Nora Jennifer Schneevoigt

Remote sensing in geomorphological and glaciological research

Thesis submitted for the degree of

Philosophiae Doctor (Ph.D.)

2012

Department of Geosciences

Faculty of Mathematics and Natural Sciences

University of Oslo

the essence

lies

in every detail
and
in the great entirety

at the same time
and
on far more different levels

than we can possibly perceive
and
even imagine

or maybe there is simply
no
discernable essence

at all

Contents

List of dissertation papers

The seven dissertation papers are listed in the thematic order of their appearance in the successive chapters. In the introductory overview (Chapter 1), they are referred to by their Roman numerals as Paper I to Paper VII. All published papers are peer-reviewed. Paper IV received a 'Best Paper Award for Young Authors' at the 9th International Symposium on High Mountain Remote Sensing Cartography (HMRSC-IX), Graz, Austria.

Paper I:
Schneevoigt, N.J. (subm.):
Review article: Is remote sensing proper science?
Manuscript submitted to Norsk Geografisk Tidsskrift.

Paper II:
Schneevoigt, N.J. & L. Schrott (2006):
Linking geomorphic systems theory and remote sensing. A conceptual approach to Alpine landform detection (Reintal, Bavarian Alps, Germany).
Geographica Helvetica 61(3): 181-190.

Paper III:
Schneevoigt, N.J., van der Linden, S., Thamm, H.-P. & L. Schrott (2008):
Detecting Alpine landforms from remotely sensed imagery. A pilot study in the Bavarian Alps.
Geomorphology 93: 104-119.

Paper IV:

Schneevoigt, N.J., van der Linden, S., Kellenberger, T., Kääb, A. & L. Schrott (2011):

Object-oriented classification of alpine landforms from an ASTER scene and digital elevation data (Reintal, Bavarian Alps).

Grazer Schriften der Geographie und Raumforschung 45: 53-62.

Paper V:

Ortega, R.Z. & N.J. Schneevoigt (2012):

Modelling potential debris flows from SRTM data in the upper Chama river watershed, northwestern Venezuela.

Revista Geográfica Venezolana 53(1): 93-108.

Paper VI:

Schneevoigt, N.J., Sund, M., Bogren, W., Kääb, A. & D.J. Weydahl (2012):

Glacier displacement on Comfortlessbreen, Svalbard, using 2-pass differential SAR interferometry (DInSAR) with a digital elevation model.

Polar Record 48(244): 17-25.

Paper VII:

Sund, M., Eiken, T., Schneevoigt, N.J. & J.O. Hagen (in prep.):

Towards a revised and synthesized conceptual surge model.

In: Sund, M. (2011): On the dynamics of surge-type and tidewater glaciers in Svalbard. PhD thesis, Department of Geosciences. Series of dissertations submitted to the Faculty of Mathematics and Natural Sciences, University of Oslo, No. 1147. ISSN 1501-7710.

Acronyms

ACIA	Arctic Climate Impact Assessment
ASAR	Advanced Synthetic Aperture Radar
ASTER	Advanced Spaceborne Thermal Emission and Reflection Radiometer (sensor onboard the Terra satellite)
C-band	radar wavelengths (between 3.7 and 7.5 cm)
CNES	Centre National d'Etudes Spatiales ('French Space Agency')
COSMO-SkyMed	COnstellation of small Satellites for the Mediterranean basin Observation
DEM	digital elevation model
DFG	Deutsche ForschungsGemeinschaft ('German Research Foundation')
DMRN	Distributed Melton´s Ruggedness Number
DSM	digital surface model
DTM	digital terrain model
DInSAR	differential SAR interferometry
ERS-1/-2	European Remote Sensing satellites 1 and 2
ERSDAC	Earth Remote Sensing Data Analysis Center
ESA	European Space Agency
EOS	Earth Observing System (satellite series programme)
FCC	false colour composite
GCP	ground control point
GEOBIA	geographic object-based image analysis

GIS	geographical information system
Glaciodyn	The dynamic response of Arctic glaciers to global warming (research project)
GNSS	Global Navigation Satellite System
HMRSC	High Mountain Remote Sensing Cartography
HRS	high resolution stereoscopic
ICRSS	International Circumpolar Remote Sensing Symposium
InSAR	SAR interferometry
IPCC	Intergovernmental Panel on Climate Change
IPY	International Polar Year (2007-2009)
ISPRS	International Society for Photogrammetry and Remote Sensing
LiDAR	Light Detection And Ranging
L-band	radar wavelengths (between 15 and 30 cm)
L1 - L4	the four levels of the main eCognition project
MCF	minimum cost flow (unwrapping technique)
MFDA	multiple-flow direction algorithm
MLI	multilook image (radar data format)
MRN	Melton´s ruggedness number
MSFM	modified single flow model
NASA	National Aeronautics & Space Administration
NDVI	normalised difference vegetation index
NPI	Norwegian Polar Institute
OBIA	object-based image analysis
ODE	Oxford dictionary of English
RADAR	RAdio Detection And Ranging
RDC	radar doppler coordinates
RGB	red, green and blue (channels in satellite image representation)
RMSE	root mean square error
SAR	synthetic aperture radar

SAVI	soil-adjusted vegetation index
SEDAG	SEDiment cascades in Alpine Geosystems (research project)
SLC	single look complex (radar data format)
SLR	sea level rise
SPIRIT	SPOT 5 stereoscopic survey of Polar Ice: Reference Images and Topographies (IPY project)
SPOT	Satellite Pour l'Observation de la Terre ('Earth observation satellite')
SWIR	short wave infrared (wavelengths between 1.4 and 3 μm)
SRTM	Shuttle Radar Topography Mission
SVM	support vector machine
TanDEM-X	TerraSAR-X Add-oN for Digital Elevation Measurement (radar satellite)
TerraSAR-X	Terra SAR X-band (radar satellite)
TIN	triangular irregular network
TIR	thermal infrared (wavelengths between 3 and 15 μm)
TLS	terrestrial laser scanning
UNEP	United Nations Environment Programme
USGS	United States Geological Survey
UTM	Universal Transverse Mercator
VHR	very high resolution
VNIR	visible and near-infrared (wavelengths between 0.4 and 1.4 μm)
X-band	radar wavelengths (between 2.5 and 3.7 cm)
ZFL	Zentrum für Fernerkundung der Landoberfläche ('Center for Remote Sensing of Land Surfaces')

Acknowledgements

The years of involvement in academia and its workings have been an interesting and eye-opening venture, which has broadened my horizons in many ways. My gratitude goes to all who have contributed to the completion of this work, including those not explicitly mentioned here.

First, thanks are due to my supervisors. Dr. Dan Johan Weydahl´s constructive, down-to-earth approach and encouragement were much appreciated. Prof. Dr. Andreas Kääb was readily available for meetings and for offering expert feedback. Advice and assistance with matters of organisation were provided by Prof. Dr. Lothar Schrott at the outset and by Prof. Dr. Jon Ove Hagen at the end of this work. Special thanks go to Prof. Dr. Elisabeth Alve and Petter Hovind, without whose support it would not have been finished.

I am grateful to Prof. Dr. Björn Waske, Dr. Ulrike Falk and the Center for Remote Sensing of Land Surfaces (ZFL), University of Bonn, and to Dr. Tobias Kellenberger and the Remote Sensing Laboratories, University of Zurich, for so kindly accommodating me as a visiting researcher.

Besides, I should like to give thanks to the institutions producing the data for this thesis. The Advanced Spaceborne Thermal Emission and Reflection Radiometer (ASTER) science team, the National Aeronautics & Space Administration (NASA) and the United States Geological Survey (USGS) provided the ASTER and the Shuttle Radar Topography Mission (SRTM) data. The synthetic aperture radar (SAR) data is curtesy of the European Space Agency (grant AOPOL 4127), the Satellite Pour l'Observation de la Terre (SPOT)

data of the French Space Agency. Elevation data also came from the Bavarian Geodetic Survey and the Norwegian Polar Institute.

This work was mainly funded by the Department of Geosciences, University of Oslo. I would also like to thank the Daimler and Benz Foundation for awarding a Research Abroad Fellowship for Zurich and Oslo. Further financial support came through the SEDiment cascades in Alpine Geosystems (SEDAG) project collection funded by the German Research Foundation (grant Schr 648/1-3). Other funding included a Conference Travel Grant by Industrial Liaisons, Department of Geosciences, University of Oslo, and an Early Career Scientist Travel Grant by the UK Polar Network.

Competent IT specialists ensured the smooth running of my workplaces and were always available to help with computer problems. Fellow students and colleagues brightened up the daily routine and are all thanked very much for the good company, especially Dr. Evy Glørstad-Clark, Dr. Anna Sinisalo, Dr. Karianne Staalesen Lilleøren, Stefanie Stenzel and Olena Dubovyk. Very special thanks go to the great staff of ZFL for always providing such a pleasant and supportive working atmosphere.

Moreover, I would like to express my sincere gratitude to Dr. Monica Sund, Dr. Sebastian van der Linden, Dr. Geir Moholdt and Wiley Bogren for sharing their knowledge with me. Those discussions taught me a lot, thus making my work more rewarding. The comments by Dr. Silvia Huber, Dr. Sven Nussbaum, Dr. Monica Sund, Dr. Sebastian van der Linden and Frank Thonfeld helped to improve the introductory overview of the thesis. Vivien Campbell and Norbert Schneevoigt kindly proofread the entire manuscript.

Of utmost importance, my most heartfelt thanks go to my family and friends for their constant encouragement, which was so crucial for the completion of this dissertation. Carla Schneevoigt, Dr. Pengxin Zhang, Dr. Silvia Huber, Sofie Xiaofen Gjerull, Ruth Schneevoigt and Dr. Marija Rosić Pavlović, in particular, made a huge difference - thanks a million!

Abstract

Cold environments are highly variable and play an important role in the global change debate. At freezing point temperatures, they react sensitively even to minor climatic variations and therefore they need to be monitored closely and constantly. The relative inaccessibility of alpine and polar regions can be partly compensated for by the almost global availability of remote sensing data. Due to high relief energy, cloud, snow and ice cover, it is challenging to monitor these regions from a distance. This interdisciplinary feasibility study analyses remote sensing from a theoretical point of view and in three exemplary high mountain case studies. The potential of remote sensing for monitoring cold climate environments in lower (European Alps, Venezuelan Andes) and higher latitudes (Spitsbergen) is investigated with data from passive optical and active radar satellite sensors.

First of all, the scientific basis of remote sensing is examined, and the question is raised as to whether it is science or method. It is argued that sciences nowadays can hardly be separated from the methodologies and technologies they make use of for their advancement. The myth of the supremacy of science over technology may prove to be an outdated remnant of former, less technologised times. The elusiveness of the terms 'science' and 'remote sensing' is symptomatic of a general problem of categorisation found in modern sciences.

For the first case study, the characteristic features of geomorphological landforms are initially identified. In a segment-based approach on four scales, an optical Advanced Spaceborne Thermal Emission and Reflection Radiometer (ASTER) satellite scene and a digital elevation model (DEM) are then clas-

sified hierarchically with fuzzy membership functions. The resulting thematic map of the Reintal catchment reaches an overall accuracy of 92 % and a kappa coefficient of 0.915. It is possible to identify both sediment stores and activity status within the alpine sediment cascade system.

The second case study examines mass movements in the Venezuelan Andes with a DEM and an ASTER scene. The potential occurrence of debris flows is modelled as a function of topography and sediment dynamics. The results represent a realistic first hazard assessment of qualitative debris flow probabilities in the region and underline the importance of further displacement measurement, modelling and monitoring.

Glacier mass movement is the focus of the third case study. Synthetic aperture radar (SAR) scenes by the European Remote Sensing satellites ERS-1 and ERS-2 are used for differential interferometry along with a DEM. An average of a few centimetres per day and maximum horizontal displacements of 18 to 20 cm d^{-1} indicate pre-surge conditions on Comfortlessbreen in 1996. These and other data as well as previous surge studies are then turned into a synthesized conceptual model, which accommodates both temperate and polythermal glacier surges and also accounts for processes prior to surge visibility.

This work shows the usefulness of multi-sensor remote sensing for spatial mapping, monitoring and modelling in cold climate environments. One universal approach for all possible research questions does not exist; adequate data and methods have to be chosen in accordance with their respective strengths for the particular topic. The findings are not only of interest for applied research questions, but also exemplify the need for further theory formation.

Sammendrag

Kalde områder er svært omskiftelige og spiller en viktig rolle i den globale klimadebatten. De reagerer sensitivt selv på små klimatiske variasjoner, ettersom temperaturene fluktuerer rundt frysepunktet. Det er derfor behov for grundig og konstant overvåkning. Utilgjengeligheten i alpine og polare områder kan delvis kompenseres med fjernmålingsdata med tilnærmet global dekning. På grunn av høy reliefenergi, skyer, snø- og isdekke er det utfordrende å overvåke disse områdene fra rommet. I denne tverrfaglige geografiske mulighetsstudien diskuteres fjernanalyse fra et teoretisk ståsted og eksemplifiseres ved tre anvendelser fra høyfjellsområder. Potensialet fjernanalyse har for måling av klimatisk kalde områder i lavere (europeiske Alper, venezuelanske Andesfjellene) og høyere (Svalbard) breddegrader, blir undersøkt med data fra både passive optiske og aktive radar satellittsensorer.

Først og fremst undersøkes det vitenskapelige grunnlaget for fjernanalyse, og det diskuteres hvorvidt det er en metode eller en vitenskap. Det argumenteres for at vitenskap i dag knapt kan skilles fra metoder og teknologi som benyttes i vitenskapens framgang. Myten om at vitenskapen er overordnet teknologien kan vise seg å være en utdatert rest fra tidligere, mindre teknologiske tider. De vanskelig definerbare termene 'vitenskap' og 'fjernanalyse' gjenspeiler et generelt problem med kategorisering i den moderne vitenskapen.

I det første studieområdet identifiseres de karakteristiske geomorforlogiske landformene. Deretter klassifiseres et optisk ASTER (Advanced Spaceborne Thermal Emission and Reflection Radiometer) satellittbilde og en digital terrengmodell (DTM) hierarkisk med fuzzy medlemskapsfunksjoner i en segment-

basert tilnærming i fire skalaer. Det resulterende tematiske kartet av Reintal har en samlet nøyaktighet på 92 % og en kappa-koeffisient på 0,915. Det påviser både sedimentlagre og deres aktivitetsnivå innen det alpine sediment systemet.

I det andre studieområdet undersøkes, ved hjelp av en radar DTM og et ASTER-bilde, massebevegelse i de venezuelanske Andesfjellene. Den mulige forekomsten av løsmasse- og sørpeskred blir modellert som en funksjon av topografi og sedimentdynamikk. Resultatet representerer en realistisk initiell risikovurdering av kvalitativ sannsynlighet for løsmasse- og sørpeskred i området, og understreker viktigheten av videre måling, modellering og over våkning av bevegelse.

I det tredje studieområdet fokuseres det på bevegelse i ismasser. Synthetic aperture radar (SAR) bilder fra satellittene ERS-1 og ERS-2 (European Remote Sensing) benyttes sammen med en DTM til differensiel interferometri. Et gjennomsnitt på noen få centimeter per dag og maksimal horisontal forflytning på 18 til 20 cm d^{-1} indikerer forholdene før surge på Comfortlessbreen i 1996. Sammen med andre data og tidligere surgestudier inngår disse resultatene deretter i en samlet konseptuell surgemodell. Denne omfatter surge i både tempererte og polytermale breer, så vel som prosessene før den synlige surgen.

Dette arbeidet viser anvendeligheten av multi-sensor fjernanalyse for romlig kartlegging, overvåkning og modellering i kalde miljøer. En universal tilnærming for alle mulige forskningsspørsmål finnes ikke; adekvate data og metoder bør velges ut fra deres respektive styrke i forhold til det bestemte emnet. Funnene er ikke bare av interesse for den anvendte vitenskapen, men eksemplifiserer også behovet for ytterligere teoretisk utvikling.

1 Introductory overview

Field research in alpine[1] and polar regions provides important insights into global and climate change, amongst other things (Eiken et al., 1997; Hagen et al., 2003, 2005; Chiverrell et al., 2008; Otto & Schrott, 2010; Keiler et al., 2012), but encounters limitations in terms of accessibility, expense and repeatability. Remote sensing[2] offers a valuable additional dimension of feature monitoring: it enables us to operate on global scales with uniform data sets and measuring methods, thus providing long, continuous and intercomparable series of measurements (Hall & Martinec, 1986; Haeberli et al., 2002; Kääb, 2005a; Wangensteen, 2006; Lubin & Massom, 2007; Skorve, 2007; Smith & Pain, 2009; Kääb, 2010; Copland et al., 2011; Riedel et al., 2011; Wilson, 2012). Moreover, mapping and monitoring with remote sensing data is relatively cost- and time-effective (Konecny, 1999; Kääb, 2005b; Lubin & Massom, 2007; Rees & Pellikka, 2010; Joughin et al., 2010a; Debella-Gilo, 2011; Heid, 2011).

Improvements in geometric, spectral and radiometric resolution in the multitude of air- and spaceborne sensors available today enable a remote assessment of alpine and polar features at least to a certain extent (Richards, 2005; Lubin & Massom, 2007; Rott, 2009; Smith & Pain, 2009; Pellikka & Rees,

[1] In this thesis, the capitalised adjective *Alpine* designates features of the European Alps, whereas *alpine* with a small letter is used with the meaning 'high mountain', 'of high mountains'.

[2] *Remote sensing* refers to satellite and aerial sensors in this work, cf. Ch. 2.1. Photogrammetry, ground penetrating radar, sonar etc. are not explicitely targeted, although overlaps do exist.

2010; ESA, 2012; Wilson, 2012). Yet the rapid advancements in image aquisition coverage and volumes are not matched by the current level of image analysis (Debella-Gilo, 2011; Riedel et al., 2011; Bishop et al., 2012; Casey et al., 2012): a wealth of data slumbers in the remote sensing data archives, the potential of which remains to be unlocked.

While a lot of new sensors with enhanced resolutions have become operational since the turn of the millenium (cf. ESA, 2012), many research questions want to look further back in time in order to derive trends and developments over time. Archived data is cheaper than preordered new acquisitions or even available for free, as e.g. the optical Landsat archives, RAdio Detection And Ranging (radar) data on certain earthquake events or the Shuttle Radar Topography Mission (SRTM) digital elevation model (DEM) (cf. ESA, 2012). Data quality can be directly assessed in the archives and the best suitable scenes selected, unlike with new orders. Older data can thus be used to close data gaps in research projects.

In this thesis, remote sensing is used in three exemplary case studies to investigate cold climate mountainous landscapes (Fig. 1.1). These regions are formed and characterised by the past and present existence of ice and water above and below the ground (Thorn, 1992; Haeberli, 1996; Shroder Jr. & Bishop, 2004; Kääb, 2005b; Gruber & Haeberli, 2007; Gruber et al., 2009; Band et al., 2012; Zwieback et al., 2012). Over a long period of time, glacial erosion can outperform the effects of denudative and fluvial erosion (Hallet et al., 1996; Brocklehurst & Whipple, 2002). As glacial and geomorphologic activity, change and process rates are significantly more accelerated there than elsewhere (Caine, 1974; Abele et al., 1993; Slaymaker, 2010; Keiler et al., 2012), glacial and periglacial dynamics rapidly and effectively shape the landscapes of high elevations and latitudes (Thorn, 1992; Haeberli, 1996; Band et al., 2012).

The effects of global change may increase the already high process activity in those regions (Gude et al., 2002; Gruber & Haeberli, 2007; Lubin & Massom, 2007; Gruber et al., 2009; Stoffel, 2010; Stoffel & Huggel, 2012; Goode et al.,

2012), leading to even less stable geomorphological and glaciological process-form-relationships, which need to be further monitored. A step in this direction is undertaken in this dissertation.

Landforms and glaciers cannot always be observed in total from the ground due to relative terrain inaccessibility, while satellite scenes can be purchased for most parts of the Earth. In order to find out more about the possibilities and limitations of cold climate remote sensing, both optical and radar satellite images as well as elevation data have been analysed in this thesis. Yet areas with high relief energy make image processing a challenge due to high variability in topography and illumination (Kääb, 2005b; Smith et al., 2006; d'Oleire-Oltmanns et al., 2012). Snow and ice offer little visual contrast, and snow and vegetation often cover the target features on the ground (Lubin & Massom, 2007; Smith & Pain, 2009; Pellikka & Rees, 2010). Hence this thesis investigates to what extent multi-sensor satellite remote sensing can further alpine geomorphological and glaciological investigations.

Knowledge of surface characteristics is a key to understanding the processes taking place and long-term landscape evolution (Abele et al., 1993; Hutchinson & Gallant, 2000; Gude et al., 2002; Bishop & Shroder, 2004; Lubin & Massom, 2007; Wilson 2012). Environmental assessments form the basis of many research questions, but also of political decision-making and surveying (Lubin & Massom, 2007; Smith & Pain, 2009; Klemenjak et al., 2012). Innovative land-cover mapping and classification is the first and foremost application of remote sensing (Waske, 2007) and considered a "major research theme" (Bishop et al., 2012: 17), just as exact quantifications of sediment and glacier mass budgets and dynamics (Gude et al., 2002; Bartsch et al., 2009; Burt & Allison, 2010; Otto & Schrott, 2010). Remote sensing can provide new insights into research questions which have been pending for a long time (Lubin & Maasom, 2007; Sund et al., 2009; Burgess et al., 2012; Paper VII), which also promotes theory formation.

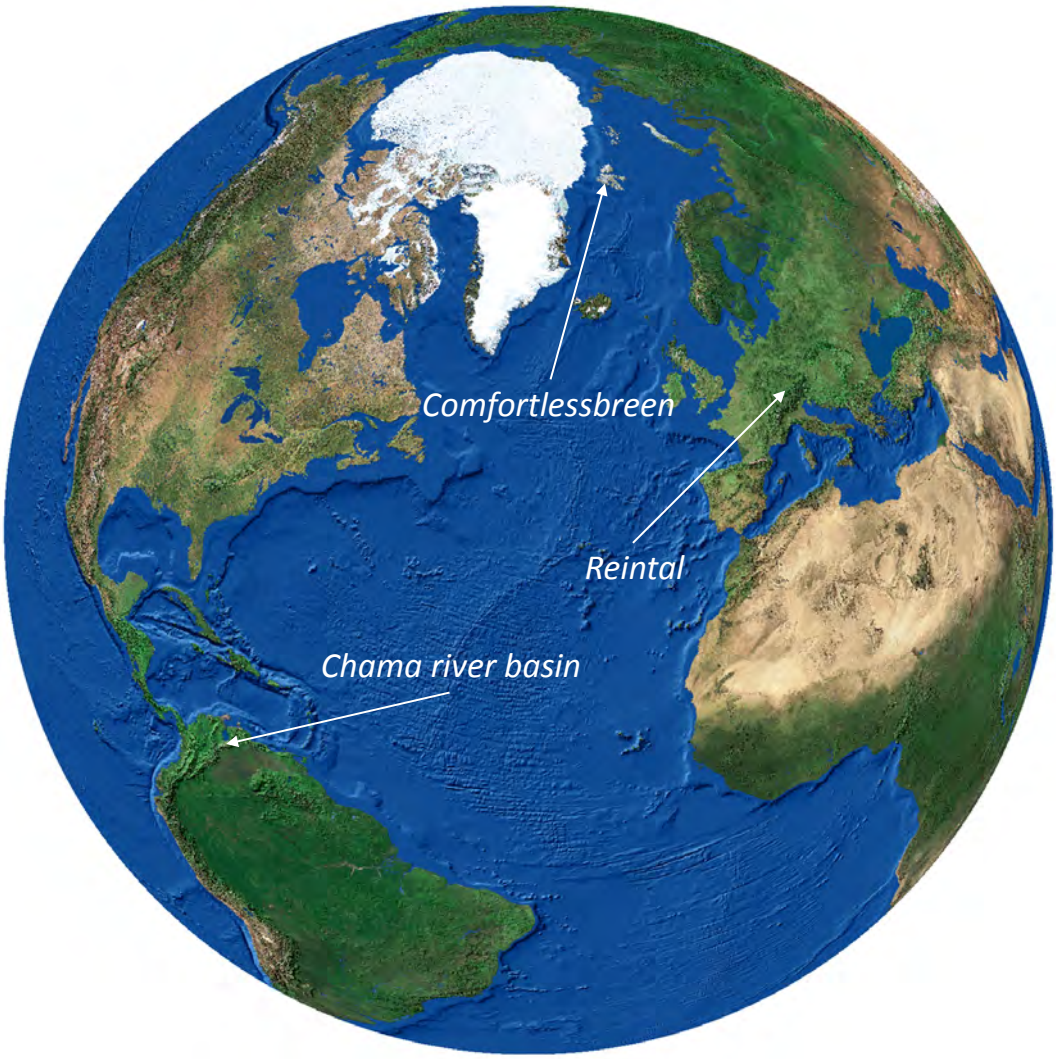

Figure 1.1: Study Areas in the Alps, the Andes and on Svalbard

Comfortlessbreen glacier near Ny Ålesund on Svalbard, the Reintal valley in the Bavarian Alps, and the upper Chama river basin in Venezuela.

1.1 Objectives

The major goal of this thesis is to use satellite remote sensing data for assessing cold climate environments. Both passive and active sensors should be considered in order to make optimal use of the optical and radar data available for the chosen study test areas. The remote investigation of alpine and polar terrain represents a challenge, which is why the applicability of various approaches to mountainous regions has to be tested and adapted accordingly.

The exact identification of geomorphological landforms and processes is demanding both in the field and in remote sensing data. Characteristic features have to be found which allow for their recognition in image and elevation data. This requires knowledge of the spatial linkages between geomorphologic processes and sediment storage types in catchments. Precise descriptions of the target classes and their typical features form the necessary prerequisite of classification, which is why this data base has to be assembled first.

The suitability of satellite and elevation data for detecting rock and sediment storage areas is tested in the Bavarian Alps with the objective of finding a way of classifying spectrally and topographically often rather similar landforms. The superordinate goal of this is to further the research on the functioning of sediment stores as components of the sediment cascade. The identification of storage type patterns and the classification of geomorphological units, ultimately aims at an integrative model describing landform development in high mountain regions (Schrott & Dikau, 1998; Schrott et al., 2002).

The appropriateness of satellite elevation data for modelling and validating debris flows is studied in the Venezuelan Andes. The DEM has to be corrected and adequate parameters and models must befound in order to be able to calculate the debris flow probability at a reginal scale. The ultimate goal is to deliver a first hazard assessment of the study area, which was lacking prior to this study. The contribution of debris flows to the sediment dynamics of the regional river system also needs further investigation.

Active and passive satellite remote sensing for movement measurements is investigated in Spitsbergen, Svalbard. Appropriate archived data has to be found for the mid-1990s to close an existing data gap, as ground truth is lacking for that period of time. In order to gain more insight into surge patterns (Sund et al., 2009), glacier velocities are to be derived in the area of interest. Out of different existing approaches, an adequate technique has to be chosen for doing so. This case study ultimately aims at more thoroughly describing surge behaviour to develop an integrative conceptual surge model.

Although the term 'remote sensing' has been used since the 1960s, the nature of the term still needs to be defined properly: is it a real science or a mere method which is being used? Therefore a clarification of the theoretical scientific basis of remote sensing is aimed at by analysing the ontology of remote sensing, i.e. its metaphysical nature from a philosophy of science point of view. Definitions of both the terms 'science' (Ch. 2.2) and 'remote sensing' are attempted at (Ch. 2.1, 2.3) by means of a literature review. Similarly, image segmentation techniques and geomorphological systems theory are theoretically linked/coupled in order to show parallels between these two approaches from two unrelated fields of research.

In summary, the following objectives are pursued in this work:

- to further the theoretical foundations of remote sensing by clarifying its ontology and by coupling image segmentation with systems theory,
- to detect alpine landforms by assembling their characteristics and by finding a suitable approach to classifying them in remote sensing data,
- to derive processes and (potential) displacement by means of assessing process activity, modelling flow paths and measuring movement from space,
- to assess both optical and radar data in search of their most appropriate usage in the given study areas, thus combining passive and active sensors.

1.2 Structure of the thesis

This feasibility study analyses the drawbacks and opportunities of satellite remote sensing of landforms and movements. Three case studies cover cold climate environments in lower and higher latitudes, i.e. in the European Alps, the Venezuelan Andes and in Spitsbergen, Svalbard (Fig. 1.1). The study areas are further detailed in the respective papers (Chs. 4.2, 5.2, 6.2, 7.2). Alpine landforms are looked at in the first case study. Landform changing surface processes can involve mass movements such as debris flows, the potential occurence of which is investigated in the second case study. Finally, glacier movement itself is tackled in the third case study in order to find out more about the surge phenomenon.

The case studies are bracketed by theoretical considerations. The practical applications of remote sensing, which are suitable for many different topics of research as exemplified in this thesis, make it scientifically valuable. However, every science needs a theoretical basis on which the research dwells, in the name of which it is conducted. Does remote sensing have such a theoretical foundation? The scientific framework of the remote sensing discipline is examined at the beginning of the thesis. The surge study eventually leads to a revised and synthesised conceptual surge model at the very end of the thesis, thus coming back to theory formation.

The introductory overview chapter puts the content of the dissertation papers into context and elaborates on their common ground. Remote sensing forms the leitmotiv around which the dissertation papers evolve. Their scientific background and geographical context is presented. Particular attention is paid to Earth system science and the global change debate. Matters are elaborated upon which have not received much attention in the papers, but which further clarify the scientific context. Some additional material is presented as well. When issues have been discussed extensively in a paper, the relevant paper section is referred to. The content of each paper is summarised

Table 1.1: Overview of Dissertation Paper Topics

Paper / Topic	I	II	III	IV	V	VI	VII
Remote sensing	X	X	X	X	X	X	X
Optical data		X	X	X	X	X	X
Radar data					X	X	X
Geomorphology		X	X	X	X	(X)	
Glaciology			X			X	X
Forms and shapes		X	X	X	X		
Movement					X	X	X
Theory of science	X	X	(X)		(X)		X
Didactics	X	X				X	

at the beginning of the respective chapter, corresponding to the publication's abstract. The subsequent seven chapters reproduce Papers I to VII (see p. IX). Some of these contain minor changes to the published versions not only in the interest of readability, but also to offer added value. This does not alter nor update their peer-reviewed content, but only its presentation, and is indicated above the paper reference at the beginning of each chapter.

Paper I is a theoretical review article analysing the nature of both science in general and remote sensing in particular, thus laying some theoretical foundations for the practise of remote sensing. The next three papers form a logical sequence around the first case study in the Bavarian Alps (Figs. 1.1, 1.2), departing from and further developing Schneevoigt (2004). Geomorphic systems theory and segment-based remote sensing have been linked in Paper II in order to convey the conceptual background of the study. Its geomorphic side is accentuated in Paper III, which particularly stresses the nature and characteristics of the Alpine landforms examined and to what extent they can

be classified. Paper IV describes the remote sensing methods employed in further depth, i.e. the segmentation-based classification hierarchy. The second case study modelling potential debris flows in the Venezuelan Andes (Fig. 1.1) is described in Paper V, which is partly based on Ortega (2007). The last two papers focus on the third case study on Svalbard (Figs. 1.1, 1.3). Paper VI derives glacier movement by means of radar interferometry. Paper VII uses these and other measurements to develop a new conceptual surge model, which takes the dissertation full circle and back to theory formation.

This work thus unites diverse spheres of research which have not been linked in this way before. In sum, the thesis deals with active and passive remote sensing applied to several fields of research: scientific theory and philosophy of science, geomorphology and glaciology, while a certain emphasis has also been placed on didactics and understandability when presenting the work (Tab. 1.1). This makes it interdisciplinary and very geographical by its nature, similar to e.g. Earth system studies.

1.3 Scientific background

This section is organised as follows, inductively moving from practical to abstract issues: remote sensing is useful for the monitoring of global change, of which glaciers are prime indicators (Ch. 1.3.1). Glacier movement, especially in the form of surge (Ch. 1.3.2), can be likened to mass movement, e.g. debris flow (Ch. 1.3.3). Such sediment fluxes control landform development (Ch. 1.3.4) and move down-slope through sediment cascade systems, a branch of systems theory (Ch. 1.3.5). This finally leads to the theoretical concept of remote sensing (Ch. 1.3.6).

Figure 1.2: View of the Oversteepened Rockwalls of the Reintal
The dammed lake on Vordere Gumpe foodplain in the foreground, the Zugspitzplatt plateau in the background, view facing west. Photo by L. Schrott, 2001.

1.3.1 Cold climate environments and global change

The global interest in cold climate environments (i.e. high altitudes and high latitudes) stems from the fact that they form strongholds of resources, energy production, biodiversity, biotic refugia (survival habitats) and recreation (Fig. 1.2), amongst other things (Briggs et al., 1997; Ives et al., 1997; Ives & Messerli, 2001; Davies & Korup, 2010; Keiler et al., 2012). These regions are highly variable and react sensitively to even minor climatic or environmental change (Caine, 1974; Abele et al., 1993; Lubin & Massom, 2007; Humlum et al., 2011; Stoffel & Huggel, 2012). Because of their closeness to the melting point, often in combination with the pronounced relief energy of alpine terrain, even small changes in temperatures can lead to movements in wa-

ter/ice and sediment, which quickly engender modifications of landforms and glaciers (Abele et al., 1993; Orwin et al., 2010; Bimböse et al., 2011; Debella-Gilo, 2011; Stoffel & Huggel, 2012). Climate change has already led to a considerable melt of glaciers, ice caps and permafrost, and consequent hydrological changes and mass movements may endanger humans and infrastructure (Maisch, 1995; Haeberli et al., 1999; Kääb, 2003, 2005b; Gruber & Haeberli, 2007; Gruber et al., 2009; Thomas et al., 2009; Slaymaker, 2010; Debella-Gilo, 2011; Zemp, 2011; Radić & Hock, 2011; Stoffel & Huggel, 2012). In order to monitor such changes, it is important to closely observe those landscapes as well as specific processes which may alter them, for instance debris flows (Ch. 1.3.3) and glacier surges (Ch. 1.3.2).

Global change also affects mountains and highlands in their function as natural "water towers" in global hydrology, as they supply up to 95 % of the available freshwater (Briggs et al., 1997; Ives & Messerli, 2001; Viviroli et al., 2003; Viviroli & Weingartner, 2008; Radić & Hock, 2011; Bolch et al., 2012; Kääb et al., 2012). This is significant both on local scales regarding watersheds and inhabitants and on a global perspective: for Earth system sciences, the global ice masses in the form of glaciers, ice caps and permafrost constitute both the most important freshwater store and the most important indicator of climate and global change (IPCC, 2001, 2007; Kääb, 2005b; UNEP, 2007; Kääb, 2010; Kääb et al., 2012).

The ice of glaciers and ice caps, the Earth´s most important freshwater reservoirs, hold an amount equivalent to almost 70 m of potential sea level rise (SLR) (IPCC, 2007; UNEP, 2007). Most of it ($>$ 99 %) is contained in Antarctica and Greenland ($\sim$ 61 and $\sim$ 7 m, respectively), while the remaining smaller glaciers and ice caps hold only $\sim$ 0.6 m (IPCC, 2007; UNEP, 2007; Radić & Hock, 2011; Paul, 2011). However, the latter contribute with $\sim$ 60 % to current eustatic SLR induced by ice melt, which is responsible for about half of today's SLR - the other half resulting from thermal expansion of the warming oceans (IPCC, 2007; Meier et al., 2007; Hock et al., 2009; Radić &

Figure 1.3: Surge Crevasses on upper Comfortlessbreen
Photo of the upper portion of the glacier, taken during ongoing surge by M. Sund, 2009.

Hock, 2011; Gardner et al., 2011; Jacob et al., 2012). Uncertainties regarding regional SLR contributions and SLR estimates are large (IPCC, 2007; Thomas et al., 2009; Paul, 2011; Gardner et al., 2011; Jacob et al., 2012; Kääb et al., 2012). Meier et al. (2007) and Błaszczyk et al. (2009) argue for a more pronounced eustatic SLR through glaciers and ice caps outside Antarctica and Greenland than estimated by IPCC (2007).

The global ice masses are primary climate indicators: close to the melting point, they respond sensitively to climatic variations (IPCC, 2001, 2007; Kääb, 2005b; Humlum et al., 2011; Zemp, 2011; Bolch et al., 2012; Kääb et al., 2012). Glaciers can be seen as indicators of climate change in a twofold way: firstly, their surface mass balance, i.e. the 'vertical' difference in thickness between snow and ice accumulation and ablation, directly reflects snowfall and melt

and hence short-time trends in precipitation and temperature (Hagen et al., 2005; Zemp, 2011; Bolch et al., 2012). Secondly, overall 'horizontal' glacier geometry indirectly expresses changes in climate over longer periods of time, dating as far back as it takes for the glacier ice to travel down to the terminus, the glacier tongue (Jóhannesson & Sigurdsson, 1998; Zemp, 2011; Bolch et al., 2012).

However, glacier surges, i.e. the phenomenon of sudden glacier speed-ups, complicate the picture (Ch. 1.3.2, Fig. 1.3). Most likely, internal glacier instabilities drive the cyclic surge reoccurrence rather than climate change (Meier & Post, 1969; Raymond, 1987; Sund et al., subm.); the cause of these instabilities is still unknown. Yet the influence of surge dynamics can blur the long-term climate signal contained in glaciers (Jóhannesson & Sigurdsson, 1998), which has not been taken sufficiently into account in recent studies: while quiescent build-up phases may delay reactions on global change, accentuated mass loss and thus SLR can occur when warming and surge phases coincide (Sund et al., subm.). More knowledge of surges is all the more important as of all latitudes, global (glacier mass) change is most marked in the Arctic (ACIA, 2005; IPCC 2007; Jacob et al., 2012), and Svalbard is considered especially climate-sensitive (Serreze & Francis, 2006; Błaszczyk et al., 2009; Humlum et al., 2011). The project 'The dynamic response of Arctic glaciers to global warming' (Glaciodyn) investigates selected glaciers to better understand their reactions to and interactions with their environment, and to derive enhanced input for climate models.

1.3.2 Glacier movement and surge

Most of Svalbard´s glaciers are *polythermal*, i.e. partly at the pressure-melting point (warm-based), a prerequisite for fast flow, and partly frozen to the ground (cold-based), which impedes flow (Hagen & Sætrang, 1991; Mansell et al, 2012; Sund, 2011). In contrast, *temperate* glaciers are at melting point, apart from

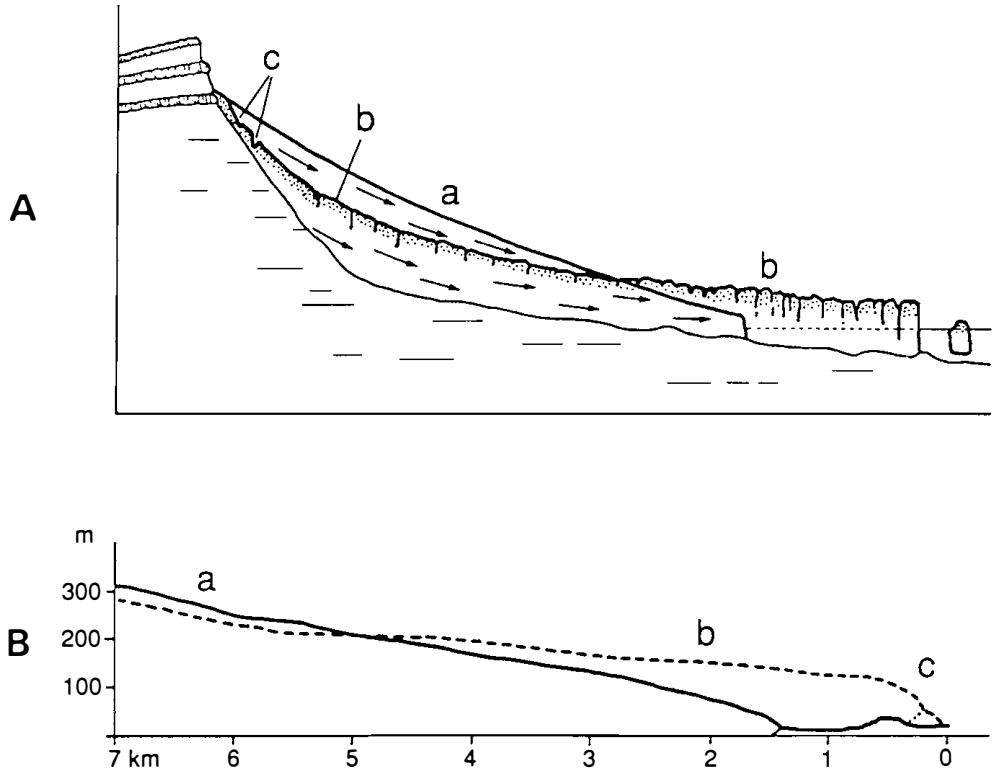

Figure 1.4: Schematical Surge Advance

Longitudinal glacier profile changes from Hagen et al. (1993). The overthickened reservoir zone is quickly lowered by up to 100 m, feeding into the receiving zone which gains mass significantly. A: Calving glacier with crevasses (c). B: Land-terminating glacier with its marked convex terminus (c). Shown are glacier surfaces before (a) and after surge (b).

a colder surface layer, whereas *cold* glaciers remain at freezing temperatures throughout (Cuffey & Paterson, 2010). Glaciers move down-slope under the influence of gravity via basal sliding and internal plasticity (Cuffey & Paterson, 2010). Through this movement, a glacier adapts to the given climate conditions: if in dynamic equilibrium and at balance flux, the glacier keeps its steady-state surface profile (Cuffey & Paterson, 2010; Dunse, 2011). Meier & Post (1969) first defined glacier surges as quasi periodic oscillations between longer quiescent phases of slow flow and shorter intervals of highly accelerated glacier movement with 10 to 100 times higher velocities. Murray et al. (2003a, b) even speak of speed increases of up to 1000 times. Such speeds imply basal

motion, through which much faster flow than in plastic deformation becomes possible. While changes in accumulation and ablation can trigger glacier response of up to centuries, changes in the basal thermal regime or hydrology provoke glacier reactions within days or months, thus facilitating surges (Cuffey & Paterson, 2010; Dunse, 2011).

Svalbard's surges tend to show especially long quiescent phases of up to 500 years (Dowdeswell et al., 1991; Solheim, 1991) and comparatively slow surge velocities due to high mass turnover (Hagen et al., 1993; Dowdeswell et al., 2001; Błaszczyk et al., 2009; Eiken & Sund, 2012). Oscillation intervals vary for each glacier individually, yet some general patterns do exist which most surges follow at least in parts (cf. Meier & Post, 1969; Fowler, 1987; Raymond, 1987; Lefauconnier & Hagen, 1991; Hagen et al., 1993): the origin of surge behaviour lies in flow rates which are too low to transport all ice accumulation from the surge reservoir to the receiving zone. Hence mass builds up in the reservoir zone, causing surface gradient and basal shear stress to increase (Fig. 1.4).

At some critical, but unknown threshold value, the slow glacier switches mode and becomes very fast flowing. This results from the heating of the glacier bed via high ice overburden pressure; frictional heat due to motion further lubricates the bed. This is sometimes accompanied by an advance of the terminus; up to 20 km have been observed on Svalbard (Liestøl, 1969; Schytt, 1969). However, the surge front may also stop before reaching the terminus (Meier & Post, 1969; Fowler et al., 2001; Sund et al., 2009; Sund & Eiken, 2010). Marked longitudinal and transverse crevassing (Fig. 1.3) of the glacier surface reflects the stress build-up and release of the whole process (Lefauconnier & Hagen, 1991; Hagen et al., 1993). Figure 1.4 represents the typically changing geometries.

Surge-type glaciers are unequally distributed and clustered on Svalbard, Greenland, Iceland, in Alaska, the Canadian Arctic, the Karakoram, the Pamirs and the Andes (Clarke et al., 1984). They supposedly constitute ~ 1 % of glaciers worldwide (Raymond, 1987; Jiskoot et al., 2000; Murray et al.,

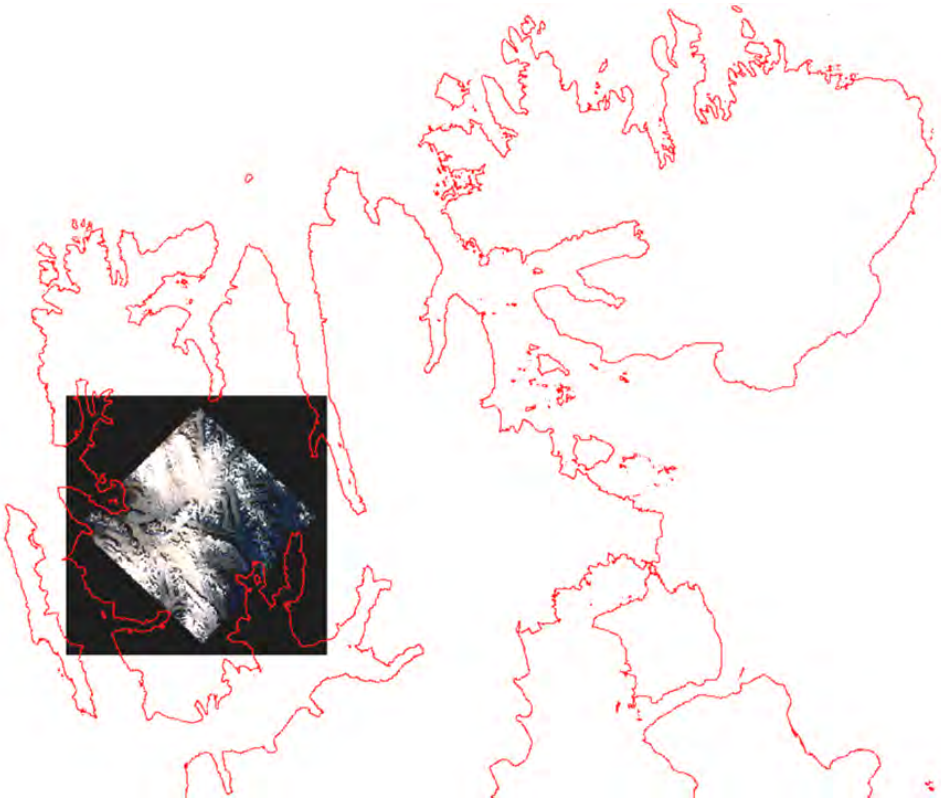

Figure 1.5: ASTER scene with Svalbard Coast Lines

Contour lines of north-western Svalbard archipelago. Behind its largest island, Spitsbergen, an optical ASTER scene, which roughly covers the area of interest near Ny Ålesund, of 17 August 2000 provided by NASA and the US/Japan ASTER science team.

2003a, b). Yet this percentage may not be exact, as recent research indicates a greater frequency of surges (Copland et al., 2003, 2011; Grant et al., 2009; Sund et al., 2009; Błaszczyk et al., 2009). On Svalbard (Figs. 1.1, 1.5), the percentage of surging glaciers is estimated to lie between 13 % (Jiskoot et al., 1998) and 90 % (Lefauconnier & Hagen, 1991), which shows how great the uncertainties in surge research still are. The trigger of the internal instabilities causing surges (Meier & Post, 1969) is still uncertain. A possible environmental or climatic control in global surge distribution is being debated; while Raymond (1987) denies it, Murray et al. (2000) object that the regional clustering hints at exactly such a control, e.g. deformable glacier bed geology. Surge recurrence intervals may be modified or even stopped because of

constrained accumulation in the reservoir zone in a changing climate (Hagen et al., 1993; Dowdeswell et al., 1995). Thermal trigger mechanisms have been proposed (Schytt, 1969; Clarke, 1976; Fowler et al., 2001) as well as changes in the subglacial drainage system (Clarke et al., 1984; Kamb et al., 1985).

In order to find out about possible surge behaviour, glacier flow velocities have to be obtained. In this thesis, this is done for Comfortlessbreen (c. 65 km^2, 15 km long), a partly tidewater glacier south of Ny Ålesund on Spitsbergen, Svalbard (Figs. 1.1, 1.5, 7.1), which recently surged (Sund et al., 2009; Sund & Eiken, 2010). Amongst other things, glacier movement can be derived from optical or radar data via image matching (e.g. Berthier et al., 2005; Kääb et al., 2005b; Debella-Gilo, 2011; Heid, 2011) or from radar data by means of offset tracking or interferometry (e.g. Mohr et al., 1998; Dowdeswell et al., 1999; Strozzi et al., 2002; Eldhuset et al., 2003; Pritchard et al., 2005; Joughin et al., 2010a; Mansell et al., 2012).

1.3.3 Mass movement and debris flow

Mass movement or wasting is defined as any gravitational down-slope displacement of earth material, possibly also involving water (Ritter, 2011). Mountainous terrain is characterised by mass movement, which occurs due to "slope instability or 'failure'" (Gruber et al., 2009: 527) when a certain relief energy is given. Mass deformation, detachment and finally displacement result once the withholding shear strength of the material is surpassed by the gravitational stress it is exposed to (Abele et al., 1993; Debella-Gilo, 2011; Ritter, 2011). Common types of mass movement are (land-) slide, slump, (rock) fall, (soil) creep, solifluction and (debris, earth, mud) flow (Dikau, 1996; Gruber et al., 2009; Ritter, 2011; Ch. 4.3.1). Mass movement thus most commonly refers to deforming and moving earth materials, yet Gruber et al. (2009) also include snow avalanches, and Debella-Gilo (2011) glacier ice flow, which is why the glacier movement studied in this thesis can also be subsumed under mass

movement. Debris flows mostly consist of water-saturated soil, sediments, regolith, rocks and water moving downhill (Dikau, 1996; Haeberli, 1996; Ritter, 2011; Yu, 2011; Ch. 4.3.1). These poorly sorted mass movements usually show sediment concentrations of $\geq 60\%$ and deposit *en masse*, which places them somewhere between landslides and runoff (Rickenmann, 1999; Lavigne & Thouret, 2002; Mergili et al., 2012; Worni et al., 2012; Kaitna et al., 2013; Rickenmann & Scheidl, 2013). Their activity is characterised by certain frequencies and magnitudes (Stoffel, 2010; Kaitna et al., 2013). Steep slopes and abundant sediment stores are the essential prerequisite for their formation, which is mostly triggered by rainfall (Dikau, 1996; Haeberli, 1996; Yu, 2011). Debris flows as further described in Chapters 4.3.1 and 6.1 show site-specific variations (Ingeomin, 2007) and occur frequently in the Venezuelan Andes (Laffaille, 2005), which are characterised by high sediment transfer rates and geomorphologic processes activity. Its central region in the Mérida Mountain Range (Fig. 6.1; Ch. 6.2) is investigated, i.e. the upper Chama river basin (1900 km^2).

Cold-climate mountain environments feature steep slopes, abundant sediment supply and vaste amounts of frozen water, essential prerequisites for debris flows. In a warming climate, rising temperatures, increased precipitation and accelerated melt lead to rising pore water pressure and reduced shear strength in mountain (ice) masses (Debella-Gilo, 2011; Band et al., 2012; Stoffel & Huggel, 2012). This creates more possible source areas for mass movement and thus increases the hazard potential in these regions (Salzmann et al., 2004; Kääb et al., 2005a; Gruber & Haeberli, 2007; Gruber et al., 2009; Otto & Schrott, 2010; Orwin et al., 2010; Debella-Gilo, 2011; Bimböse et al., 2011; Hölbling et al., 2012; Huggel et al., 2012; Stoffel & Huggel, 2012). Geohazards put humans and infrastructure at risk and can cause casualties and high costs by quickly remodelling the landscape, e.g. via debris flows, landslides, damming of rivers, lake outburst floods, snow and ice avalanches or rock falls (Kääb, 2003, 2005b; Salzmann et al., 2004; Kääb et al., 2005a; Noetzli et al., 2006; Debella-Gilo, 2011; Zemp, 2011; Stoffel & Huggel, 2012; Worni et

al., 2012; Hölbling et al., 2012; Huggel et al., 2012). It is therefore necessary to monitor geohazards such as the highly destructive debris flows (Davies & Korup, 2010; Yu, 2011) and the impact of global change.

1.3.4 Geomorphological target landforms

Alpine landforms are an expression of ongoing processes, i.e. sediment or mass movements, which constantly remodel cold climate environments. Alpine, periglacial and glacial regions display complex landform associations (Fig. 3.1): from earliest deglacion onwards, climatic and vegetative variations have influenced geomorphological process activity and hence landform evolution. Due to morphometric changes over time, some forms were ruled by different parameters in the past than they are nowadays, some have been overprinted by more recent processes (Dikau, 1996; Bartsch et al., 2002; Gude et al., 2002; Schrott et al., 2003; Bishop et al., 2012). Our incomplete knowledge about the geomorphological processes involved complicates the choice of the best parameters for analysis (Etzelmüller et al., 2001; Evans, 2011; Wilson, 2012; Tabs. 4.1, 4.2). The exact identification of geomorphological landforms therefore represents a challenge both in the field and in remote sensing data (Bartsch et al., 2002; Gude et al., 2002; Drăguţ & Blaschke, 2008; Berthling, 2011; Bishop et al., 2012; d'Oleire-Oltmanns et al., 2012; Wilson, 2012), but remote sensing can continuously monitor otherwise inaccessible terrain (Skorve, 2007; Kääb, 2010; Bishop et al., 2012). The detection of alpine landforms incorporates the third dimension to a great extent. Different landforms are often covered by the same kind of vegetation, sediment or ground and therefore cannot be differentiated by their spectral characteristics alone, but only with the help of a DEM and its derivatives (Bishop et al., 2012; Wilson, 2012; Tabs. 4.1, 4.2).

The first case study concentrates on the spatial extension of sediment stores, covering the scales of the Reintal catchment (c. 17 km^2) to the smallest landforms of a few metres extension, hence mesoscale according to Slay-

maker (1991). The "interaction between topography, lithology, and climate in mountain environments leads to the development of a particular landform assemblage" (Schrott et al., 2003: 58): the Reintal (Figs. 1.1, 1.2, 4.2, 5.1) forms an example of a now deglaciated valley, "one of the most prominent U-shaped valleys in the German Alps" (Schrott et al., 2003: 47; Fig. 1.2), whose present shape results from several Pleistocene glaciations. Therefore, the Holocene Reintal can be divided into three vertical zones (crest regions, rockwalls and valley bottom) which play an important role in the landform classification scheme (Chs. 4.3, 5.3). The oversteepened rock faces of the orographically right valley side sloping above 70° (Fig. 1.2) challenge remote sensing approaches.

Target landforms as defined in Chapters 3.2.1 and 4.3.1 originate from interacting, partly equifinal processes, and therefore often show fuzzy boundaries (Fig. 3.1; Schrott et al., 2003; Drăguţ & Blaschke, 2008; Berthling, 2011). Their morphometry also varies and overlaps, so that 'natural' and unequivocal devides between forms often cannot be found (Berthling, 2011), yet characteristic attributes have to be found for target class identifiction. Increased knowledge of target classes leads to more possibilities for feature analysis and differentiation in classification. As the identification of sediment–landform assemblages helps to ascertain the central processes responsible for landform and landscape development (Chiverrell et al., 2008; Berthling & Etzelmüller, 2011), more insights into sediment systems can be simultaneously gained.

1.3.5 Sediment cascade systems

Systems theory stands for the general study of systems, which aims at unifying principles inherent in all systems disregarding their scientific origins. The term, which still needs further definition, further generalises systems science. It was first coined by von Bertalanffy (1950, 1975) and further developed by Lazlo (1972a, b, 1996) and e.g. Luhmann (1984) within sociology. With its inter- and

transdisciplinary orientation, it bridges philosophy, computer sciences, physics, engineering, as well as geography, politics and sociology, amongst other disciplines. Systems theory seems very geographical by nature (cf. Ch. 2.4; Blotevogel, 1997; Castree, 2005), as it stimulates cross-disciplinary exchange. Yet even human and physical geographers do not have the same concepts and epistemologies, i.e. perceptions and theories of knowledge and its generation, of systems (Egner & von Elverfeldt, 2009). Interestingly, von Bertalanffy (1950, 1975) delineates systems inquiry within three central fields of study: philosophy, science and technology, the core of Paper I. Strahler (1950, 1952) already stresses the necessity of quantitative process monitoring in order to draw conclusions about landform evolution and adapts the concept of open systems by von Bertalanffy (1950) to geomorphology. The systems approach within process-orientated geomorphology is described in Chapter 3.2.2.

Cascade systems transfer material and energy from source to sink (Chorley & Kennedy, 1971; Burt & Allison, 2010). Akin to water cascades, sediment cascade systems picture the pathways of sediment and water from their generation in upland environments via transfer and intermediate storage to sediment sinks (Becht et al., 2005; Davies & Korup, 2010; Burt & Allison, 2010). Exact quantifications of sediment transfers and budgets at catchment scales in time and space and their transformation into efficient models represent today's main research challenges (Gude et al., 2002; Schrott et al., 2002, 2006; Burt & Allison, 2010; Trimble, 2010; Keiler et al., 2012). In order to understand natural sediment cascades, both sediment delivery systems and the thereby formed and interacting landscape components need to be investigated (Schrott et al., 2006; Burt & Allison, 2010). Through coupling and buffering process links within the system, the build-up and depletion of sediment stores can happen suddenly, sometimes even dramatically (Davies & Korup, 2010; Harvey, 2010; Keiler et al., 2012), as in the Reintal dambreak flood in 2005 (Bimböse et al., 2011). The detection and volumetric assessment of mobilisable sediment stores are also crucial for land management and hazard monitoring and prediction, e.g. regarding debris flows (Becht et al., 2005; Yu, 2011; Paper V).

The case study on geomorphological landforms (Papers II to IV) forms part of the project collection 'SEDiment cascades in Alpine Geosystems' (SEDAG). Until 2008, SEDAG aimed at developing a model describing landform development in high mountain regions. The present-day pattern of sediment storage types, geomorphological units and process activity were examined to decipher the functioning of the alpine sediment cascade (Schrott & Dikau, 1998; Schrott et al., 2002, 2003, 2006).

1.3.6 Remote sensing concept and foundation

Space- and airborne remote sensing lets us get unprecedented perspectives onto and insights into spatial patterns on Earth, and it has been successfully applied for the generation of knowledge for decades now (Casey, 2011). But what actually is remote sensing? Scientific work is thought to depart from a theoretical background. At the onset of modern scientific endeavour, theoretical considerations, philosophy of science and reflection on the nature of research were constitutional, fundamental and essential questions which scientists pondered over, possibly because the scope of sophisticated practical applications was still limited. Science was necessarily more theoretically based and oriented than in today's technical world. Nowadays, these questions have moved into the background, largely replaced by very concrete and applied scientific problem definitions, as, for instance, described by IPCC (2001, 2007). Scepticism towards theory and philosophy of science is common in the domains of applied sciences (Wolpert, 1992; Malanson, 1999; Pernu, 2008; von Elverfeldt & Glade, 2011; Ruse, 2012). The problems of the world are concrete and practical, approaches for their solution require further research, so why do we need abstract metaphysics?

"Whenever anyone mentions theory to a geomorphologist, he instinctively reaches for his soil auger" (Chorley, 1978: 1). According to Cox (2007), this quote is still valid; empirical research remains the order of the day. Nobel

prize laureate Richard Feynman stated that philosophy of science "is about as useful to scientists as ornithology is to birds" (Pernu, 2008: 30; Ruse, 2012: 47). Such words from a theoretical physicist may seem surprising. "It is a good thing that Feynman clarified this, since one could easily have been led into making the mistake of thinking that nothing could be more useful to birds than ornithology. After all, [...] the very existence of many bird species is dependent on our knowledge about their ecology, physiology, and genetics. In fact, [...] the only reason why it makes sense to say that ornithology is not useful to birds is that birds are not clever enough to understand it. Should Feynman be interpreted as implying that there is a similar relationship between philosophy and scientists? Hopefully not" (Pernu, 2008: 30f.).

To take a meta-level perspective of one's own subject can help finding the solutions we are looking for. In interdisciplinary research projects, which are at the scientific forefront today, it is particularly important to realise that our theoretical background determines our perception (Rhoads & Thorn, 1996; von Elverfeldt & Glade, 2011; von Elverfeldt, 2012). Regarding cold climate mountainous landscapes (which themselves need forther definition, cf. Berthling & Etzelmüller, 2011), a geographer sees different overlapping physical and human spheres shaping specific spatial patterns, a geomorphologist focuses on forms and formative processes, a glaciologist looks at ice and its behaviour, and a geodesist finds survey points to measure planimetric geometries. An economist may wonder how most economically to get rid of all the debris and rubble, build a scenic hotel and refinance the project within five years. What would a remote senser see? What is more, is there such a category as a 'remote senser' per se, or is remote sensing just a technique used by e.g. one of the specialists named above?

Practitioners of empirical science may not always be aware of this, but "there is no observation, no explanation, no research design without theory, and the respective results are strongly dependent on theoretical backgrounds" (von Elverfeldt & Glade, 2011: 88). It is therefore useful to know what our

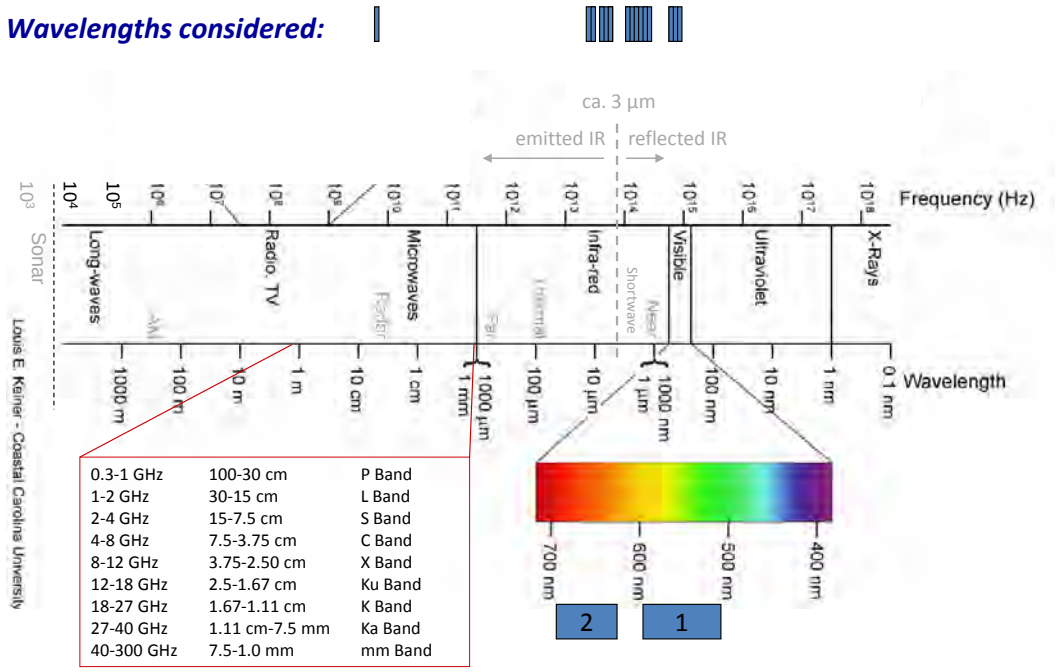

Figure 1.6: ASTER Spectral Bands in Comparison to C-Band

Multispectral optical and microwave satellite bands considered in this thesis. Their wavelengths and frequencies within the electromagnetic spectrum are indicated by the blue rectangles above and below the spectrum beam. The 14 rectangles to the right represent the 14 ASTER bands, the one to the left above the microwave range stands for radar C-band (modified from L.E. Keiner and A. Kääb).

theoretical background actually is. There is also "the knock-out argument that science is not scientific without a coherent foundation in theory and epistemology" (von Elverfeldt & Glade, 2011: 88). Hence it is worthwhile taking a dispassionate look at the nature or ontology of remote sensing in order to clarify the theoretical background of the applied research and case studies conducted in its name. Although the term 'remote sensing' has been used since the 1960s, the nature of the term still needs to be defined properly: is it a real science or a mere method which is being used? Self-image, professional ethos and practical organisational matters at geography departments and within working groups would benefit from a clarification. This is not only an academic question; on a very practical departmental level, it is relevant to know whether either a

method should be taught or a legitimate scientific discipline stimulated and supported (Wright et al., 1997). After all, budget allocations also depend on the importance assigned to a research field (Jones, 1988).

1.4 Remote sensing data sets

Because of frequent cloud cover and changeable weather and illumination conditions over cold climate mountainous landscapes, both optical and radar sensors are considered in this thesis. The image and elevation data analysed here stem preponderantly from spaceborne sensors.

1.4.1 Optical data

Optical images depict the ground in the visible and infrared portion of the electromagnetic spectrum (Fig. 1.6). Surfaces reflect and emit radiances which vary according to their specific properties, which allows for target class determination in image classification (Lillesand et al., 2008; Rees & Pellikka, 2010).

Optical images from the Advanced Spaceborne Thermal Emission and Reflection Radiometer (ASTER) onboard the Terra satellite (Figs. 1.5, 1.6) are used in this thesis. ASTER ground resolution varies between 15 m in the three visible and near-infrared (VNIR) bands, 30 m in the six short wave infrared (SWIR) bands and 90 m in the five thermal infrared (TIR) ones, as shown in Figures 1.6 and 4.4. ASTER scenes cover an area of 60 x 60 km (Fig. 1.5) and are further described in Chapter 4.3.2 as well as by Abrams & Hook (2002) and ERSDAC (2005). Their spectral resolution in SWIR and TIR is unique, yet since April 2008, the SWIR bands are no longer usable (Casey, 2011; ESA, 2012). An ASTER scene from 29 May 2001 (Fig. 4.2) proved most suitable for landform detection, and one from 1 February 2004 (Fig. 6.7) for debris flow assessment.

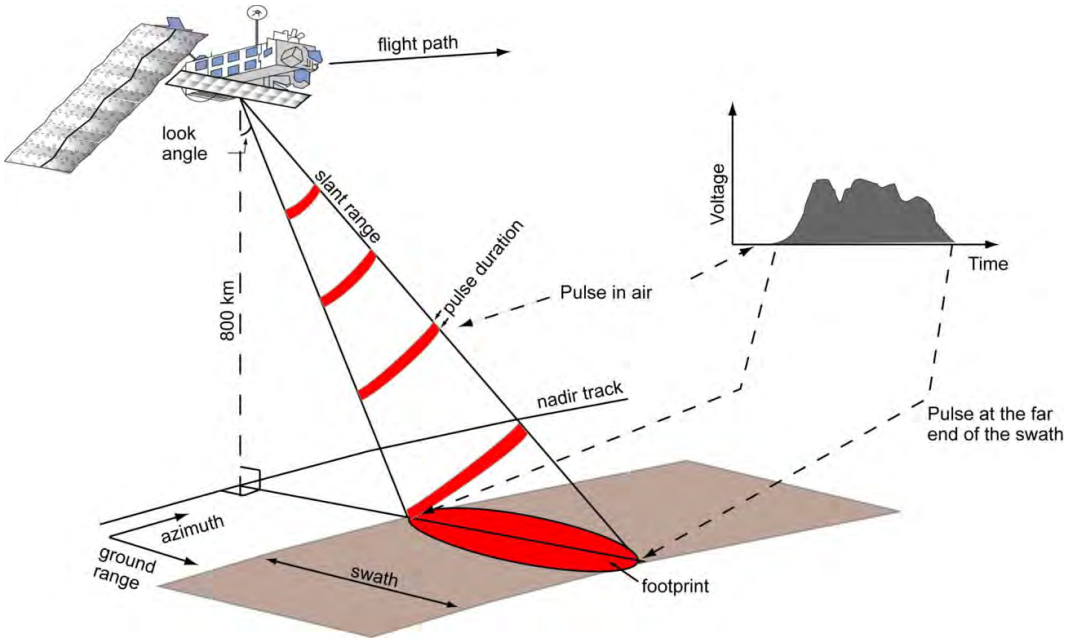

Figure 1.7: SAR Terminology and Viewing Geometry

Emission of a pulsed radar beam by an active antenna, its footprint on the ground and its backscattered return recorded at sensor over time. The satellite flies in azimuth direction and looks into range direction. The sideward viewing geometry helps disambiguating ground target echoes and leads to a distinct radar image geometry as shown in Figure 1.8 (from Langley, 2007).

Scenes by the Satellite Pour l'Observation de la Terre 3 (SPOT 3, French for 'Earth observation satellite 3') are also assessed. They have a panchromatic resolution of 10 m and a multispectral one of 20 m, respectively, and also cover 60 x 60 km.

1.4.2 Radar data

While cloudy or overcast skies and darkness hamper optical data, *radar data* is independent of cloud cover and daylight: an active antenna emits radar pulses in the microwave portion of the electromagnetic spectrum (Fig. 1.6), the returns of which are then recorded by the sensor. Yet its sideward viewing geometry (Fig. 1.7) results in distortions such as foreshortening, layover and radar shadow (Fig. 1.8) in synthetic aperture radar (SAR) imagery (Wey-

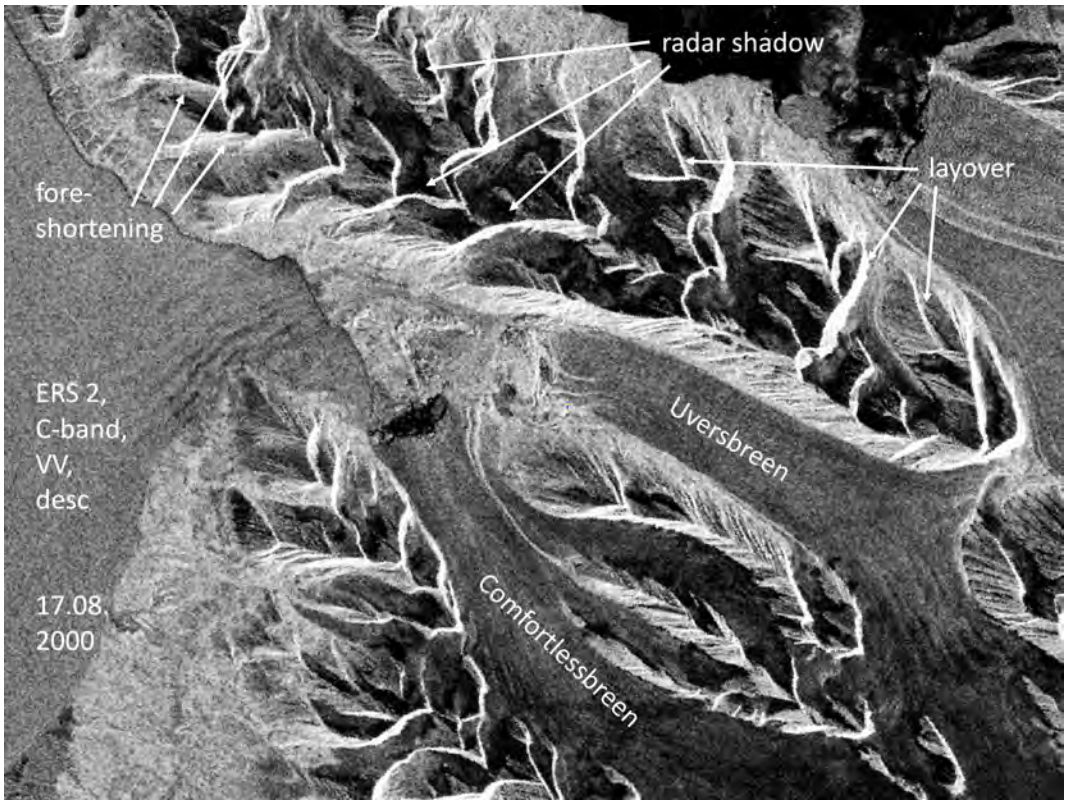

Figure 1.8: ERS SAR amplitude Image of north-west Svalbard
Radar scene with strong, bright backscatter returns and darker, weaker responses. Forshortening, layover and radar shadow are relief displacements in radar imagery due to the sideward radar viewing geometry, where *foreshortening* leads to compressed slopes in slant-range towards the sensor, *layover* to first returns of tops of tall features and *radar shadow* to missing returns where the radar beam cannot reach surfaces facing away from the sensor. SAR data provided by ESA.

dahl, 1998; Rott, 2009). The radar signal penetrates the ground to a certain extent; its amplitudinal backscatter depends on humidity, amongst other factors. Backscatter, polarisation and interferometric phase coherence provide information on e.g. surface humidity, roughness, facies, melting and changes (e.g. Kelly et al., 1997; Engeset & Weydahl, 1998; Weydahl, 1998; Braun, 2001; Rignot et al., 2001; Weydahl, 2001; König, 2004; Brown et al., 2005; Langley, 2007; Langley et al., 2008, 2009; Rees & Pellikka, 2009; Høgda et al., 2010; Müller, 2011; Gardelle et al., 2012; Kääb et al., 2012; Zwieback et al., 2012).

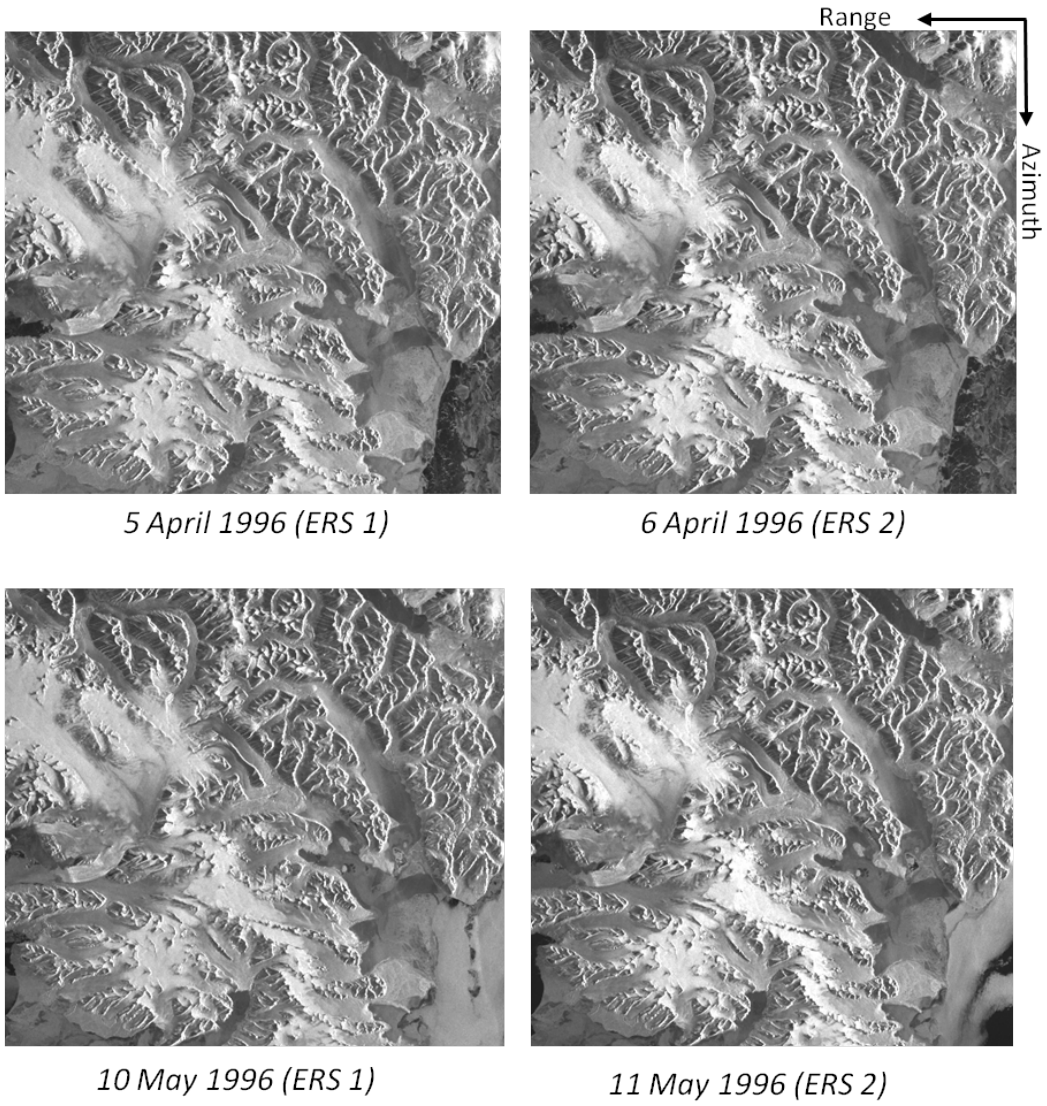

Figure 1.9: The two SAR Amplitude one-day Tandem Image Pairs
Azimuth and range arrows indicate the satellite flight path and radar viewing directions respectively. Offset estimation via image matching is used to co-register the image pairs. Image size ca. 100 x 100 km. SAR data provided by ESA.

A SAR scene contains a real-valued image consisting of radar pulse backscatter amplitude values from the ground (Figs. 1.7 to 1.9), as well as complex radar phase information. The phase differences or interferometric phases between two SAR images acquired over the same area using the same satellite orbit (Fig. 1.9) can be used for interferometry (Gens & van Genderen, 1996). The interferometric SAR technique is best utilized when high correlation or coherence is found between the image pairs. However, high coherence poses problems in high latitudes like Svalbard with its very changeable weather and precipitation conditions (Moholdt, 2010).

Because of their very short, one-day interval, the data from the 1996 repeat-pass tandem mission (from April 1995 to July 1996) of the European Remote Sensing satellites 1 and 2 (ERS-1/-2) are characterised by a remarkably high coherence potential, which substantiates their special scientific value to this day (Rott, 2009; Strozzi et al., 2010b; Sansosti et al., 2010). Four C-band ERS-1/-2 SAR scenes from April and May 1996 (Fig. 1.9, Tab. 7.1) were chosen amongst other things because of their good coherence according to Weydahl (1998, 2001). They cover an area of ca. 100 x 100 km (Fig. 1.9) and are further described in Weydahl (1998).

1.4.3 Elevation data

A digital elevation model (DEM) represents a tridimensional surface. Sometimes, albeit not in this introductory overview, a difference is made between digital surface models (DSMs), which also contain raised features, i.e. vegetation and buildings, and digital terrain models (DTMs) depicting solely the ground (Kääb, 2005b; Nuth, 2011).

The DEM used within the Reintal study has 5 m ground resolution and a vertical accuracy better than 0.5 m (further details in Chapter 4.3.2 and Schrott et al., 2003). Five DEM derivatives (geomorphometric grids of horizontal, vertical and total curvature, slope and aspect) are derived from it.

A SPOT 5 HRS (High Resolution Stereoscopic) SPIRIT (SPOT 5 stereoscopic survey of Polar Ice: Reference Images and Topographies) DEM from 2007, thoroughly described by Korona et al. (2009), with 40 m resolution and 5 m height accuracy is employed in the Svalbard study, while a DEM from 1990 (20 m resolution, 1 m height accuracy) compiled by the Norwegian Polar Institute is additionally assessed.

A Shuttle Radar Topography Mission (SRTM) DEM (90 m resolution, 10-16 m height accuracy) from an InSAR campaign in February 2000, collected in C-band (Kääb, 2005b; Farr et al., 2007; Paul & Hendriks, 2010b; Nuth & Kääb, 2011; Bishop et al., 2012; Frey & Paul, 2012, for more information), was used in the Venezuela study.

1.5 Image classification

Image classification is used to (semi-)automatically assign the pixels in an image to specific classes or themes; this can be done pixel by pixel or in a segment-based approach as described in Ch. 1.5.1. While unsupervised methods cluster classes automatically, supervised approaches require expert knowledge and ground truth for reference. Hard classifiers assign one pixel exactly to one class, whereas soft or fuzzy classifiers rely on class-specific likelihoods for each pixel (Jensen, 2005; Kääb, 2005b; Waske, 2007; Lillesand et al, 2008 for more information).

1.5.1 Segment-based landform classification

In order to establish meaningful form-process connections in accordance with the sediment cascade (Ch. 1.3.5; Fig. 3.2), neighbourhoods as well as sub- and superordinations should also be taken into account by the Reintal landform classification scheme. Image segmentation, an approach which dates back to the 1970s, allows for this. A considerable number of algorithms have been

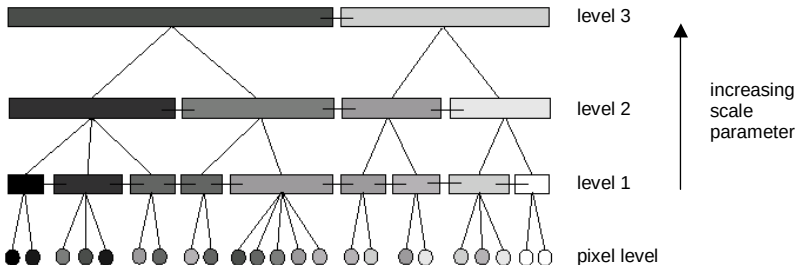

Figure 1.10: Hierachical Multiresolution Segmentation Levels
Features are increasingly averaged and homogenised in the higher segmentation levels (modified from Baatz et al., 2002)

developed since, by Haralik (1973), Baatz & Schäpe (2000), Evans (2002) and Tarabalka et al. (2012) amongst others. Yet those algorithms only became operational with enhanced computing capacities (Baatz & Schäpe, 2000; Richards, 2005; Waske & van der Linden, 2008; Minár & Evans, 2008; Blaschke, 2010). Segmentations are increasingly used as input for modelling and complex image analysis (Hay & Castilla, 2008; Drăguţ & Blaschke, 2008; Drăguţ & Eisank, 2011).

Segmentation algorithms assume that adjacent pixels showing certain similarities belong to one group, so that an entire scene is segmented into image objects (Figs. 1.10, 4.5). Not only are the spectral characteristics of each pixel considered individually; relationships, neighbourhoods and similarities are also taken into account (Blaschke et al., 2002, 2008). Each image object can be described by a multitude of features, such as mean value, standard deviation and ratio of the incorporated pixels next to geometric features (Baatz & Schäpe, 2000; Blaschke et al., 2008; Addink et al., 2012; Chs. 3.3.2, 5.3.2).

This approach is also called Object-based Image Analysis (OBIA) (Blaschke et al., 2008) or more specificly Geographic or Geospatial Object-Based Image Analysis (GEOBIA) (Hay & Castilla, 2008; Blaschke, 2010; Addink et al., 2012). Yet the terms are often used synonymously (Blaschke, 2010). The adjective *object-oriented* also refers to a computer programming concept. *Object-based* can lead one to assume that the algorithm truly describes existing ob-

jects, while image objects are purely based on statistics, not nature. The user tries to match the statistical image objects to the desired target classes. As *segment-based* appears most neutral, it is used in this introductory summary.

Segment-based class descriptions thus go far beyond spectral information alone if the segmentation process is able to produce objects which describe natural features geometrically well. DEM and other additional information can be integrated and analysed for each object individually. This asset outweighs the fact that segmentation prior to classification introduces an additional, time-consuming step: segment-based image analysis unites the spectral interpretation capacities of remote sensing and the geometric tools of geographical information systems (GIS) in one desktop environment. In this respect, segment-based analysis is superior to pixel-oriented approaches, especially when dealing with high mountain data (Blaschke, 2000; Blaschke & Hay, 2001; Blaschke et al., 2002; Hay & Castilla, 2008; Drăguţ et al., 2011; Drăguţ & Eisank, 2011; Addink et al., 2012; Romstad & Etzelmüller, 2012).

In the Reintal study, alpine landforms are assessed with a segment-based, hierarchical approach based on initial image segmentation and subsequent classification (Figs. 3.3, 4.1), which is extensively described in Chapter 5.3. Optical ASTER imagery and various ratios, e.g. the Normalised Difference Vegetation Index (NDVI; cf. Mao et al., 2011; Fensholt & Proud, 2012 for more information), are analysed in combination with the Reintal DEM. Geomorphological maps of the Reintal valley (Schrott et al., 2003; Fig. 4.3) and photos of the study area serve as ground truth and reference. The segmentation scales for generating adequately sized image objects have to be determined and the corresponding number of hierarchical working levels created (Fig. 1.10). The levels are classified individually in a second but separate step, where the most suitable classifier can be chosen for each segmentation level. Only on the finest level L1, which focusses on spectral land cover characteristics alone, is a nearest neighbour classifier used; all other levels are based on an iteratively generated fuzzy membership function hierarchy (Fig. 5.2).

1.5.2 Accuracy assessment

Statistical accuracy assessments are used to judge the quality of the classification (cf. Ch. 5.4). In an error matrix, also called contingency or confusion table, classification results are compared to ground truth (Richards & Jia, 2006; Lillesand et al., 2008). In the Reintal, test areas are selected manually and without regular spatial pattern, the most appropriate image objects or clusters being chosen according to field evidence.

By dividing of the correctly classified pixels of one class (from the major diagonal in Tab. 5.2) by the total of test area pixels (the pixel sum of that same column), producer´s accuracy is calculated. In contrast, the division of the correctly classified pixels by the row total of the respective class gives the user´s accuracy. As a measure of omission (i.e. exclusion; given by the matrix columns) error, the producer's accuracy expresses how exactly the test area pixels of this class are assigned. In contrast, the division of the correctly classified pixels by the row total of the respective class gives the user´s accuracy. By analogy to commission (i.e. inclusion; represented by the rows of the matrix) error, it indicates the probability of a user finding the L2 classification result in situ (Congalton & Green, 1999; de Lange, 2006).

For overall accuracy, the sum of correctly classified pixels is divided by the total number of pixels (Jensen, 2005, Congalton & Green, 1999). The kappa coefficient κ determines the difference between the result of the given classification and a randomly produced one (Cohen, 1960; Lillesand et al., 2008). Fuzzy classification stability and best membership assignments of the hierarchical classification scheme are also assessed.

1.6 Displacement measurements and modelling

Displacement can be measured, analysed and modelled by means of a large variety of methods and techniques. As in-situ measurements are spatially and temporally limited by feasibility and expense, remote sensing approaches are welcome alternatives (Joughin et al., 2010a; Debella-Gilo & Kääb, 2012), an overview of which is given in Kääb (2005b). Amongst other things, movement can be derived from optical or radar data via image matching, and from radar data by means of speckle, coherence or offset tracking and interferometry (cf. Kääb, 2005b; Høgda et al., 2010; Joughin et al., 2010a; Debella-Gilo, 2011; Heid, 2011).

Image matching compares overlapping repeat images from the same area in order to find similarities between them, aiming at e.g. geometric image registration, image fusion or change tracking (Brown, 1992; Zitová & Flusser, 2003; Debella-Gilo, 2011). This can be done via feature-based or area-based matching, by looking for prominent features or by comparing grey value intensities of image subsets or templates. Area-based similarity measures include normalized cross-correlation and least squares matching (Brown, 1992; Zitová & Flusser, 2003; Kääb, 2005b; Debella-Gilo, 2011).

Tracking in SAR data is yet another form of image matching. Speckle tracking exploits the correlated noise or speckle, a salt-and-pepper effect due to the many scatterers within one image pixel, in coherent real-valued SAR amplitude images. Coherence tracking relies on the complex phase information, and also requires high correlation between the images. In contrast, offset or feature tracking estimates the offset between image pairs from prominent visible features (e.g. glacier crevasses) in the respective amplitudes alone and is therefore independent of coherence. Temporal decorrelation, the shortcoming of all coherence-based SAR applications, hence becomes therefore much less of a problem. Yet the measurement precision is lower in offset tracking and lies within the range of meters (cf. Weydahl, 1998; Høgda et al., 2010).

1.6.1 Differential interferometry

SAR interferometry (InSAR) is a technique for analysing both topography and movement information inherent in SAR data, for which a high correlation or coherence between the the tandem SAR image pairs is needed. It is the most accurate means of measuring movement in slant-range direction as it detects changes on a scale of milli- and centimetres from space (Gabriel et al., 1989; Goldstein et al., 1993; Weydahl, 2001; Strozzi et al., 2002, Høgda et al., 2010). Offset estimation via image matching is used to co-register the image pairs with sub-pixel precision (Fig. 1.9). Interferogram generation includes "flat Earth" correction and unwrapping (Fig. 1.11; Kwok & Fahnestock, 1996; Rott, 2009). Phase unwrapping means transforming the interferometric phase, which is initially wrapped around 2π and thus repeatedly reset to 0, into continuous values which constantly augment from one single initial 0-value Fig. 1.11). This is a crucial and difficult undertaking, all the more in rugged terrain (Gens & van Genderen 1996; Wegmüller & Werner 1997; Strozzi et al., 2004, 2010a; Moholdt 2010).

Differential SAR interferometry (DInSAR) is a means of separating displacement from topographic information by subtracting one interferometric phase from the other one. Hence pure displacement can be obtained without residual height information in it or vice versa - topographical information can be freed from any displacement on the ground. However, when aiming at glacier velocities as e.g. in the Svalbard case study, only the component of movement in line-of-sight direction with the satellite sensor, i.e. in range direction, is depicted in a differential interferogram (Cumming et al., 1989; Kwok & Fahnestock, 1996; Rott, 2009; Joughin et al., 2010a).

There are several ways of doing DInSAR; 2-pass DInSAR with two tandem SAR scenes and a DEM as first described by Cumming et al. (1989), or by combining three (3-pass DInSAR), four (4-pass DInSAR) or more satellite scenes from the same orbit. The basic principle behind those different

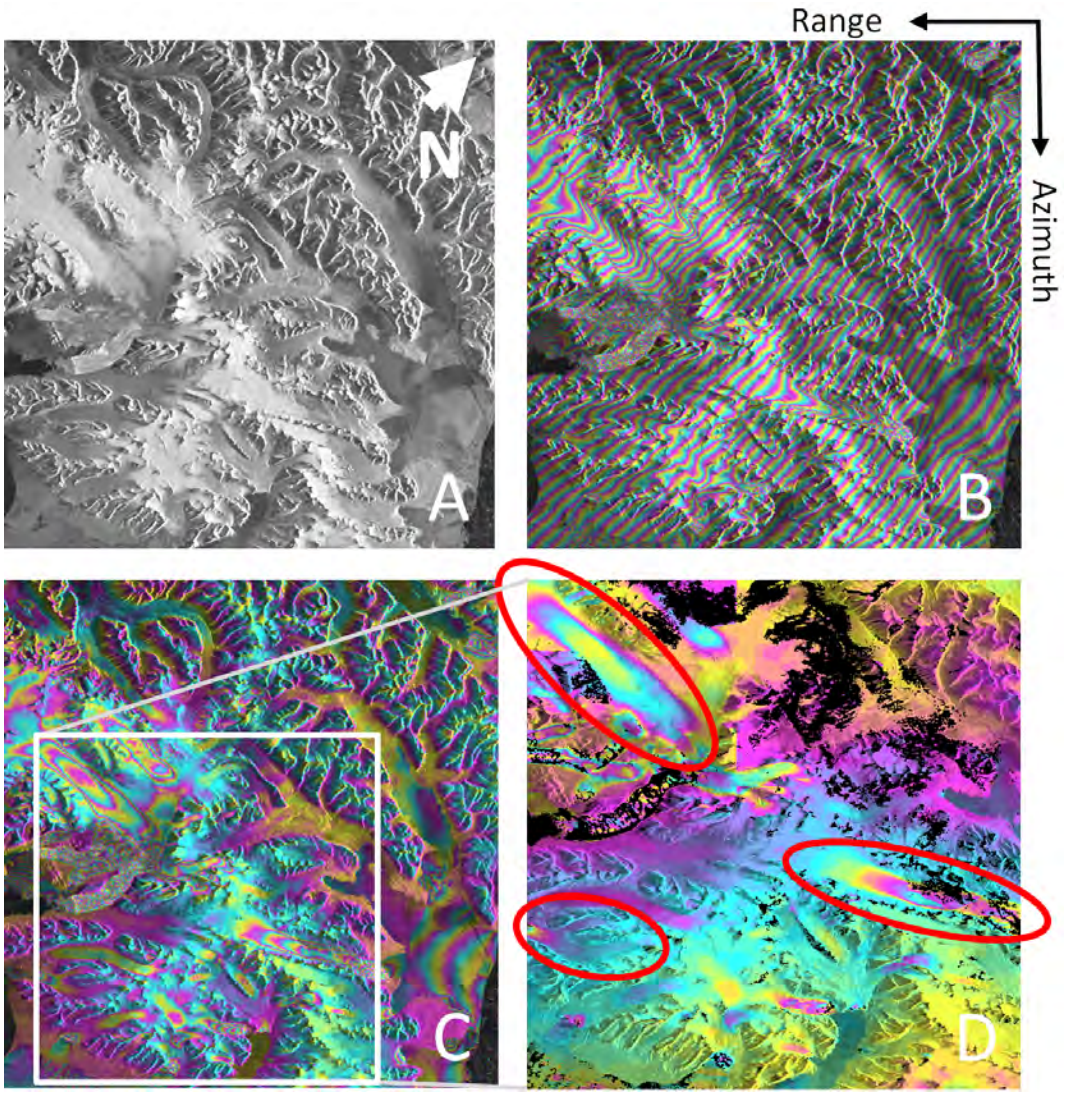

Figure 1.11: SAR Interferogram Generation and Correction

A: SAR amplitude image of 5 April 1996. B: Interferogram of 5-6 April 1996, amplitude image as background. Fringe structures from "flat Earth", topography and movement. C: Interferogram of 5-6 April 1996, "flat Earth" corrected. Remaining fringes from topography and movements. D: Unwrapped interferogram where the fringes represent continuous values (793 m per colour cycle) instead of modulo 2 π. Marked areas indicate fringe deformation due to glacier movement.

approaches is that two interferograms are first generated and then subtracted from one another (Joughin et al., 1996; Kwok & Fahnestock, 1996; Eldhuset et al., 2003; Joughin et al., 2010a).

2-pass DInSAR is applied in this study, which means that in addition to one conventional interferogram generated from the two SAR scenes of two satellite passes on the same orbit, a reference interferogram with phases corresponding to surface topography is simulated from a DEM which has to be transferred into radar geometry. Differential interferograms then result from subtracting the simulated from the conventional interferogram. Glacier velocities are obtained from the interferometric fringe structures. The exact workflow, including preprocessing, intermediate image products, unwrapping and generation of displacement maps, are thoroughly detailed in Chapter 7.4. It deliberately offers the InSAR beginner many illustrations of the different processing steps in order to facilitate the use of this technique. Focus has been placed on didactics and understandability when presenting the workflow.

1.6.2 Digital terrain modelling

Digital terrain modelling comprises the methods and techniques for visualising and analysing topography, often in the form of DEMs (Pike, 1995, 2000; Wilson, 2012; Romstad & Etzelmüller, 2012). Quantitative topographic data assessment is also referred to as geomorphometry, which combines morphometric and geomorphological enquiries (Pike, 1995, 2000; Li et al. 2005; Zhou et al., 2008; Hengl & Evans, 2009; Hengl & Reuter, 2009; Wilson, 2012). For the most part, continuous land surfaces are numerically analysed, yet also discrete features such as landforms (cf. Chs. 1.3.4, 4.3.1) and watersheds (cf. Chs. 1.3.3, 6.2) can be in the focus of interest (Hengl & Evans, 2009).

Modelling procedures involve surface sampling, DEM generation/correction, and deriving and applying primary and secondary land surface parameters (Hengl & Evans, 2009, Wilson, 2012) This is further detailed in e.g. Salzmann

et al. (2004), Noetzli et al. (2006), Band (2012), Bishop (2012), Evans (2012) and Mitášová et al. (2012) with respect to different terrain modelling and landform classification approaches (Wilson, 2012). Parameter values are usually initially obtained from in-situ observations or scientific literature (Lavigne & Thouret, 2002; Salzmann et al., 2004; Worni et al., 2012). Topographic attributes are then mostly calculated by pixel from the gridded DEM, where the challenge lies in the meaningful assignment of landform patterns and systems, as context is hardly considered (Romstad & Etzelmüller, 2012).

After SRTM DEM correction, morphometric and geomorphological parameters are derived from the DEM of the Chama river watershed in the Venezuelan Andes. Amongst other things, they are used to determine potential debris flow source areas by means of the Distributed Melton's Ruggedness Number (DMRN), a dimensionless index of basin ruggedness (Jackson et al., 1987; Marchi & Fontana, 2005; Rowbotham et al., 2005) explained in Chapter 6.3.2.

Suitability for the research goal determines the choice between simple parameterisation models such as the one used in the Venezuela study and more complex models based on physical processes (Gruber et al., 2009). The Modified Single Flow Model (MSFM) is used to model debris flows along the Chama River and its tributaries as a function of topography and sediment dynamics. The MSFM uses the single-flow direction algorithm introduced by O'Callaghan and Mark (1984) and developed by Huggel et al. (2003, 2004) to model flow propagation at regional scales in mountainous environments (Huggel et al., 2008; Gruber et al., 2009). Based on a qualitative probability function (Huggel et al., 2003, 2008), it calculates flow trajectories and runout areas as further described by Gruber et al. (2009) and in Chapter 6.3.3. Modelling the flow and runout of debris flows is similar to detecting snow or debris avalanches or lahars (Huggel et al., 2003, 2004, 2008; Salzmann et al., 2004; Rickenmann & Scheidl, 2013).

1.7 Results and discussion

1.7.1 Science and remote sensing

In search of a definition of 'science' (Paper I), literature relating to various scientific concepts is here reviewed. Empirical induction, positivism and logical empirism are considered first, followed by empirical falsification and critical rationalism (Popper, 1989, 1998). The picture is rounded off by sociological and postmodernist views on science (Kuhn, 1996; Lakatos, 1970; Feyerabend, 1998; Zieman, 1968; Knorr, 1979). These considerations show that science is not easy to grasp and its definition depends on whom one reads and quotes. Yet science may not be as noble and rigorous as often claimed (Chs. 2.2, 2.4, 2.5). Subsequently, remote sensing is subsumed under these different ontological concepts in order to find out whether it belongs more to the realm of science or of technology. This is partly based on a debate between Curran (1987a, b) and Fussell et al. (1986, 1987). The reasoning suggests that remote sensing can be understood as developing from a method to an applied science.

When differentiating between science and methods or technology (or scientific methods), borderlines and overlaps abound, not only regarding remote sensing but also computer sciences and GIS. Wilson (2012: 107) writes about "the science of digital terrain modeling", and Pike et al. (2009: 29) define geomorphometry as "the science of quantitative land-surface analysis. A mix of Earth and computer science, engineering, and mathematics, it is a new field paralleling analytical cartography and GIS". Is the term 'science' used correctly or just uncritically in these examples? This leads to the question of how most natural sciences nowadays can be distinguished from the technologies they use. Even if this distinction is still possible today, no modern applied natural science will be likely to function and to define itself without regress to technology in the future. Hence the entire differentiation between science and methodology may prove to be an artificial, outdated distinction between the flip sides of one coin (Chs. 2.3, 2.4, 2.5).

Science and technology are moving closer together. In a high-tech scientific world, methodology and its scientific application can no longer be clearly distinguished from one another. Modern ontologies of both science and remote sensing remain ambiguous and complex; they depend largely on the quoted source (Paper I). In general, categorisations and demarcations appear less clear-cut today than in the past. Remote sensing started out as a method, but is turning into an applied science with many technological qualities. Yesterday´s reassuring simplicity seems to be gone for good: it is becoming increasingly difficult to make a clear distinction between science, non-science and technology . The elusiveness of terminology, definition and categorisation constitutes a feature of modern science or possibly of modern society in general.

The prevailing disdain for philosophy of science within applied sciences leads to a lack of exchange between these disciplines, although philosophy of science and ethics belong to the mandatory curriculum at many universities. This can be traced down to the current scientific practise where peer-review and impact factors "encourage both scientists and philosophers to stay within the boundaries of well-defined questions, concepts, and paradigms. [B]reaching these boundaries, one risks the chance of slipping in between fields and finding oneself doing work that no one finds relevant. It is better to play it safe and stick to one's last" (Pernu, 2008: 32). However, just as remote sensing looks at things from a distance and gives us get precedented perspectives on and insights into spatial patterns on Earth, a philosophical "gazing at things from a distance and getting a view of the big picture can provide us with understanding about science, just as ornithology provides understanding about birds, even though the objects themselves are oblivious to it" (Pernu, 2008: 31). More exchange between disciplines, including those which are not directly related and therefore speak different scientific languages, could be beneficial for all involved. Natural scientists for instance still claim to be practising positivist and empirical science, and assume that philosophers of science are doing the same. However, the concept of positivism started to become historic

within philosophy even in the 1950s (Pernu, 2008). "So if positivism continues to do harm, it is because scientists continue to cling to it. Philosophers let it go decades ago" (Pernu, 2008: 31). Maybe it is time to drop soil augurs and to start dialoguing. There needs to be more room for theoretical debate in geosciences (Malanson, 1999; Cox, 2007; Egner & von Elverfeldt, 2009; von Elverfeldt & Glade 2011; von Elverfeldt, 2012).

1.7.2 Systems theory and segmentation

Geomorphic systems theory is related to segment-based remote sensing and relationships established between them (Chs. 3.2.2, 3.2.3). Surprisingly many parallels can be found between the completely distinct approaches from two entirely different fields of research: systems theory facilitates the delimitation of individual system components by allowing the user to zoom into systemic details while placing all components into subsystems and superordinate systems, thus restoring the entirety of landscape and, for example, leading to the conceptional Alpine sediment cascade (Fig. 3.2).

This corresponds to the way how image segmentation works, which combines the spectral analyses of remote sensing and the geometric tools of GIS: a simultaneous depiction of several image levels segmented at different scales by multiresolution segmentation (Figs. 1.10, 3.3) leads to relationships, sub- and superordinations, morphometric and class-related features which can be used for class descriptions (Papers III, IV). Through spectral generalisation, results appear more homogeneous, thus smoothing out irregular pixel-dominated patterns and creating more realistic forms (Baatz & Schäpe, 2000; van der Linden et al., 2007).

The theoretical and applied sides of geomorphic systems theory and segment-based remote sensing have a lot in common: they have regained acceptance as high-performance computing has finally allowed large datasets to be processed. They meet the demand for hierarchical and scale-dependent analyses

made both in remote sensing and in geomorphology, thus helping to overcome scale problems in space. Multiscalar, segment-based approaches take the hierarchical organisation of alpine topography into account. As meaningful form-process connections in accordance with the the sediment cascade (Fig. 3.2) were to be established, neighbourhoods as well as sub- and superordinations had to be accessible in the classification scheme. A hierarchical, segment-based detection method is thus most appropriate for addressing alpine landforms, as also shown by van Niekerk (2010), Drăguţ & Eisank (2011), Romstad & Etzelmüller (2012).

When developing the classification hierarchy, the iterative insertion of information by fuzzy descriptions can be likened to fractal net evolution: on multiple levels of abstraction, a process akin to human visual perception occurs (Blaschke & Hay, 2001; Blaschke et al., 2002; Addink et al., 2012). Multiscalar levels focussing on different-sized landforms imitate the geomorphic systems approach, allowing for detailed and general views at the same time (Paper II). It is of interest here that some authors (e.g. Hay & Castilla, 2008) are now beginning to liken the advent of the segment-based approach to a paradigm shift, a scientific revolution (or rather evolution) in the Kuhnian sense (Kuhn, 1996). Meanwhile, geomorphology has also matured, progressively evolving from quantitative and systems considerations to a unification phase indicative of a 'modern science', where complex conceptual and multidisciplinary questions are brought into focus (Bauer, 2004; Smith & Pain, 2009). Technology in the form of remote sensing and GIS plays a decisive role in this development (Smith & Pain, 2009).

To further the dialogue on systems theory, Egner & von Elverfeldt (2009) explain and bridge the differences between the concepts of systems in physical versus human geography, where a second-order sociological systems approach based on Luhmann (1984) is used. The concept of open geomorphic systems implies ambiguous system confines and logical fallacies regarding equilibrium and cause-and-effect relationships (von Elverfeldt & Glade, 2011). Introducing

self-reference, autopoiesis and operative closeness of systems, a paradigm shift within the theoretical foundations of geomorphology is proposed (Egner & von Elverfeldt 2009; von Elverfeldt & Glade, 2011). Finally, von Elverfeldt (2012) develops a stringent geomorphological system theory, which facilitates exchange with neighbouring disciplines.

The argumentation convinces, but a footnote is puzzling. "Within the framework of general systems theory, we observe the world in terms of systems. It has to be emphasized, however, that it is only a way to look at the respective objects of interest: Systems do not exist. Therefore, whenever a phrase similar to 'the system is (open/isolated/...)' is used in this paper it does not connote any ontological statement" (von Elverfeldt & Glade, 2011: 88). At the same time, the paper attempts to answer the question 'What is a system?' (von Elverfeldt & Glade, 2011: 91), which looks like an ontological question by its very nature. Does everything invisible and intangible not exist? That seems to put the discussion back to before Popper; then all abstractions, conceptualisations and models would not exist, maybe not even philosophy of science and theoretical discourse as such. The existence of the quoted papers could literally prove otherwise, and another issue is put up for discussion: when do conceptual models start to exist?

1.7.3 Alpine landform detection

A literature survey has resulted in an extensive overview of alpine landform features and characteristics as displayed in Tables 4.1 and 4.2. These tables distinguish between fourteen landforms and twelve landform characteristics. These characteristics can be divided into four greater categories: visible material, particle size and superficial sorting describe the *sediment surface*, while slope, horizontal and vertical curvature constitute *form parameters*. In contrast, *spatial distribution* comprises the spatial extent, location in the valley and the process link of the different landforms. The categories activity status,

vegetation cover, dominant process and processual link specify the *processes* involved. These tables form the foundation of the classification of geomorphological landforms. The proposed landform subdivisions take the concept of fuzzy boundaries into account, but are necessarily arbitrary to a certain degree. More work on landform and landscape definitions is required when assessing today's wealth of remote sensing data (Berthling, 2011; Berthling & Etzelmüller; Evans, 2012).

In the multiscale project, the segmentations with different scale parameters (Fig. 3.4) make it possible to focus on different features on each of the four levels: the first level L1 based on pure spectral ASTER information defines all boundaries of the project at a very high resolution, resulting in a classic remotely sensed land cover map (Fig. 4.6). The coarsest Level L4 displays the altitudinal strata mask generated in a separate project, while L3 focuses on eastern and western walls of cirques and hanging valleys in the upper valley portions (Fig. 3.4). L2 is designed for merging the information of all four levels. In the final landform classification on level L2 (Figs. 3.4, 5.3), the majority of classes such as cirques, rockwalls, floodplains and sediments are accurately assigned. Detection limits are reached with moraine and rockfall deposits which have been overprinted by more recent processes for centuries or millennia (Schrott et al., 2003). Some target classes (Tab. 3.1) are more precisely differentiated than previously expected (Tab. 4.3), e.g. vegetation-covered slopes and talus cover, leading to 20 final thematic landform classes. The resulting thematic map shows the present-day pattern of geomorphological process units in the entire valley up to its less accessible upper regions (Figs. 3.4, 4.6, 5.3), whilst previously only the valley floor could be mapped in situ. Many other segment-based landform classification do not produce coherent maps, but just aim at certain landforms of interest, e.g. Eisank et al. (2010, 2011), Ferentinou et al. (2011), d'Oleire-Oltmanns et al. (2012) and Hölbling et al. (2012). Van Niekerk (2010) stresses the particular sensitivity of the multi-resolution segmentation algorithm to morphological discontinuities, which makes it most appropriate for detecting land units from DEM.

From these results, it becomes evident that the geomorphic (in-)activity of an area is spectrally better defined than the actual type of landform present. The classification of geomorphological activity or possibly geomorphic process units (i.e. areas with homogeneous process types and rates; cf. Gude et al., 2002; Bartsch et al., 2002, 2009) seems therefore easier than assessing landforms, as one form is often made up of areas with changing activity and cover. Through the NDVI, the degree of vegetative cover can be determined quickly (cf. Mao et al., 2011; Fensholt & Proud, 2012), and hence also process activity. However, soil-adjusted vegetation indices (SAVIs) should be tested against the performance of the NDVI (Huete et al., 1985; Baret & Guyot, 1991; García-Haro et al., 1996; Gilabert et al., 2002; Ch. 4.5.2). Yet SAVIs require soil-line or brightness information, which may hamper transferability. Machine learning approaches (cf. Ch. 1.7.4) could render the intermediate step via spectral indices obsolete.

While the sediment cascade of the Reintal forms a closed system characterised by sediment input and a high inactivity rate in the studied data sets (Ch. 3.2.3), some changes have taken place on the valley floor since. After a high magnitude dambreak flood on Vordere Gumpe floodplain (Figs. 1.2, 4.3) in 2005, the (re-)coupling and activity of sediment stores has increased considerably in this area, as quantified by Terrestrial Laser Scanning (TLS) amongst other things (Morche et al., 2007, 2008; Bimböse et al., 2010, 2011). The system has switched to a state of disequilibrium and an imbalance in favour of sediment output: sediment stores continue to be depleted, yet quantitative fluxes are declining with time as is customary after extreme events (Morche et al., 2008; Bimböse et al., 2011). TSL makes it possible to compare intra- and interannual sediment dynamics from the slopes to the catchment exit, and to conclude that the sediment budget is now negative, but the role of fluvial transit and stores requires further study (Morche et al., 2008; Bimböse et al., 2011). It is uncertain whether the changes on the valley floor due to that dambreak flood could be detected in ASTER data; maybe by means of novel segment-based, sub-pixel mapping models to solve the mixed pixel prob-

lem and increase classification results through post-processing (Li et al., 2011; Ling et al., 2012). Yet new and high-resolution remote sensing images and DEMs allow for more scrutinous and sophisticated extractions of form features today (Smith & Pain, 2009; Ch. 1.7.8). Hillslope-glacier coupling and glacial erosion (Scherler et al., 2011) as well as supraglacial debris flux patterns (Casey et al., 2012) have been successfully studied by remote sensing, which can benefit sediment cascade research. Quantifications of sediment fluxes and stores over different time scales are needed (Schrott et al.,2002, 2006; Otto & Schrott, 2010). Due to close connexions and interlinkages at various scales, the influence of individual systemic parts is still hard to assess (Smith & Pain, 2009; Slaymaker, 2010; Keiler et al., 2012).

It remains to be investigated to which extend a purely pixel-based classification scheme may handle this data. To further evaluate the results, the exact influences of image and DEM data respectively should be assessed by analysing them individually. Recent studies have analysed DEM segmentation and its potentials for landform discrimination (Drăguţ & Blaschke, 2006; Drăguţ et al., 2010, 2011; Drăguţ & Eisank, 2011; Drăguţ & Eisank, 2012; Matsuura & Aniya, 2012; Romstad & Etzelmüller, 2012). A purely spectral SVM classification has been used by van der Linden et al. (2007) to compare spectral properties and generalisations to pixel-based results, where both approaches reached comparable accuracies, yet the segment-based results were more homogeneous.

1.7.4 Classification accuracy and transferability

A kappa coefficient of 0.915 confirms the good match of the L2 classification results to ground truth. Overall accuracy amounts to 92 % for L2, while producer's and user's accuracies also generally score high. Bartsch et al. (2002) obtain accuracies between 85 % and 93 % in their identification of geomorphic process units. Saadat et al. (2008) reach even higher accuracies in their

intricate landform classification approach based on polygons and segmentation. Fuzzy classification stability comes out a little lower in the Reintal, but best membership assignments generally turn out high (see Ch. 5.4 and Fig. 5.4 for details). Drăguţ & Blaschke (2008) also find fuzzy stability to score lower than other methods for assessing DEM-based classifications.

The simple overall accuracy ignores wrongly classified pixels (i.e. errors of commission and omission), but allows for chance agreements, which is why high accuracies in the single classes and the kappa coefficient have more analytical significance (Cohen, 1960; Kellenberger, 1996). Kappa statistics also allow comparisons between matrices of different data sets, which makes them the most objective accuracy measure (Kellenberger, 1996; Lillesand et al., 2008). Yet Pontius Jr. & Millones (2011) draw attention to repeated past criticism of kappa indices and conclude that they are of no use for practical remote sensing, declaring death to kappa and birth to quantity disagreement and allocation disagreement, which should be assessed for the Reintal.

The accuracy values given are based on manually chosen image objects, not individual pixels. While manual selection ensures the quality and correctness of the assessments, it makes them also more subjective, less random and less easily transferrable to other regions. The accuracy assessment could be optimised by choosing test areas according to a random or regular spatial pattern, and by using individual pixels instead of image objects. While van der Linden et al. (2007) note slightly lower accuracies with segmented data, especially with increasing segment size, Waske (2007) and Waske et al. (2008) found that both image segmentation and multilevel information lead to significantly increased classification accuracies. Therefore a pixel-based accuracy assessment may just lower the accuracies per se, without giving further evidence on the quality of the values given in Table 5.2 (cf. Pontius Jr. & Millones, 2011). It may not be usefully applicable to segment-based classifications at all, as segment-based spatial generalisations risk to be evaluated as errors (Castilla et al., 2012; Marinho et al., 2012). For comparison, the accuracy assessments

of contextual, segment-based classification results as proposed by Castilla et al. (2012), Marinho et al. (2012) and Thoonen et al. (2012) should be evaluated.

The applicability of the Reintal study to other regions remains to be investigated. Blaschke et al. (2002), Drăguţ & Blaschke (2006) and Drăguţ & Eisank (2011) argue that segment-based classification leads to better transferability, as variations in reflectances and atmospheric influences are levelled out to a certain extent (Ch. 5.6). However, the number of segment-based studies has not increased in as spectacularly as expected at the turn of the millennium. As both segmentation and classification need to be adjusted to other data sets, it is generally more difficult to transfer segment-based schemes to different study areas than single step classifications. The more supervised, knowledge-based steps have to be taken, the less universal a method becomes (Eisank et al., 2011; d'Oleire-Oltmanns et al., 2012; Zwieback et al., 2012).

As all cirques in the Reintal align from north to south, for example, cirque segmentation rests on aspect and slope in our study. If it were based on watersheds as in Romstad & Etzelmüller (2012), application to other regions may be facilitated. Yet Drăguţ & Blaschke (2006) stress the importance of slope aspect in segmentation and classification and see its enhanced utilisation as a major research priority. Minár and Evans (2008) introduce small elementary forms as indivisible basic units in relief segmentation, which may facilitate transferability. Attempts at objectivising landform descriptions by introducing semantic models (Eisank et al., 2010, 1011) go in the same direction. Drăguţ et al. (2010) propose a tool to objectivise the selection for appropriating scales for segmentation, and Drăguţ & Eisank (2012) suggest an automated segment-based classification method for topography from SRTM data, which should be considered in future work. All of these findings indicate that the segmentation part of the Reintal study could be made transferrable.

The trend in classification is going from statistical to more elaborate classifiers (cf. Richards, 2005; Pal & Mather, 2006; Waske, 2007; Waske & van der Linden, 2008; van der Linden, 2008; Drăguţ & Eisank, 2011; Shoa & Lunetta,

2012), i.e. artificial neural networks (Benediktsson et al., 1990; Ferentinou et al., 2011), self-learning decision trees (Friedl & Brodley, 1997) or support vector machines (SVMs) which fit optimal hyperplanes for class separation (Huang et al., 2002; Waske, 2007; van der Linden et al., 2007; van der Linden, 2008; Waske & van der Linden, 2009; Riedel et al., 2011; Klemenjak et al., 2012). For comparisons of different classifiers, see Waske (2007), Waske & van der Linden (2009), Brenning et al. (2012) and Shao & Lunetta (2012) amongst others. Best performances vary, but SVM can outperform the other approaches in land cover classification (Shao & Lunetta; 2012) and facilitate the updating of land cover maps (Bruzzone & Marconcini, 2009).

Prerequisites for the application of the classification hierarchy to other regions and data sets are its optimisation and generalisation. However, landforms of such different sizes can hardly be captured by one single segmentation level. Waske and van der Linden (2008) argue that the information of different individual levels may be relevant for the classification decision, but that the decision does not have to be taken on the respective level. They classify pixels by including the information from very many levels of segmentation by means of decision fusion during classification. Advanced classifiers, e.g. SVM or random forest classifier systems based on a set of decision trees (cf. Breiman, 2001; Waske, 2007; Waske et al., 2012), select the most suitable level per pixel and target class in a user-controlled way within supervised classification. Hence a supervised step occurs only once, but replaces the two steps of segmentation and classification; both optical and radar data can be analysed in this way. The marker-based method for image and elevation data by Tarabalka et al. (2012) goes in the same direction, which may be applied for locally optimising the Reintal study. A wrapper approach (cf. Kohavi & John, 1997) for feature selection and morphological profiles (i.e. chains of mathematical operators to analyse the image surface) as suggested by Waske et al. (2009) could also be useful. in general, the combination of one supervised and one unsupervised processing step seems most appropriate for transferability.

1.7.5 Potential debris flows

53 potential source areas for debris flows are found with the help of the DMRN (Fig. 6.5) and 48 potential debris flow runouts with the MSFM (Fig. 6.6). Five runouts are missing because they slope below 11°, the stopping threshold value of the model. The DMRN also shows the level of dissection of the watershed based on relief variation, by means of which areas with high versus low sediment dynamics can be distinguished (cf. Jackson et al., 1987; Marchi & Fontana, 2005; Rowbotham et al., 2005).

These results are qualitatively assessed with the orthorectified ASTER image (Fig. 6.7), a historical aerial photo (Fig. 6.8) and a morphopedological map. This is validated through three fieldwork excursions, which proved the consistency of the results. However, the overall slope threshold of 11°, which stems from the Swiss Alps (Huggel et al., 2003, 2004), does not always reflect the Venezuelan reality. The DEM dependency of the model also introduces some errors (cf. Miliaresis, 2008; Ch. 6.8), but in general, the SRTM DEM allows us to calculate realistic results, and this is congruent with the SRTM evaluation of Huggel et al. (2008). The hazard maps produced (Figs. 6.5, 6.6, 6.10) reflect the given sediment dynamics and are consistent with other recent vulnerability and susceptibility studies (cf. Maldonado, 2007; Roa, 2007; Caritas, 2010).

A simple parameterisation model such as the MSFM is well suited for larger areas such as the 1900 km^2 evaluated in the Chama river basin. Model and SRTM DEM limitations are reached when one is interested in specific sediment volumes and types. More precise DEMs and more complex and detailed models based on physical processes, for instance 3D dynamic models should be considered for this effect (Gruber et al., 2009; Bell et al., 2012). For example, Becht et al. (2005) analyse and model debris flow events on one talus in the Reintal, concluding that debris flows remove far greater sediment volumes from the cascade than rockfalls put in, so that the talus sediment sources are

currently depleting. Yet this precise piece of evidence implies considerable downscaling, from watershed dimensions to the scope of one talus and annexes. "At present, no generally applicable model is able to cover the range of all possible material mixtures and event scenarios. This complexity results in different torrential processes and results in a large variety of approaches to predict debris-flow mobility" (Rickenmann & Scheidl, 2013: 75).

Band et al. (2012) propose an optimised estimation of slope instability sites without a priori, in-situ ground knowledge: the integrated modelling of slope stability as a function of geomorphological, hydrological and ecosystem processes may be an alternative for debris flow source area detection and provide more insights into systemic connections in watersheds. What is more, the GIS-based geomorphological mapping method presented by Theler et al. (2010) focuses explicitly on the sediment source areas and their potential for debris flow generation, translating the sediment cascade model into a cartographic system. Brenning (2009) and Brenning et al. (2012) test several predictor variables for debris flow pattern recognition via modelling and classification techniques. They find that image classification leads to an enhanced spatial predictability and transferability of the texture attributes when compared to linear and additive statistical modelling. Therefore classification methods as decribed in Chapters 1.6, 1.7.4 and 1.7.5 should be considered in further research on Venezuelan debris flows. A combination of segmentation and InSAR as proposed by Hölbling et al. (2012) should be evaluated. Sediment volumes and transfer rates involved may be quantified following Bartsch et al. (2009).

The evaluation of remote sensing data can be extremely helpful in assessing potential mass movements and can form the only available source of information (Kääb et al., 2005a; Gruber et al., 2009; Sund et al., 2009; Kääb, 2010; Debella-Gilo, 2011; Bell et al., 2012; Debella-Gilo & Kääb, 2012; Eiken & Sund, 2012). To date, major changes in sediment supply and mass-movement activity have not been documented, but the potential for them to occur is given (Goode et al., 2012; Stoffel & Huggel, 2012). Yet global change may also

deplete some sediment sources or decouple them from the sediment cascade, as "slope stability and mass movements in high-mountain regions are complex and highly interlinked systems" (Stoffel & Huggel, 2012: 430). Recent investigations hint at unprecedented reactions, events and magnitudes triggered by a warming climate, which is why sediment and process cascades have to be monitored closely and further (Stoffel, 2010; Stoffel & Huggel, 2012; Goodfellow & Boelhouwers, 2012; Goode et al., 2012).

1.7.6 Glacier displacement and surge

In the rugged terrain around Ny Ålesund, the minimum cost flow (MCF) technique with a triangular irregular network (TIN) described by Costantini (1998) led to better interometric phase unwrapping results than the branch-cut algorithm by Goldstein et al. (1988). Glacier velocities in line-of-sight of the sensor are obtained from the differential phase after filtering and unwrapping by MCF, leading to orthonormal displacement maps for horizontal, vertical and look vector movement components (Fig. 7.9). Horizontal displacements of $\sim$ 20 cm d^{-1} (5-6 April 1996) and $\sim$ 18 cm d^{-1} (10-11 May 1996) are found at the glacier terminus and $<$ 3 cm d^{-1} in the middle and upper portions of Comfortlessbreen (Fig. 7.9). The cirque area (Figs. 1.3, 1.12), however, shows velocities of around 6 cm d^{-1} both in April and May 1996. DInSAR allows us to look into the past of Comfortlessbreen to retrospectively deduce 1996 velocities and thereby fill an existing data gap. The DInSAR displacement rates are consistent for both April and May 1996. They hint at a pre-surge velocity level of the glacier in 1996, which underwent full surge a decade later (Sund et al., 2009; Sund & Eiken, 2010; Eiken & Sund, 2012). Surge-type glaciers on Svalbard are mostly characterised by low velocities of around 10 m a^{-1} during quiescence (cf. Nuttall et al., 1997; Melvold et al., 1998) because of their polythermal regime, as indicated by the velocities found. Tidewater glaciers usually increase velocities towards the terminus (Vieli et al., 2004), as is the case on Comfortlessbreen in 1996 (Fig. 7.9).

Figure 1.12: View of the Cirque Region of Comfortlessbreen
The uppermost area of the glacier, where velocities were possibly higher than further downglacier in 1996. Photo taken by M. Sund in 2009 during glacier surge as indicated by the crevasses.

The errors within the velocity maps (Figs. 7.8, 7.9) produced cannot be precisely calculated within Gamma for all pixel values of a DInSAR scene. Crosetto et al. (2008) and Strozzi et al. (2010) assume an error in line-of-sight displacement of < 0.7 cm for ERS-1/-2. As shown in Equations 7.4 and 7.5, contributions from atmospheric influences and noise are still contained in the generated differential interferograms (Weydahl et al., 2001; Li et al., 2003; Rott, 2009; Danklmayer et al., 2009). This is difficult to amend because the necessary additional meteorological data is not available (Gens & van Genderen, 1996; Hanssen, 2001; Rott, 2009). Signal noise can be reduced by transforming the SAR image into a multilook image (MLI). However, this implies a reduction of the spatial resolution (Kwok & Fahnestock, 1996), which

is inconvenient for a small glacier such as Comfortlessbreen. MLI generation can be used to find out how much noise is left in the interferograms; therefore different MLI parameter settings should be compared to the DInSAR results obtained.

Testing all possible combinations of the ERS-1/-2 SAR scenes together with several DEMs represents a means of producing more DInSAR results. A comparison of those results with 3- and 4-pass DInSAR may make it possible to account for the potential error sources in DInSAR and to filter out noise (Sansosti et al., 2010; Current et al., 2012), yet DEM errors would still be contained as well. Advanced algorithms such as persistent scatterer interferometry (cf. Ferretti et al., 2000; Werner et al., 2003; Hooper et al., 2004, 2007; Hölbling et al., 2012), small baseline interferometry (cf. Berardino et al., 2002; Schmidt and Bürgmann, 2003; Lauknes et al., 2010b; Henderson et al., 2011) or combinations of both (Hooper, 2008; Lauknes, 2010; Lauknes et al., 2010a) can help filter out atmospheric effects and noise (Li et al. 2003; Ferretti et al., 2000; Berardino et al., 2002; Sansosti et al., 2010).

Knowledge of displacement rates is of central importance in alpine and polar settings regarding analysis and modelling of e.g. glacier surges, glacier dynamics, calving, rock glacier creep, rock slope deformation, sediment fluxes and budgets, slope instabilities. Studies on InSAR and glacier displacement abound (e.g. Joughin et al., 1998; Mohr et al., 1998; Dowdeswell et al., 1999; Michel & Rignot, 1999; Rosen et al., 2000; Joughin, 2002; Eldhuset et al., 2003; Strozzi et al., Luckman et al., 2002, 2007; Palmer et al., 2009; Quincey et al., 2009; Joughin et al., 2010b; Kumar et al., 2011), most of them also involving ERS-1 and/or ERS-2 data. InSAR for the study of slope deformation, rock- and landslides (Osmundsen et al., 2009; Lauknes et al., 2010; Henderson et al., 2011) provides important insights into alpine sediment systems, or even into deformation patterns and mechanisms of seismic activation (Currenti et al., 2012). But InSAR has also been successfully applied to rock glaciers (Strozzi et al., 2004, 2008, 2010a, 2010b), which couple glacier and alpine landform.

In an approach similar to the Svalbard study, Strozzi et al. (2010b) detect rock glacier movement of ≥ 1 cm d^{-1} in ERS-1/-2 tandem data, in three-day repeat ERS-1 images from 1991 and in terrestrial DInSAR. They argue that such speeds can hardly be detected with present satellite SAR data because the 35-, 46- and 11-day repeat intervals (corresponding to C-, L- and X-band data currently available) lead to decorrelation. This applies all the more to Comfortlessbreen with its considerably higher velocities of up to ≤ 20 cm d^{-1} even in quiescence. By combining ascending and descending orbit passes with slope information, a full 2-D or 3-D flow velocity field can be derived (Joughin et al., 1998; Palmer et al., 2009), so that also glaciers flowing perpendicularly to the line of sight of the sensor can be measured by InSAR.

Not only does DInSAR yield glacier displacement, but also SAR speckle, coherence and feature offset tracking (e.g. Lucchitta et al., 1995; Michel & Rignot, 1999; Strozzi et al., 2002, 2008; Pritchard et al., 2005; Burgess et al., 2012; cf. Ch. 1.7). These different approaches have been combined and compared by e.g. Michel & Rignot (1999), Joughin (2002), Strozzi et al. (2002), Luckman et al. (2007), Quincey et al. (2009), Joughin et al. (2010a) and Kumar et al. (2011). The great advantage of feature offset estimation lies in the fact that unambiguous values are produced, so that phase unwrapping, the most intricate part of InSAR, can be avoided (Strozzi et al., 2008). Mansell et al. (2012) study Comfortlessbreen by feature tracking on pairs of ERS-1/-2. Their resulting velocity maps seem to mainly cover the lower glacier portions and the frontal areas, probably due to the fact that feature tracking cannot capture the very slow speeds further up, whereas DInSAR accurately measures the flow of the entire glacier (Fig. 7.9; Palmer et al., 2009). While their surge flow speeds of 2008 correspond to the ones described by Sund & Eiken (2010), they report just small terminus variations before surge onset, which matches the pre-surge velocity levels described in Chapter 7.5.

In a changing climate, glacier mass accumulation and hence glacier velocities, particularly of mountain and land-terminating glaciers, could decrease on

regional scales (Heid & Kääb, 2012a). Yet melt-induced speed-ups have also been observed, especially in tidewater, but also in land-terminating glaciers (Thomas et al., 2009; Sundal et al., 2011). More monitoring and comparisons with earlier glacier velocities are necessary for the assessment of climate change, especially over large areas (Lubin & Maasom, 2007; Joughin et al., 2010b; Haug et al., 2010; Casey et al., 2012; Heid & Kääb, 2012a; Kääb et al., 2012).

The new tandem missions are of special interest as they provide data for interferometric analyses again, e.g. the COnstellation of small Satellites for the Mediterranean basin Observation (COSMO-SkyMed) with its possibility of either one-day, four-day, eight-day or 16-day tandem recording. The X-band SAR satellite TerraSAR-X and its twin satellite TerraSAR-X Add-oN for Digital Elevation Measurement (TanDEM-X) or the C-band Radarsat Constellation Mission should also be considered for further interferometric study, while the existing full and underused data archives ought to be remembered as well (ESA, 2012; Debella-Gilo, 2011; Sansosti et al., 2010; Joughin et al., 2010a).

1.7.7 Towards a new glacier surge model

In a paper entitled "Is there a single surge mechanism?", the strong contrast in surge dynamics between Svalbard and other regions makes Murray et al. (2003b) conclude that there are at least two distinct surge mechanisms: Svalbard-type, in which polythermal glaciers are controlled by thermal mechanisms as modelled by Fowler et al. (2001), and Variegated-type named after the fast temperate Variegated glacier surge in Alaska described by Kamb et al. (1985) and Kamb (1987) which is hydraulically controlled. Sund et al. (2009) propose three surge stages, the first of which comprises initial features which have not been associated with surge before. Remote sensing enables the detection of small changes which often occur years before the first typical, visible surge characteristics (Chs. 8.1, 8.2)

Taking Sund et al. (2009) and the results from Paper VI as points of departure, Paper VII suggests one common surge theory for all types of observations. Svalbard´s surge-type glaciers are polythermal; only their margins and lower reaches are frozen to the ground, which hinders flow. Yet temperate conditions dominate their upper portions (e.g. Hagen & Sætrang, 1991; Björnsson et al., 1996; Ødegård et al., 1997; Melvold & Hagen, 1998; Sund & Eiken, 2004). This corresponds to the thermal regime of polythermal surge-type glaciers in other regions (e.g. Clarke et al, 1984; Grant et al., 2009). Hence the upper portions of both temperate and polythermal glaciers are characterised by the same basic conditions and determining factors. It is suggested that surges initiate in these upper regions (Sund et al., 2009; Chs. 8.2, 8.3). The greater DInSAR velocities of around 6 cm d^{-1} in the cirque area (cf. Ch. 7.5; Figs. 1.3, 1.12) could constitute a first indicator of surge initiation, surge stage 1 as suggested by Sund et al. (2009) and Chapter 8.3. This contrasts with other studies on tidewater-terminating glaciers (e.g. Rolstad et al., 1997; Luckman et al., 2002; Dowdeswell & Benham, 2003; Murray et al., 2003a), which assume surges to initiate in the lower glacier reaches.

As Chapter 8.3 proposes a conceptual surge model which includes a stage before any visible surge signs can be observed (Figs. 8.2, 8.3), these findings need not contradict one another. A joint perspective on surge initiation both in polythermal and temperate glaciers is therefore proposed in Chapter 8.3. The coupling between build-up and surge initiation is evidenced as well as prerequisites for build-up, primary controls for surge initiation and individual glacier (secondary controls) of surge propagation. As the example of Comfortlessbreen shows, changes in flow velocities and surface elevation over time are observed (Fig. 8.1). The DInSAR velocities obtained for 1996 and Global Navigation Satellite System (GNSS) velocity measurements in 2001 make it possible to conclude on upglacier changes in mass movement (Ch. 8.2.3). These results, further remote sensing findings and a reinterpretation and synthesis of previous studies leads to a synthesised conceptual surge model (Ch. 8.3; Figs. 8.2, 8.3), which is applicable to both temperate and polythermal glaciers.

Various processes occurring during surge are similar to those occurring in non-surge-type glaciers, i.e. regarding glacier hydrology (e.g. Raymond et al., 1995). Surges may then result from a certain series of ordered factors, processes and reactions. The generalised model aims at illustrating this order of surge process activity, from which individual glaciers may deviate due to secondary controls. This does not necessarily contradict the divergent earlier theories on surges: the apparent differences in dynamics can be seen as variations in already ongoing surges, which stem from different thermal regimes, glacier properties and surge stages. Budd (1975) had already suggested that surge process features were not basically different from those observed in non-surge-type glaciers. The model offers a new perspective and framework for future surge studies, and may be further fine-tuned, just as sediment cascade models have been developed and refined over time (cf. Ch. 3.2.2). Scherler et al. (2011) present a conceptual model coupling hillslope and glacier dynamics, which explains relief and landscape evolution in cold climate environments. The alpine sediment cascade, glacier movement and theoretical models are thus closely connected.

1.7.8 Optical as opposed to radar data

Traditional remote sensing often focuses either on optical (e.g. Paul, 2000; Dowdeswell & Benham, 2003; Kääb et al., 2003, 2005b; Berthier et al., 2005, 2006; Liu et al., 2009; Casey et al., 2012) or on microwave imagery (e.g. Kelly et al., 1997; Dowdeswell et al., 1999; Engeset, 1999; Braun, 2001; Palmer et al., 2009). Studies based on the combination of both are still rare, which is largely due to the different geometries in optical as opposed to radar data. This has also hindered them being linked to the desired degree within this thesis. Moreover, the limited availability of optical and radar data from the same place and time restricts research possibilities more than previously estimated. It is also unclear from which calendaric dates the optical and radar data should be for combination. Data from as proximate calendaric dates as possible may

not show the same surface, because the radar signal penetrates the surface to a certain extent (Kelly et al., 1997; Brown et al., 2005). SAR backscatter from glaciers partly depicts the previous summer surface or even subsurface features (Langley et al., 2008, 2009; Müller, 2011).

Frequent cloud cover over alpine, nordic and polar regions limits the choice of usable optical satellite scenes (Weydahl, 1998), which has hindered the combined analysis of optical and radar data in the Svalbard study. For instance, when aiming at optical image matching for combination with the DInSAR results on glacier displacement described in Paper VI, optical scenes turned out to be very scarce over the research area around 1996: no Landsat scenes are available over Ny Ålesund between 1993 and 1999. Only a few SPOT 3 scenes taken between 3 and 27 August 1996 can be found, many of them misty, cloudy and with poor optical contrast. Even in a set dating from 3 and 17 August 1996 from the same orbit track and frame, topographical distortions and haze blur potential movement. Besides, the short time interval between those SPOT scenes results in hardly any displacement signal exceeding the statistical significance level.

New satellite missions are characterised by increased spatial resolution and shorter revisit times (Liu et al., 2009; ESA, 2012), so that the optical data pool is constantly being enlargened. Optical satellite sensors have been detecting at high resolutions for more than a decade now. Recent missions such as Formosat (cf. Liu et al., 2009), WorldView, GeoEye and the upcoming Pleiades and Sentinels continue the trends set by e.g. Ikonos, Quickbird and OrbView. The Landsat Data Continuity Mission follows up on the thermal dimensions of the Landsat series and ASTER (cf. ESA, 2012). When working in the visible spectral range, interpretations appear quite straightforward. Reconnaissance, understanding and the spread of methods to larger user groups benefit from the fact that optical data roughly depict the ground as it is perceived by the human eye. This holds especially for geometries; the multispectral bands of optical data contain far more information. For instance, false colour compos-

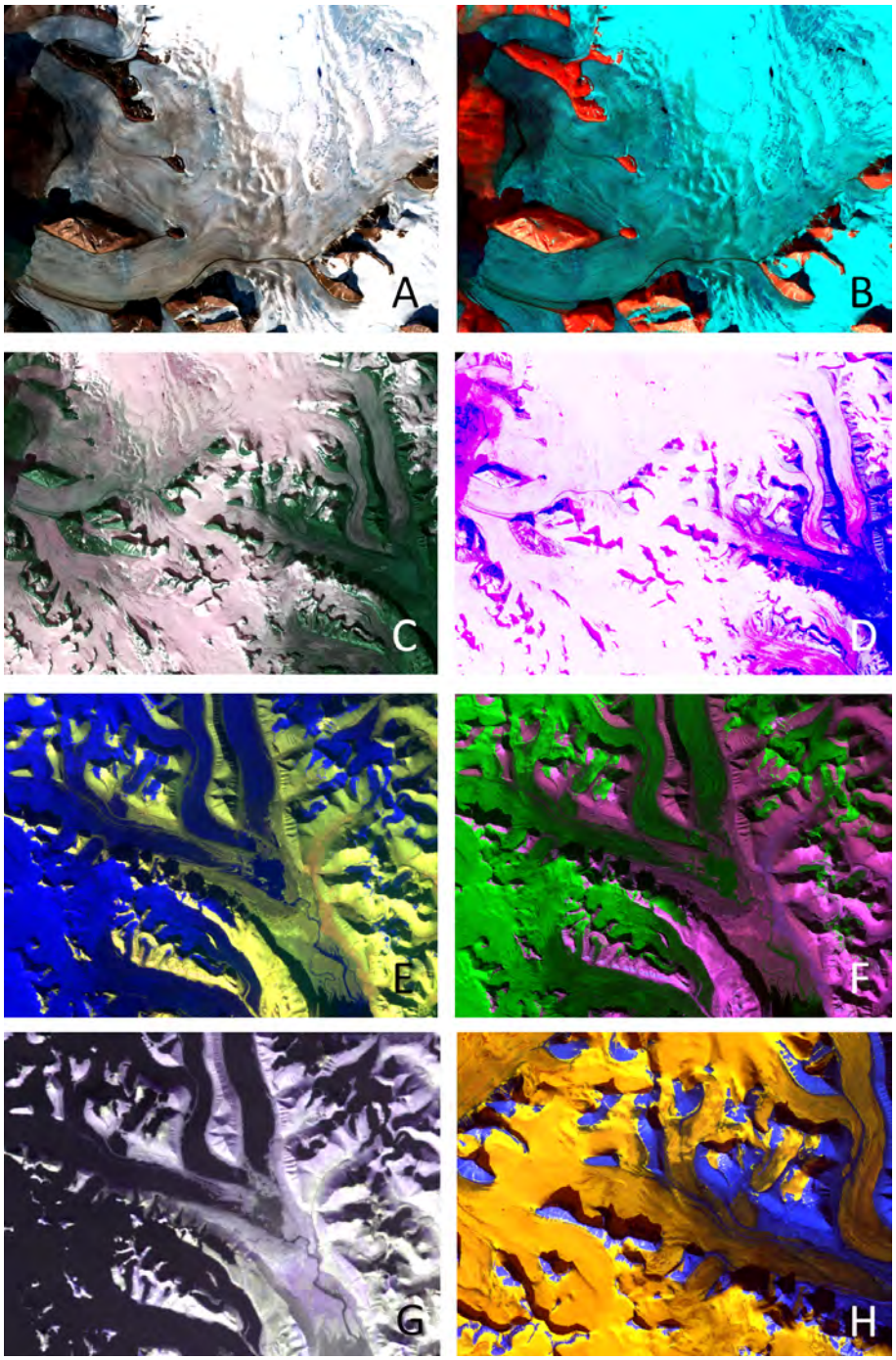

Figure 1.13: False Colour Composites of northern Svalbard

Different combinations of ASTER spectral bands (17 August 2000). A: ASTER bands 3-2-1 for the red, green and blue (RGB) image channels, the band combination for closest approximation of human vision. B: RGB 4-3-2 for distinguishing snow from ice. C: RGB 1-3-2 with linear stretch and normal brightness. D: RGB 1-3-2 without linear stretch and with increased brightness. E: RGB 4-5-3 differentiates the glacier forefield. F: RGB 7-3-4 illustrates glacier flow structures and debris cover. G: RGB 10-12-14 for masking out glaciers. H: RGB 1-3-4 highlights snow and ice surface structures.

ites (FCCs, Fig. 1.13) combine other bands than the three conventional red, green and blue (RGB) channels approximating the human visual experience (cf. Kääb, 2005b; Paul et al., 2007; Błaszczyk et al., 2009; Paul & Hendriks, 2010a). They sometimes allow for a neater distinction between surface features (Fig. 1.13). Besides, a vast number of optical images are available in extensive archives.

Because they are not dependent on daylight and clear skies, radar data can be more convenient for studies in these regions, yet until 2007, commercially available SAR resolution was still rather coarse (cf. Rott, 2009; ESA, 2012). Such small landforms as on the Reintal valley floor would not have been detectable, so optical data was the only option at hand then. Yet with Radarsat-2, the COnstellation of small Satellites for the Mediterranean basin Observation (COSMO-SkyMed), TerraSAR-X and TanDEM-X, the commercial SAR product range has been widened considerably and made more flexible (Weydahl et al., 2008; Yoon et al., 2009; Høgda et al., 2010; Mittermayer et al., 2010; Sansosti et al., 2010; Thonfeld & Menz, 2011). SAR resolutions have been brought down to the 1 m range, thus approaching the very high optical resolutions, which makes the microwave spectrum a lot more attractive for many small-scale applications in geomorphology and glaciology today.

The methods applied in this thesis offer multiple possibilities for a synergistic usage of optical and radar data. Segmentation of SAR intensity images is possible, yet variations in backscatter and speckle can make an exact delineation of ground features difficult, which is why object shapes may be best derived from optical data alone in combined analyses (Thonfeld & Menz, 2011). Classification accuracies rise, especially when using SVM and random forest classifiers on optical and (even multipolarised) radar data (Waske, 2007; Waske & Benediktsson, 2007; McNairn et al., 2009; Riedel et al., 2011; Klemenjak et al., 2012). New processing chains aim at increasing degrees of automation, also regarding training area selection, for the integrated assessment of optical and radar data (Bruzzone et al., 2004; Bruzzone & Marconcini, 2009; Baraldi

et al., 2010; Riedel et al., 2011; Bishop et al., 2012; Klemenjak et al., 2012; Zwieback et al., 2012). High automation is an asset for operational and large scale monitoring as it reduces user input and ground truth requirements to a minimum (Bishop et al., 2012; Klemenjak et al., 2012).

The choice of SAR image pairs suitable for interferometric analysis is limited (Rott, 2009), which is also why scenes of 1996 are used in Paper VI. When aiming at glacier observation in Svalbard with its highly changeable weather conditions and consequent rapid loss of coherence, this relative scarcety of InSAR-compliant data will persist to a certain degree, even though new tandem missions have been installed, e.g. the COSMO-SkyMed constellation (Sansosti et al., 2010; Stramondo et al., 2011; Currenti et al., 2012) with its current four satellites (X-band SAR), TerraSAR-X and TanDEM-X (Weydahl et al., 2008; Yoon et al., 2009; Mittermayer et al., 2010) or the planned C-band Radarsat Constellation Mission. In contrast, feature offset tracking offers more possibilities for change detection as larger temporal intervals can be covered by this technique than by InSAR. When coherence does not matter, a wider range of SAR data beyond tandem missions can be used for glacier flow measurements, from e.g. the planned Sentinel missions or the entire ERS-1/-2 archives.

When aiming at change or movement detection, be it in sediment or glacier dynamics, pronounced changes or displacements appear blurred in interferometric applications due to decorrelation. While InSAR is well suited for rock glaciers and the accumulation area of a glacier, which is dominated by slow movements and little melting (Toutin, 1995, 2000; Toutin & Gray, 2000; Eldhuset et al., 2003; Strozzi et al., 2004, 2008, 2010a, 2010b; Paper VI), it often fails in the ablation zone, which changes quickly (Fig. 7.3). For example, fast flowing Kronebreen with its 2 m d^{-1} (Weydahl, 2001; Eldhuset et al., 2003; Kääb et al., 2005b; Błaszczyk et al., 2009) decorrelates in Figure 7.3 (cf. Ch. 7.6). Similar velocities were measured in the Comfortlessbreen surge in 2008 (Sund & Eiken, 2010; Eiken & Sund, 2012; Mansell et al., 2012). They lie

beyond the scope of DInSAR; SAR feature offset tracking and optical image matching are complementary alternatives (Berthier et al., 2005; Kääb et al., 2005b; Luckman et al., 2007; Haug et al., 2010; Joughin et al., 2010a; Mansell et al., 2012).

Radar and its optical counterpart, airborne or terrestrial laser scanning (TLS) or Light Detection And Ranging (LiDAR), have taken DEM generation to the next level (Geist & Stötter, 2010; Moholdt & Kääb, 2012; Wilson, 2012). LiDAR's high spatial and vertical resolution depicts even small-scale geomorphological features with unprecedented clarity (Chiverell et al., 2008; Bimböse et al., 2010; Bell et al., 2012). TanDEM-X and TerraSAR-X have meanwhile covered the entire Earth, which will result in a high-precision DEM of Earth (ESA, 2012). A combination of optical and radar may also be beneficial for optimised DEM compilation (Toutin, 2000; Karkee et al., 2006). It is an open question whether this should best be done after or during the actual DEM generation process. In the latter case, either the radar information can be introduced into the matching process based on optical data, or the optical data can be embedded in the unwrapping of the interferometric phase. Error propagation and the derivation of changes in elevation constitute other fields of further research concerning combined DEMs.

In short, multi-sensor remote sensing promises an increased gain in information: concurrent analyses based on both optical and radar data can complement one another with their respective strengths (e.g. Toutin, 1995, 2000; Honikel, 1999, 2002; Weydahl, 1998; Jansa et al., 2002; Kääb, 2005a; Kääb et al., 2005b; Richards, 2005; Karkee, 2006; Luckman et al., 2007; Waske, 2007; Waske & van der Linden, 2008; Joughin et al., 2010a; Riedel et al., 2011) and thereby further research on cold climate landscape evolution.

1.8 Conclusions and perspectives

This thesis has assessed the potential of passive and active satellite remote sensing for investigating cold climate environments. Three exemplary case studies focused on process units and mass movements. They evidence the need to choose different data and methods according to the particular research questions, which is also highlighted by e.g. Brenning (2009), Brenning et al. (2012), Marmion et al. (2008) and Mountrakis et al. (2011). Although new sensors are customarily regarded as the frontline of research, the existing data archives are underused and of scientific potential (Sansosti et al., 2010; Debella-Gilo, 2011; Heid, 2011). The following conclusions can be drawn from this work:

With respect to its theoretical background, remote sensing initially was a method, but is gradually moving towards being regarded as an applied science. Yet both the nature of remote sensing and of science can hardly be defined unequivocally, all the more so in today's high-tech scientific world, where formerly distinct categories and domains are moving closer together. This is illustrated by the fact that two seemingly unrelated approaches from distinct scientific disciplines, namely geomorphic systems theory and segment-based image classification, show surprisingly many similarities.

As segment-based class descriptions go beyond spectral per-pixel analysis and allow for the incorporation of DEM and other spatial information, they are especially suited for three-dimensional applications in rugged terrain. The identification of geomorphological process units, even with regard to their activity status, becomes possible. The inaccessible upper alpine regions have also been mapped for the first time. The necessity of four differently scaled levels in the classification hierarchy shows the scale dependency of feature extraction. The Reintal case study hence forms a valid approach for both the thematic mapping of alpine landforms and the monitoring of accelerated landscape development.

It remains to be investigated to what extent a purely pixel-based classification scheme may handle this data. Before 2008, available SAR resolutions were too coarse for the landforms investigated, yet the new generation of radar satellite sensors, e.g. Radarsat-2 and TerraSAR-X, should be considered along with recent very high resolution optical data. The latest classficators should be tested as well. The segmentation and classification hierarchy can be extended to other reseach questions, e.g. the space-time variations of landscape and radiation or erosive processes. It may also benefit and assist studies on glacier mass and sediment balance, to name just some examples of important fields in (peri-)glacial research (cf. Bishop & Shroder Jr., 2004; Bishop et al., 2012).

For the upper Chama river watershed, a regional debris flow hazard assessment was lacking prior to the Venezuelan case study. In spite of the complex terrain and certain model limitations, the chosen parameterisation in combination with the SRTM DEM proved to be suitable for assessing geomorphologic processes at regional scales. New and enhanced DEMs, e.g. by TerraSAR-X and TanDEM-X data, may facilitate the downscaling of the modelling approach to achieve a more specific investigation of selected sites of interest.

The Svalbard case study shows that 2-pass DInSAR makes it possible to derive coherent glacier displacement rates which cover the entire Comfortlessbreen from the cirque area to its terminus. This fills an existing data gap and allows us to deduce the surge stage of the glacier in 1996, which corresponds to pre-surge conditions at the time, with surge initiation possibly detected in the cirque regions. In general, InSAR better reflects slow displacement. Faster movement or pronounced change is detectable by SAR feature offset tracking or in the visible range of the electromagnetic spectrum, where optical image matching produces suitable results. These methods should be used in a combined approach to assess other and also faster flowing glaciers than Comfortlessbreen, also integrating recent interferometry-compliant data from the new tandem missions with their shorter revisit times.

The resulting conceptual surge model implies that the three surge stages described in Sund et al. (2009) and Paper VII underlie the development of all surge behaviour in both temperate and polythermal glaciers, thus synthesising earlier surge theories. The wealth of archived and new, enhanced remote sensing data in combination with remote sensing and photogrammetric analyses (Joughin et al., 2010a; Eiken & Sund, 2012) make surge research at large scales possible. Thus the validity of the model can be further investigated.

In short, segment-based classification is applicable to spatial mapping and monitoring research questions in cold climate environments where the features of interest can only be differentiated by combining different sources of information. Process activity can also partially be observed this way, while potential movements and pending hazards should rather be modelled. Ongoing movement is detected at milli- to centimetre range by SAR interferometry, limited only by the relative scarcety of coherent data. Yet existing archived remote sensing data can be used retrospectively in order to fill data gaps in time series.

Several subjects and methods of research have been tackled in this thesis, but they could be combined within one single study as well. For instance, Parry (2011) applies geomorphological mapping for landslide, i.e. movement hazard modelling and assessment. If glacial hazards and small-scale measurements of movement were involved, too, all practical aspects of this thesis would be covered. In general, theoretical considerations and hypothesis formation form the starting point of any scientific research (Papers I, II). Terrain sounding and mapping is a prerequisite in most research projects and can be aided by space-borne data and segment-based classification (Papers III, IV). The modelling of hazard potential (Paper V) and movement detection (Paper VI) often accompany one another. In cold climate environments, geomorphological (Papers II, III, IV, V) and glaciological (Papers VI, VII) spheres overlap and are closely coupled, as the sediment cascade (Papers II, III, IV) initiates in the glacial domain.

To further the knowledge of glacial and geomorphological processes and to assess to what extent global change is actually happening (cf. Humlum et al., 2011), global monitoring and interdisciplinary research is needed which unites both remote sensing and in-situ data analysis to be able to model future trends. This will enhance the scientific understanding of cold climate landscape evolution through ice and sediment dynamics.

The following perspectives for future work can be deduced from the work presented in this thesis:

- If remote sensing really is being regarded as a science, then one should not only invest in applied research, but also strengthen and develop its theoretical foundations.
- The segment-based approach can deal with alpine terrain and landforms and leads to sound results. The exact influences of image and DEM data respectively should be assessed by analysing them individually. The degree of transferability of both segmentation and classification schemes to different study areas and kinds of data, e.g. high resolution optical and radar, remains to be investigated, as well as the utility of new classifiers.
- For debris flow investigations, a downscaling of the approach presented and the integration of other topographic parameters is suggested. An enhancement via land cover classification with an emphasis on stream channel domains should be considered.
- DInSAR can be used retrospectively in order to draw conclusions on earlier glacier surge stages; analysis ought to be extended to other glaciers. The results are also valuable with regard to new tandem missions which allow for interferometric analyses again and thus for a better quantification and understanding of temporal deformation patterns, which will benefit further surge research.
- The combination of optical and radar data promises to provide an increase in information. Further research into spectral and polarimetric

analyses of combined optical and SAR data on a multitemporal and multifrequency basis is needed.

- Scientific literature on glacier surges has been published for 50 years now; scientific observations date back even further. Yet in spite of an increasing number of surge studies especially in the last two decades, the phenomenon has not been fully understood as yet; more work needs to be done. Therefore, the investigation of the question of whether all glacier surges could be explained by a single, unified surge theory as presented in Paper VII necessarily reflects the knowledge about surges which has been published to date - further corrections and amendments are possible and probable. Besides, as not ALL glacier surges have been studied yet, the initial question can, in fact, never be answered with an unequivocal 'yes', at least not from a philosophy of science point of view: even if all observations indicated one single surge mechanism, at least the possibility of a so-far unobserved exception to the rule is always present - the logical error of induction or the principle of empirical falsification (Popper, 1989; Curran, 1987).

1.9 References

Abele, G., Barsch, D., Garleff, K., Haeberli, W. & Höfner, T. (1993): Aktuelle Geomorphodynamik im Hochgebirge. In: Barsch, D. & Karrasch, H. (eds.): Geographie und Umwelt, Franz Steiner Verlag, Stuttgart, 325–346.

Abrams, M. & Hook, S. (2002): The ASTER User Handbook. Version 2. Pasadena, Sioux Falls. http://asterweb.jpl.nasa.gov/content/03_data/04_Documents/aster_user_guide_v2.pdf, 04.11.2011.

ACIA (2005): Arctic Climate Impact Assessment. Cambridge University Press, Cambridge.

Addink, E.A., van Coillie, F.M.B. & de Jong, S.M. (2012): Introduction to the GEOBIA 2010 special issue: From pixels to geographic objects in remote sensing image analysis. International Journal of Applied Earth Observation and Geoinformation 15, 1-6.

Baatz, M. & Schäpe, A. (2000): Multiresolution segmentation - an optimization approach for high quality multi-scale image segmentation. In: Strobl, T., Blaschke, T. & Griesebner, G. (eds.): Angewandte Geographische Informationsverarbeitung XII. Beiträge zum AGIT-Symposium Salzburg 2000. Herbert Wichmann Verlag, Heidelberg, 12-23.

Band, L.E., Hwang, T., Hales, T.C., Vose, J. & Ford, C. (2012): Ecosystem processes at the watershed scale: mapping and modeling ecohydrological controls of landslides. Geomorphology 137(1), 159-167.

Baraldi, A., Durieux, L., Simonetti, D., Conchedda, G., Holecz, F. & Blonda, P. (2010): Automatic spectral-rule-based preliminary classification of radiometrically calibrated SPOT-4/-5/IRS, AVHRR/MSG, AATSR, IKONOS/QuickBird/OrbView/GeoEye, and DMC/SPOT-1/-2 imagery – Part I: system design and implementation. IEEE Transactions on Geoscience and Remote Sensing 48(3), 1299 – 1325.

Baret, F. & Guyot, G. (1991): Potentials and limits of vegetation indices for LAI and APAR assessment. Remote Sensing of Environment 35, 161-173.

Bartsch, A., Gude, M. & Gurney, S.D. (2009): Quantifying sediment transport processes in periglacial mountain environments at a catchment scale using geomorphic process units. Geografiska Annaler 91A(1), 1–9.

Bartsch, A., Gude, M., Jonasson, C., & Scherer, D. (2002): Identification of geomorphic process units in Kärkevagge, northern Sweden, by remote sensing and digital terrain analysis. Geografiska Annaler 84A(3-4), 171–178.

Bauer, B.O. (2004): Geomorphology. In: Goudie, A.S. (ed.): Encyclopedia of Geomorphology 1, Routledge, London, 428–435.

Becht, M. (1998): Sedimentkaskaden in alpinen Geosystemen (SEDAG). DFG-Bündelantrag, Technische Universität München, Munich (unpublished).

Becht, M., Haas, F., Heckmann, T. & Wichmann, V. (2005): Investigating sediment cascades using field measurements and spatial modelling. Pro-

ceedings of the International Symposium on Sediments Budgets (at Foz do Iguaco, Brazil. IAHS Publications 291, IAHS Press, Wallingford, 206-213.

Bell, R., Petschko, H., Röhrs, M. and Dix, A., 2012. Assessment of landslide age, landslide persistence and human impact using airborne laser scanning DTMs. Geografiska Annaler 94A(1), 135-156.

Benediktsson, J.A., Swain, P.H. & Ersoy O.K. (1990): Neural network approaches versus statistical-methods in classification of multisource remote-sensing data. IEEE Transactions on Geoscience and Remote Sensing 28(4), 540-552.

Benz, U.C., Hofmann, P., Willhauck, G., Lingenfelder, I. & Heynen, M. (2004): Multiresolution, object-oriented fuzzy analysis of remote sensing data for GIS-ready information. ISPRS Journal of Photogrammetry & Remote Sensing 58, 239-258.

Berardino, P., Fornaro, G., Lanari, R., & Sansosti, E. (2002): A new algorithm for surface deformation monitoring based on small baseline differential SAR interferograms. IEEE Transactions on Geoscience and Remote Sensing 40(11), 2375-2383.

Berthier, E., Arnaud, Y., Kumar, R., Ahmad, S., Wagnon, P. & Chevallier, P. (2007): Remote sensing estimates of glacier mass balances in the Himachal Pradesh (Western Himalaya, India). Remote Sensing of Environment 108, 327-338.

Berthier, E., Vadon, H., Baratoux, D., Arnaud, Y., Vincent, C., Feigl, K.L., Rémy, F. & Legresy, B. (2005): Surface motion of mountain glaciers derived from satellite optical imagery. Remote Sensing of Environment 95, 14-28.

Berthling, I. (2011): Beyond confusion: rock glaciers as cryo-conditioned landforms. Geomorphology 131, 98–106.

Berthling, I. & Etzelmüller, B. (2011): The concept of cryo-conditioning in landscape evolution. Quaternary Research 75(2), 378-384.

Bimböse, M., Nicolay, A., Bryk, A., Schmidt, K.-H. & Morche, D. (2011): Investigations on intra- and interannual coarse sediment dynamics in a high-mountain catchment. Zeitschrift für Geomorphologie 55(2): 67–81.

Bimböse, M., Schmidt, K.-H. & Morche D. (2010): High resolution quantification of slope-channel coupling in an Alpine geosystem. IAHS Publication 337. IAHS Press, Wallingford, 300–308.

Bishop, M.P., James, L.A., Shroder Jr., J.F. & Walsh, S.J. (2012): Geospatial technologies and digital geomorphological mapping. Concepts, issues and research. Geomorphology 137(1), 5-26.

Bishop, M.P. & Shroder Jr., J.F. (2004): GIScience and mountain geomorphology: Overview, feedbacks, and research directions. In: M. P. Bishop & Shroder Jr., J.F. (eds.): Geographic Information Science and Mountain Geomorphology. Springer Verlag, Berlin, Heidelberg, 1-31.

Björnsson, H., Gjessing, Y., Hamran, S.-E., Hagen, J.O., Liestøl, O., Pálsson,

F. & Erlingsson, B. (1996): The thermal regime of sub-polar glaciers mapped by multi-frequency radio-echo sounding. Journal of Glaciology 42(140), 23-32.

Blaschke, T. (2000): A multi-scalar GIS/image processing approach for landscape monitoring of mountainous areas. In: R. Bottarin, Tappeiner, U. (eds.): Interdisciplinary Mountain Research. Blackwell Verlag, Bozen, 44-57.

Blaschke, T., Gläßler, C. & Lang, S. (2002): Bildverarbeitung in einer integrierten GIS/Fernerkundungsumgebung - Trends und Konsequenzen. In: Blaschke, T. (ed.): Fernerkundung und GIS. Neue Sensoren - innovative Methoden. Herbert Wichmann Verlag, Heidelberg, 1-9.

Blaschke, T. (2010): Review article: Object based image analysis for remote sensing. ISPRS Journal of Photogrammetry and Remote Sensing 65, 2-16.

Blaschke, T. & Hay, G. (2001): Object-oriented image analysis and scale-space: theory and methods for modeling and evaluating multiscale landscape structure. International Archives of Photogrammetry and Remote Sensing 34(4/W5), 22-29.

Blaschke, T., Lang, S. & Hay, G.J. (2008): Object-based image analysis. Spatial concepts for knowledge-driven remote sensing applications. Springer Verlag, Berlin, Heidelberg.

Błaszczyk, M., Jania, J. A. & Hagen, J.O. (2009): Tidewater glaciers of Svalbard: Recent changes and estimates of calving fluxes. Polish Polar Research 30(2), 85-142.

Blotevogel, H.H. (1997): Einführung in die Wissenschaftstheorie: Konzepte der Wissenschaft und ihre Bedeutung für die Geographie. Diskussionspapier 1/1997, Geographisches Institut, Duisburg.

Bolch T., Kulkarni, A., Kääb, A., Huggel, C., Paul, F., Cogley, J.G., Frey, H., Kargel, J.S., Fujita, K., Scheel, M., Bajracharya, S. & Stoffel, M. (2012): The State and Fate of Himalayan Glaciers. Science 336(6079), 310-314.

Braun, M. (2001): Ablation on the ice cap of King George Island (Antarctica). An approach from field measurements, modelling and remote sensing. PhD thesis, Department of Physical Geography, Albert–Ludwigs–Universität Freiburg.

Breiman, L. (2001): Random forests. Machine Learning 45(1), 5-32.

Brenning, A. (2009): Benchmarking classifiers to optimally integrate terrain analysis and multispectral remote sensing in automatic rock glacier detection. Remote Sensing of Environment 113, 239–247.

Brenning, A., Long, S. & Fieguth, P. (2012): Detecting rock glacier flow structures using Gabor filters and IKONOS imagery. Remote Sensing of Environment 125, 227-237.

Briggs, D.J., Smithson, P., Addison, K., & Atkinson, K. (1997): Fundamentals of the Physical Environment. Routledge, London, New York.

Brocklehurst, S. & Whipple, K. (2002): Glacial erosion and relief production in the Eastern Sierra Nevada, California. Geomorphology 42, 1–24.

Brown, I.A., Klingbjer, P. & Dean A. (2005): Problems with the retrieval of glacier net surface balance from SAR imagery. Annals of Glaciology 42(1), 209-216.

Brown, L.G. (1992): A survey of image registration techniques. Computing Surveys 24(4), 325–376.

Bruzzone, L. & Marconcini, M. (2009): Toward the automatic updating of land-cover-maps by a domain-adaptation SVM classifier and a circular validation strategy. IEEE Transactions on Geoscience and Remote Sensing 47(4), 1108–1122.

Bruzzone, L., Marconcini, M., Wegmüller, U. & Wiesmann, A. (2004): An advanced system for the automatic classification of multitemporal SAR images. IEEE Transactions on Geoscience and Remote Sensing 42(6), 1321–1334.

Budd, W.F. (1975): A first simple model for periodically self-surging glaciers. Journal of Glaciology 14(70), 3-21.

Burgess, E.W., Forster, R.R., Larsen, C.F. & Braun, M. (2012): Surge dynamics on Bering Glacier, Alaska, in 2008–2011. The Cryosphere Discussions 6, 1181-1204, doi:10.5194/tcd-6-1181-2012.

Burt, T.P. & Allison, R.J. (2010): Sediment cascades in the environment: an integrated approach. In: Burt, T.P. & Allison, R.J. (eds.): Sediment cascades: an integrated approach. John Wiley & Sons, Chichester, UK, 1-15.

Caine, N. (1974): The geomorphic processes of the alpine environment. In: Ives, J. & Barry, R. (eds.): Arctic and Alpine Environments, Methuen, London, 721-748.

Caritas (2010): Zonificación de las areas suceptibles a procesos hidrogeomorfológicos en el eje Vega de San Antonio, urbanización Don Perucho - El Arenal - La Pueblita, Municipio Libertador, Estado Mérida. http://www.caritasvenezuela.org.ve/zonificacion.pdf (30.11.2010).

Casey, K.A. (2011): Supraglacial dust and debris characterization via in situ and optical remote sensing methods. PhD thesis, Department of Geosciences, University of Oslo.

Casey, K., Kääb A. & Benn D. (2012): Geochemical characterization of supraglacial debris via in situ and optical remote sensing methods: a case study in Khumbu Himalaya, Nepal. The Cryosphere 6(1), 85-100.

Castilla, G., Hernando, A., Zhang, C., Mazumdar, D. & McDermid, G.J. (2012): An integrated framework for assessing the accuracy of GEOBIA land cover products. Proceedings of the 4th GEOBIA, Rio de Janeiro, 572-575.

Castree, N. (2005): Is geography a science? In: Castree, N., Rogers, A. & Sher-

man, D.J. (eds.): Questioning geography: fundamental debates. Blackwell Publishing, Malden, Oxford, Carlton.

Chiverrell, R.C., Thomas, G.S.P. & Foster, G.C. (2008): Sediment–landform assemblages and digital elevation data: Testing an improved methodology for the assessment of sand and gravel aggregate resources in north-western Britain. Engineering Geology 99(1–2), 40-50.

Chorley, R.J. (1978): Bases for theory in geomorphology. In: Embleton, C., Brunsden, D. & Jones, D.K.C. (eds.): Geomorphology: present problems and future prospects. Oxford University Press, Oxford, 1–13.

Chorley, R.J. & Kennedy, B. (1971): Physical geography - A systems approach. Prentice Hall, London.

Clarke, G.K.C., Collins, S.G. & Thompson, D.E. (1984): Flow, thermal structure and subglacial conditions of a surge-type glacier. Canadian Journal of Earth Sciences 21(2), 232-240.

Clarke, G.K.C. (1976): Thermal regulation of glacier surging. Journal of Glaciology 16(74), 231-250.

Cohen, J. (1960): A coefficient of agreement for nominal scales. Educational and Psychological Measurement 20, 37–46.

Congalton, R. & Green, K. (1999): Assessing the Accuracy of Remotely Sensed Data: Principles and Practices. Lewis Publishers, New York.

Copland, L., Sharp, M. & Dowdeswell, J.A. (2003): The distribution and flow characteristics of surge-type glaciers in the Canadian High Arctic, Annals of Glaciology 36, 73-81.

Copland, L. Sylvestre, T., Bishop, M.P., Shroder, J.F., Seong, Y.B., Owen, L.A., Bush, A., & Kamb, U. (2011): Expanded and recently increased glacier surging in the Karakoram. Arctic, Antarctic, and Alpine Research 43(4), 503-516.

Costantini, M. (1998): A novel phase unwrapping method based on network programming. IEEE Transactions on Geoscience and Remote Sensing 36(3), 813–821.

Cox, N.J. (2007): Kinds and problems of geomorphological explanation. Geomorphology 88(1–2), 46–56

Crosetto, M., Monserrat, O., Bremmer, C., Hanssen R., Capes, R. & Marsh, S. (2008): Ground motion monitoring using SAR interferometry: quality assessment. European Geologist 26, 12–15.

Cuffey, K. & Paterson, W.S.B. (2010[4]): The physics of glaciers. Butterworth-Heinemann, Elsevier, Burlington, MA.

Cumming, I., Valero, J.L., Vachon, P.W., Mattar, K. Geudtner, D. & Gray, L. (1997): Glacier flow measurements with ERS tandem mission data. Proceedings of the ESA Fringe 1996, Zurich (ESA SP–406), 353–362.

Curran, P.J. (1987a): On defining remote sensing. Photogrammetric Engineering and Remote Sensing 53(3), 305-306.

Curran, P.J. (1987b): Review article: Remote sensing methodologies and geography. International Journal of Remote Sensing 8(9), 1255-1275.

Currenti, G. Solaro, G., Napoli, R., Pepe, A., Bonaccorso, A., Del Negro, C. & Sansosti, E. (2012): Modeling of ALOS and COSMO-SkyMed satellite data at Mt Etna: Implications on relation between seismic activation of the Pernicana fault system and volcanic unrest. Remote Sensing of Environment 125, 64-72.

Danklmayer, A., Doring, B.J., Schwerdt, M. & Chandra, M. (2009): Assessment of Atmospheric Propagation Effects in SAR Images. IEEE Transactions on Geoscience and Remote Sensing 47(10), 3507-3518.

Davies, T.R.H. & Korup, O. (2010): Sediment cascades in active landscapes. In: Burt, T.P. & Allison, R.J. (eds.): Sediment cascades: an integrated approach. John Wiley & Sons, Ltd, Chichester, UK, 89-115.

Debella-Gilo, M. (2011): Matching of repeat remote sensing images for precise analysis of mass movements. PhD thesis, Department of Geosciences, University of Oslo.

Debella-Gilo, M. & Kääb, A. (2012): Measurement of surface displacement and deformation of mass movements using least squares matching of repeat high resolution satellite and aerial images. Remote Sensing 4(1), 43-67.

de Lange, N. (2006^2): Geoinformatik in Theorie und Praxis. Springer, Berlin, Heidelberg.

Dikau, R. (1996): Geomorphologische Reliefklassifikation und -analyse. In: Mäus-
bacher, R. & Schulte, A. (eds.): Beiträge zur Physiogeographie: Festschrift für Dietrich Barsch. Heidelberger Geographische Arbeiten 104, 15-23.

d'Oleire-Oltmanns, S., Eisank, C., Drăguţ, L., Schrott, L., Marzolff, I. & Blaschke, T. (2012): Object-based landform mapping at multiple scales from Digital Elevation Models (DEMs) and aerial photographs. Proceedings of the 4th GEOBIA, Rio de Janeiro, 496-500.

Dowdeswell, J.A. & Benham, T.J. (2003): A surge of Perseibreen, Svalbard, examined using aerial photography and ASTER high-resolution satellite imagery. Polar Research 22(2), 373–383.

Dowdeswell, J.A., Hamilton, G.S. & Hagen, J.O. (1991): The duration of the active phase on surge-type glaciers - contrasts between Svalbard and other regions. Journal of Glaciology 37, 388-400.

Dowdeswell, J.A., Hodgkins, R., Nuttall, A.M., Hagen, J.O. & Hamilton, G.S. (1995): Mass-Balance Change as a Control on the Frequency and Occurrence of Glacier Surges in Svalbard, Norwegian High Arctic. Geophysical Research Letters 22, 2909-2912.

Dowdeswell, J.A., Unwin, B., Nuttall, A.M. & Wingham, D.J. (1999): Velocity structure, flow instability and mass flux on a large Arctic ice cap from satellite radar inferometry. Earth and Planetary Science Letters 167(3-4),

131-140.

Drăguţ, L. & Blaschke, T. (2006): Automated classification of landform elements using object-based image analysis. Geomorphology 81, 330-344.

Drăguţ, L. & Blaschke, T. (2008): Terrain segmentation and classification using SRTM data. In: Zhou, Q., Lees, B. & Tang, G. (eds.): Advances in digital terrain analysis. Springer, Berlin, Heidelberg, 141-158.

Drăguţ, L. & Eisank, C. (2012): Automated object-based classification of topography from SRTM data. Geomorphology 141, 21-33.

Drăguţ, L. & Eisank, C. (2011): Review paper: Object representations at multiple scales from digital elevation models. Geomorphology 129(3–4), 183-189.

Drăguţ, L., Eisank, C. & Strasser, T. (2011): Local variance for multi-scale analysis in geomorphometry. Geomorphology 130(3-4), 162-172.

Drăguţ, L., Tiede, D. & Levick, S.R. (2010): ESP: a tool to estimate scale parameter for multiresolution image segmentation of remotely sensed data. International Journal of Geographical Information Science 24(6), 859-871.

Dunse, T. (2011): Glacier dynamics and subsurface classification of Austfonna, Svalbard: Inferences from observations and modelling. PhD thesis, Department of Geosciences, University of Oslo.

Egner, H. & von Elverfeldt, K. (2009): A bridge over troubled waters? Systems theory and dialogue in geography. Area 41(3), 319-328.

Eiken, T., Hagen, J.O. & Melvold, K. (1997): Kinematic survey of geometry changes on Svalbard glaciers. Annals of Glaciology 24, 157-163.

Eiken, T. & Sund, M. (2012): Photogrammetric methods applied to Svalbard glaciers: accuracies and challenges. Polar Research 31(18671), http://dx.doi.org/10.3402/polar.v31i0.18671.

Eisank, C., Drăguţ, L. & Blaschke, T. (2011): A generic procedure for semantics-oriented landform classification in object-based image analysis. In: Hengl, T., Evans, I.S., Wilson, J.P. & Gould, M. (eds.): Proceedings of Geomorphometry 2011, Redlands, CA, 125-128.

Eisank, C., Drăguţ, L., Götz, J. & Blaschke, T. (2010): Developing a semantic model of glacial landforms for object-based terrain classification - the example of glacial cirques. In: Addink, E.A. & Van Coillie, F.M.B. (eds.): GEOBIA 2010 - Geographic Object-Based Image Analysis. Ghent, Belgium. ISPRS XXXVIII-4/C7, ISSN 1682-1777.

Eldhuset, K., Andersen, P.H., Hauge, S., Isaksson, E. & Weydahl, D.J. (2003): ERS tandem InSAR processing for DEM generation, glacier motion estimation and coherence analysis on Svalbard. International Journal of Remote Sensing 24(7), 1415-1437.

Engeset, R.V. (1999): Comparison of annual changes in winter ERS-1 SAR images and glacier mass balance of Slakbreen, Svalbard. International Journal of Remote Sensing 20(2), 259-271.

Engeset, R.V. & Weydahl, D.J. (1998): Analysis of glaciers and geomorphology on Svalbard using multitemporal ERS-1 SAR images. IEEE Transactions on Geoscience and Remote Sensing 36(6), 1879-1887.

ERSDAC (2005): ASTER User's guide - Part I. http://www.science.aster.ersdac. or.jp/en/documnts/users_guide/part1/pdf/Part1_4E.pdf, 04.11.2011.

ESA (2012): Earthnet Online: Missions. https://earth.esa.int/web/guest/missions (12.09.2012).

Etzelmüller, B., Ødegård, R., Berthling, I., & Sollid, J. (2001): Terrain parameters and remote sensing data in the analysis of permafrost distribution and periglacial processes: principles and examples from southern Norway. Permafrost and Periglacial Processes 12, 79-92.

Evans, I.S. (2012): Geomorphometry and landform mapping: What is a landform? Geomorphology 137, 94-106.

Evans, C., Jones, R., Svalbe, I. & Berman, M. (2002): Segmenting Multispectral Landsat TM Images into Field Units. IEEE Transactions on Geoscience and Remote Sensing 40(5), 1054-1064.

Farr, T.G., Rosen, P.A., Caro, E., Crippen, R., Duren, R., Hensley, S., Kobrick, M., Paller, M., Rodriguez, E., Roth, L., Seal, D., Shaffer, S., Shimada, J., Umland, J., Werner, M., Oskin, M., Burbank, D. & Alsdorf, D. (2007): The Shuttle Radar Topography Mission. Reviews of Geophysics 45, RG2004, doi:10.1029/2005RG000183.

Fensholt, R. & Proud, S.R. (2012): Evaluation of Earth Observation based global long term vegetation trends — Comparing GIMMS and MODIS global NDVI time series. Remote Sensing of Environment 119, 131–147.

Ferentinou, M., Karymbalis, E., Charou, E. & Sakellariou, M. (2011): Using self organising maps in applied geomorphology. In: Mwasiagi, J.I. (ed.): Self organizing maps - applications and novel algorithm design. InTech, Rijeka, 274-298.

Ferretti, A., Prati, C. & Rocca, F. (2001): Permanent scatterers in SAR interferometry. IEEE Transactions on Geoscience and Remote Sensing 39(1), 8–20.

Feyerabend, P. (1998[3]): How to defend society against science. In: Klemke, E.D., Hollinger, R., Rudge, D.W. & Kline, A.D. (eds.): Introductory readings in the philosophy of science. Prometheus Books, Amherst.

Fowler, A.C. (1987): A theory of glacier surges. Journal of Geophysical Research 92(B9), 9111-9120.

Fowler, A.C., Murray, T. & Ng, F.S.L. (2001): Thermally controlled glacier surging. Journal of Glaciology 47(159), 527-538.

Friedl, M.A. & Brodley, C.E. (1997): Decision tree classification of land cover from remotely sensed data. Remote Sensing of Environment 61(3), 399-409.

Frey, H. & Paul, F. (2012): On the suitability of the SRTM DEM and ASTER GDEM for the compilation of topographic parameters in glacier inventories.

International Journal of Applied Earth Observation and Geoinformation 18, 480–490.

Fussell, J., Rundquist, D. & Harrington, J.A. (1986): On defining remote sensing. Photogrammetric Engineering and Remote Sensing 52(9), 1507-1511.

Fussell, J., Rundquist, D. & Harrington, J.A. (1987): On defining remote sensing, a response. Photogrammetric Engineering and Remote Sensing 53(8), 1096.

Gabriel, A.K., Goldstein, R.M. & Zebker, H.A. (1989): Mapping small elevation changes over large areas: differential radar interferometry. Journal of Geophysical Research 94(B7), 9183–9191.

García-Haro, F., Gilabert, M. & Melía, J. (1996): Linear spectral mixture modelling to estimate vegetation amount from optical spectral data. International Journal of Remote Sensing 17(17), 3373-3400.

Gardelle, J., Berthier, E. & Arnaud, Y. (2012): Impact of resolution and radar penetration on glacier elevation changes computed from multi-temporal DEMs. Journal of Glaciology 58, 419–422.

Gardner, A.S., Moholdt, G., Wouters, B., Wolken, G.J., Burgess, D.O., Sharp, M.J., Cogley, J.G., Braun, C. & Labine, C. (2011): Sharply increased mass loss from glaciers and ice caps in the Canadian Arctic Archipelago. Nature 473, 357-360.

Geist, T. & Stötter, J. (2010): Airborne laser scanning in glacier studies. In: Pellikka, P. & Rees, W.G. (eds.): Remote sensing of glaciers. Techniques for topographic, spatial and thematic mapping of glaciers. Taylor & Francis, London, 179-194.

Gens, R. & van Genderen, J.L. (1996): SAR interferometry – issues, techniques, applications. International Journal of Remote Sensing 17(10), 1803–1835.

Gilabert, M., Gonzáles-Piqueras, J., García-Haro, F., & Melía, J. (2002): A generalized soil-adjusted vegetation index. Remote Sensing of Environment 82, 303-310.

Goldstein, R.M., Engelhard, R., Kamb, B. & Frolich, R. (1993): Satellite radar interferometry for monitoring ice sheet motion: application to an Antarctic ice stream. Science 262, 1525– 1530.

Goldstein, R.M., Zebker, H.A. & Werner, C.L. (1988): Satellite radar interferometry: two–dimensional phase unwrapping. Radio Science 23(4), 713–720.

Goode, J.R., Luce, C.H. & Buffington, J.M. (2012): Enhanced sediment delivery in a changing climate in semi-arid mountain basins: Implications for water resource management and aquatic habitat in the northern Rocky Mountains. Geomorphology 139-140, 1–15.

Goodfellow, B.W. & Boelhouwers, J. (2012): Hillslope processes in cold envi-

ronments: An illustration of high latitude mountain and hillslope processes and forms. In: Shroder, J. Jr, Marston R.A., & Stoffel, M. (eds.): Treatise on geomorphology: Mountain and hillslope geomorphology. Academic Press, San Diego, CA.

Grant, K.L., Stokes, C.R. & Evans, I.S. (2009): Identification and characteristics of surge-type glaciers on Novaya Zemlya, Russian Arctic. Journal of Glaciology 55(194), 960-972.

Gruber, S. & Haeberli, W. (2007): Permafrost in steep bedrock slopes and its temperature-related destabilization following climatic change. Journal of Geophysical Research 112, F02S18.

Gruber, S., Huggel, C. & Pike, R. (2009): Modelling mass movements and landslide susceptibility. In: Hengl, T. & Reuter, H.I. (eds.): Geomorphometry: concepts, software, applications. Developments in Soil Science 33. Elsevier, Amsterdam, Oxford, 527-550.

Gude, M., Daut, G., Dietrich, S., Mäusbacher, R., Jonasson, C., Bartsch, A. & Scherer, D. (2002): Towards an integration of process measurements, archive analysis and modelling in geomorphology – the Kärkevagge experimental site, Abisko area, northern Sweden. Geografiska Annaler 84A(3–4), 205–212.

Haeberli, W. (1996): On the morphodynamics of ice/debris-transport systems in cold mountain areas. Norsk Geografisk Tidsskrift – Norwegian Journal of Geography 50, 3–9.

Haeberli, W., Frauenfeld, R., Hoelzle, M. & Maisch, M. (1999): On the rates and acceleration trends of global glacier mass changes. Geografiska Annaler 81A(4), 585-591.

Haeberli, W., Maisch, M. & Paul, F. (2002): Mountain glaciers in global climate-related observation networks. WMO Bulletin 51(1), 18-25.

Hagen, J.O., Eiken, T., Kohler, J. & Melvold, K. (2005): Geometry changes on Svalbard glaciers - mass balance or dynamic response? Annals of Glaciology 42(1), 255-261.

Hagen, J.O., Liestøl, O., Roland, E. & Jørgensen, T. (1993): Glacier atlas of Svalbard and Jan Mayen. Meddelelser 129, Norsk Polarinstitutt, Oslo.

Hagen, J.O., Melvold, K., Pinglot, J.F. & Dowdeswell, J.A. (2003): On the net mass balance of the glaciers and ice caps in Svalbard, Norwegian Arctic. Arctic, Antarctic and Alpine Research 25(2), 264-270.

Hagen, J.O. & Sætrang, A. (1991): Radio-echo soundings of sub-polar glaciers with low-frequency radar. Polar Research 9, 99-107.

Hall, D. & Martinec, J. (1986): Remote sensing of ice and snow. Chapman and Hall, London, New York.

Hallet, B., Hunter, L., & Bogen, J. (1996): Rates of erosion and sediment evacuation by glaciers: A review of field data and their implications. Global and Planetary Change 12, 213–235.

Hanssen, R.F. (2001): Radar interferometry: data interpretation and error analysis. Remote sensing and digital image processing. Kluwer, Dordrecht.

Haralick, R., Shanmugan, K. & Dienstein, I. (1973): Textural features for image classification. IEEE Transactions on Systems, Man and Cybernetics 3(1), 610–621.

Harvey, A.M. (2010): Local buffers to the sediment cascade. In: Burt, T.P. & Allison, R.J. (eds.): Sediment cascades: an integrated approach. John Wiley & Sons, Chichester, UK, 153-180.

Haug, T., Kääb, A. & Skvarca, P. (2010): Monitoring ice shelf velocities from repeat MODIS and Landsat data - a method study on the Larsen C ice shelf, Antarctic Peninsula, and 10 other ice shelves around Antarctica. The Cryosphere 4(1), 161-178.

Hay, G.J. & Castilla, G. (2008): Geographic Object-Based Image Analysis (GEOBIA): A new name for a new discipline. In: Blaschke, T., Lang, S. & Hay, G.J. (eds.): Object-based image analysis. Spatial concepts for knowledge-driven remote sensing applications. Springer Verlag, Berlin, Heidelberg, 75-89.

Heid, T. (2011): Deriving glacier surface velocities from repeat optical images. PhD thesis, Department of Geosciences, University of Oslo.

Heid, T. & Kääb, A. (2012a): Repeat optical satellite images reveal widespread and long term decrease in land-terminating glacier speeds. The Cryosphere 6, 467-478.

Henderson, I.H.C., Lauknes, T.R., Osmundsen, P.T., Dehls, J., Larsen, Y. & Redfield, T.F. (2011): A structural, geomorphological and InSAR study of an active rock slope failure development. In: Jaboyedoff, M. (ed.): Slope Tectonics. Special Publications 351. Geological Society, London, 185–199.

Hengl, T. & Evans, I.S. (2009): Mathematical and digital models of the land surface. In: Hengl, T. & Reuter, H.I. (eds.): Geomorphometry: concepts, software, applications. Developments in Soil Science 33, Elsevier, Amsterdam, Oxford, 31-64.

Hengl, T. & Reuter, H.I. (eds., 2009): Geomorphometry: concepts, software, applications. Developments in Soil Science 33, Elsevier, Amsterdam, Oxford.

Hock, R., de Woul, M., Radic, V. & Dyurgerov, M. (2009): Mountain glaciers and ice caps around Antarctica make a large sea-level rise contribution. Geophys. Res. Lett. 36, L07501 (2009).

Høgda, K.A., Storvold, R. & Lauknes, T.R. (2010): SAR imaging of glaciers. In: Pellikka, P. & Rees, W.G. (eds.): Remote sensing of glaciers. Techniques for topographic, spatial and thematic mapping of glaciers. Taylor & Francis, London, 153-178.

Hölbling, D., Füreder, P., Antolini, F., Cigna, F., Casagli, N. & Lang, S. (2012): A semi-automated object-based approach for landslide detection

validated by persistent scatterer interferometry measures and landslide inventories. Remote Sensing 4(5), 1310-1336.

Honikel, M. (1999): Strategies and methods for the fusion of digital elevation models from optical and SAR data. Proceedings of the Joint ISPRS/EARSeL Workshop 'Fusion of Sensor Data, Knowledge Sources and Algorithms for Extraction and Classification of Topographic Objects', Valladolid, Spain, 83-89.

Honikel, M. (2002): Fusion of spaceborne stereo-optical and interferometric SAR data for digital terrain model generation. Mitteilungen des Institutes für Geodäsie und Photogrammetrie 76, Eidgenössisch-Technische Hochschule, Zurich.

Hooper, A. (2008): A multi-temporal InSAR method incorporating both persistent scatterer and small baseline approaches. Geophysical Research Letters 35, L16302, doi:10.1029/2008GL034654.

Hooper, A., Segall, P. & Zebker, H. (2007): Persistent scatterer interferometric synthetic aperture radar for crustal deformation analysis, with application to Volcán Alcedo, Galápagos. Journal of Geophysical Research 112, B07407, doi:10.1029/2006JB004763.

Hooper, A., Zebker, H., Segall, P. & Kampes, B. (2004): A new method for measuring deformation on volcanoes and other natural terrains using InSAR persistent scatterers. Geophysical Research Letters 31, L23611, doi:10.1029/2004GL021737.

Huang, C., Davis, L.S. & Townshend J.R.G. (2002): An assessment of support vector machines for land cover classification. International Journal of Remote Sensing 23(4), 725-749.

Huete, A., Jackson, R. & Post, D. (1985): Spectral response of a plant canopy with different soil backgrounds. Remote Sensing of Environment 17, 37-53.

Huggel, C., Clague, J.J. & Korup, O. (2012): Is climate change responsible for changing landslide activity in high mountains? Earth Surface Processes and Landforms 37, 77–91.

Huggel, C., Kääb, A., Haeberli, W. & Krummenacher, B. (2003): Regional scale GIS models for assessment of hazards from glacier lake outbursts: evaluation and application in the Swiss Alps. Natural Hazards and Earth Systems Sciences 3, 647-662.

Huggel, C., Kääb, A. & Salzmann, N. (2004): GIS-based modeling of glacial hazards and their interactions using Landsat-TM and IKONOS imagery. Norsk Geografisk Tidsskrift 58, 61-73.

Huggel C., Schneider, D., Julio Miranda, P., Delgado Granados, H. & Kääb, A. (2008): Evaluation of ASTER and SRTM DEM data for lahar modeling: A case study on lahars from Popocatépetl Volcano, Mexico. Journal of Volcanology and Geothermal Research 170(1-2), 99-110.

Humlum, O., Solheim, J.-E. & Stordahl, K. (2011): Identifying natural con-

tributions to late Holocene climate change. Global and Planetary Change 79, 145–156.

Hutchinson, M.F. & Gallant, J.C. (2000): Digital elevation models and representation of terrain shape. In: Wilson, J.P., Gallant, J.C. (eds.): Terrain Analysis: Principles and Applications. John Wiley and Sons, New York, 29–50.

Ingeomin (2006): Efecto social del evento de Santa Cruz de Mora. Emergencia en el Mocotíes. Encuentro Binacional Colombo-Venezolano en el marco del Proyecto Multinacional Andino: Geociencias para las Comunidades Andinas. Instituto Nacional de Geología y Minería de Venezuela. Mérida, Venezuela.

IPCC (2001): Climate Change 2001. The Scientific Basis. In: Houghton, J.T., Ding, Y., Griggs, D.J., Noguer, M., van der Linden, P.J., Dai, X., Maskell, K. & Johnson, C.A. (eds.): Contribution of Working Group I to the Third Assessment Report of the Intergovernmental Panel on Climate Change (IPCC). Cambridge University Press, Cambridge, New York.

IPCC (2007): Climate Change 2007. The Physical Science Basis. In: Solomon, S., Qin, D., Manning, M., Chen, Z., Marquis, M., Averyt, K.B., Tignor, M. & Miller, H.L. (eds.): Contribution of Working Group I to the Fourth Assessment Report of the Intergovernmental Panel on Climate Change (IPCC). Cambridge University Press, Cambridge, New York.

Ives, D. & Messerli, B. (2001): Perspektiven für die zukünftige Gebirgsforschung und Gebirgsentwicklung. Geographische Rundschau 53(12), 4–7.

Ives, J., Messerli, B. & Spiess, E. (1997): Mountains of the World - A Global Priority. In: Messerli, B. & Ives, J. (eds.): Mountains of the World. A Global Priority. Parthenon, New York, 1-15.

Jackson, E., Kostaschuk, A. & MacDonald, M. (1987): Identification of debris flow hazard on alluvial fans in the Canadian Rocky Mountains. In: Costa, J.E. & Wieczorek, G.F. (eds.): Debris flows/avalanches: process, recognition and mitigation. Geological Society of America, Boulder, Colorado, 115-124.

Jacob, T., Wahr, J., Pfeffer, W.T. & Swenson, S. (2012): Recent contributions of glaciers and ice caps to sea level rise. Nature 482, 514–518.

Jansa, J., Blöschl, G., Kirnbauer, R., Kraus, K. & Kuschnig, G. (2002): Schneemonitoring mittels Fernerkundung. In: Blaschke, T. (ed.): Fernerkundung und GIS. Neue Sensoren - innovative Methoden. Herbert Wichmann Verlag, Heidelberg, 241-250.

Jensen, J.R. (2005[3]): Introductory digital image processing: a remote sensing perspective. Prentice Hall, Upper Saddle River.

Jiskoot, H., Boyle, P. & Murray, T. (1998): The incidence of glacier surging in Svalbard: evidence from multivariate statistics. Computational Geosciences 24(4), 387–399.

Jiskoot, H., Murray, T. & Boyle, P. (2000): Controls on the distribution of surge-type glaciers in Svalbard. Journal of Glaciology 46(154), 412–422.

Johannesson, T. & Sigurdsson, O. (1998): Interpretation of glacier variations in Iceland 1930–1995. Jökull 45, 27–33.

Jones, A.D. (1988): Remote sensing and geography. Australian Geographical Studies 26(1), 63-69.

Joughin, I. (2002): Ice-sheet velocity mapping: a combined interferometric and speckle-tracking approach. Annals of Glaciology 34, 195–201.

Joughin, I., Kwok, R. & Fahnestock, M.A. (1998): Interferometric estimation of three-dimensional ice-flow using ascending and descending passes. IEEE Transactions on Geoscience and Remote Sensing 36(1), 25-37.

Joughin, I., Smith, B.E. & Abdalati, W. (2010a): Glaciological advances made with interferometric synthetic aperture radar. Journal of Glaciology 56(200), 1026-1042.

Joughin, I., Smith, B.E., Howat, I.M., Scambos, T.A. & Moon, T. (2010b): Greenland flow variability from ice-sheet-wide velocity mapping. Journal of Glaciology 56(197), 415–430.

Joughin, I., Tulaczyk, S., Fahnestock, M.A. & Kwok, R. (1996): A mini–surge on the Ryder Glacier, Greenland, observed by satellite radar interferometry. Science 274, 228–230.

Kääb, A. (2003): Rapid ASTER imaging facilitates timely sssessment of glacier hazards and disasters. EOS Transactions 84(13), 117–124.

Kääb, A. (2005a): Combination of SRTM3 and repeat ASTER data for deriving alpine glacier flow velocities in the Bhutan Himalaya. Remote Sensing of Environment 94(4), 463-474.

Kääb, A. (2005b): Remote sensing of mountain glaciers and permafrost creep. Habilitation thesis, Department of Geography, Schriftenreihe Physische Geographie 48, Zürich.

Kääb, A. (2010): The role of remote sensing in worldwide glacier monitoring. In: Pellikka, P. & Rees, W.G. (eds.): Remote sensing of glaciers. Techniques for topographic, spatial and thematic mapping of glaciers. Taylor & Francis, London, 286-296.

Kääb, A., Berthier, E., Nuth, C., Gardelle, J. & Arnaud, Y. (2012): Contrasting patterns of early twenty-first-century glacier mass change in the Himalayas. Nature 488(7412), 495-498.

Kääb, A., Huggel, C., Fischer, L., Guex, S., Paul, F., Roer, I., Salzmann, N., Schlaefli, S., Schmutz, K., Schneider, D., Strozzi, T. & Weidmann, Y. (2005a): Remote sensing of glacier- and permafrost-related hazards in high mountains: an overview. Natural Hazards and Earth System Science 5(4), 527-554.

Kääb A., Huggel, C., Paul, F., Wessels, R., Raup, B., Kieffer H. & Kargel, J. (2003): Glacier monitoring from ASTER imagery: accuracy and ap-

plications. Proceedings of the EARSeL LISSIG Workshop 'Observing our Cryosphere from Space', Bern, March 2002, EARSeL e-Proceedings 2, 43-53.

Kääb, A., Lefauconnier, B. & Melvold, K. (2005b): Flow field of Kronebreen, Svalbard, using repeated Landsat 7 and ASTER data. Annals of Glaciology 42(1), 7-13.

Kaitna, R., Schneuwly-Bollschweiler, M., Sausgruber, T., Moser, M., Stoffel, M. & Rudolf-Miklau, F. (2013): Susceptibility and triggers for debris flows: emergence, loading, release and entrainment. In: Schneuwly-Bollschweiler, M., Stoffel, M. & Rudolf-Miklau, F. (eds.): Dating torrential processes on fans and cones. Methods and their application for hazard and risk assessment. Advances in Global Change Research 47(1), Springer Science+Business Media, Dordrecht, 33-49.

Kamb, B. (1987): Glacier Surge Mechanism Based on Linked Cavity Configuration of the Basal Water Conduit System. Journal of Geophysical Research 92(B9), 9083-9100.

Kamb, B., Raymond, C.F., Harrison, W.D., Engelhardt, H., Echelmeyer, K., Humphrey, N., Brugman, M.M. & Pfeffer, T. (1985): Glacier surge mechanism: 1982–1983 surge of Variegated Glacier, Alaska. Science 227, 469–479.

Karkee, M., Kusanagi, M. & Steward, B.L. (2006): Fusion of optical and InSAR DEMs: improving the quality of free data. Paper 061172, ASABE Annual Meeting, Portland, Oregon.

Keiler, M., Kellerer-Pirklbauer, A. & Otto, J.-C. (2012): Concepts and implications of environmental change and human impact: studies from Austrian geomorphological research. Geografiska Annaler 94A(1), 1–5.

Kellenberger, T. W. (1996): Erfassung der Waldfläche in der Schweiz mit multispektralen Satellitenbilddaten. Grundlagen, Methodenentwicklung und Anwendung. Geographisches Institut der Universität Zürich, Remote Sensing Series 28, Zurich.

Kelly, R.E.J., Engeset, R., Kennett, M., Barrett, E.C. & Theakstone, W. (1997): Characteristic snow and ice properties of a Norwegian ice cap determined from complex ERS SAR. Proceedings of the 3rd ERS Symposium (ESA), Florence, CD-ROM.

Klemenjak, S., Waske, B., Valero, S. & Chanussot, J. (2012): Automatic detection of rivers in high-resolution SAR data. IEEE Journal of Selected Topics in Applied Earth Oberservation and Remote Sensing 5(5), 1-9.

Knorr, K.D. (1979): Tinkering towards success: Prelude to a theory of scientific practice. Theory and Society 8(3), 347-376.

Koch, B., Jochum, M., Ivits, E. & Dees, M. (2003): Pixelbasierte Klassifizierung im Vergleich und zur Ergänzung zum objektbasierten Verfahren. Photogrammetrie Fernerkundung Geoinformation 3, 195-204.

Kohavi, R. & John, G.H. (1997): Wrappers for feature subset selection. Arti-

ficial Intelligence 97, 273-324.

Konecny, G. (1999): Mapping from Space. Proceedings of the ISPRS Workshop 'Sensors and Mapping from Space 1999', Hannover. http://www.ipi.uni-hannover.de/128.html?iykibawfdqrlyuz, 27.11.2011.

König, M. (2004): Observing glaciers from space: surface type detection and mass balance monitoring using SAR satellite images. PhD thesis, Department of Geosciences, University of Oslo.

Korona, J., Berthier, E., Bernard, M., Remy, F. & Thouvenot, E. (2009): SPIRIT. SPOT 5 stereoscopic survey of polar ice: reference images and topographies during the fourth International Polar Year (2007-2009). ISPRS Journal of Photogrammetry and Remote Sensing 64, 204-212.

Kuhn, T.S. (1996[3]): The structure of scientific revolutions. University of Chicago Press, Chicago.

Kumar, V., Venkataraman, G., Larsen, Y., Høgda, K.A. (2011): SAR interferometry and offset tracking approaches for glacier movement estimation in the Himalaya. IEEE Proceedings of the International Geoscience and Remote Sensing Symposium (IGARSS) 2011, Vancouver, 3175–3178.

Kwok, R. & Fahnestock, M.A. (1996): Ice sheet motion and topography from radar interferometry. IEEE Transactions on Geoscience and Remote Sensing 34(1), 189–200.

Lafaille, J. (2005): Antecedentes de los eventos meteorológicos ocurridos en el valle del río Mocotíes y su impacto geomorfológico. Revista Geográfica Venezolana, Número Especial 1, 297-311.

Lakatos, I. (1970): Falsification and the methodology of scientific research programmes. In: Lakatos, I. & Musgrave, A. (eds.): Criticism and the growth of Knowledge. Cambridge University Press, Cambridge, 91-196.

Langley, K. (2007): Glacier subsurface interpretation combining ground penetrating radar and satellite synthetic aperture radar. PhD thesis, Department of Geosciences, University of Oslo.

Langley, K., Hamran, S.-E., Høgda, K.A., Storvold, R., Brandt, O., Kohler, J. & Hagen, J.O. (2008): From glacier facies to SAR backscatter zones via GPR. IEEE Transactions on Geoscience and Remote Sensing 46(9), 2506-2516.

Langley, K., Lacroix, P., Hamran, S.-E. & Brandt, O. (2009): Sources of backscatter at 5.3GHz from a superimposed ice and firn area revealed by multi-frequency GPR and cores. Journal of Glaciology 55(190), 373-383.

Laszlo, E. (1972a): The systems view of the world: the natural philosophy of the new developments in the sciences. George Braziller, New York.

Laszlo, E. (1972b): Introduction to systems philosophy: toward a new paradigm of contemporary thought. Gordon and Breach, New York.

Laszlo, E. (1996): The systems view of the world: a holistic vision for our time. Hampton Press, Cresskill, New Jersey.

Lauknes, T.R. (2010): Rockslide mapping in Norway by means of interferometric SAR time series analysis. PhD thesis, Department of Physics and Technology, University of Tromsø.

Lauknes, T.R., Piyush Shanker, A., Dehls, J.F., Zebker, H.A., Henderson, I.H.C. & Larsen, Y. (2010a): Detailed rockslide mapping in northern Norway with small baseline and persistent scatterer interferometric SAR time series methods. Remote Sensing of Environment 114(9), 2097-2109.

Lauknes, T.R., Zebker, H.A. & Larsen, Y. (2010b): InSAR deformation time series using an L1-norm small baseline approach. IEEE Transactions on Geoscience and Remote Sensing 49, 536-546.

Lavigne, F. & Thouret, J.C. (2002): Sediment transportation and deposition by rain-triggered lahars at Merapi Volcano, Central Java, Indonesia. Geomorphology 49, 45–69.

Lefauconnier, B. & Hagen, J.O. (1991): Surging and calving glaciers in eastern Svalbard. Meddelelser 116, Norsk Polarinstitutt, Oslo.

Li, Z.W., Ding, X.L. & Liu, G.X. (2003): Atmospheric effects on InSAR measurements - a review. Geomatics Research Australasia 79, 43-58.

Li, Z., Zhu, Q. & Gold, C. (2005): Digital terrain modeling: principles and methodology. CRC Press, Boca Raton.

Liestøl, O. (1969): Glacier surges in West Spitsbergen. Canadian Journal of Earth Sciences 6(4), 895–897.

Lillesand, T.M., Kiefer, R.W & Chipman, J.W. (2008[6]): Remote sensing and image interpretation. Wiley, Hoboken.

Liu, C.-C., Chang, Y.-C., Huang, S., Yan, S.-Y., Wu, F., Wu, A.-M., Kato, S. & Yamaguchi (2009): Monitoring the dynamics of ice shelf margins in Polar Regions with high-spatial- and high-temporal-resolution space-borne optical imagery. Cold Regions Science and Technology 55, 14–22.

Ling, F., Li, X., Xiao, F., Fang, S. & Du, Y. (2012): Object-based sub-pixel mapping of buildings incorporating the prior shape information from remotely sensed imagery. International Journal of Applied Earth Observation and Geoinformation 18, 283-292.

Lubin, D. & Massom, R. (2007): Remote sensing of Earth's polar regions. Opprotunities for computational science. Computing in Science and Engineering 9(1), 58-71.

Lucchitta, B.K., Rosanova, C.E. & Mullins, K.F. (1995): Velocities of Pine Island Glacier, West Antarctica, from ERS-1 SAR images. Annals of Glaciology 21, 277–283.

Luckman, A., Murray, T. & Strozzi, T. (2002): Surface flow evolution throughout a glacier surge measured by satellite radar interferometry. Geophysical Research Letters 29, 2095, doi: 10.1029/ 2001GL014570.

Luckman, A., Quincey, D. & Bevan, S. (2007): The potential of satellite radar interferometry and feature tracking for monitoring flow rates of Himalayan

glaciers. Remote Sensing of Environment 111, 172–181.

Luhmann, N. (1984): Soziale Systeme. Grundriss einer allgemeinen Theorie. Suhrkamp, Frankfurt.

Maisch, M. (1995): Gletscherschwundphasen im Zeitraum des ausgehenden Spätglazials (Egesen-Stadium) und seit dem Hochstand von 1850 sowie Prognosen zum künftigen Eisrückgang in den Alpen. In: Schweizerische Akademie der Naturwissenschaften (eds.): Gletscher im ständigen Wandel. Jubiläums-Symposium der Schweizerischen Gletscherkommission 1993, Verbier: 100 Jahre Gletscherkommission - 100 000 Jahre Gletschergeschichte. vdf, Zürich, 81-100.

Malanson, G.P. (1999): Considering Complexity. Annals of the Association of American Geographers 89(4), 746–753.

Maldonado, J.J. (2007): Propuesta para la zonificación de vulnerabilidad socionatural de la microcuenca Quebrada La Resbalosa, Mérida. Master's thesis, Department of Geography, University of Ejido, Venezuela (unpublished).

Mansell, D., Luckman, A. & Murray, T. (2012): Dynamics of tidewater surge-type glaciers in northwest Svalbard. Journal of Glaciology 58(207), 110-118.

Mao, D., Wang, Z., Luo, L. & Ren, C. (2011): Integrating AVHRR and MODIS data to monitor NDVI changes and their relationships with climatic parameters in Northeast China. International Journal of Applied Earth Observation and Geoinformation 18, 528-536.

Marchi, L. & Fontana, G. (2005): GIS morphometric indicators for the analysis of sediment dynamics in mountain basins. Journal of Environmental Geology 48(2), 218-228.

Marinho, E., Fasbender, D. & Kok, R. (2012): Spatial assessment of categorical maps: A proposed framework. Proceedings of the 4th GEOBIA, Rio de Janeiro, Brazil, 602-607.

Marmion, M., Hjort, J., Thuiller, W. & Luoto, M. (2008): A comparison of predictive methods in modelling the distribution of periglacial landforms in Finnish Lapland. Earth Surface Processes and Landforms 33, 2241–2254.

Matsuura, T. & Aniya, M. (2012): Automated segmentation of hillslope profiles across ridges and valleys using a digital elevation model. Geomorphology (in press), http://dx.doi.org/10.1016/j.geomorph.2012.07.024.

McNairn, H., Champagne, C., Shang, J., Holmstrom, D. & Reichert, G. (2009): Integration of optical and Synthetic Aperture Radar (SAR) imagery for delivering operational annual crop inventories. ISPRS Journal of Photogrammetry and Remote Sensing 64(5), 434-449.

Meier, M.F., Dyurgerov, M.B., Rick, U.K., O'Neel, S., Pfeffer, W.T., Anderson, R.S., Anderson, S.P., & Glazovsky, A.F. (2007): Glaciers dominate eustatic sea-level rise in the 21st century. Science 317(5841), 1064–1067.

Meier, M.F. & Post, A. (1969): What are glacier surges? Canadian Journal of Earth Sciences 6, 8907-8917.

Melvold, K. & Hagen, J.O. (1998): Evolution of a surge– type glacier in its quiescent phase: Kongsvegen, Spitsbergen, 1964–95. Journal of Glaciology 44(147), 394– 404.

Mergili, M., Fellin, W., Moreiras, S.M. & Stötter, J. (2012): Simulation of debris flows in the Central Andes based on Open Source GIS: possibilities, limitations, and parameter sensitivity. Natural Hazards 61, 1051–1081.

Michel, R. & Rignot, E. (1999): Flow of Glaciar Moreno, Argentina, from repeat-pass Shuttle Imaging Radar images: comparison of the phase correlation method with radar interferometry. Journal of Glaciology 45(149), 93–100.

Miliaresis, G.C. (2008): The landcover impact on the aspect/slope accuracy dependence of the SRTM-Elevation Data for the Humboldt Range. Sensors 8, 3134-3149.

Minár, J. & Evans, I.S. (2008): Elementary forms for land surface segmentation: the theoretical basis of terrain analysis and geomorphological mapping. Geomorphology 95, 236–259.

Mitášová, H., Harmon, R.S., Weaver, K.J., Lyons, N.J. & Overton, M.F. (2012): Scientific visualization of landscapes and landforms. Geomorphology 137(1), 122-137.

Mittermayer, J., Younis, M., Metzig, R., Wollstadt, S., Marquez Martinez, J. & Meta, A. (2010): TerraSAR-X system performance characterization and verification. IEEE Transactions on Geoscience and Remote Sensing 48(2), 660-676.

Moholdt, G. (2010): Elevation change and mass balance of Svalbard glaciers from geodetic data. PhD thesis, Department of Geosciences, University of Oslo.

Moholdt, G. & Kääb, A. (2012): A new DEM of the Austfonna ice cap by combining differential SAR interferometry with ICESat laser altimetry. Polar Research 31(18460), http://dx.doi.org/10.3402/polar.v31i0.18460.

Mohr, J.J., Reeh, N. & Madsen, S.N. (1998): Three-dimensional glacial flow and surface elevation measured with radar interferometry. Nature 391, 273-276.

Morche, D., Schmidt, K.-H., Heckmann, T. & Haas, F. (2007): Hydrology and geomorphic effects of a high magnitude flood in an Alpine river. Geografiska Annaler 89A(1), 5-19.

Morche, D., Schmidt, K.-H., Sahling, I., Herkommer, M. & Kutschera, J. (2008): Volume changes of Alpine sediment stores in a state of post-event disequilibrium and the implications for downstream hydrology and bed load transport. Norsk Geografisk Tidsskrift – Norwegian Journal of Geography 62(2), 89-101.

Mountrakis, G., Im, J. & Ogole, C. (2011): Support vector machines in remote sensing: a review. ISPRS Journal of Photogrammetry and Remote Sensing

66, 247–259.

Müller, K. (2011): Microwave penetration in polar snow and ice: implications for GPR and SAR. PhD thesis, Department of Geosciences, University of Oslo.

Murray, T., Luckman, A., Strozzi T. & Nuttall, A.M. (2003a): The initiation of glacier surging at Fridtjovbreen, Svalbard. Annals of Glaciology 36, 110-116.

Murray, T., Strozzi, T., Luckman, A., Jiskoot, H. & Christakos, P. (2003b): Is there a single surge mechanism? Contrasts in dynamics between glacier surges in Svalbard and other regions. Journal of Geophysical Research 108, B5 2237, doi:10.1029/ 2002JB001906.

Murray, T., Stuart, G.W., Miller, P.J., Woodward, J., Smith, A.M., Porter, P.R. & Jiskoot, H. (2000): Glacier surge propagation by thermal evolution at the bed. Journal of Geophysical Research 105(B6), 491-507.

Noetzli, J., Huggel, C., Hoelzle, M. & Haeberli, W. (2006): GIS-based modelling of rock/ice avalanches from Alpine permafrost areas. Computers and Geosciences 10(2), 161–178.

Nuth C. (2011): Quantification and interpretation of glacier elevation changes. PhD thesis, Department of Geosciences, University of Oslo.

Nuth C. & Kääb A. (2011): Co-registration and bias corrections of satellite elevation data sets for quantifying glacier thickness change. The Cryosphere 5, 271-290.

Nuttall, A.M., Hagen, J.O. & Dowdeswell, J. (1997): Quiescent–phase changes in velocity and geometry of Finsterwalderbreen, a surge–type glacier in Svalbard. Annals of Glaciology 24, 249–254.

O'Callaghan, J.F. & Mark, D.M. (1984): The extraction of drainage networks from digital elevation data. Computer Vision, Graphics, and Image Processing 28, 323–344.

Ødegård, R., Hagen, J.O. & Hamran, S.-E. (1997): Comparison of radio-echo sounding (30-1000 MHz) and high-resolution borehole-temperature measurements at Finsterwalderbreen, southern Spitsbergen, Svalbard. Annals of Glaciology 24, 262-267.

Ortega, R. (2007): Modelling potential debris flows on soil-covered catchment areas along the Upper Chama River Basin, north-western Venezuela. Master's thesis, Department of Geosciences, University of Oslo.

Orwin, J.F., Lamoureux, S.F., Warburton, J. & Beylich, A. (2010): A framework for characterizing fluvial sediment fluxes from source to sink in cold environments. Geografiska Annaler 92A(2), 155–176.

Osmundsen, P.T., Henderson, I.H.C., Lauknes, T.R., Larsen, Y., Redfield, T. & Dehls, J. (2009): Active normal fault control on landscape and rock-slope failure in northern Norway. Geology 37(2), 135–138.

Otto, J.-C. & Schrott, L. (2010): Quantifizierung von rezenten und post-

glazialen Sedimentflüssen in den Ostalpen. Salzburger Geographische Arbeiten 46, 1-13.

Pal, M. & Mather, P.M. (2006): Some issues in the classification of DAIS hyperspectral data. International Journal of Remote Sensing 27(14), 2895-2916.

Palmer, S., Shepherd, A., Björnsson, H. & Pálsson (2009): Ice velocity measurements of Langjökull, Iceland, from interferometric synthetic aperture radar (InSAR). Journal of Glaciology 55(193), 834-838.

Parry, S. (2011): The application of geomorphological mapping in the assessment of landslide hazard in Hong Kong. In: Smith, M.J. Paron, P. & Griffiths, J.S. (eds.): Geomorphological Mapping. Methods and Applications. Developments in Earth Surface Processes 15, Elsevier, Amsterdam, Oxford, 413-441.

Paul, F. (2000): Evaluation of different methods for glacier mapping using Landsat-TM data. In: Wunderle, S. (ed.): EARSeL Workshop on Remote Sensing of Land Ice and Snow, Juni 2000, Dresden, 239-245.

Paul, F. (2011): Melting glaciers and ice caps. Nature Geoscience 4(2), 71-72.

Paul, F. & Hendriks, J. (2010a): Optical remote sensing of glacier extent. In: Pellikka, P. & Rees, W.G. (eds.): Remote sensing of glaciers. Techniques for topographic, spatial and thematic mapping of glaciers. Taylor & Francis, London, 137-152.

Paul, F. & Hendriks, J. (2010b): Detection and visualization of glacier area changes. In: Pellikka, P. & Rees, W.G. (eds.): Remote sensing of glaciers. Techniques for topographic, spatial and thematic mapping of glaciers. Taylor & Francis, London, 231-243.

Paul, F., Huggel C. & Kääb, A. (2004): Combining satellite multispectral image data and a digital elevation model for mapping debris-covered glaciers. Remote Sensing of Environment 89(4), 510-518.

Pellikka, P. & Rees, W.G. (2010): Glacier parameters monitored using remote sensing. In: Pellikka, P. & Rees, W.G. (eds.): Remote sensing of glaciers. Techniques for topographic, spatial and thematic mapping of glaciers. Taylor & Francis, London, 41–66.

Pernu, T.K. (2008): Philosophy and the front line of science. The Quarterly Review of Biology 83(1), 29-36.

Pike, R.J. (1995): Geomorphometry — progress, practice and prospect. Zeitschrift für Geomorphologie 101(7), 221–238.

Pike, R.J. (2000): Geomorphometry — diversity in quantitative surface analysis. Progress in Physical Geography 24(1), 1–20.

Pike, R.J., Evans, I.S. & Hengl, T. (2009): Geomorphometry. A brief guide. In: Hengl, T. & Reuter, H.I. (eds.): Geomorphometry: concepts, software, applications. Developments in Soil Science 33, Elsevier, Amsterdam, Oxford, 3-30.

Pontius Jr., R.G. & Millones, M. (2011): Death to Kappa: birth of quantity disagreement and allocation disagreement for accuracy assessment. International Journal of Remote Sensing 32(15), 4407-4429.

Popper, K.R. (1989[9], 1st ed. 1934): Logik der Forschung. Mohr, Tübingen.

Popper, K.R. (1998[3]): Conjectures and refutations. In: Klemke, E.D., Hollinger, R., Rudge, D.W. & Kline, A.D. (eds.): Introductory readings in the philosophy of science. Prometheus Books, Amherst.

Pritchard, H., Murray, T., Luckman, A., Strozzi, T. & Barr, S. (2005): Glacier surge dynamics of Sortebrae, East Greenland from synthetic aperture radar feature tracking. Journal of Geophysical Research 110, F03005, doi:1029/2004JF000233.

Quincey, D.J., Luckman A. & Benn, D. (2009): Quantification of Everest region glacier velocities between 1992 and 2002, using satellite radar interferometry and feature tracking. Journal of Glaciology 55(192), 596–606.

Radić , V. & Hock, R. (2011): Regionally differentiated contribution of mountain glaciers and ice caps to future sea-level rise. Nature Geoscience 4, 91–94.

Raymond, C.F. (1987): How do glaciers surge? A review. Journal of Geophysical Research 92, 9121–9134.

Raymond, C.F., Benedict, R., Harrison, W.D., Echelmeyer, K.A. & Sturm, M. (1995): Hydrological discharges and motion of Fels and Black Rapids Glaciers, Alaska, U.S.A.: implications for the structure of their drainage systems. Journal of Glaciology 41(138), 290-304.

Rees, W.G. & Pellikka, P. (2010): Principles of remote sensing. In: Pellikka, P. & Rees, W.G. (eds.): Remote sensing of glaciers. Techniques for topographic, spatial and thematic mapping of glaciers. Taylor & Francis, London, 1–20.

Rhoads, B.L. & Thorn, C.E. (1996): Observation in geomorphology. In: Rhoads, B.L. & Thorn, C.E. (eds.): The scientific nature of geomorphology. Proceedings of the 27th Binghamton Symposium on Geomorphology, 32–56.

Richards, J.A. (2005): Analysis of remotely sensed data: The formative decades and the future. IEEE Transactions on Geoscience and Remote Sensing 43(3), 422-432.

Richards, J.A. & Jia, X. (2006[4]): Remote Sensing Digital Image Analysis. An introduction. Springer, Berlin, Heidelberg.

Rickenmann, D. (1999): Empirical relationships for debris flows. Natural Hazards 19, 47–77.

Rickenmann, D. & Scheidl, C. (2013): Debris-flow runout and deposition on the fan. In: Schneuwly-Bollschweiler, M., Stoffel, M. & Rudolf-Miklau, F. (eds.): Dating torrential processes on fans and cones. Methods and their application for hazard and risk assessment. Advances in Global Change

Research 47(1), Springer Science+Business Media, Dordrecht, 75-93.

Roa, J.G. (2007): Identifying landslides hazards in a tropical mountain environment, using geomorphologic and probabilistic approaches. PhD thesis, Department of Geography, University of Maryland.

Riedel, T., Elbertzhagen, I., Menz, G. & Schmullius, C. (2011): Synergistische Nutzung von hochauflösenden optischen und SAR-Daten zur automatischen Ableitung von Landbedeckungsprodukten. In: Borg, E. & Daedelow, H. (eds.): RapidEye Science Archive (RESA) - Erste Ergebnisse. Tagungsband zum 3. RESA Workshop der DLR, 165-175.

Rignot, E., Echelmeyer, K. & Krabill, W. (2001): Penetration depth of interferometric synthetic-aperture radar signals in snow and ice. Geophysical Research Letters 28, 3501–3504.

Ritter, M.E. (2011[3]): The physical environment: an introduction to physical geography. http://www.earthonlinemedia.com/ebooks/tpe_3e/title_page.html, 29.08.2012.

Roa, J.G. 2007. Identifying landslides hazards in a tropical mountain environment, using geomorphologic and probabilistic approaches. University of Maryland. Maryland, USA, 182 pp. (Inédito). http://drum.lib.umd.edu/handle/1903/7825, last access: December 1, 2010.

Rolstad, C., Amlien, J., Hagen, J.O. & Lundén, B. (1997): Visible and near-infrared digital images for determination of ice velocities and surface elevation during a surge on Osbornebreen, a tidewater glacier in Svalbard. Annals of Glaciology 24, 255–261.

Romstad, B. & Etzelmüller, B. (2012): Mean-curvature watersheds: A simple method for segmentation of a digital elevation model into terrain units Geomorphology 139-140, 293-302.

Rosen, P.A., Hensley, S., Joughin, I.R., Li, F.K., Madsen, S.N., Rodriguez, E. & Goldstein, R.M. (2000): Synthetic aperture radar interferometry. Proceedings of the IEEE 88(3), 333– 382.

Rott, H. (2009): Advances in interferometric synthetic aperture radar (InSAR) in earth system science. Progress in Physical Geography 33(6), 769–791.

Rowbotham, D., Scally, D.F. & John, L. (2005): The identification of debris torrent basins using morphometric measures derived within a GIS. Geografiska Annaler 87A(4), 527-537.

Ruse, M. (2012): The gym teachers of academia. The Philosophers' Magazine 58(3), 47-52.

Saadat, H., Bonnell, R., Sharifi, F., Mehuys, G., Namdar, M. & Ale-Ebrahim, S. (2008): Landform classification from a digital elevation model and satellite imagery. Geomorphology 100, 453–464.

Salzmann N., Kääb, A., Huggel, C., Allgöwer, B. & Haeberli, W. (2004): Assessment of the hazard potential of ice avalanches using remote sensing and GIS-modelling. Norwegian Journal of Geography 58, 74-84.

Sansosti, E., Casu, F., Manzo, M. & Lanari, R. (2010): Space-borne radar interferometry techniques for the generation of deformation time series: an advanced tool for Earth surface displacement analysis. Geophysical Research Letters 37, L20305, doi:10.1029/2010GL044379.

Scherler, D., Bookhagen, D. & Strecker, M.R. (2011): Hillslope-glacier coupling: The interplay of topography and glacial dynamics in High Asia. Journal of Geophysical Research 116, F02019, doi:10.1029/2010JF001751.

Schmidt, D.A., & Bürgmann, R. (2003): Time-dependent land uplift and subsidence in the Santa Clara valley, California, from a large InSAR data set. Journal of Geophysical Research 108(B9), doi:10.1029/2002JB002267.

Schneevoigt, N.J. (2004): To what extent can Alpine geomorphological landforms be detected from remotely sensed imagery? A case study in the Reintal catchment, Bavarian Alps. Diploma thesis, Department of Geography, Rheinische Friedrich-Wilhelms-Universität Bonn (unpublished).

Schrott, L. & Dikau, R. (1998): Die Rolle von Sedimentspeichern im geomorphologischen Prozessgefüge alpiner Kaskadensysteme. Forschungsantrag zum DFG-Teilprojekt Schr 648/1, Bonn (unpublished).

Schrott, L., Götz, J., Geilhausen, M. & Morche, D. (2006): Spatial and temporal variability of sediment transfer and storage in an Alpine basin (Reintal valley, Bavarian Alps, Germany). Geographica Helvetica 61(3), 191-200.

Schrott, L., Hufschmidt, G., Hankammer, M., Hoffmann, T. & Dikau, R. (2003): Spatial distribution of sediment storage types and quantification of valley fill deposits in an alpine basin, Reintal, Bavarian Alps, Germany. Geomorphology 55, 45–63.

Schrott, L., Niederheide, A., Hankammer, M., Hufschmidt, G. & Dikau, R. (2002): Sediment storage in a mountain catchment: geomorphic coupling and temporal variability (Reintal, Bavarian Alps, Germany). Zeitschrift für Geomorphologie N.F., Suppl. 127, 175–196.

Schytt, V. (1969): Some comments on glacier surges in eastern Svalbard. Canadian Journal of Earth Sciences 6, 867-871.

Serreze, M.C. & Francis, J.A. (2006): The Arctic amplification debate. Climatic Change 76(3–4), 241-264.

Shao, Y. & Lunetta, R.S. (2012): Comparison of support vector machine, neural network, and CART algorithms for the land-cover classification using limited training data points. ISPRS Journal of Photogrammetry and Remote Sensing 70, 78–87.

Shroder Jr., J.F. & Bishop, M.P. (2004): Mountain geomorphic systems. In: Bishop, M.P. & Shroder Jr., J.F. (eds.): Geographic Information Science and Mountain Geomorphology. Springer, Chichester, 33-73.

Skorve, J. (2007): Megaton nuclear underground tests and catastrophic events on Novaya Zemlya - A satellite study. Paper 716, Norsk Utenrikspolitisk Institutt (NUPI), Oslo.

Slaymaker, O. (1991): Mountain geomorphology: a theoretical framework for measurement programms. Catena 18, 427–437.

Slaymaker, O. (2010): Mountain hazards. In: Alcántara- Ayala, I. & Goudie, A. (eds): Geomorphological hazards and disaster prevention. Cambridge University Press, Cambridge, 33–47.

Smith, M.J. & Pain, C.F. (2009): Applications of remote sensing in geomorphology. Progress in Physical Geography 33(4), 568-582.

Smith, M.J., Rose, J. & Booth, S. (2006): Geomorphological mapping of glacial landforms from remotely sensed data: an evaluation of the principal data sources and an assessment of their quality. Geomorphology 76(1–2), 148-165.

Solheim, A. (1991): The depositional environment of surging sub-polar tidewater glaciers. A case study of the morphology, sedimentation and sediment properties in a surge affected marine basin outside Nordaustlandet, the Northern Barents Sea. Norsk Polarinstitutts Skrifter 194, Oslo.

Stoffel, M. (2010): Magnitude-frequency relationships of debris flows – a case study based on field surveys and tree-ring records. Geomorphology 116, 67–76.

Stoffel, M. & Huggel, C. (2012): Effects of climate change on mass movements in mountain environments. Progress in Physical Geography 36, 421–439.

Strahler, A. (1950): Davis' concepts of slope development viewed in the light of recent quantitative investigations. Annals of the Association of American Geographers 40, 209–213.

Strahler, A. (1952): Dynamic basis of geomorphology. Geological Society of America Bulletin 63, 923–938.

Stramondo, S., Chini, M., Bignami, C., Salvi, S. & Atzori, S. (2011): X-, C-, and L-band DInSAR investigation of the April 6, 2009, Abruzzi earthquake. IEEE Geoscience and Remote Sensing Letters 8(1), 49-53.

Strozzi, T., Delaloye, R., Kääb, A., Ambrosi, C. Perruchoud, E. & Wegmüller, U. (2010a): Combined observations of rock mass movements using satellite SAR interferometry, differential GPS, airborne digital photogrammetry, and airborne photography interpretation. Journal of Geophysical Research 115, F01014, doi:10.1029/2009JF001311.

Strozzi, T., Delaloye, R., Raetzo, H. & Wegmüller, U. (2010b): Radar interferometric observations of destabilized rockglaciers. Proceedings of the 'Fringe 2009 Workshop', Frascati, ESA SP-677, 1-5.

Strozzi. T, Kääb, A. & Frauenfelder, R. (2004): Detecting and quantifying mountain permafrost creep from in situ inventory, space-borne radar interferometry and airborne digital photogrammetry. International Journal of Remote Sensing 25(15), 2919–2931.

Strozzi, T., Luckman, A., Murray, T., Wegmüller, U. & Werner, C.L. (2002): Glacier motion estimation using SAR offset-tracking procedures. IEEE

Transactions on Geoscience and Remote Sensing 40(11), 2384-2391.

Sund, M., Błaszczyk, M., Eiken, T. & Jania, J. (subm.): The implications of surge and tidewater glacier dynamics in relation to the climate change response of Svalbard glaciers. Manuscript submitted to Annals of Glaciology.

Sund, M. & Eiken, T. (2004): Quiescent-phase dynamics and surge history of a polythermal glacier: Hessbreen, Svalbard. Journal of Glaciology 50(171), 547-555.

Sund, M., & Eiken, T. (2010): Correspondence: Recent surges of Blomstrandbreen, Comfortlessbreen and Nathorstbreen, Svalbard. Journal of Glaciology 56(195), 182-184.

Sund, M., Eiken, T., Hagen, J.O. & Kääb, A. (2009): Svalbard surge dynamics derived from geometric changes. Annals of Glaciology 50(52), 50–60.

Sundal, A.V., Shepherd, A., Nienow, P., Hanna, E., Palmer, S. & Huybrechts, P. (2011): Melt-induced speed-up of Greenland ice sheet offset by efficient subglacial drainage. Nature 469(7331), doi:10.1038/nature09740.

Tarabalka, Y., Tilton, J.C., Benediktsson, J.A. & Chanussot, J. (2012): A marker-based approach for the automated selection of a single segmentation from a hierarchical set of image segmentations. IEEE Journal of Selected Topics in Applied Earth Observations and Remote Sensing 5(1), 262-272.

Theler, D., Reynard, E., Lambiel, C., Bardou, E. (2010): The contribution of geomorphological mapping to sediment transfer evaluation in small alpine catchments. Geomorphology 124(3–4), 113-123.

Thomas, R., Frederick, E., Krabill, W., Manizade, S. & Martin, C. (2009): Recent changes on Greenland outlet glaciers. Journal of Glaciology 55(189), 147-162.

Thonfeld, F. & Menz, G. (2011): Coherence and multitemporal intensity metrics of high resolution SAR images for urban change detection. Proceedings of the 4th TerraSAR-X Science Team Meeting, Oberpfaffenhofen, 1-9.

Thoonen, G., Hufkens, K., Vanden Borre, J., Spanhove, T. & Scheunders, P. (2012): Accuracy assessment of contextual classification results for vegetation mapping. International Journal of Applied Earth Observation and Geoinformation 15, 7-15.

Thorn, C. (1992): Periglacial geomorphology: what, where, when? In: Dixon, J.C. & Abrahams, A.D. (eds.): Periglacial geomorphology. Wiley, New York, 1-30.

Toutin, T. (1995): DEM generation with a photogrammetric approach: examples with VIR and SAR images. EARSeL Advances in Remote Sensing 4(2), 110-117.

Toutin, T. (2000): Stereo-mapping with SPOT-P and ERS-1 SAR images. International Journal of Remote Sensing 21(8), 1657-1674.

Toutin, T. & Gray, L. (2000): State-of-the-art of elevation extraction from satellite SAR data. Review paper. ISPRS Journal of Photogrammetry and

Remote Sensing 55(1), 13-33.

Trimble, S.W. (2010): Streams, valleys and floodplains in the sediment Cascade. In: Burt, T.P. & Allison, R.J. (eds.): Sediment cascades: an integrated approach. John Wiley & Sons, Chichester, UK, 307-343.

UNEP (2007): Global Outlook for Ice and Snow. United Nations Environment Programme (UNEP) Publications. Birkeland Trykkeri, Birkeland, Norway.

van der Linden, S. (2008): Investigating the potential of hyperspectral remote sensing data for the analysis of urban imperviousness - a Berlin case study. PhD thesis, Department of Geography, Humboldt-Universität zu Berlin.

van der Linden, S., Janz, A., Waske, B., Eiden, M. & Hostert, P. (2007): Classifying segmented hyperspectral data from a heterogeneous urban environment using support vector machines. Journal of Applied Remote Sensing 1, 013543, doi: 10.1117/1.2813466.

van Niekerk, A. (2010): A comparison of land unit delineation techniques for land evaluation in the Western Cape, South Africa. Land Use Policy 27, 937–945.

Vieli, A., Jania, J., Blatter, H. & Funk, M. (2004): Short–term velocity variations on Hansbreen, a tidewater glacier in Spitsbergen. Journal of Glaciology 50(170), 389–398.

Viviroli, D. & Weingartner, R. (2008): 'Water Towers' — a global view of the hydrological importance of mountains. In: Viviroli, D. & Weingartner, R. (eds.): Mountains: sources of Water, Sources of Knowledge. Advances in Global Change Research, 31(1), 15-20.

Viviroli, D., Weingartner, R. & Messerli, B. (2003): Assessing the hydrological significance of the World´s mountains. Mountain Research and Development 23(1), 32–40.

von Bertalanffy, L. (1950): An outline of general system theory. The British Journal for the Philosophy of Science 1(2), 134-165.

von Bertalanffy, L. (1975): Perspectives on general system theory: scientific-philosophical studies. Taschdjian, E. (ed.). George Braziller, New York.

von Elverfeldt, K. (2012): System theory in geomorphology - Challenges, epistemological consequences and practical implications. Doctoral thesis, Department of Geography, University of Vienna, Austria. Springer Science+Buisiness Media, Dordrecht.

von Elverfeldt, K. & Glade, T. (2011): Systems theory in Geomorphology. A challenge. Zeitschrift für Geomorphologie 55(3), 87–108.

Wangensteen, B. (2006): Remote sensing-based quantification and analysis of earth surface processes in periglacial and glacial environments - case studies from Iceland, Svalbard and southern Norway. PhD thesis, Department of Geosciences, University of Oslo.

Wangensteen, B., Weydahl, D.J. & Hagen, J.O. (2005): Mapping glacier velocities on Svalbard using ERS tandem DInSAR data. Norwegian Journal

of Geography 59, 276-285.

Waske, B. (2007): Classifying multisensor remote sensing data: concepts, algorithms and applications. PhD thesis, Department of Geography, Rheinische Friedrich-Wilhelms-Universität Bonn.

Waske, B. & Benediktsson, J.A. (2007): Fusion of support vector machines for classification of multisensor data. IEEE Transactions on Geosciences and Remote Sensing 45(12), 3858-3866.

Waske, B. & van der Linden, S. (2008): Classifying multilevel imagery from SAR and optical sensors by decision fusion. IEEE Transactions on Geosciences and Remote Sensing 46(5), 1457-1466.

Waske, B., van der Linden, S., Benediktsson, J., Rabe, A. & Hostert, P. (2009): Impact of different morphological profiles on the classification accuracy of urban hyperspectral data. Proceedings of the 1st Workshop on Hyperspectral Image and Signal Processing: Evolution in Remote Sensing, Grenoble, France.

Waske, B., van der Linden, S., Oldenburg, C., Jakimow, B., Rabe, A., & Hostert, P. (2012): imageRF - A user-oriented implementation for remote sensing image analysis with Random Forests. Environmental Modelling & Software 35, 192-193.

Wegmüller, U. & Werner, C. (1997): Gamma SAR processor and interferometry software. ERS Third ERS symposium on space at the service of our environment, Florence, Italy, 1687–1692.

Werner, C., Wegmüller, U., Strozzi, T. & Wiesmann, A. (2003): Interferometric point target analysis for deformation mapping. IEEE Proceedings of the International Geoscience and Remote Sensing Symposium (IGARSS) 2003, Toulouse, France, 4362-4364.

Weydahl, D.J. (1998): Analysis of satellite SAR images for change detection over land areas. Doctoral thesis, FFI/Publication-98/04969, Forsvarets Forskningsinstitutt, Kjeller.

Weydahl, D.J. (2001): Analysis of ERS tandem SAR coherence from glaciers, valleys, and fjord ice on Svalbard. IEEE Transactions on Geoscience and Remote Sensing 39(9), 2029-2039.

Weydahl, D.J., Eldhuset, K. & Hauge, S. (2001): Atmospheric effects on advanced modes. Norwegian Defence Research Establishment (Report 2001/04826), Kjeller.

Weydahl, D.J., Simensen, S.H. & Dick, Ø.B. (2008): Analysis of the first TSX images and future plans. Proceedings of the Third TerraSAR-X Workshop at DLR, Munich, 1-4.

Wilson, J.P. (2012): Digital terrain modeling. Geomorphology 137(1), 107-121.

Worni, R., Huggel, C., Stoffel, M. & Pulgarín, B. (2012): Challenges of modeling recent, very large lahards at Nevado del Huila Volcano, Colombia.

Bulletin of Volcanology 74, 309-324.

Wright, D.J., Goodchild, M.F. & Proctor, J.D. (1997): GIS: tool or science? Annals of the Association of American Geographers 87(2), 346-362.

Yoon, Y.T., Eineder, M., Yague-Martinez, N. & Montenbruck, O. (2009): TerraSAR-X precise trajectory estimation and quality assessment. IEEE Transactions on Geoscience and Remote Sensing 47(6), 1859-1868.

Yu, B. (2011): Research on prediction of debris flows triggered in channels. Natural Hazards 58, 391-406.

Zemp, M. (2011): The monitoring of glaciers at local, mountain, and global scale. Habilitation thesis, Department of Geography, University of Zurich.

Zhou, Q., Lees, B.G., Tang, G.-A. (eds., 2008): Advances in digital terrain analysis. Springer Lecture Notes in Geoinformation and Cartography, Berlin.

Ziman, J.M. (1968): Public knowledge: an essay concerning the social dimension of science. Cambridge University Press, Cambridge.

Zitova, B. & Flusser, J. (2003): Image registration methods: a survey. Image and Vision Computing 21(11), 977–1000.

Zwieback, S., Bartsch, A., Melzer, T. & Wagner, W. (2012): Probabilistic Fusion of Ku- and C-band Scatterometer Data for Determining the Freeze/Thaw State. IEEE Transactions on Geoscience and Remote Sensing 50(7), 2583-2594.

3 Paper II
Linking geomorphic systems theory and segmentation

published in a shortened version as
Schneevoigt, N.J. & L. Schrott (2006):
Linking geomorphic systems theory and remote sensing. A conceptual approach to Alpine landform detection (Reintal, Bavarian Alps, Germany).
Geographica Helvetica 61(3): 181-190.

Although the global importance of high mountains is increasingly being recognised, their geomorphic process system has not been completely understood as yet. While systems theory and geographical information systems (GIS) approaches have long been applied in the alpine geomorphology community, the implementation of remote sensing software is just beginning. However, object-oriented image analysis lends itself to alpine applications, as it unites the benefits of remote sensing and GIS.

Taking the Reintal (Bavarian Alps) as an example, the systems approach and the object-oriented classification of an Advanced Spaceborne Thermal Emission and Reflection Radiometer (ASTER) satellite scene with digital elevation information are parallelised. In a hierarchical, multiscale data segmen-

tation and classification, Alpine landforms can be detected with high accuracy. Hence remote sensing techniques represent a valuable tool for geomorphologic research in high mountains, especially in otherwise inaccessible terrain.

3.1 Introduction

Mountain regions have moved into the focus of scientific attention: chapter 13 of the Agenda 21 is dedicated to the world´s mountains (United Nations, 1992; Ives et al., 1997), 2002 was declared 'International Year of the Mountain' by the United Nations (Ives & Messerli, 2001), and the German Geographers Day 2003 had as its motto 'Alpine World - Mountain World: Islands, Bridges, Borders'. The sustainable preservation of alpine regions is a global issue, because a tenth of the world´s population lives in mountain regions, while a much larger number indirectly depend on mountain resources (United Nations, 1992).

Geomorphologic activity in alpine regions is significantly increased when compared to their forelands. Therefore, mountain environments display quick changefulness in time and space (Caine, 1974) and hence react very sensitively to global change (Kääb, 2002). However, scientific knowledge about their geomorphologic process structure remains sketchy, especially quantitatively. Similarly, the question of potentially mobilisable sediments in the upper regions of high mountain catchments still calls for an answer (Schrott et al., 2002, 2003). As upper areas, for the most part, cannot be observed from the ground, remote sensing applications lend themselves to closing this gap which impedes a full understanding of the alpine sediment cascade.

While research on high mountain geomorphology often uses GIS coupled with remote sensing data, only few genuine remote sensing techniques are employed. Difficulties in the accurate designation of high mountain landforms add to the general intricacy of handling alpine data in remote sensing. Yet object-oriented classification constitutes a new and promising approach which combines the advantages of GIS and remote sensing.

This paper pursues the following objectives:

- To convey the theoretical and conceptual background of a study on object-oriented classification of geomorphological landforms.
- To link geomorphic systems theory and object-oriented remote sensing in order to draw a parallel between those two approaches from completely different scientific disciplines, thus showing how they complement each other.
- To illustrate the potential of remote sensing as a tool in high mountain geomorphology within the context of systems approaches to alpine sediment fluxes and deposits.

3.2 Allocation of landforms in alpine regions

In order to detect landforms by remote sensing, a compilation of their distinctive features is required. The better the knowledge about the target classes (Tab. 3.1), the more possibilities arise to differentiate between them in image data (Schneevoigt et al., 2008). Landforms are systematically distributed in landscape, but varying geomorphic process activity results in a patchwork structure of landforms (Fig. 3.1). Activity status and the processes involved play an important role in their space- and airborne detection: texture and spectral characteristics of individual landforms can be very heterogeneous.

Table 3.1: Target Groups of Alpine Landform Classification

crest regions	rockwalls	valley bottom	
cirques & hanging valleys	avalanche & debris flow tracks	avalanche & debris flow tracks	avalanche & debris flow deposits
less inclined bare rock	vegetation covered slopes	talus sheets & cones	rockfall partly/ fully overgrown
free faces	free faces	alluvial fans	rockfall deposits
snow & ice	loose sediments	floodplains	moraine deposits

3.2.1 Target landforms

A landform is defined by its particular shape. However, strict delineations of landforms rarely exist in landscape, as many forms show no clear boundaries (Fig. 3.1). Moreover, landforms often form part of other landforms - scale and specific objectives determine where to set a division (Mark & Smith, 2004). Depending on the geographic situation, age, maturity and markedness of a landform, its geomorphometry varies enormously (Dikau, 1994; Rasemann et al., 2004).

Detection of landforms can also be hindered by the fact that many landforms originate from interacting processes and display complex assemblages instead of clear features (Fig. 3.1). Besides, equifinality blurs underlying processes: different processes can produce the same landform shapes, which however should bear different names according to the building process. For instance, a strict separation of avalanche from debris flow deposits is neither always possible in situ (Fig. 3.1) nor hence in a satellite scene. As partially interfingered deposits are frequent, form characteristics deviate from the ideal. This "fuzzy nature of most high-mountain terrain features" (Kääb, 2002: 50) makes it neccessary to consider context to achieve sound classifications.

Geomorphological landforms result from spatially distributed and interlinked geomorphologic processes, which consecutively model the landscape by filling and emptying different types of stores. Monocausal, linear process-form relations cannot be established because of interactions which vary spatially and temporally. As a result, alpine sediment transport, storage and their processual links need further investigation to enable us to fully understand landform development in high mountains (Jordan & Slaymaker, 1991; Haeberli, 1996; Schrott et al., 2002, 2003; Krautblatter & Moser, 2005; Becht et al., 2005). Remote sensing applications also benefit from increased knowledge relating to target classes (Tab. 3.1), as more possibilities of feature analysis arise in classification hierarchies.

Figure 3.1: Alpine Landform Assemblage in the Reintal

Photo by L. Schrott, 2001, overlaid with landform denominations around Hintere Gumpe floodplain, view facing south-east.

The difficulty in deciphering sediment flow and storage lies in their sophistication: a focus on single events or forms ignores greater context (Fig. 3.1), whereas a large-scale perspective cannot fully grasp the complexity of landform assemblages. A systemic approximation unites those antipodes: on the one hand, it facilitates the delimitation of single components by making it possible to zoom into systemic details. On the other hand, its holistic approach places all components into subsystems and these into greater superordinate systems, thus restoring the entirety of landscape.

Hence systems theory, in conjunction with object-oriented remote sensing, helps to overcome the scale problematics in space. As the temporal aspect of remote sensing is limited, the following section focuses on the micro time scale of the present according to Slaymaker (1991).

3.2.2 Systemic approach to sediment fluxes and deposits

With the onset of process-orientated geomorphology, Strahler (1952) stresses the need for quantitative process monitoring to comprehend landform evolution. He adapts the concept of open systems to geomorphology: in- and output of energy and matter characterise these flow systems striving for a steady state, i.e. an equilibrium of transfers in the system as a whole. Hack (1960) refers to the dynamic relationships between process components: as soon as a system contains negative feedback loops, it shows a tendency to establish a dynamic equilibrium, because hence a capability of compensation is given. Within a certain expanse frame specific to the form and its given surroundings, landforms thus develop to a state of maturity, which is constantly destroyed and subsequently reattained.

Chorley (1962) and Chorley & Kennedy (1971) further promote general systems theory, focusing on structure or inner complexity: they perceive environment as a hierarchy of organised and interlinked subsystems. Dynamic cascading systems prevail in mountainous regions. Ahnert (1994) remarks that not all processes involved work in a downslope direction like a cascade and proposes the term 'process system'. Yet 'sediment cascade' has gained general acceptance for designating alpine material transport. It is defined as a structure in which the output of one subsystem forms the input of another (Fig. 3.2). In between subsystems, 'throughput' or mere transmission also occurs. Likewise, energy and matter can be transferred into stores and thus be withheld from the cascade (Chorley & Kennedy, 1971).

Any movement is determined by regulators at the interfaces between processes and forms (Fig. 3.2), i.e. by the disposition, presence or absence of geomorphological variables (e.g. infiltration capacity, storage potential, slope). Internal thresholds of the individual variables interfere with external thresholds of other regulators in the same or surrounding subsystems. Together with their discontinuity in time and space, allowing for reaction intervals and different

reaction patterns of adjacent forms, this explains the complexity and nonlinearity of alpine systems. Generally speaking, high rates of energy transfer result in rapid sediment turnover in alpine environments (Chorley & Kennedy, 1971; Caine, 1974).

Despite its benefits, the systems approach initially did not gain general acceptance on account of limitations in quantification and modelling. With the advent of more powerful computer systems in the 1990s, paradigms in geomorphology changed: with the increasing improvement of memory space, the systems approach regained vitality. Recent research on the coupling of sediment transport systems increasingly captures qualitative and quantitative simulation of the sediment cascade in (peri-)glacial environments, e.g. Haeberli (1996), Ballantyne (2002), Otto & Dikau (2004), Becht et al. (2005), Zemp et al. (2005) and Rothenbühler (2006).

3.2.3 The Alpine sediment cascade of the Reintal

The project 'SEDiment cascades in Alpine Geosystems' ('Sedimentkaskaden in Alpinen Geosystemen' - SEDAG) models the Alpine sediment cascade, integrating qualitative and quantitative sediment turnover (Unbenannt, 2002; Schrott et al., 2002, 2003; Becht et al., 2005; Krautblatter & Moser, 2005; Schmidt & Morche, 2006). The identification of different storage types (Tab. 3.1) and an analysis of their present-day spatial pattern forms part of this. Remote sensing hence represents a helpful tool, especially considering the higher, inaccessible parts of the valley (Fig. 3.1; Schneevoigt et al., 2008).

The conceptional Alpine sediment cascade (Fig. 3.2) by Schrott et al. (2002) is based on systems theory, synthesising Chorley & Kennedy´s hierarchical cascading systems concept (1971) and Caine´s alpine sediment transfer model (1974). With symbols after Chorley & Kennedy (1971), it shows the spatial distribution of storage types in the Reintal in three subsystems: I (free faces and cirques), II (slopes below rockwalls) and III (valley floor and

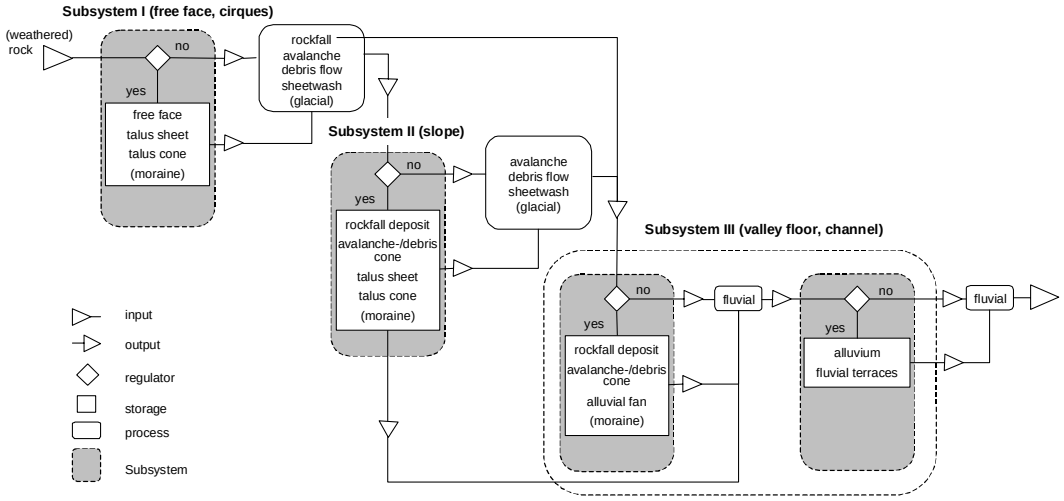

Figure 3.2: Conceptual Alpine Sediment Cascade of the Reintal
Symbols after Chorley & Kennedy´s (1971) systems representations, taken from Schrott et al. (2002).

channel). These subsystems form a cascade linked by processes (rockfalls, avalanches, debris flow, sheetwash and fluvial processes) in the direction of drop. Today, 79% of the sediment stores representing geomorphic process units in the Reintal are inactive, overgrown (Fig. 3.1) and decoupled from the cascade system.

As hardly any sediment leaves the subcatchment, the Reintal equals a nearly closed sediment system (Unbenannt, 2002). This is possible because karst limestone allows for considerable subterranean drainage, while two rockfalls and a major cirque threshold form natural dams trapping sediment in natural sinks (Schrott et al., 2002). An imbalance in favour of input neither allows the onset of a steady state nor of a general dynamic equilibrium. It leads to a reinforced building up of sediment stores, exemplified in very high mean sedimentation rates between 18 and 27 mm a^{-1} (Schrott et al., 2002, 2006). These stores form buffers which can trap material for centuries and millennia (Jordan & Slaymaker, 1991). They thus introduce major temporal variations into the entire system, leading to the sediment delivery problem. The heterogeneity of alpine regions and recent climate change add to the dif-

ficulty of designing universally applicable schemes of sediment fluxes. Thus overall, quantitative models of sediment cascades fully describing landscape development are still lacking.

3.3 Optical remote sensing in alpine geomorphology

High mountains must be further monitored in order to better understand their complex material flow systems engendering high landscape variability and natural hazards (Kääb et al., 2005). To that effect, remote sensing constitutes an adequate tool, as it permits global, regular coverage of remote areas at a wide range of scales. However, alpine terrain poses problems for remote sensing: extreme altitudinal differences within small horizontal intervals may result in offsets of several pixels or hundreds of meters if scanned at disadvantageous angles. Illumination and shading vary enormously because of relief influences.

Nonetheless, high mountain geomorphologists increasingly recognise the potential of remote sensing applications for their interests (Bishop & Shroder Jr., 2004). The long-distance perspective facilitates pattern detection and monitoring of otherwise inaccessible landscape sections: remotely sensed imagery and digital elevation models (DEM) complement one another for geomorphological analyses based on automated applications from the remote sensing community (Giles & Franklin, 1998).

3.3.1 GIS versus remote sensing

According to Bishop & Shroder Jr. (2004), GIS is favoured in alpine geomorphology because spatial analysis in the form of statistical arithmetics, neighbourhood relationships, regional clusters, continuities and discontinuities can be used to differentiate patterns in landscape. While first order descriptive

statistics comprise calculations such as minima, maxima, means or standard deviations, second order statistics imply spatial texture analysis. First order calculations per cell have belonged to geomorphic standard repertoire for long now, applied for an automated extraction and frequency analysis of geomorphometric mountain properties such as slope, aspect and curvature (Bishop & Shroder Jr., 2004). Second order digital terrain analyses have only been operationalised in GIS environments of late, e.g. (semi-) empirical GIS modelling. Several studies confirm the potential of optical imagery and GIS for the assessment, modeling and monitoring of geomorphic forms and processes (e.g. McDermid & Franklin, 1994; Walsh et al., 1998; Etzelmüller et al., 2001). The same goes for glacier observation (e.g. Paul et al., 2002; Huggel et al., 2004).

Whereas GIS approaches to analyse remote sensing data in general are manifold, studies employing remote sensing methodology occur less frequently in the field of high mountain geomorphology. Snow and ice monitoring represents the foremost research topic when it comes to genuine remote sensing, as field measurements quickly reach their limits here. For more than two decades now, the full range of possibilities concerning optical satellite data on snow applications has been exploited (e.g. Hall & Martinec, 1986; Schaper, 2000). Due to its relative independence from weather conditions, radar data is also employed (e.g. Haefner et al., 2000). As foreshortening, layover and shadow effects exorbitantly increase, stereo pairs of radar images are often dealt with in alpine terrain.

Rock glaciers and debris-covered glaciers are also increasingly investigated by remote sensing (Kääb et al., 2003; Paul, 2000; Paul et al., 2004). The Global Land Ice Measurements from Space (GLIMS) programme represents a scientific project centred on the ASTER sensor, scenes of which also form the basis of this study. For climate monitoring, an inventory of global land-ice extension is thus being developed by a worldwide consortium combining remote sensing and GIS (Schaper, 2000; Kääb, 2002, Kääb et al., 2003). Here a trend towards GIS integration into remote sensing applications is emerging.

Recent developments lead to a coalescence of GIS and remote sensing: current object-oriented software unites remote sensing tools with with first and second order GIS statistics into one desktop environment. Remote sensing imagery can be interpreted in a pixel- or in an object-oriented mode. While the former analyses each single pixel individually according to its spectral characteristics, the latter also considers the neighbourhood of a pixel. It assumes that adjacent pixels showing certain similarities belong to one group, so that the entire scene is divided into image segments (Fig. 3.3) before classifying it in a second but separate step. This method produces more homogeneous results through spectral generalisation, thus smoothing out irregular pixel-dominated patterns and creating more realistic forms (Baatz & Schäpe, 2000; Blaschke & Hay, 2001; Koch et al., 2003).

3.3.2 Segmenting images into objects

The idea of image segmentation arose in the 1970s. A considerable number of algorithms have been developed since, but they only became operational with the improved computer systems of the 1990s. Segmentation techniques are used to deal with intensified in-class variability brought forth by increasing spectral and spatial image resolution (Baatz & Schäpe, 2000; Schiewe & Tufte, 2002). Object-orientation implies two steps: first, the data set is split up into image objects (Fig. 3.3). Only afterwards can it be classified by assigning the objects to different classes or themes (Fig. 3.3). Supervised classification relies on interaction with an operator. With a priori terrain knowledge, the latter has to select representative areas or features of the different target classes to be detected in the scene (Tab. 3.1). This allows a focus on specific classes of interest, also in the high mountain context. Regarding alpine relief, Giles & Franklin (1998) classify slope units in a moderate- to high-relief area in southwest Canada. The studies show that prior image segmentation and assemblage of specific geomorphic signatures for landform discrimination produces sound results.

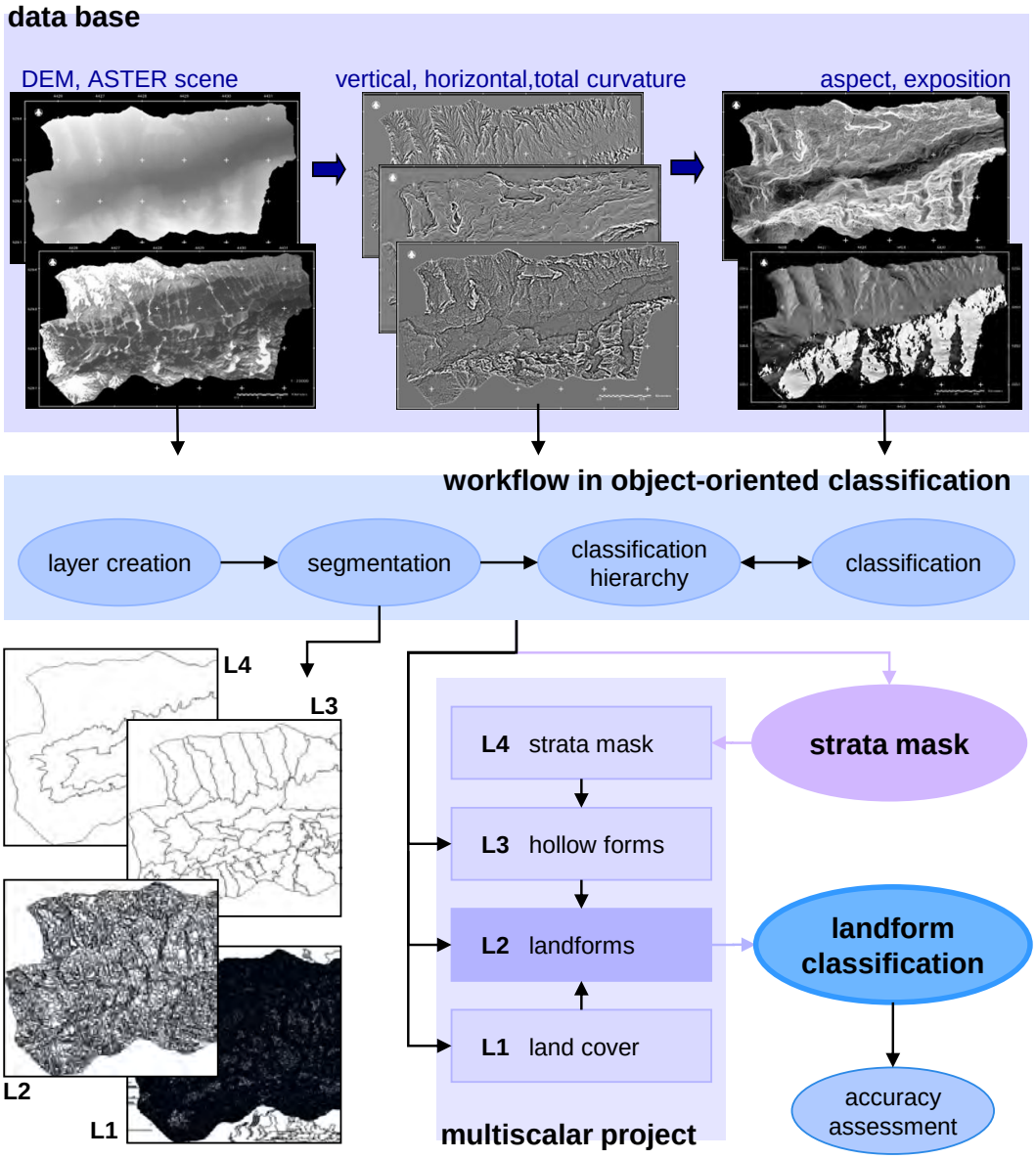

Figure 3.3: Input and Steps of Object-oriented Classification.

Top: Input data for object-oriented analysis: ASTER satellite scene (15 m resolution resampled to 5 m), DEM (5 m resolution) and five DEM derivatives (5 m resolution). Bottom left: Segmentation on four hierarchical levels L1 to L4. Bottom right: Classifications of different land cover features on four levels L1 to L4.

The spectral properties of image objects are addressed by mean values, standard deviations and ratios of the incorporated pixels. Image objects also comprise geometric features, as image objects vary in shape and extent (Fig. 3.3, Bottom left). Neighbourhood relationships, sub- and superordinations, morphometric and class-related features can be analysed as well (Blaschke & Hay, 2001; Baatz & Schäpe, 2000; Benz et al., 2004). As object-based class descriptions hence reach far beyond spectral information, they are well suited for three-dimensional alpine applications, where spectral input alone does not suffice (Giles & Franklin 1998; Schneevoigt et al., 2008).

The object-oriented software eCognition segments an image in a knowledge free way via *region-growing*, an automatized heuristic optimization method: a 'composition of homogeneity' criterion assesses potential increase of spectral heterogeneity in a merge weighed by the size of two pixels or segments considered. Next to this colour criterion based on spectral information alone, shape parameters can be used to correct highly textured data which otherwise would produce frayed and distorted segments. This constitutes an advantage especially in high mountain data. Yet it must be applied carefully, as it implies an arbitrary divergence from the given spectral information based on pure arithmetics (Baatz & Schäpe, 2000).

From the colour and shape input, the region-growing algorithm produces image objects with a minimized average heterogeneity in any desired resolution or scale. However, vital information for the desired classes often cannot be displayed in one single resolution, while segmentation must be applied to an entire image with one single scale parameter. Multiresolution segmentation allows a simultaneous depiction of several image levels segmented at different scales (Benz et al., 2004; Blaschke & Hay, 2001; Schiewe & Tufte, 2002). For example, a small scale parameter best conveys the heterogeneous Reintal ground surface, whereas the delineation of a mask encompassing three altitudinal subsystems

(Figs. 3.2, 3.4) implies a very high scale parameter. The final classification should be executed at an intermediate level, not too detailed but showing also relatively small landforms.

This meets the demand for hierarchical and scale dependent remote sensing classifications. Dikau (1994) states that the hierarchical organisation of topography has not yet been taken appropriately into account in studies on mountain geomorphology. Multiscalar approaches can correct for this defect (Figs. 3.3, 3.4).

3.3.3 Hierarchical landform classification

An ASTER satellite scene, a DEM (5 m resolution, generated in the ArcInfo spline algorithm Topogrid from data by the Bavarian Geodetic Survey) and its derivatives were assessed at four levels ranging from very small spectral units to the altitudinal strata mask (Fig. 3.3). The finest level L1 was segmented based on spectral (colour) information only, while the coarsest layer, L4, represents a strata mask made in a separate object-oriented project.

All segmented levels were then classified individually (see Schneevoigt et al., 2010 for details) with a knowledge base containing features immanent in a class itself and inherited ones passed on by parent classes in the classification hierarchy. Thus, working on multiscalar levels focussing on differently sized landform features imitates the systems approach, allowing for detailed and general views at once (Figs. 3.2, 3.3). The L1 classification renders ground land cover, level L3 eastern and western walls of cirques and hanging valleys, all of which leads to a sound L2 landform classification shown in Figure 3.4 (see Schneevoigt et al., 2008, 2010 for more information). The good fit of the results to ground truth is demonstrated in Schneevoigt et al. (2008). Detection limitations are reached with landforms such as moraine and rockfall deposits (which have been overprinted by more recent processes for centuries or millennia) and some complex alluvial fans. The majority of classes such as

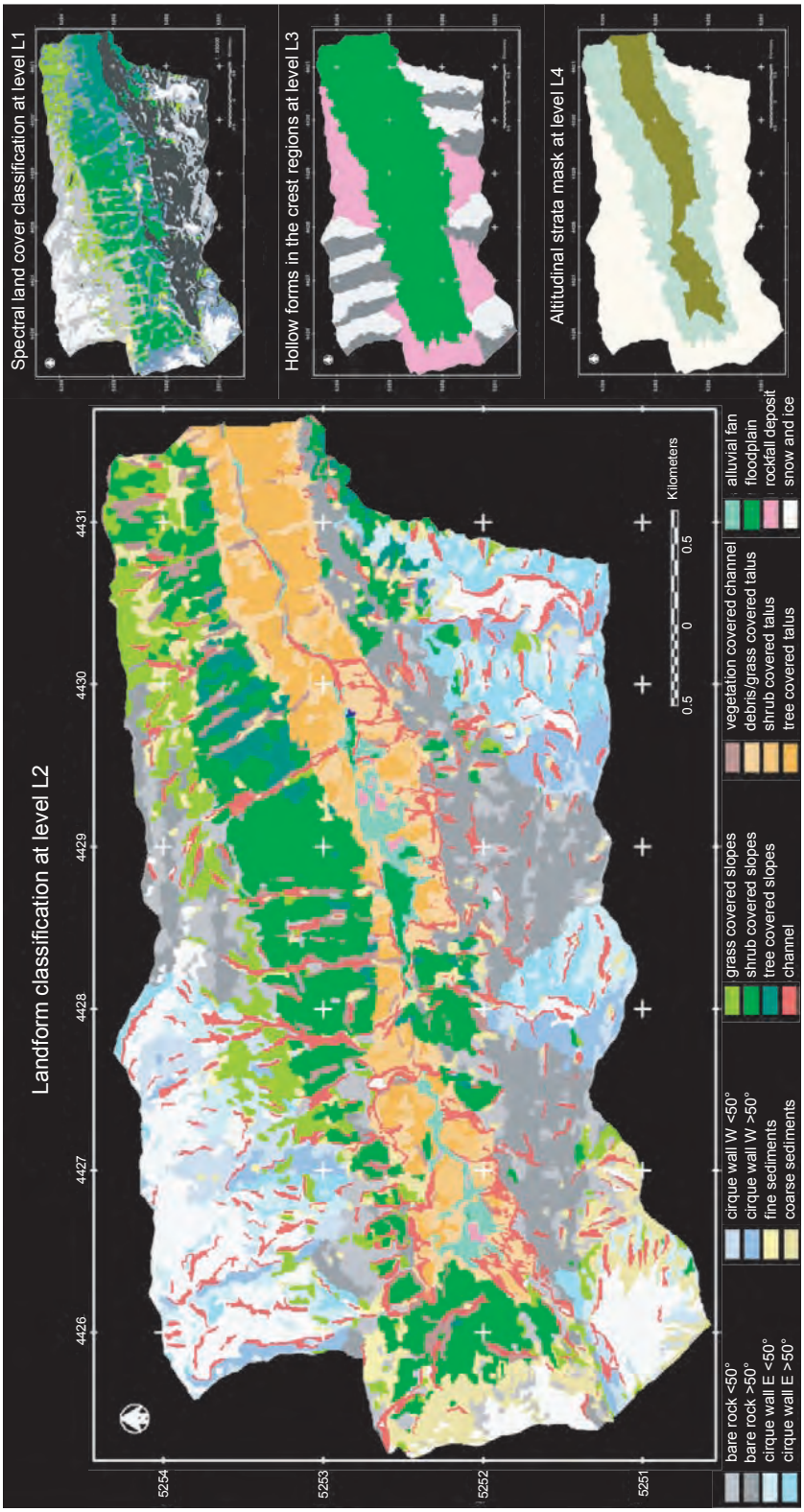

Figure 3.4: Object-oriented Classification Results on four Levels
Spectral land cover classification on level L1, landform classification on level L2, hollow forms in the crest regions on level L3, altitudinal strata mask on level L4.

cirques, rockwalls, floodplains, fine and coarse sediments were well assessed, and some could even be differentiated more than previously expected, e.g. the vegetation covered slopes and talus cover, leading to twenty final thematic landform classes (Fig. 3.4).

3.4 Conclusions

Remote sensing applications with geometrically medium-resolved, multispectral image data allow the classification of Alpine landforms or geomorphic process units to a great extent, even when dealing with such small landscape units as on the valley bottom of the Reintal (Fig. 3.1). Thus, remote sensing constitutes a valuable tool in the elaboration of the Alpine sediment cascade, particularly on account of its high detection capacity in otherwise inaccessible crest regions and rockwalls. Object-oriented classification rules should be transferable to other regions, as they depend less on reflection values, atmospheric conditions and arbitrarily selected training areas than pixel-based ones (Blaschke et al., 2002). Application of the approach to different study areas will show whether or not it prepares the ground for a semi-automatic landform classification scheme.

3.5 Acknowledgements

We thank the Remote Sensing Laboratories, University of Zurich (T. Kellenberger, K. Itten), the Center for Remote Sensing of Land Surfaces (S. Schiefer, M. Braun) and the Remote Sensing Research Group (H.-P. Thamm, G. Menz), both University of Bonn, for their cooperation. SEDAG has been funded by the German Research Foundation since 2000 (Schr 648/1- 3). N.J. Schneevoigt was supported by the German National Scholarship Foundation, SEDAG and the International Fellowship Programme of the Gottlieb Daimler and Karl Benz Foundation.

3.6 References

Ahnert, F. (1994): Equilibrium, Scale and Inheritance in Geomorphology. Geomorphology 11(2): 125-140.

Baatz, M. & A. Schäpe (2000): Multiresolution segmentation - an optimization approach for high quality multi-scale image segmentation. In: T. Strobl, T. Blaschke, & G. Griesebner (ed.): Angewandte Geographische Informationsverarbeitung XII. Beiträge zum AGIT-Symposium Salzburg 2000. Heidelberg, Herbert Wichmann Verlag: 12-23.

Ballantyne, C. K. (2002): A general model of paraglacial landscape response. Holocene 12(3): 371-376.

Becht, M., Haas, F., Heckmann, T. & Wichmann, V. (2005): Investigating sediment cascades using field measurements and spatial modelling. IAHS Publications 291: 206-213.

Benz, U. C., Hofmann, P., Willhauck, G., Lingenfelder, I., & M. Heynen (2004): Multiresolution, object-oriented fuzzy analysis of remote sensing data for GIS-ready information. ISPRS Journal of Photogrammetry & Remote Sensing 58: 239-258.

Bishop, M. P. & J. F. Shroder Jr. (2004): GIScience and mountain geomorphology: Overview, feedbacks, and research directions. In: M. P. Bishop & J. F. Shroder Jr. (ed.): Geographic Information Science and Mountain Geomorphology. Berlin, Heidelberg, Springer Verlag: 1-26.

Blaschke, T., Gläßler, C., & S. Lang (2002): Bildverarbeitung in einer integrierten GIS/Fernerkundungsumgebung - Trends und Konsequenzen. In: T. Blaschke (ed.): Fernerkundung und GIS. Neue Sensoren - innovative Methoden. Heidelberg, Herbert Wichmann Verlag: 1-9.

Blaschke, T. & G. Hay (2001): Object-oriented image analysis and scale-space: theory and methods for modeling and evaluating multiscale landscape structure. International Archives of Photogrammetry and Remote Sensing 34(4/W5): 22-29.

Caine, N. T. (1974): The geomorphic processes of the alpine environment. In: J. Ives & R. Barry (ed.): Arctic and Alpine Environments. London, Methuen: 721-748.

Chorley, R. (1962): Geomorphology and general systems theory. U.S. Geological Survey Professional Paper 500B, Washington: 1-10.

Chorley, R. & B. Kennedy (1971): Physical geography - a systems approach. London, Prentice Hall International.

Dikau, R. (1994): Computergestützte Geomorphographie und ihre Anwendung in der Regionalisierung des Reliefs. Petermanns Geographische Mitteilungen 138: 99-114.

Etzelmüller, B., Ødegard, R., Berthling, I. & J. Sollid (2001): Terrain parameters and remote sensing data in the analysis of permafrost distribution

and periglacial processes: principles and examples from southern Norway. Permafrost and Periglacial Processes 12: 79-92.

Geographie Innsbruck (2011): Tirol Atlas. http://tirolatlas.uibk.ac.at/maps/interface/topo.py/index (03.03.2011).

Giles, P. T. & S. E. Franklin (1998): An automated approach to the classification of the slope units using digital data. Geomorphology 21(3-4): 251-264.

Hack, J. (1960): Interpretation of erosional topography in humid temperate regions. American Journal of Science 258A: 80-97.

Haeberli, W. (1996): On the morphodynamics of ice/debris-transport systems in cold mountain areas. Norsk Geografisk Tidsskrift 50: 3-9.

Haefner, H., Small, D., Biegger, S., Hoffmann, H. & D. Nüesch (2000): Small-scale monitoring of wet snow cover with RADARSAT-ScanSAR data. EARSeL eProceedings 1: 339-347.

Hall, D. & J. Martinec (1986): Remote sensing of ice and snow. London, New York, Chapman and Hall.

Huggel, C., Kääb, A. & N. Salzmann (2004): GIS-based modeling of glacial hazards and their interactions using Landsat-TM and IKONOS imagery. Norsk Geografisk Tidsskrift 58: 61-73.

Ives, D. & B. Messerli (2001): Perspektiven für die zukünftige Gebirgsforschung und Gebirgsentwicklung. Geographische Rundschau 53(12): 4–7.

Ives, J., Messerli, B. & E. Spiess (1997): Mountains of the world - a global priority. In: B. Messerli & J. Ives (ed.): Mountains of the world. A global priority, New York: 1-15.

Jordan, P. & Slaymaker, O. (1991): Holocene sediment production in Lillooet River Basin, British Columbia: a sediment budget approach. Géographie Physique et Quaternaire 45(1): 45-57.

Kääb, A. (2002): Monitoring high-mountain terrain deformation from repeated air- and spaceborne optical data: examples using digital aerial imagery and ASTER data. ISPRS Journal of Photogrammetry & Remote Sensing 57: 39-52.

Kääb, A., Huggel, C., Paul, F., Wessels, R., Raup, B., Kieffer, H. & J. Kargel (2003): Glacier monitoring from ASTER imagery: accuracy and applications. EARSeL eProceedings 2: 43-53.

Kääb, A., Huggel, C., Fischer, L., Guex, S., Paul, F., Roer, I., Salzmann, N., Schlaefli, S., Schmutz, K., Schneider, D., Strozzi, T. & Y. Weidmann (2005): Remote sensing of glacier- and permafrost-related hazards in high mountains: an overview. Natural Hazards and Earth System Sciences 5: 527-554.

Koch, B., Jochum, M., Ivits, E. & M. Dees (2003): Pixelbasierte Klassifizierung im Vergleich und zur Ergänzung zum objektbasierten Verfahren. Photogrammetrie Fernerkundung Geoinformation 3: 195-204.

Krautblatter, M. & M. Moser (2005): Die Implikationen einer vierjährigen quantitativen Steinschlagmessung für Gefahrenabschätzung, Risikoverminderung und die Ausgestaltung von Schutzmaßnahmen. Tagungsband zur 15. Tagung für Ingenieurgeologie, Erlangen: 67-72.

Mark, D. M. & B. Smith (2004): A science of topography: From qualitative ontology to digital representations. In: M. P. Bishop & J. F. Shroder Jr. (ed.): Geographic information science and mountain geomorphology. Berlin, Heidelberg, Springer Verlag: 75-100.

McDermid, G. & S. Franklin (1994): Spectral, spatial, and geomorphometric variables for the remote sensing of slope processes. Remote Sensing of Environment 49: 57-71.

Otto, J.-C. & R. Dikau (2004): Geomorphologic system analysis of a high mountain valley in the Swiss Alps. Zeitschrift für Geomorphologie 48, 3: 323-341.

Paul, F. (2000): Evaluation of different methods for glacier mapping using Landsat-TM data. EARSeL eProceedings 1: 239-245.

Paul, F., Huggel, C. & A. Kääb (2004): Combining satellite multispectral image data and a digital elevation model for mapping debris-covered glaciers. Remote Sensing of Environment 89: 510-518.

Paul, F., Kääb, A., Maisch, M., Kellenberger, T. & W. Haeberli (2002): The new remote sensing derived Swiss glacier inventory: I. Methods. Annals of Glaciology 34: 355-361.

Rasemann, S., Schmidt, J., Schrott, L. & R. Dikau (2004): Geomorphometry in mountain terrain. M. P. Bishop & J. F. Shroder Jr. (ed.): Geographic Information Science and Mountain Geomorphology. Berlin, Heidelberg, Springer Verlag: 101-146.

Rothenbühler, C. (2006): GISALP. Räumlich - zeitliche Modellierung der klimasensitiven Hochgebirgslandschaft des Oberengadins. PhD Dissertation, Geographisches Institut der Universität Zürich.

Schaper, J. (2000): Fernerkundungsbasierte Kartierung von Schnee- und Eisflächen hochalpiner Gebiete. Ein Beitrag zur Abflussmodellierung und Bewertung der Auswirkungen potentieller Klimaänderungen. Remote Sensing Series, 34: 1-99.

Schiewe, J. & L. Tufte (2002): Potenzial regionen-basierter Verfahren für die integrative Auswertung von GIS- und Fernerkundungsdaten. T. Blaschke (ed.): Fernerkundung und GIS. Neue Sensoren - innovative Methoden. Heidelberg, Herbert Wichmann Verlag: 42-52.

Schmidt, K.-H. & Morche, D. (2006): Sediment output and effective discharge in two small high mountain catchments in the Bavarian Alps, Germany. Geomorphology 80: 131-145.

Schneevoigt, N.J., van der Linden, S., Kellenberger, T., Kääb, A. & L. Schrott (2010): Object-oriented classification of alpine landforms from an ASTER

scene and digital elevation data (Reintal, Germany). Grazer Schriften der Geographie und Raumforschung 45: 53-62.

Schneevoigt, N.J., van der Linden, S., Thamm, H.-P. & L. Schrott (2008): Detecting Alpine landforms from remotely sensed imagery. A pilot study in the Bavarian Alps. Geomorphology, 93: 104-119.

Schrott, L., Niederheide, A., Hankammer, M., Hufschmidt, G. & R. Dikau (2002): Sediment storage in a mountain catchment: geomorphic coupling and temporal variability (Reintal, Bavarian Alps, Germany). Zeitschrift für Geomorphologie N.F., Suppl. 127: 175-196.

Schrott, L., Hufschmidt, G., Hankammer, M., Hoffmann, T. & R. Dikau (2003): Spatial distribution of sediment storage types and quantification of valley fill deposits in an alpine basin, Reintal, Bavarian Alps, Germany. Geomorphology 55: 45-63.

Schrott, L., Götz, J., Geilhausen, M. & D. Morche (2006): Spatial and temporal variability of sediment transfer and storage in an Alpine basin (Bavarian Alps, Germany). Geographica Helvetica 3: 191-201.

Slaymaker, O. (1991): Mountain geomorphology: a theoretical framework for measurement programms. Catena 18: 427-437.

Strahler, A. (1952): Dynamic basis of geomorphology. Geological Society of America Bulletin 63: 923-938.

Unbenannt, M. (2002): Fluvial sediment transport dynamics in small alpine rivers - first results from two upper Bavarian catchments. Zeitschrift für Geomorphologie N.F., Suppl. 127: 197-212.

United Nations (1992): Earth Summit: Agenda 21. The United Nations Programme of Action from Rio. Rio de Janeiro, Brazil.

Walsh, S. J., Butler, D. R. & G. P.Malanson (1998): An overview of scale, pattern, process relationships in geomorphology: a remote sensing and GIS perspective. Geomorphology 21: 183-205.

4 Paper III
Detecting geomorphic landforms from optical imagery

published as
Schneevoigt, N.J., van der Linden, S., Thamm, H.-P. & L. Schrott (2008):
Detecting Alpine landforms from remotely sensed imagery. A pilot study in the Bavarian Alps.
Geomorphology 93: 104-119.

This study investigates the suitability of remote sensing for detecting rock and sediment storage areas in the Reintal subcatchment (17 km^2) east of Zugspitze, Germany. First, characteristic features of Alpine landforms such as curvature, process coupling or type of deposited sediment were compiled. Based on this, a landform classification was performed: topographical information from a digital elevation model (DEM) and spectral data from an Advanced Spaceborne Thermal Emission and Reflection Radiometer (ASTER) satellite scene were classified using a multiscale, object-oriented approach comprising four differently scaled levels. The complex decision-tree hierarchy is based for the most part on fuzzy membership functions and to a lesser extent on the hard nearest neighbour classifier. The results show that both an identification of

the present-day pattern of storage types and the classification of geomorphologic units, also with regard to their activity status and complexity, is largely possible. Moreover, the methodology developed in this study permits a first assessment of the upper regions of the study area which could not be included in any previous survey because of their inaccessibility. Coherent landform classification using remote sensing methods, as developed in this study, constitutes a promising scientific approach, especially with regard to the enhanced spatial and spectral resolution of modern satellite systems.

4.1 Introduction

Whereas many high alpine areas are only accessible to a certain extent, remotely sensed imagery is available for most regions in the world. Moreover, mapping with remote sensing data is relatively cost and time efficient (Konecny, 1999). However, high mountain regions represent difficult terrain for remote sensing applications: extreme altitudinal differences occur within small horizontal intervals and may result in offsets of several pixels or hundreds of meters if scanned at disadvantageous angles. Illumination varies enormously because of relief influences. For instance, dark shadows hamper more than half of the imagery evaluated for this work.

Studies using remote sensing applications and focussing on high mountain landforms are rare. Etzelmüller et al. (2001) and Bartsch et al. (2002), for example, try to identify geomorphological process units by integrating remote sensing information into a geographic information system (GIS) environment. Snow and glacier investigations rely more often on remote sensing alone (Hall and Martinec, 1986; Hall et al., 1995; Haefner et al., 1997; Rango, 1999; Paul, 2000), but overlaps with GIS applications are also frequent in this field (Jansa et al., 2002; Paul et al., 2002, 2004; Kääb et al., 2002, 2003a,b). Yet the relatively recent trend of image segmentation and object-oriented image interpretation allows new ways of linking remote sensing and GIS. It has found

its way into high mountain applications, e.g. with Giles (1998) and Giles and Franklin (1998) classifying geomorphological slope units or Blaschke (2000) extracting image objects for monitoring purposes.

At present, sensor development is constantly bringing forth improvements in spatial and spectral resolution, which leads to increased spectral heterogeneity within target classes. Conventional classification per pixel forms clusters based on spectral similarities alone and can result in many dispersed classes (salt-and-pepper effect) which often do not grasp the essence of the information inherent in the scene (Kartikeyan et al., 1998).

In contrast, image segmentation prior to classification helps to manage increased geometric resolution by merging adjacent pixels based on grey value homogeneity and form parameters. It assumes that proximate pixels with certain similarities represent the same kind of surface or feature on the ground. Thus the entire image is divided into spectrally akin objects which vary in shape and extent. Simultaneously, object outlines or borders represent transitions between heterogeneous surfaces. Consequently, the spectral generalisation inherent in pixel-mergers counteracts the salt-and-pepper effect by producing more homogeneous results. This is why segmentation techniques are increasingly used to deal with intensified in-class variability (Kartikeyan et al., 1998; Hill, 1999; Rodríguez-Yi et al., 2000; Blaschke et al., 2002; Neubert and Meinel, 2002; Schiewe and Tufte, 2002; Koch et al., 2003; Schneevoigt and Schrott, 2006).

This study presents a coherent landform classification with complete spatial coverage of the study area from DEM information and a satellite scene. It forms part of a set of projects called 'Sediment Cascades in Alpine Geosystems' (SEDAG), which are jointly aiming at developing a model to describe landform evolution in high mountain regions. At present, the Universities of Eichstätt, Erlangen, Halle and Bonn (all in Germany) are cooperating within SEDAG. The database gathered since 2000 gave rise to the idea of using that knowledge to test remote sensing methods for sediment storage detection.

The first part of this paper describes the exact spatial setting and processual order of Alpine storage types and gives a general overview of characteristical landform features derived from literature and field data. This information is utilised in a landform classification of the Reintal based on previously segmented image data (Fig. 4.1). These objectives are pursued in the following:

- to develop an inventory of landforms present in the Reintal, a prerequisite for the remote sensing applications,
- to find out which landforms are detectable by a semiautomatic classification scheme,
- to classify alpine landforms even in inaccessible crest regions,
- to show the potential of object-oriented image analysis as an efficient mapping tool.

4.2 Geological and geomorphological settings of the study area

The Reintal valley is situated in the Bavarian Alps, a part of the Northern Calcareous Alps (Fig. 4.2A), where the valley extends in an east-westerly direction along the Austro-German border. Excluding the Zugspitzplatt plateau to the west, a subcatchment of 17 km^2 was considered in this study (Fig. 4.2B), mostly consisting of dolomitized limestone (Wettersteinkalk). The relative relief within the high mountainous study area amounts to 1692 m from a minimum of 1052 m asl at the valley entrance to a maximum of 2744 m asl (Fig. 4.2B).

Due to former glacial erosion, the Reintal is divided into three vertical zones, namely upper regions (with cirques and hanging valleys), oversteepened rockwalls and a broadened valley bottom. However, with the climatic snowline lying at around 2700 m asl, no glaciers remain today. Vegetation belts

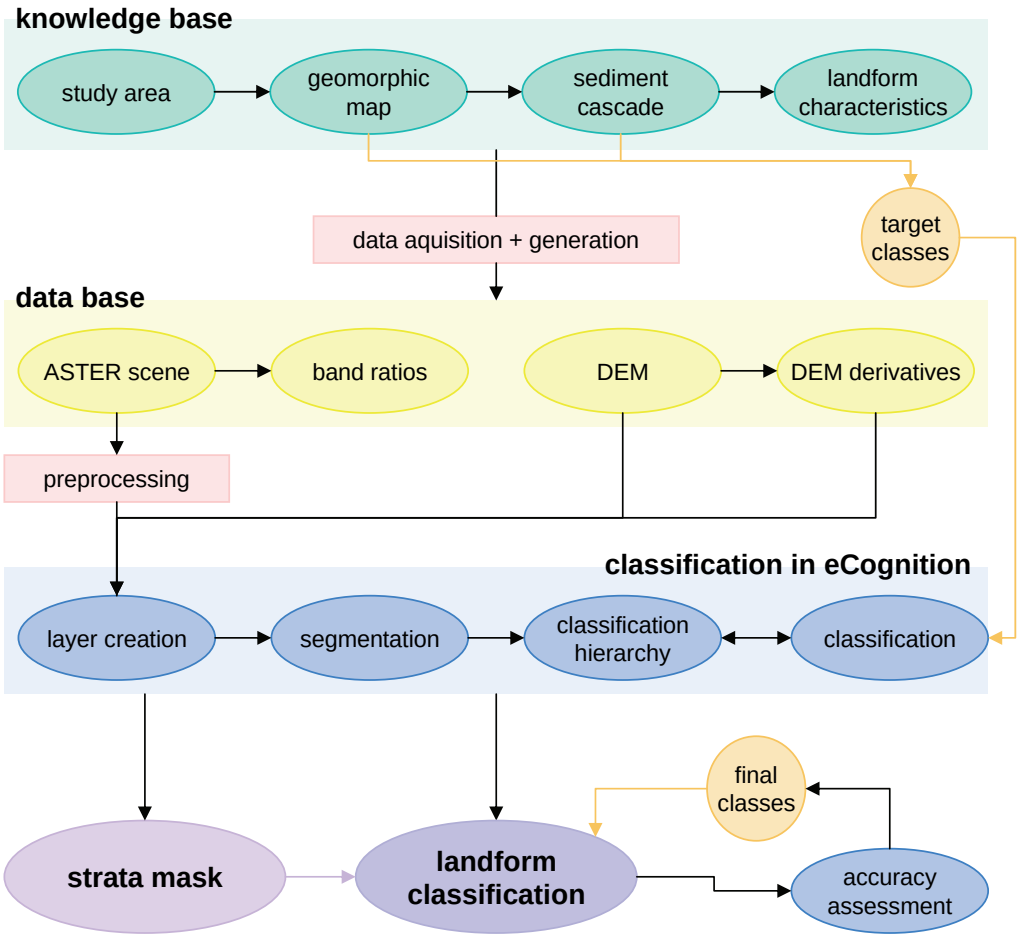

Figure 4.1: Representation of the Workflow followed in this Study

stretch from upper montane to nival zone; the Alpine tree line is located at around 1700 m. Both the precipitous rock faces and extensive tree cover raise problems for image segmentation and subsequent classification.

The landforms in the *valley bottom*, covering an area of 5.9 km length and maximum 700 m width, were mapped by Schrott et al. (2002) (for details see Fig. 4.3), with a terminology following Ballantyne and Harris (1994). The spatial distribution of these sediment storage types (Figs. 3.1, 4.3) exemplarily illustrates the conditions in a high mountain drainage basin: typically, talus sheets and cones dominate the overall picture with 41% and 26% of the valley

floor respectively. Rock falls (11%), alluvial fans (9%), floodplains and fluvial deposits (6%) cover another quarter of that area. The share of debris cones amounts to 5% and of avalanche deposits to only 1%, however the latter partially overprint the former, larger storage types. Thus the actual occurrence of debris and avalanche deposits in situ exceeds the figures given, while the other mapped landforms to some extent incorporate such deposits (Schrott et al., 2002). Manual mapping of the rockwalls and upper regions in the field was impossible due to the inaccessibility of the higher regions. However, the most important landforms in terms of area coverage are free faces, hanging valleys and cirques in the upper regions of the Reintal.

4.3 Methods and techniques

In order to distinguish landforms by remote sensing techniques, a compilation of their distinctive features is necessary. The better the knowledge basis concerning the target classes, the more possibilities arise to extract them from satellite and DEM data (Figs. 4.1, 4.2). Therefore, the first step within this study was to assemble the characteristics of the different landforms occurring in the Reintal (see Section 4.3.1), which also facilitates the understanding of their systematic distribution in landscape. As shown in Fig. 4.1, information from an ASTER scene and a DEM were subsequently examined and classified in an object-oriented approach (see Section 4.3.2) on four different scales with varying foci.

4.3.1 Alpine landform characteristics

According to Mark and Smith (2004), a landform is a "part of the Earth's surface that is characteristically apprehended as a unitary entity because of its particular shape" (p. 78). Geomorphological landforms result from spatially distributed and interlinked geomorphological processes, which are consecu-

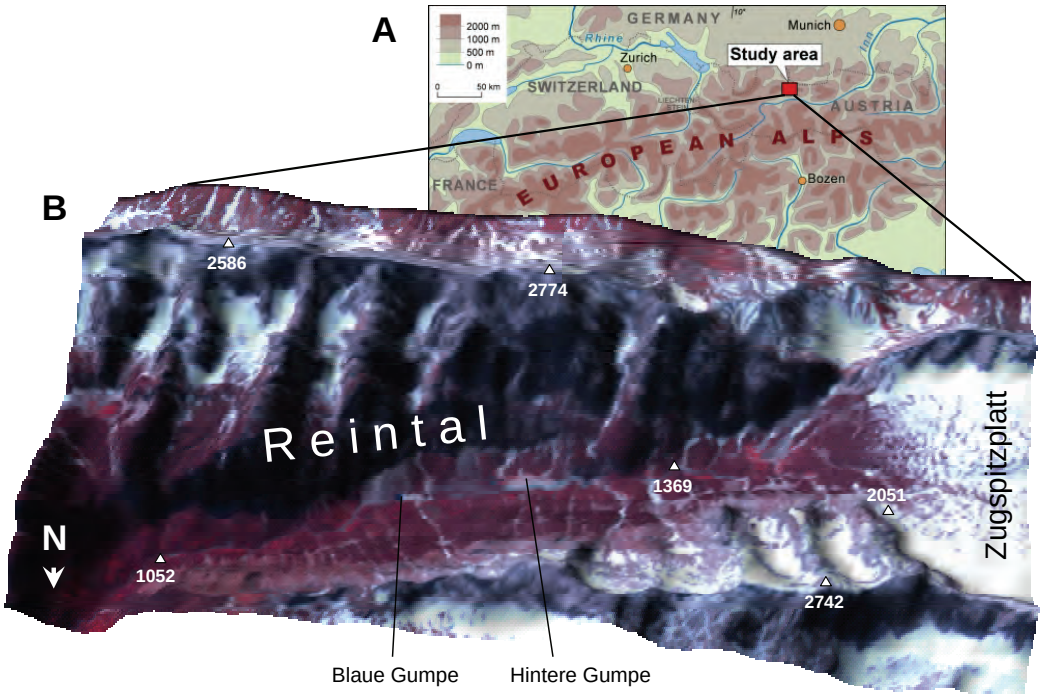

Figure 4.2: Reintal valley Drape and Location

(A) Geographical location of the Reintal study area in the Northern Calcareous Alps. (B) The 2001 ASTER scene in RGB 3-1-2 draped over the DEM (view from north). The valley stretches in an east-westerly direction along the Austro-German border, which runs on the southern valley crest.

tively modelling landscape by filling and emptying different types of sediment stores (Dikau, 1996; Schrott et al., 2003). As many forms are vague or graded, they do not display clear boundaries in landscape. Moreover, landforms often form part of other landforms — scale and given interest determine where a spectator would set a division (Mark and Smith, 2004). Depending on geographic situation, age, maturity and markedness of a landform, its geomorphometry varies also (Dikau, 1994; Rasemann et al., 2004). Monocausal linear process-form relations cannot be established because of mutual influences and interactions which vary spatially and temporally (Schrott et al., 2003). However, target classes must be defined for classification, so the characteristic features of the landforms occurring in the Reintal (Fig. 3.1) are described in the following (see Tabs. 4.1 and 4.2).

Glacial erosion has led to an extreme oversteepening of the *rockwalls*, especially obvious in the almost vertical free faces of the southern valley side (Figs. 1.3, 3.1), leading to a mean slope angle of 41.2° in the subcatchment (Unbenannt, 2002). Rapp (1960) and Bartsch et al. (2002) delimit steep slopes to values above 40°. In the classification hierarchy, a fuzzy threshold from 45° to 55° served best for separating free faces from steep talus and less inclined rockwalls by the DEM slope criterion.

The delimiting upper crests as well as the bottoms of *cirques* and *hanging valleys*, snow-covered for most of the year, can be easily discerned in aerial and satellite images (Fig. 4.2B). However, remote sensing applications hardly detect them from spectra or DEM because of relatively smooth transitions stretching over several pixels. Five hanging valleys and three cirques were detectable by aspect and height in the DEM in the Reintal, though. In accordance with the valley bottom, the threshold of the different hollow forms lowers from c. 1900 m asl in the west to c. 1600 m asl in the east (Fig. 4.2B), values circumscribing them in the DEM.

As typical, the *talus sheets* and *cones* in the Reintal are coupled with steep slopes (Fig. 3.1). Yet they show internal sorting, which is seldom found and implies that not only gravitative fall must have contributed to talus formation, but also to a large extent sheetwash and wet snow avalanches (Schrott et al., 2003). Hence the Reintal limestone taluses differ from the usual rockfall talus described in crystalline alpine areas such as Northern Scandinavia, the Canadian Rocky Mountains or the French Alps (Rapp, 1960; Luckman, 1976; Jomelli and Francou, 2000). As with internal sorting, sheetwash also leads to a lowering of slope, a feature which facilitates talus detection in the DEM. Active avalanche taluses show extensive vertical concavity and mostly angles below 30°, since the avalanche debris tends to be reworked successively downslope by later events, leaving the talus tongue to stretch all across the valley basin (Caine, 1974; Jomelli and Francou, 2000). In the Reintal, talus activity is higher on the southern slopes than on the northern ones, but in

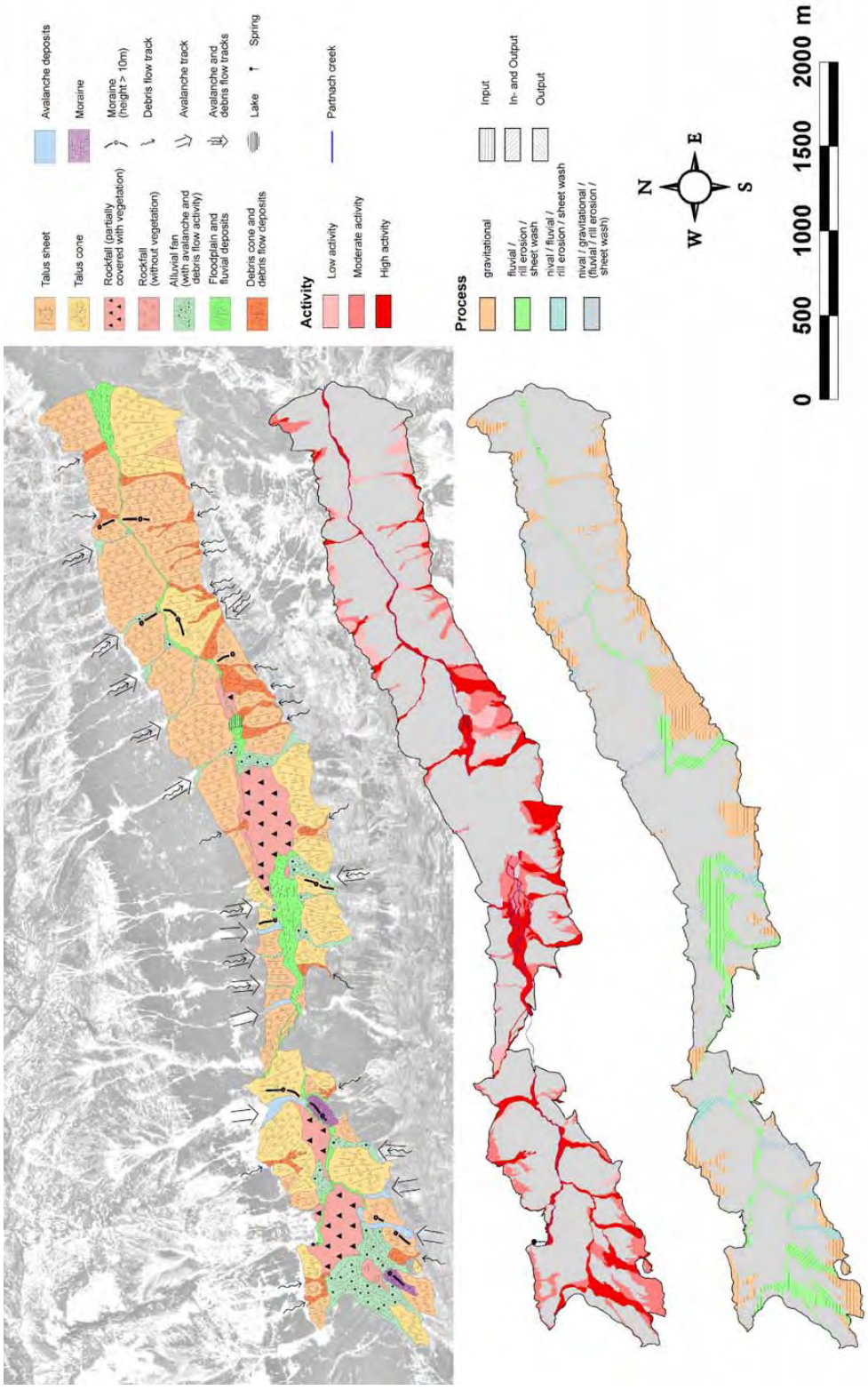

Figure 4.3: Geomorphological Maps of the Reintal valley Floor

Maps after Schrott et al. (2003), highlighting the distribution of sediment storage types, their process activity status and process coupling with respect to sediment input, sediment output or both.

general, talus sheets and cones belong rather to areas with moderate to no activity. More than 85% of the taluses are completely covered by vegetation without receiving any noticeable quantities of sediment (Figs. 4.2, 4.3, 3.1). These relict landforms hence experience neither input nor output (Fig. 4.3, Schrott et al., 2002, 2003).

Five *rockfall deposits* are discernable in the Reintal (Schrott et al., 2003) (Fig. 4.3), but three of them form relict and overprinted features. They constitute the only landforms in the valley exclusively built up by gravitational processes and shape the landscape by damming vast floodplains and lakes behind them, if they exceed a certain volume (Figs. 3.1, 4.3). Their very diverse extension, form and vegetation cover hinder their remote classification as one single class, but curvature may allow detection individually.

Alluvial fans should be extractable from DEM and curvature files by their concave long-profiles and convex cross-profiles with mean slopes between 2° and 12° (Blair and McPherson, 1994), but they slope more in the Reintal DEM. They occur in areas levelling out and are mostly linked to sheet flow, rather than veritable fluvial activity. Both eroded material from upslope and undercut sediments from adjacent stores contribute to their development (Fig. 3.1). Fans represent predominantly active landforms (Fig. 4.3), which are responsible for most of actual sediment transport in the valley (Schrott et al., 2003).

Unlike alluvial fans, *floodplains* hardly show any inclination with slopes of maximum 2° (Mark and Smith, 2004), but again were found to slope more in the Reintal DEM. Channel courses change rapidly, which leads to the development of a broad braided river system with terraces. Although floodplains cover only 6% of the valley bottom (Fig. 4.3), they impressively imprint landscape with formative sediment stores (Fig. 3.1).

Debris flows initiate in unconsolidated sediment that rests at angles between 25° to 46° (Dikau, 1996; Haeberli, 1996) above couloirs (Schrott et al.,

2003). Their flow tracks drop down between 24° and 35° (Zimmermann, 1996) and lie in the middle of boulder levées as a vertically rectilinear hollow form. The corresponding U-shaped cross-profile constitutes another clear indicator of debris flow, but this feature was not assessable in the 5 m DEM. *Debris cones* slope between 12° to 25° and thus flatter than talus cones due to their higher water content, which reduces shear strength. Superficial sorting does not occur, but rather internal stratification from overlying lobes (Zimmermann, 1996). In the Reintal, most debris flows originate at the border between rockwalls and taluses (Figs. 4.3, 3.1). They rarely form separate forms, but rather overprint other, older storage types, constituting a palimpsest of systems (Dikau, 1996; Schrott et al., 2003). Moreover, they are often associated with avalanche tracks.

Avalanche tracks, chutes or couloirs develop where plant growth proves impossible on account of repeated devastating events. These concave channels mostly lie below cirques in the rockwalls. Regular avalanche events lead to *avalanche deposits* in the form of narrow cones or elongated tongues (Jomelli and Francou, 2000). Valley geomorphology encourages avalanche activity in the Reintal, where avalanches often deposit on other landforms (Fig. 3.1), e.g. on floodplains (Heckmann et al., 2002; Schrott et al., 2002). Hence avalanche deposits labelled as such in Fig. 4.3 comprise only very active ones refilled more than once annually (Schrott et al., 2003). Typically, they display vertically rectilinear profiles and horizontal breadths of 10 to 20 m.

Moraine deposits cover 1% of the geomorphically mapped area (Fig. 4.3), but these relict landforms occur more frequently in the valley. They are covered by younger sediments and are only revealed when exposed by erosion, which is why their detection by remote sensing seems highly unlikely.

Schrott et al. (2002) developed a conceptual Alpine sediment cascade depicting the spatial distribution of storage types in the Reintal in a cascade linked by processes. Today, 79 % of the sediment stores in the valley bottom are considered to be relict forms and completely decoupled from the sedi-

ment cascade system (Schrott et al., 2002; Schneevoigt and Schrott, 2006). Avalanche and debris-flow tracks, alluvial fans and floodplains represent the most active storage types (Fig. 4.3). The upper parts of the valley deglaciated more than 2000 years later than the lower subunits, so process activity rises with valley altitude. Very low clastic sediment output turns the Reintal into an effective serial sediment trap. As most active landforms receive input only, sediment stores build up quickly (Schrott et al., 2002, 2003). All landform characteristics are summarised in Tables 4.1 and 4.2.

4.3.2 Segmenting and classifying optical imagery

Data basis employed

In this study, the suitability of ASTER imagery for landform detection was tested, because it compromises near global coverage, acceptable resolution and pricing. Since 2000, spectral data from the ASTER sensor recording at nadir are available in scenes of 60 x 60 km. Ground resolution varies between 15min the three visible and near-infrared (VNIR) bands (no. 1–3), 30 m in the six short wave infrared (SWIR) bands (no. 4–9) and 90 m in the five thermal infrared (TIR, no. 10–14). Both spectral coverage and orbit parameters resemble the younger Landsat sensor generations, but ASTER's geometric and spectral resolution is higher and offers more differentiation in the infrared spectrum (Fig. 4.4; Kääb et al., 2003a,b).

Ten bands of an ASTER scene from 29th May 2001 (Fig. 4.2) were selected for classification, i.e. VNIR, SWIR and TIR band 11. SWIR and TIR bands are useful for the detection of snow, ice and geological features. The bands were stacked, geometrically rectified to fixed landmarks in a monochrome orthophoto of 1996 (background in Fig. 4.3) and simultaneously resampled by cubic convolution to a resolution of 5 m to match DEM resolution. The orthophoto itself did not form part of the data set to be examined due to the five-year interval between its exposure and the ASTER scene. As in other

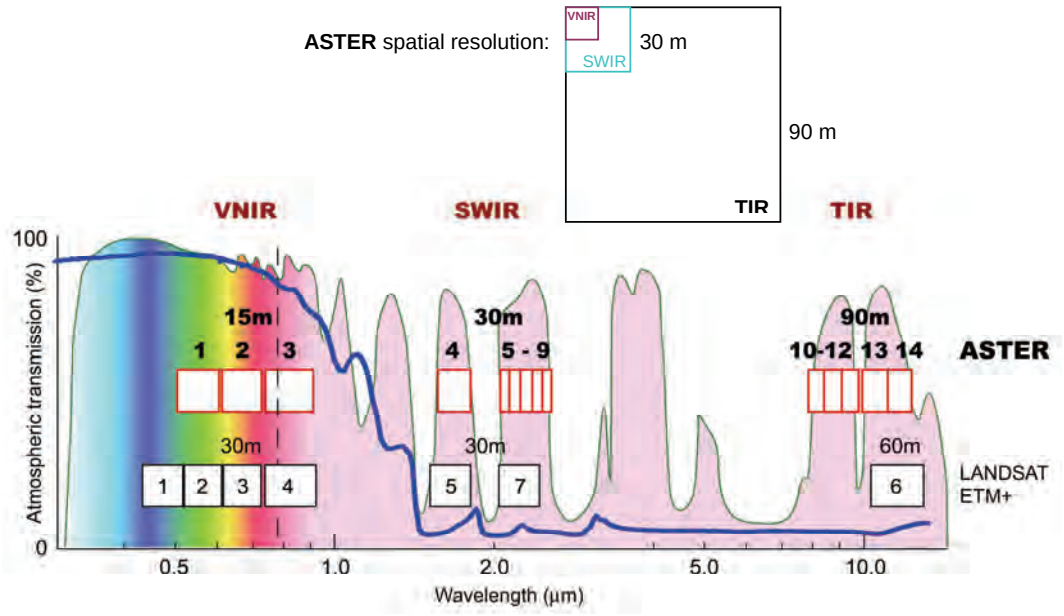

Figure 4.4: ASTER Bands in Comparison to Landsat ETM+

The upper row of rectangles represents the 14 ASTER spectral bands, the lower one the 7 Landsat ETM+ bands; their respective spatial resolutions are indicated above the rectangles. The shaded curve conveys atmospheric transmission dependent on wavelength, the thick one the spectral properties of snow. The box above the diagram shows the proportions between the different spatial ASTER band resolutions (modified from Kääb et al., 2003a).

monotemporal investigations (e.g. Hill, 1999; Etzelmüller et al., 2001; Bartsch et al., 2002), atmospheric and illumination correction were rejected, since they can introduce additional errors into the data set (Itten et al., 1992; Kellenberger, 1996; Vermote at al., 1997; Florinsky, 1998; Jansa et al., 2002; Bishop and Shroder, 2004). Atmospheric and brightness effects were counterbalanced by using a mask of different altitudinal strata (see Section 4.3.3) and band ratios (see Section 4.5.2).

A stream-corrected DEM (5 m ground resolution, vertical accuracy better than 0.5 m) served for topographical analysis. The DEM was generated by SEDAG partners using the ArcInfo spline algorithm Topogrid and photogrammetric data by the Bavarian Geodetic Survey. In this study, it served for the

generation of five DEM derivatives within ArcInfo. These geomorphometric grids of horizontal, vertical and total curvature, slope and aspect were also incorporated in the remote sensing applications. For the detection of landforms, they play a decisive role in the segmentation and classification processes, since spectral signatures alone often do not suffice for landform differentiation.

Object-oriented classification of landforms

Object-oriented approaches aim at creating areas which depict realistic forms rather than pixelled landscapes. However, segmenting a scene into objects implies more than a mere merging of pixels: while all pixels constitute equally sized squares, the different image objects vary in shape and extent. Thus also geometric features are extractable from the data, which can be helpful in classification. In addition, the spectral properties of image objects can be described both by mean values, standard deviations and ratios of the incorporated pixels. Working on several levels of abstraction is also possible. Finally, context emerges from considering neighbourhood relationships, sub- and superordinations, object-based morphometric and class-related features (Blaschke and Strobl, 2001; Baatz et al., 2002; Blaschke et al., 2002; Neubert and Meinel, 2002; Benz et al., 2004).

Object-based class descriptions hence reach beyond spectral information, provided that segmentation leads to objects which describe natural features geometrically well. In particular, DEM and other additional information can be usefully integrated and analysed for each object individually. This asset outweighs the fact that segmentation prior to classification represents an additional, time-consuming step: object-oriented image analysis unites the spectral interpretation capacities of remote sensing and the geometric tools of GIS into one desktop environment, hence combining both approaches. This constitutes an advantage in comparison to pixel-oriented analysis, especially when dealing with high mountain data (Giles, 1998; Giles and Franklin, 1998; Blaschke,

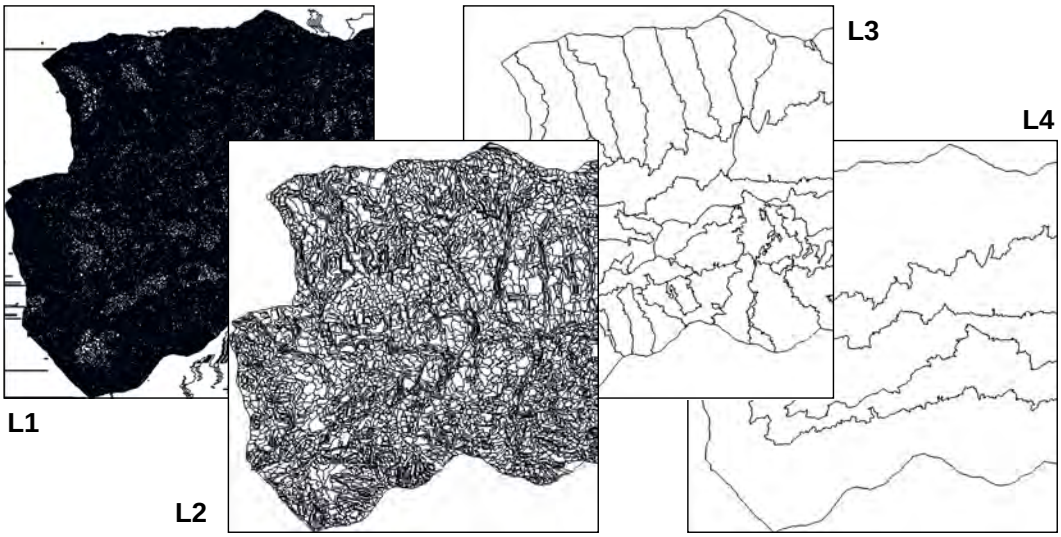

Figure 4.5: Multiresolution Segmentation of the four Levels
Displayed are the image object outlines of the four hierarchical layers L1 to L4.

2000; Schneevoigt and Schrott, 2006). However, the degree of transferability of both segmentation and classification schemes to different study areas remains to be investigated in further studies.

Objects which result from an image segmentation at a certain scale often depict certain class features very well, but do not render vital information for other classes because this information can only be displayed in another resolution. For example, a small scale parameter is very useful for precisely conveying the spectral information of the heterogeneous structure of the Reintal, whereas a division of the valley into three functional and altitudinal subsystems requires a very high scale parameter. The final classification, however, is best executed on an intermediate level in order not to show too heterogeneous details but to still capture relatively small landforms.

The multiresolution segmentation algorithm (Baatz and Schäpe, 2000) allows a simultaneous depiction of several so-called levels segmented on different scales (Blaschke and Strobl, 2001; Baatz et al., 2002; Blaschke et al., 2002;

Table 4.1: Alpine Landform Characteristics A

landform class	surface material	particle size	superficial sorting	vegetation cover	activity status	shape	slope
glacial cirque	bedrock	-	-	scarce mats of bristle grass	high	hollow form	steep head- and sidewalls, bottom <20°
hanging valley	bedrock	-	-	scarce mats of bristle grass	high	hollow form	steep head- and sidewalls, bottom <20°
free face	bedrock	-	-	none	high	extended	40°-90°
talus sheet	angular clasts	coarse gravel to boulders	coarsening downslope	high, except at apex	85% inactive; apex slightly active	extended	active: 25°-38°, inactive: >20°
talus cone	angular clasts	coarse gravel to boulders	coarsening downslope	high, except at apex; 1 cone without cover	85% inactive; apex slightly active	cone	active: 25°-38°, inactive: >20°
rockfall deposit	angular clasts	cobbles to boulders	rather unsorted; coarsening	little to high	inactive	extended to variable	<20°
alluvial fan	rounded clasts	silt to gravel	poorly to unsorted; possibly fining downslope	none to high	inactive to high	elongated, flat cone	1°-12°
floodplain, fluvial deposit	rounded clasts	mainly sand to cobbles, silt at plain foot	fining downslope	inactive to high	inactive to high	extended	<2°
debris flow track	bedrock and angular clasts	sand to boulders	unsorted	none or low	mostly high	linear	>24°
debris cone/ flow deposit	angular clasts	sand to boulders	unsorted	none or low	mostly moderate to high	cone	12°-25°
avalanche track	bedrock and angular clasts	fine gravel (grit) to boulders	unsorted	none or low	mostly high	linear	>25°
avalanche deposit	angular clasts	fine gravel (grit) to boulders	unsorted	none or low	mostly high	narrow cones or tongues	<25°
moraine deposit	angular and rounded clasts	silt to boulders	unsorted	little to high	inactive	dyke	<20°
vegetation covered slope	-	-	-	high	inactive	mostly linear	expanse

Table 4.2: Alpine Landform Characteristics B

Processes are plotted in square brackets if they are relict processes but the form they produced still today shapes the land surface.

landform class	horizontal curvature	vertical curvature	location	dominant process	further characteristics
glacial cirque	concave	concave	above 1600 m asl.	[glacial], weathering (gelifraction), rockfall, sheetwash, avalanche, debris flow	debris source for lower sediment stores
hanging valley	concave	concave	above 1600 m asl.	[glacial], weathering (gelifraction), rockfall, sheetwash, avalanche, debris flow	debris source for lower sediment stores
free face	straight	straight	upper regions	[glacial], weathering (gelifraction), rockfall, sheetwash	debris source for lower sediment stores
talus sheet	rectilinear	concave	mainly below waterfall on N-side	rockfall, sheetwash, avalanche	located below broad erosive zone in steep free face
talus cone	convex	concave	mainly on S-side; just before waterfall	rockfall, sheetwash, avalanche	located below linear ravine, gully or chute in steep free face
rockfall deposit	convex or straight	convex or straight	centre of valley floor	[gravitational fall/topple/slide], sediment accumulation	larger events create sediment sinks behind rockfall dams
alluvial fan	concave	convex	mostly to W and S of valley floor	fluvial accumulation, avalanche, debris flow	linked to drainage channels; accumulation where gradient decreases
flood-plain, fluvial deposit	slightly concave	convex	centre of valley floor	fluvial accumulation	braided river system; lake formation before rockfall deposits
debris flow track	convex-concave-convex	rectilinear	upper regions with a concentration in the E	mixture of gravitative and suspended transport	located below sediment source and above debris flow cone/alluvial fan
debris cone/ flow deposit	convex	rectilinear to convex	mainly on the S-side	accumulation of a mixture of gravitative and suspended transport	located on steep slopes (>25°) and below a sediment source; channel usually with levées
avalanche track	concave	rectilinear	mainly on the N-side	nival transport	located below cirques, above avalanche deposits/alluvial fans and perennial snow packs
avalanche deposit	convex	rectilinear to concave	mainly on the N-side	nival accumulation	below cirques, avalanche tracks and snow packs
moraine deposit	convex	rectilinear to convex	sporadicly on valley floor	glacial accumulation	[stages of glacier retreat]
vegetation covered slope	straight	mostly rectilinear	mainly on the N-side	infiltration	located above sediment stores and below rockwalls

Schiewe and Tufte, 2002; Benz et al., 2004) (Fig. 4.5). This way, natural features of various sizes can be jointly treated in an object-oriented manner. Yet the integration of additional levels only makes sense if this implies a gain of information which cannot be retrieved from the existing levels.

The pixel-based software package Erdas Imagine was used for data preparation and preprocessing, whilst the segmentation and classification process and accuracy assessment took place in the object-oriented eCognition programme. The latter allows simultaneous treatment of objects at different levels of abstraction, hence allowing for an image analysis on various, hierarchical scales (Baatz and Schäpe, 2000; Baatz et al., 2002). In order to create the boundaries needed to recognise the target landforms in the Reintal, segmentation of the data set into image objects proved to be necessary on four levels (Fig. 4.5): in a first step, the ASTER scene, the DEM and the five geomorphometric grids were used to generate a mask with the three altitudinal strata of crest regions, rockwalls and valley floor in a multiscale set of preclassifications (L4 in Fig. 4.5). After creating and segmenting the other three levels L1 to L3 (Fig. 4.5), a classification hierarchy was developed. Only level L1 employs the hard nearest neighbour classifier, all other levels use fuzzy membership functions to adjacent image objects or sub- and superobjects of other layers (Baatz and Schäpe, 2000; Baatz et al., 2002). Finally, the quality of the final L2 landform classification was evaluated. For accuracy assessment, up to ten representative test areas of ten to hundreds of pixels were chosen per landform class, depending on the availability of both unequivocal ground truth and appropriate image objects. They were selected all over the study area, conforming to 19,968 pixels in total.

4.4 Results

4.4.1 Landform characteristics condensed

The table of landform features distinguishes between fourteen landforms and twelve landform characteristics. The latter can be divided into four superordinate categories: visible material, particle size and superficial sorting describe the *sediment surface*, while slope, horizontal and vertical curvature constitute *form parameters*. In contrast, *spatial distribution* comprises the spatial extent, location in the valley and the process link of the different landforms. The categories activity status, vegetation cover, dominant process and processual link specify the *processes* involved (Tabs. 4.1, 4.2; Fig. 4.3).

4.4.2 Landform segmentation and classification

In the multiscale eCognition project, different scale parameters allowed varying features on each level (Fig. 4.5) to be recognised: the first level L1 based on pure spectral VNIR ASTER information defines all boundaries of the project at a very high resolution, rendering a classic remotely sensed land cover map. Level L4 displays the strata mask, while L3 focuses on hollow forms in the crest regions. L2 was designed for the final landform classification into which the entire information of all levels merged after their individual classification (Fig. 4.5).

All four levels were classified individually. The results of the levels L1 and L2 are displayed in Fig. 4.6. Level L3 assigns eastern and western walls of cirques and hanging valleys, while L4 represents the three altitudinal strata (shown in Schneevoigt and Schrott, 2006).

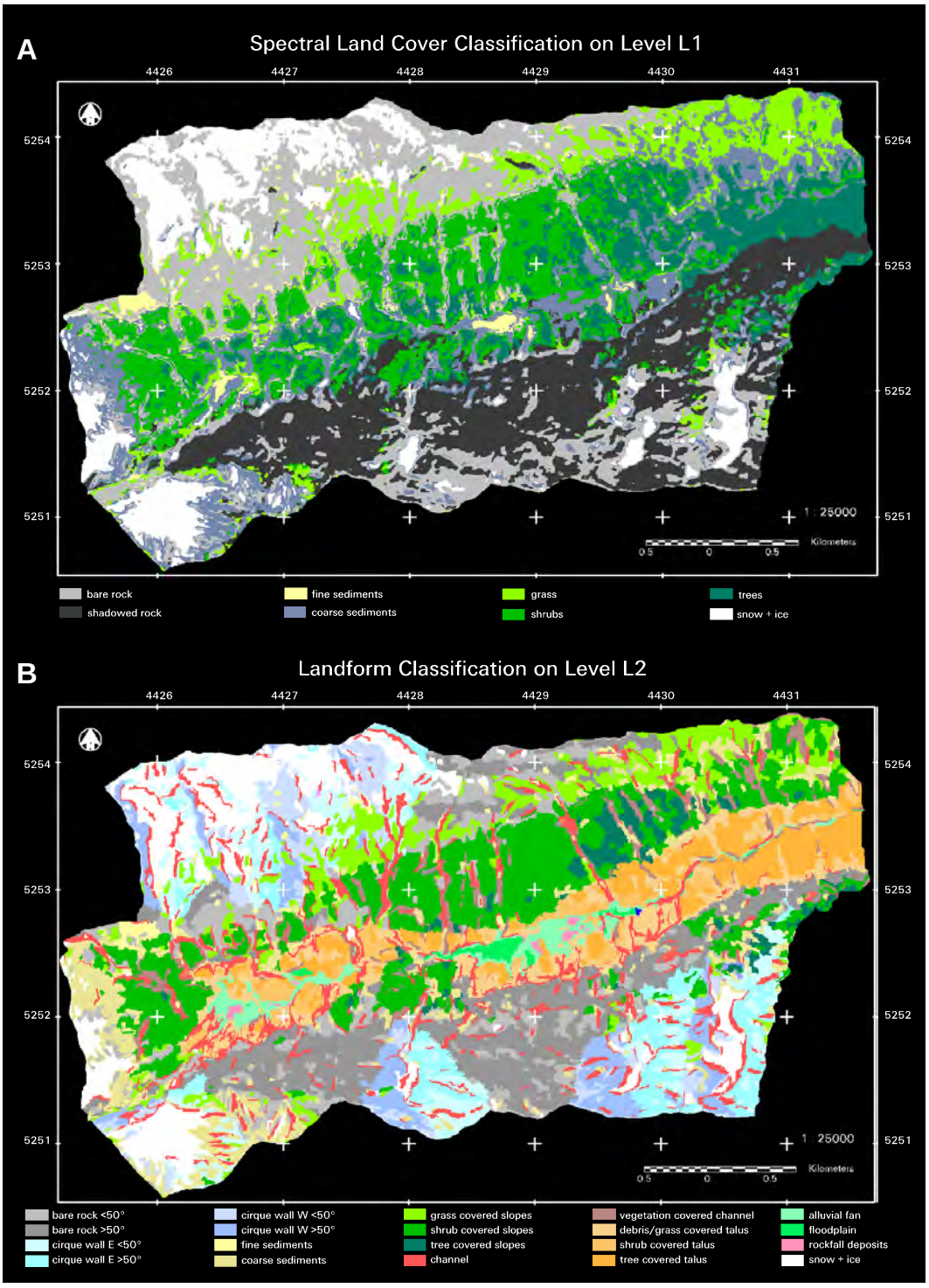

Figure 4.6: Final Classification on Levels L1 and L2
Results of the classification on level L1 focussing on surface cover (A) and on the final level L2 showing 20 landform classes and in blue the lake of Vordere Gumpe (B). For comparison, see the geomorphological map (Fig. 4.3).

4.5 Discussion

4.5.1 Comparison of classification and ground truth

In contrast to the detection of single geomorphic objects, the development of a classification scheme for a complete geomorphologic coverage represents a highly experimental approach. The intention of this study was investigating which landforms can successfully be detected in a semi-automatic, object-oriented approach. We were aware that not all landforms present in the Reintal can be detected, which is partly due to the 15 m resolution of the ASTER scene.

For ground truthing of crest areas, rockwalls and sediment stores on the valley floor, the orthophoto of 1996 and digital photos taken from opposite slopes and peaks were used, as was the geomorphological map of the Reintal bottom (Fig. 4.3, Tab. 4.3). This approach is limited, for several reasons: (I) on the ground, boundaries are blurred by landform coalescence, complexity, overlapping and vegetation cover (see Section 4.3.1), (II) surface conditions in alpine environments change rapidly (Caine, 1974; Schrott et al., 2002, 2003), and (III) traditional geomorphological mapping involves subjective and to some degree arbitrary judgments. Some geomorphological features might also be overprinted and thus were not identified in the traditional approach.

As can be seen from Fig. 4.6B, the 20 landform classes finally differentiated on level L2 (Tab. 4.3) generally closely approximate the ground truths:

- Detection accuracy of the different classes is relatively high. Landforms in the crest regions are detected particularly well as they are usually not covered by vegetation.

- In the class 'vegetation covered channels', sediment transport tracks and deposits from debris flows and avalanches occur. A further differentiation was not possible.

Table 4.3: The final Landform Classes differentiated on Level L2

Listed are the targeted landforms, the detail of classification finally obtained with L2 and comments on the classification process for each class.

target landforms	**classification on L2**	**comment**
glacial cirque and hanging valley	eastern cirque wall (<50°) eastern cirque wall (>50°) western cirque wall (<50°) western cirque wall (>50°) fine sediment coarse sediment snow and ice	classification more detailed than expected; was derived from aspect in the Reintal, but should be based on watershed outlines when applied to other study areas; distinction between sediments and talus in the cirques not possible due to lacking ground truth and snow cover in the scene
free face	bare rock (<50°) bare rock (>50°) fine sediment coarse sediment snow and ice	classification more detailed than expected
talus sheet and cone	debris/grass covered talus shrub covered talus tree covered talus	classification more detailed than expected inseparable from one another due to coalescence in the field
rockfall deposit	rockfall deposit	were only detected if recent and uncovered
alluvial fan	alluvial fan	difficult to separate from floodplains and vegetation covered channels
floodplain	floodplain	difficult to separate from alluvial fans due to very high floodplain gradients in the DEM
fluvial deposit	alluvial fan vegetation covered channel	spectrally not separable and topographically too small and indistict for a class on its own; creek slopes too much for an assignment of fluvial deposits to class "floodplain"
moraine deposit	not classified	classification impossible due to poor landform preservation
vegetation covered slope	grass covered slope shrub covered slope tree covered slope	classification more detailed than expected
debris flow debris cone avalanche track avalanche deposit	channel vegetation covered channel	equifinality hinders effective field identification of the 4 target classes

- Separation of alluvial fans and floodplains, as well as talus sheets and cones was difficult. This is at least partially based on the coalescent character of these landforms and the subjective decisions involved in field mapping. The overall largest problems for effective classification occurred with vegetation covered talus slopes.

- Relict forms are largely overprinted by more recent features in the Reintal, which often prevents their detection by satellite imagery and DEM information. At the scale parameter of L2, no distinguishing features exist for older rockfall and moraine deposits which were therefore excluded from the classification hierarchy.

The 20 landform classes (Tab. 4.3) finally differentiated on L2 score very high in the accuracy assessment with an overall accuracy of 92% and a kappa coefficient of 0.915. Fuzzy classification stability is slightly lower. These good results partially owe to the fact that two distinct data sources were combined for analysis: some target classes appear spectrally distinct (e.g. sediments, rocks vs. vegetation covered features), whereas other landforms could be separated using topographic information. Giles (1998) and Giles and Franklin (1998) reach an overall accuracy of 88.5% in a supervised classification of geomorphological slope units based on prior image segmentation and training areas. Bartsch et al. (2002) attain overall accuracies ranging from 85% to 93% for the classification of geomorphological process units by maximum likelihood. They conclude that the "synergy of remote sensing and GIS enables a sophisticated methodology for the identification of spatial distributions and interrelationships" (p. 177). Paul's (2000) maximum likelihood classification of glaciers obtains an overall accuracy of 95%.

However, our accuracy values have to be taken with care: on the one hand, object-oriented accuracy assessments tend to overestimate as they are based on averaged image objects and not on individual pixels. On the other, test areas were selected randomly, but without following a regular spatial pattern. Hence further accuracy assessment with different software is required. As older

rockfall and moraine deposits were excluded from classification, the overall accuracy of the landform detection compared to the geomorphological map will be lower than the values given above.

4.5.2 Possibilities and restraints of remote landform mapping

The L2 classification shows that landform classification based on the vegetation cover (Fig. 4.6A) is only partly successful. In the higher elevated areas, landform detection worked well because surface characteristics are not blurred by vegetation cover. Here, landforms are often correctly classified and thus detectable based on their surface characteristics (e.g. free faces, cirque walls). However, classifying accumulation forms in the valley (e.g. talus sheets, alluvial fans, floodplains) utilises more complex process and form descriptions, so that spectral information alone is insufficient. In general, a linear relationship between land cover and landform cannot be established, as similar vegetation may cover different landforms and ASTER resolution does not permit analysing sediment texture beyond 'coarse' and 'fine'. It has to be doubted if a better resolution would improve classification.

Spectral features generally reflect an area's geomorphic activity better than the type of landform present. Hence the development of a geomorphological activity classification would be an easier task than assessing landforms, which often comprise areas of varying activity. The Normalised Difference Vegetation Index (NDVI) formed an important differentiating feature in the classification hierarchy. This stresses the relative facility of assessing vegetation characteristics and hence process activity. The NDVI was chosen because it was successfully used on alpine landforms by Etzelmüller et al. (2001) and Bartsch et al. (2002). To obtain a better separation between vegetated and non-vegetated areas, the NDVI had to be adapted to the three different altitudinal strata. Even within each stratum, differences in NDVI based area assignments could

be noticed, possibly dependent on altitude or the effect of soil colour. The drawback of NDVI application in sparsely vegetated areas has been treated by Huete et al. (1985), García-Haro et al. (1996) and Gilabert et al. (2002). They found that NDVI does not reflect pure plant biotic information when spectral soil features shine through thin canopy. Yet the homogeneous lithology of the Reintal uniformly influences the NDVI, so that useful information could still be derived. When transferring the methodology to other regions, the appropriateness of NDVI application has to be established against soil-adjusted vegetation indices (SAVIs).

Shadowing constitutes another restraint for alpine remote sensing applications. Its effects can be reduced by band ratio formation, i.e. calculating the ratio of adjacent satellite image bands. This reinforces differences while similarities are eliminated: features like vegetation outlines and ice/snow are enhanced, and atmospheric and relief induced variations in illumination are diminished as they are highly correlated in neighbouring bands (Paul, 2000; Schaper, 2000). Here, the NDVI and simple ratios were successfully used for that purpose. The strata mask also compensates for variations in height and eases detection of altitude-dependent landforms. According to Florinsky (1998), such deterministic and probabilistic scene stratification prior to actual classification allows an enhanced assessment of image patterns with similar spectral responses. Itten et al. (1992), Kellenberger (1996) and Bishop and Shroder (2004) underline the use of creating areas of similar elevation as well.

Data resolution determines classification possibilities to a large extent. The relatively coarse ASTER resolution of 15 m posed an obstacle to exact landform tracing, as only landforms larger than this can be identified. For instance, finding an optimal segmentation for L2 constituted a time-consuming challenge, because the often faint signals from avalanche and debris flow tracks still had to be captured without resulting in too small a scale. Not all target classes could therefore be identified, for example a distinction of the different kinds of channels (Tab. 4.3) proved impossible. Furthermore, evaluating slope and

curvature was not possible to the extent desired, despite the high resolution DEM. The table of landform characteristics (Tabs. 4.1, 4.2, 4.3) was useful as a general lead. Yet figures (especially concerning slope angles) in the Reintal DEM sometimes diverged considerably from the values given in literature (see Section 4.3.1). This is possibly due to both, average calculation on the DEM pixels and landform coalescence on the ground. With a higher resolution in image and elevation data, figures may be better approximated. However, the majority of classes were well assessed, and some could even be further differentiated than previously expected, e.g. the vegetation covered slopes, talus cover, and cirques and hanging valleys, leading to a total of 20 landform classes that were finally satisfactorily mapped (Fig. 4.6B, Tab. 4.3).

4.6 Conclusion and perspectives

This study demonstrates the benefits of an object-oriented approach for geomorphological mapping in Alpine regions:

- Remote sensing techniques allow identification of both the present-day pattern of sediment storage types and geomorphologic units, for the later even insights in activity status and complexity.
- This methodology permits, for the first time, an assessment of the higher elevated areas of the Reintal, which could not be included in previous surveys because of inaccessibility.
- Coherent landform classification based on remote sensing data and DEM using image segmentation represents a promising new approach for geomorphic mapping, as not just individual geomorphic objects but an entire study area can be classified.

In future studies, a closer look should be taken at the particular impact of the two data sources by assessing them individually. Thus the extent can be determined to which spectral versus DEM information is responsible for

landform delineation, and whether their combined analysis results in synergetic effects. To further assess the scale-dependence of landform detection, other data sets should be evaluated, such as very high resolution imagery and DEM. Conversely, it would also be interesting to see to what extent lower resolution elevation models with near global coverage, such as from the ASTER sensor, or even from the Shuttle Radar Topography Mission (SRTM), can be integrated into this approach.

Future applications of the classification hierarchy, including the different scales of segmentation, at different study areas will show if the semi-automated landform classification scheme is transferable. Considering the very good match of this initial landform classification and ground truth, remote sensing constitutes a valuable tool for the examination of alpine geomorphic systems, particularly in otherwise inaccessible regions on crest and rock walls.

4.7 Acknowledgements

This study forms part of the SEDAG set of projects, which has been funded by the German Research Foundation (DFG) since 2000. We thank the Remote Sensing Research Group, the Center for Remote Sensing of Land Surfaces and the Geomorphological and Environmental Research Group, all located at the University of Bonn, for providing workplace and software. The internal reviews by the Glaciology and Geomorphodynamics Group (Department of Geography, University of Zurich) as well as the valuable comments of Andreas Kääb (Department of Geosciences, University of Oslo) and two anonymous reviewers were highly appreciated. Nora Jennifer Schneevoigt was supported by the German National Scholarship Foundation until 2004, then by SEDAG, and in 2006 held a scholarship within the International Fellowship Programme of the Gottlieb Daimler and Karl Benz Foundation. Sebastian van der Linden was funded within the scholarship programme of the German Federal Environmental Foundation (Deutsche Bundesstiftung Umwelt, DBU).

4.8 References

Baatz, M., Benz, U., Dehghani, S., Heynen, M., Höltje, A., Hofmann, P., Lingenfelder, I., Mimler, M., Solbach, M., Weber, M., Willhauck, G., 2002. Definiens Imaging - eCognition user guide 3. Munich.

Baatz, M., Schäpe, A., 2000. Multiresolution segmentation - an optimization approach for high quality multi-scale image segmentation. In: Strobl, T., Blaschke, T., Griesebner, G. (eds.), Angewandte Geographische Informationsverarbeitung XII, Beiträge zum AGIT-Symposium Salzburg 2000. Herbert Wichmann Verlag, Heidelberg, 12-23.

Ballantyne, C.K., Harris, C., 1994. Talus slopes and related landforms. In: Ballantyne, C.K., Harris, C. (eds.), Periglaciation of Great Britain. Cambridge University Press, Cambridge, 219-226.

Bartsch, A., Gude, M., Jonasson, C., Scherer, D., 2002. Identification of geomorphic process units in Kärkevagge, northern Sweden, by remote sensing and digital terrain analysis. Geografiska Annaler, 84A (3-4), 171-178.

Benz, U. C., Hofmann, P., Willhauck, G., Lingenfelder, I., Heynen, M., 2004. Multiresolution, object-oriented fuzzy analysis of remote sensing data for GIS-ready information. ISPRS Journal of Photogrammetry & Remote Sensing, 58, 239-258.

Bishop, M. P., Shroder Jr., J. F., 2004. Remote-sensing science and technology for studying mountain environments. In: Bishop, M.P., Shroder Jr., J.F (eds.): Geographic information science and mountain geomorphology. Springer Verlag, Berlin, Heidelberg, 147-188.

Blair, T.C., McPherson, J.G., 1994. Alluvial fans and their natural distinction from rivers based on morphology, hydraulic processes, sedimentary processes, and facies assemblages. Journal of Sedimentary Research, A 64(3), 450-489.

Blaschke, T., 2000. A multi-scalar GIS/image processing approach for landscape monitoring of mountainous areas. In: R. Bottarin, Tappeiner, U. (eds.): Interdisciplinary Mountain Research. Blackwell Verlag, Bozen, 44-57.

Blaschke, T., Gläßler, C., Lang, S., 2002. Bildverarbeitung in einer integrierten GIS/Fernerkundungsumgebung - Trends und Konsequenzen. In: T. Blaschke (ed.): Fernerkundung und GIS. Neue Sensoren - innovative Methoden. Herbert Wichmann Verlag, Heidelberg, 1-9.

Blaschke, T., Strobl, J., 2001. What´s wrong with pixels? Some recent developments interfacing remote sensing and GIS. Geo-Informationssysteme (GIS), 6, 12-17.

Caine, N.T., 1974. The geomorphic processes of the alpine environment. In: Ives, J., Barry, R. (eds.): Arctic and Alpine Environments. Methuen, London, 721-748.

Dikau, R. 1994. Computergestützte Geomorphographie und ihre Anwendung

in der Regionalisierung des Reliefs. Petermanns Geographische Mitteilungen, 138, 99-114.

Dikau, R., 1996. Geomorphologische Reliefklassifikation und -analyse. In: Mäus-
bacher, R., Schulte, A. (eds.). Beiträge zur Physiogeographie: Festschrift für Dietrich Barsch. Heidelberger Geographische Arbeiten, 104, 15-23.

Etzelmüller, B., Ødegård, R., Berthling, I., Sollid, J., 2001. Terrain parameters and remote sensing data in the analysis of permafrost distribution and periglacial processes: principles and examples from southern Norway. Permafrost and Periglacial Processes, 12, 79-92.

Florinsky, I. V., 1998. Combined analysis of digital terrain models and remotely sensed data in landscape investigations. Progress in Physical Geography, 22(1), 33-60.

García-Haro, F., Gilabert, M., Melía, J., 1996. Linear spectral mixture modelling to estimate vegetation amount from optical spectral data. International Journal of Remote Sensing, 17(17), 3373-3400.

Gilabert, M., Gonzáles-Piqueras, J., García-Haro, F., Melía, J., 2002. A generalized soil-adjusted vegetation index. Remote Sensing of Environment, 82, 303-310.

Giles, P.T., 1998. Geomorphological signatures: classification of aggregated slope unit objects from digital elevation and remote sensing data. Earth Surface Processes and Landforms, 23(6), 581-594.

Giles, P.T., Franklin, S.E., 1998. An automated approach to the classification of the slope units using digital data. Geomorphology, 21(3-4), 251-264.

Haeberli, W., 1996. On the morphodynamics of ice/debris-transport systems in cold mountain areas. Norsk Geografisk Tidsskrift, 50, 3-9.

Haefner, H., Seidel, K., Ehrler, C., 1997. Applications of snow cover mapping in high mountain regions. Physics and Chemistry of the Earth, 22(3-4), 275-278.

Hall, D., Martinec, J., 1986. Remote sensing of ice and snow. Chapman and Hall, London, New York.

Hall, D., Riggs, G., Salomonson, V., 1995. Development of methods for mapping global snow cover using Moderate Resolution Imaging Spectroradiometer data. Remote Sensing of Environment 54, 127-140.

Heckmann, T., Wichmann, V., Becht, M., 2002. Quantifying sediment transport by avalanches in the Bavarian Alps - first results. Zeitschrift für Geomorphologie N.F., Suppl. 127, 137-152.

Hill, J. 1993. High precision land cover mapping and inventory with multitemporal earth observation satellite data: The Ardèche Experiment. PhD thesis, Joint Research Centre (JRC).

Hill, R.A., 1999. Image segmentation for humid tropical forest classification in Landsat TM Data. International Journal of Remote Sensing 20(5), 1039-

1044.

Huete, A., Jackson, R., Post, D. 1985. Spectral response of a plant canopy with different soil backgrounds. Remote Sensing of Environment, 17, 37-53.

Itten, K., Meyer, P., Kellenberger, T., Leu, R., Sandmeier, S., Bitter, P., Seidel, K., 1992. Correction of the impact of topography and atmosphere on Landsat-TM forest mapping of alpine regions. Remote Sensing Series, 18, 48pp.

Jansa, J., Blöschl, G., Kirnbauer, R., Kraus, K., Kuschnig, G., 2002. Schneemonitoring mittels Fernerkundung. In: T. Blaschke (ed.). Fernerkundung und GIS. Neue Sensoren - innovative Methoden. Herbert Wichmann Verlag, Heidelberg, 241-250.

Jomelli, V., Francou, B., 2000. Comparing the characteristics of rockfall talus and snow avalanche landforms in an Alpine environment using a new methodological approach: Massif des Ecrins, French Alps. Geomorphology, 35(3-4), 181-192.

Kääb A., Huggel, C., Paul, F., Wessels, R., Raup, B., Kieffer H., Kargel, J., 2003a. Glacier monitoring from ASTER imagery: accuracy and applications. Proceedings of the EARSeL-LISSIG-Workshop "Observing our Cryosphere from Space", Bern, March 11-13, 2002. EARSeL e-Proceedings, 2, 43-53.

Kääb, A., Paul, F., Maisch, M., Hoelzle, M., Haeberli, W., 2002. The new remote sensing derived Swiss glacier inventory: II. First results. Annals of Glaciology, 34, 362-366.

Kääb, A., Wessels, R., Haeberli, W., Huggel, C., Kargel, J.S., Khalsa, S.J.S., 2003b. Rapid ASTER imaging facilitates timely assessment of glacier hazards and disasters. EOS Transactions, 84(13), 117-124.

Kartikeyan, B., Sarkar, A., Majumder, K.L., 1998. A segmentation approach to classification of remote sensing imagery. International Journal of Remote Sensing 19(9), 1695-1709.

Kellenberger, T.W., 1996. Erfassung der Waldfläche in der Schweiz mit multispektralen Satellitenbilddaten. Grundlagen, Methodenentwicklung und Anwendung. Remote Sensing Series, 28, 284pp.

Koch, B., Jochum, M., Ivits, E., Dees, M., 2003. Pixelbasierte Klassifizierung im Vergleich und zur Ergänzung zum objektbasierten Verfahren. Photogrammetrie Fernerkundung Geoinformation, 3, 195-204.

Konecny, G., 1999. Mapping from space. E-Proceedings of the ISPRS Workshop "Sensors and Mapping from Space 1999", http://www.ipi.uni-hannover.de/html/publikationen/1999.htm, 21.09.2007.

Luckman, B.H., 1976. Rockfalls and rockfall inventory data: some observations from Surprise Valley, Jasper National Park, Canada. Earth Surface Processes and Landforms, 1, 287-298.

Mark, D.M., Smith, B., 2004. A science of topography: from qualitative onto-

logy to digital representations. In: Bishop, M.P. & Shroder Jr., J.F. (eds.): Geographic information science and mountain geomorphology. Springer Verlag, Berlin, Heidelberg, 75-100.

Neubert, M., Meinel, G., 2002. Segmentbasierte Auswertung von IKONOS-Daten - Anwendung der Bildanalyse-Software eCognition auf unterschiedliche Testgebiete. In: Blaschke, T. (ed.). Fernerkundung und GIS. Neue Sensoren - innovative Methoden. Herbert Wichmann Verlag, Heidelberg, 108-117.

Paul, F., 2000. Evaluation of different methods for glacier mapping using Landsat-TM data. In: Wunderle, S. (ed.): EARSeL Workshop on Remote Sensing of Land Ice and Snow, Juni 2000, Dresden, 239-245, Dresden.

Paul, F., Huggel, C., Kääb, A., 2004. Combining satellite multispectral image data and a digital elevation model for mapping debris-covered glaciers. Remote Sensing of Environment, 89, 510-518.

Paul, F., Kääb, A., Maisch, M., Kellenberger, T., Haeberli, W., 2002. The new remote sensing derived Swiss glacier inventory: I. Methods. Annals of Glaciology, 34, 355-361.

Rango, A., 1999. Spaceborn remote sensing for snow hydrology applications. Hydrological Sciences, 41(4), 477-494.

Rapp, A., 1960. Recent development of mountain slopes in Kaerkevagge and surroundings, Northern Scandinavia. Geografiska Annaler, A 42(2-3), 71-200.

Rasemann, S., Schmidt, J., Schrott, L., Dikau, R., 2004. Geomorphometry in mountain terrain. In: Bishop, M.P., Shroder Jr., J.F. (eds.): Geographic information science and mountain geomorphology. Springer Verlag, Berlin, Heidelberg, 101-146.

Rodríguez-Yi, J.L., Shimabukuro, Y.E., Rudorff, B.F.T., 2000. Image segmentation for classification of vegetation using NOAA AVHRR data. International Journal of Remote Sensing 21(1): 167-172.

Schiewe, J., Tufte, L., 2002. Potenzial regionen-basierter Verfahren für die integrative Auswertung von GIS- und Fernerkundungsdaten. In: Blaschke, T. (ed.): Fernerkundung und GIS. Neue Sensoren - innovative Methoden. Herbert Wichmann Verlag, Heidelberg, 42-52.

Schneevoigt, N.J., Schrott, L., 2006. Linking geomorphic systems theory and remote sensing. A conceptual approach to Alpine landform detection (Reintal, Bavarian Alps, Germany). Geographica Helvetica 61(3), 181–190.

Schrott, L., Niederheide, A., Hankammer, M., Hufschmidt, G., Dikau, R., 2002. Sediment storage in a mountain catchment: geomorphic coupling and temporal variability (Reintal, Bavarian Alps, Germany). Zeitschrift für Geomorphologie N.F., Suppl. 127, 175-196.

Schrott, L., Hufschmidt, G., Hankammer, M., Hoffmann, T., Dikau, R., 2003. Spatial distribution of sediment storage types and quantification of valley

fill deposits in an alpine basin, Reintal, Bavarian Alps, Germany. Geomorphology, 55, 45 - 63.

Unbenannt, M., 2002. Fluvial sediment transport dynamics in small alpine rivers - first results from two upper Bavarian catchments. Zeitschrift für Geomorphologie N.F., Suppl. 127, 197-212.

Vermote, E., Tanré, D., Deuzé, J., Herman, M., Morcrette, J., 1994. Second Simulation of the Satellite Signal in the Solar Spectrum (6S). Technical report, Greenbelt (MD).

Zimmermann, M., 1996. Murgänge erkennen und bewerten. In: Oddsson, B. (ed.): Instabile Hänge und andere risikorelevante natürliche Prozesse. Birkhäuser, Basel, Boston, Berlin, 183-196.

5 Paper IV
Segment-based classification of optical and elevation data

published as
Schneevoigt, N.J., van der Linden, S., Kellenberger, T., Kääb, A. & L. Schrott (2011):
Object-oriented classification of alpine landforms from an ASTER scene and digital elevation data (Reintal, Bavarian Alps).
Grazer Schriften der Geographie und Raumforschung 45: 53-62.

High mountain regions represent difficult terrain for detecting rock and sediment storage areas. By means of a satellite scene by the Advanced Spaceborne Thermal Emission and Reflection Radiometer (ASTER) and a digital elevation model, the geomorphological setting of the Reintal subcatchment (17 km^2) east of the Zugspitze is analysed. Characteristic landforms are classified in an object-oriented approach comprising four spatial levels of differentiation. The complex, object-based decision tree hierarchy largely founds on fuzzy membership functions and to a lesser extent on a minimum distance classifier. The final landform classification scores high in the accuracy assessments.

The results show that an identification of the present-day pattern of geomorphological process units is possible by remote sensing. Besides, the approach provides a first insight into the otherwise inaccessible upper regions of the study area which could not be included in any previous survey.

5.1 Introduction

High mountain regions display a "geomorphic environment of considerable diversity. This variability in both time and space is perhaps the single most significant geomorphic characteristic of the alpine zone" (Caine, 1974: 722). Therefore these fragile environments react very quickly and sensitively to global change (Kääb, 2002). However, scientific knowledge about their geomorphologic process structure remains sketchy and incomplete, especially quantitatively. Similarly, the question of potentially mobilisable sediments in the upper regions of high mountain catchments still calls for an answer (Schrott et al., 2003). Within a set of projects called 'Sediment Cascades in Alpine Geosystems' (SEDAG), the universities of Eichstätt, Erlangen, Halle and Bonn/Salzburg have developed a model to describe landform evolution in high mountain regions.

This study forms part of the SEDAG research and represents the third of a series of papers: geomorphic systems theory and object-oriented remote sensing have been linked in Schneevoigt & Schrott (2006) in order to convey the theoretical and conceptual background of the analysis. Schneevoigt et al. (2008) accentuates its geomorphological side, particularly stressing the nature of the alpine landforms examined. In contrast, this paper at hand describes the remote sensing methods employed in further depth.

It aims at a semi-automatic classification scheme for geomorphological landforms, which can supply otherwise inaccessible information besides assisting landscape monitoring and mapping. As upper areas mostly cannot be observed from the ground, remote sensing applications represent a means of closing this

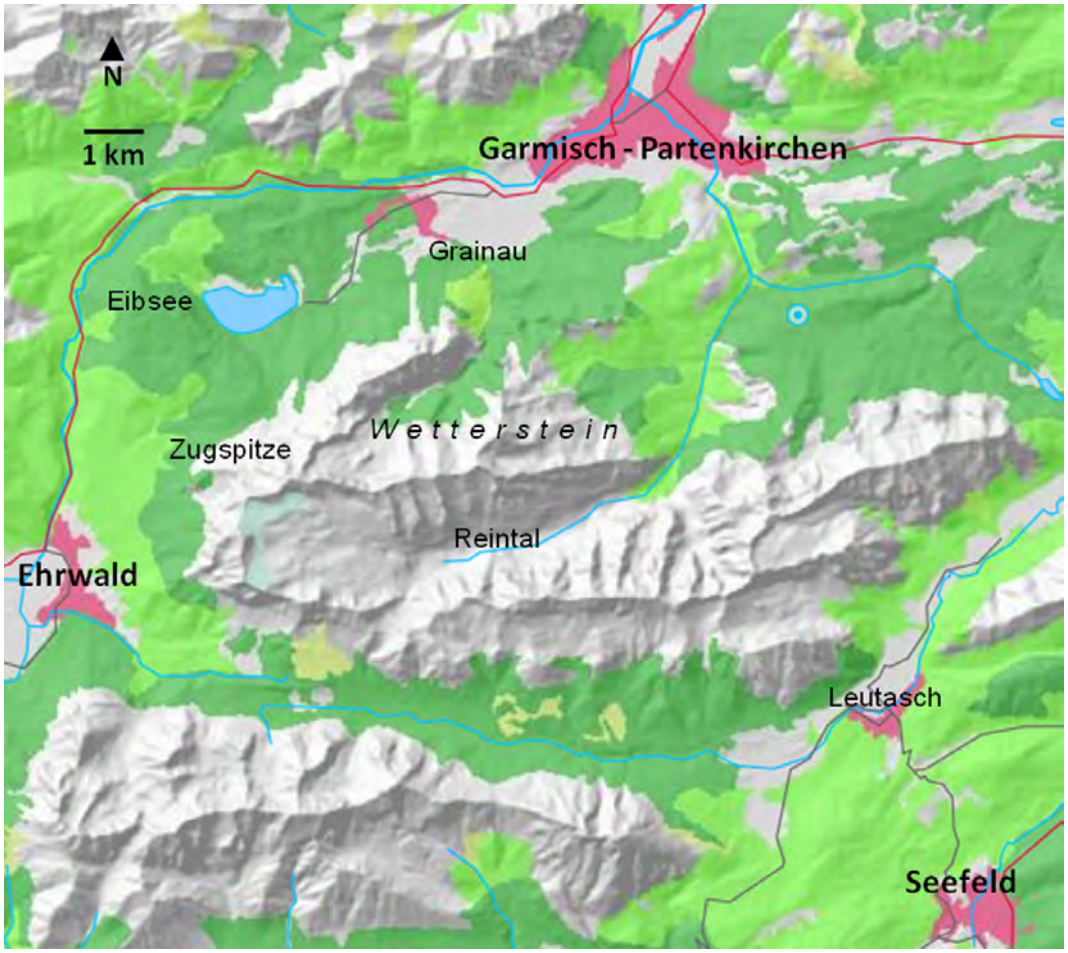

Figure 5.1: The Geographical Location of the Reintal
Location of the study area within the Wetterstein massif (The valley stretches in an east-westerly direction along the Austro- German border, which runs on the southern valley crest. Modified from Geographie Innsbruck, 2011).

gap which hampers a full understanding of the alpine sediment cascade. Many studies on high mountain geomorphology use GIS coupled with remote sensing data, whereas only few employ genuine remote sensing techniques (for details see Schneevoigt et al., 2008; Schneevoigt & Schrott, 2006). Object-oriented image segmentation prior to classification constitutes a novel and promising approach (Blaschke et al., 2002; Benz et al., 2004). This relatively new trend has also found its way into high mountain applications, e.g. with Giles & Franklin (1998) classifying geomorphological slope units.

5.2 Geographical setting

The Reintal valley is situated 7 km south of the town of Garmisch-Partenkirchen in the Bavarian Alps (Fig. 5.1). It extends over 8 km in predominantly dolomitised limestone or Wettersteinkalk. As the Zugspitzplatt is not linked to the valley in terms of sediment transfer, it has been excluded from the study area amounting to 17 km^2. No glaciers persist today, but Pleistocene glaciations have typically shaped cirques and hanging valleys in the upper regions, oversteepened rockwalls and a broadened valley bottom. The relative relief within the study area amounts to 1690 m reaching a maximum of 2744 m asl. at Hochwanner peak, a fact which amongst others confirms the high mountainous nature of the Reintal.

Today, 79% of the sediment stores on the valley floor are relict or inactive and completely decoupled from the sediment cascade system. Avalanche and debris flow tracks, alluvial fans and floodplains represent the most active storage types. In general, process activity rises with valley altitude. Very low clastic sediment output turns the Reintal into an effective serial sediment trap. As most active landforms receive input only, sediment stores build up quickly (Schrott et al., 2003).

5.3 Object-oriented landform classification

5.3.1 Optical data basis

In this study, ASTER scenes were assessed because of their spatial resolution, pricing and near global coverage (Klug, 2002, Kääb, 2002, with more information). Ten bands of an ASTER scene from 29th May 2001 (Fig. 4.2B) were selected for classification, i.e. all the visible/near-infrared (VNIR) and short wave infrared (SWIR) bands together with thermal infrared (TIR) band 11. The bands were stacked, geometrically rectified to fixed landmarks

in a monochrome orthophoto of 1996 and simultaneously resampled by cubic convolution to a resolution of 5 m to match DEM resolution. As in other monotemporal investigations, atmospheric and topographic corrections were rejected, since they can introduce additional errors into the data set (relevant reference in Schneevoigt et al., 2008). Several ratios were used in this work; the Normalised Difference Vegetation Index (NDVI) forms important thresholds in the classification hierarchy (Fig. 5.2).

A digital elevation model (DEM) of 5 m ground resolution (Fig. 3.3 top) was generated and hydrologically stream corrected by SEDAG partners using photogrammetric data by the Bavarian Geodetic Survey. It served for the generation of five DEM derivatives. These geomorphometric grids of horizontal, vertical and total curvature, slope and aspect were incorporated in the classification process in addition to the DEM (Fig. 3.3).

The landforms considered in this study are summarized in Table 5.1 (additional information can be found in Schneevoigt et al., 2008). They result from interacting and partially equifinal processes. Thus strict delimitations of landforms do not always exist in landscape: many forms show no clear boundaries (Figs. 3.1, 4.2). As partially interfingered deposits are frequent, form characteristics deviate from the ideal. This "fuzzy nature of most high mountain terrain features" (Kääb, 2002: 50) makes it necessary to consider context for sound classifications. Keeping the interval of time in mind, the orthophoto of 1996 served as ground truth for crest and rockwall regions as well as for the

Table 5.1: Target Classes in the Classification Process
Target classes sorted according to their predominant location in the study area.

upper regions	rockwalls	valley bottom	ubiquitary
snow and ice	grass covered slopes	shrub covered talus	bare rock (<50°)
eastern cirque wall (<50°)	shrub covered slopes	tree covered talus	bare rock (>50°)
eastern cirque wall (>50°)	tree covered slopes	alluvial fan	fine sediments
western cirque wall (<50°)		floodplain	coarse sediments
western cirque wall (>50°)		rockfall deposits	channel
			vegetation covered channel
			debris/grass covered talus

sediment stores on the valley floor. Digital photos taken, as far as accessible, from opposed slopes and peaks, were used for the same purpose. A geomorphological map drawn up by Schrott et al. (2003) served as reference when dealing with the Reintal valley bottom.

5.3.2 Image segmentation into objects

The object-oriented approach (not to be confused with the homonymous programming mode) consists of two separate steps. First, the data employed is segmented into homogeneous image objects through generalisation and average determination, smoothing out irregular pixel-dominated patterns and creating more realistic forms. Secondly, these entire objects are classified, not individual pixels. Object-oriented image analysis hence unites the spectral analyses of remote sensing and the geometric tools of GIS into one desktop environment.

The segmentation algorithm by Baatz & Schäpe (2000) segments an image in a knowledge-free way via region-growing, an automatized heuristic optimization method: the potential increase of spectral heterogeneity is assessed in a merge weighed by the size of two pixels or segments considered. Next to this colour criterion based on spectral information alone, shape parameters can be used to correct highly textured data which otherwise would produce frayed and distorted segments. This constitutes an advantage especially in high mountain data. Yet it must be applied carefully, as it implies an arbitrary divergence from the given spectral information based on pure arithmetics (Baatz & Schäpe, 2000).

Not only spectral data, but also DEMs and all kinds of derivatives from image and elevation information can be integrated in the segmentation process. The available sources or parameters can be weighed by factors to differentiate their respective influence on the creation of a layer. These assets compensate for the extra time-consumption of finding adequate segmentation parameters.

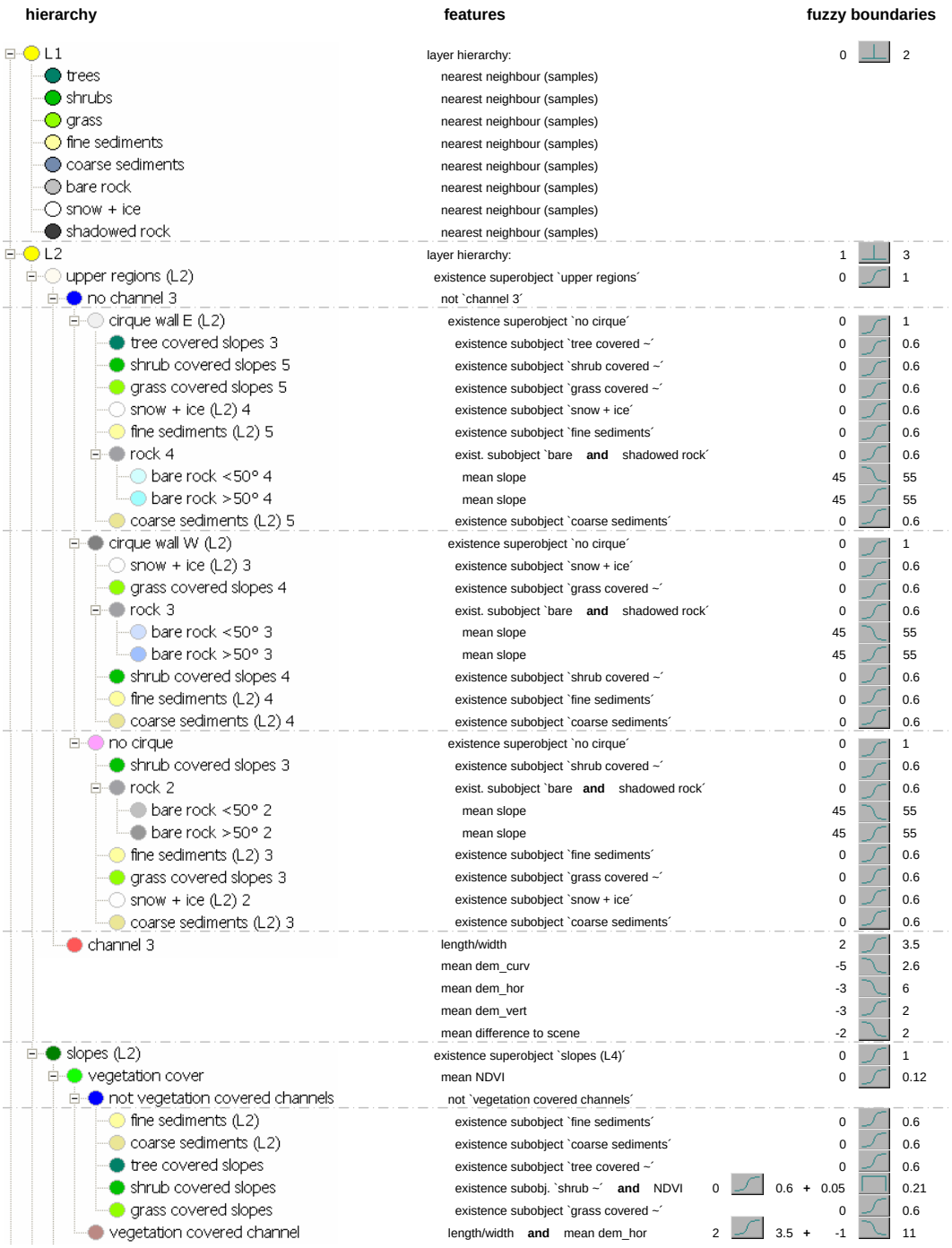

Figure 5.2: Extract of the Classification Hierarchy

The figures around the membership function icons to the right indicate the thresholds of the fuzzy areas.

To address features at different scales, individual layers must be segmented for each scale. The multiresolution segmentation algorithm (Baatz & Schäpe, 2000) permits a simultaneous depiction of several image levels segmented at various spatial resolutions (Benz et al., 2004). Yet the integration of additional levels only makes sense if this implies a gain of information which cannot be retrieved from the existing levels.

Initially, a strata mask distinguishing three altitudinal storeys was generated in an ancillary project with three levels. In this set of preclassifications, crest regions and valley bottom both carry an error of commission to guarantee inclusion of all relevant image objects. The resulting layer was imported as L4 into the main project (Fig. 3.3). Here, segmentation on four levels was necessary in order to create the boundaries for all target classes. A small scale parameter conveys the spectral ground information of the Reintal (L1, Fig. 3.3). Conversely, the imported mask of three altitudinal subsystems (L4) requires a very high scale parameter, and the cirques and hanging valleys (L3) a relatively high one. An intermediate level serves for the final classification (L2), so that smaller landforms can be displayed while preserving a certain degree of generalization.

The segmentation of level L2 comprises the scales and parameters necessary to optimally depict the different landforms. For example, decreasing the colour criterion improves the representation of water bodies, but worsens the taluses at the same time. VNIR bands and DEM derivatives were brought into an equilibrium of 4:3, so that spectral information dominates. Scale 13 guaranteed the existence of necessary boundaries; decisive further ameliorations only set in below scale 10. However, this would have increased the project and processing times on the one hand, while leading to a lesser degree of abstraction due to small image objects on the other. Hence parameterisation resulted in level L2 illustrated in Figure 3.3.

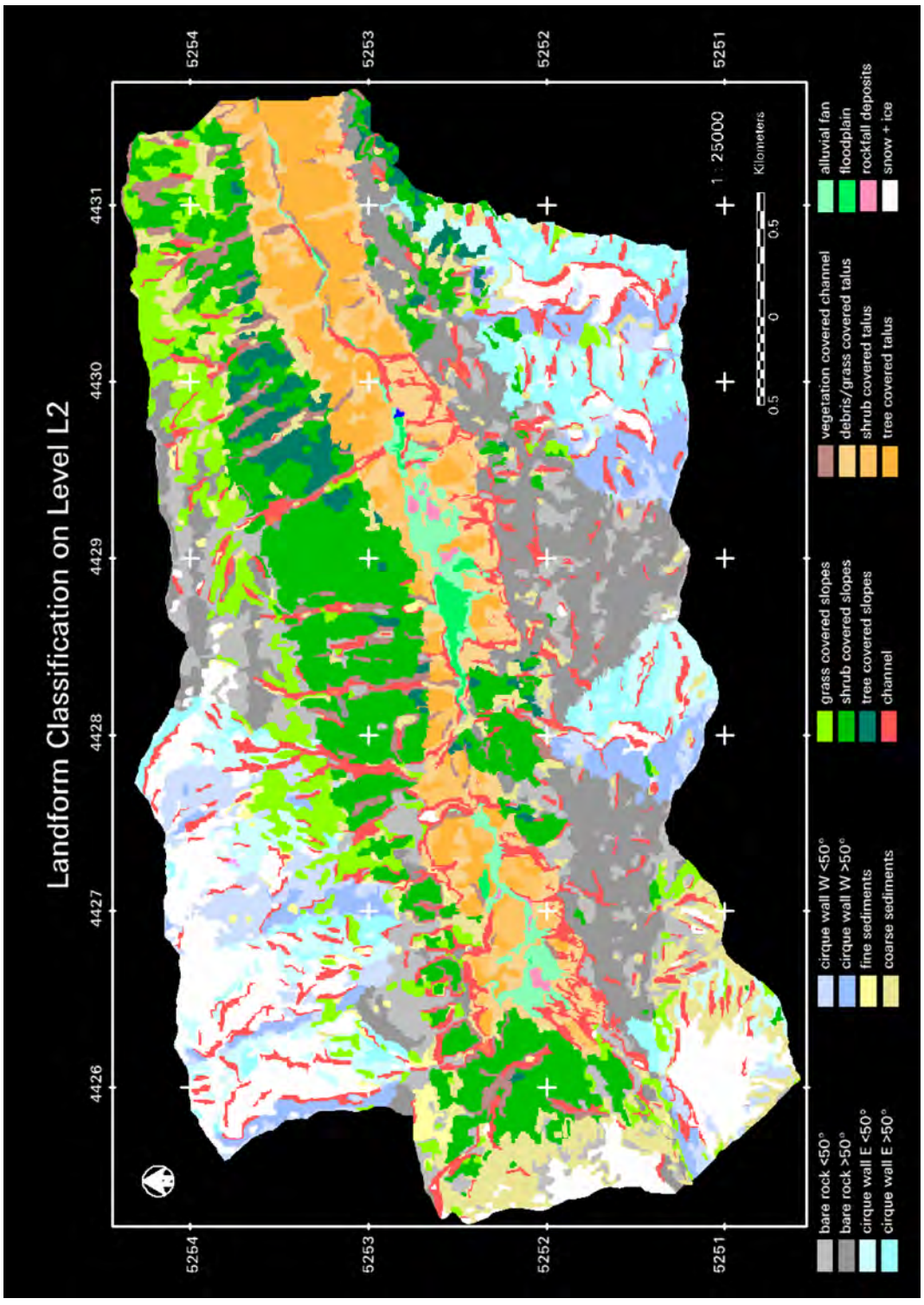

Figure 5.3: The final Landform Classification on Level L2
Its 20 distinct classes completely cover the study area, leading to a coherent thematic map which approximates ground truth well.

5.3.3 Classification of the image objects on four levels

Each image object can be addressed by mean value, standard deviation and ratio of the incorporated pixels next to its individual geometric features and its neighbourhood. When working on several image levels, relationships, sub- and superordinations, morphometric and class-related features can also be used for class descriptions (Benz et al., 2004; Blaschke et al., 2002). This accommodates three-dimensional alpine applications, provided that segmentation leads to objects which describe natural features geometrically well (Schneevoigt et al., 2008).

The four segmented levels were classified individually after developing the corresponding classification hierarchy (Fig. 5.2). This knowledge base is edited from class descriptions, which divide into contained features immanent in a class itself and inherited ones passed on by parent classes in the class hierarchy. A combination of hard (L1) and soft (L2, L3, L4) classifiers enables this approach generally resting on fuzzy logic. Hereby, floating thresholds provide a margin for the attribution of an object to a class (Fig. 5.2, right). Soft membership classifiers return fuzzy values between 0 (no assignment at all) and 1 (full assignment) for each feature and image object considered. Besides, fuzzy logic operators, which produce for instance sums, subsets and means, link different feature terms (Baatz & Schäpe, 2000).

5.4 Results

The classification of level L1 renders ground land cover, level L4 the strata mask, level L3 eastern and western walls of cirques and hanging valleys (see Schneevoigt & Schrott, 2006). This leads to a sound L2 landform classification (Fig. 5.3). The majority of classes such as cirques, rockwalls, floodplains and sediments are identified well. Detection limits are reached with moraine and rockfall deposits, because they have been overprinted by more recent processes

Table 5.2: Confusion Table of the L2 Classification

L2 \ test areas	shrub covered talus	tree covered talus	debris/grass covered talus	floodplain	grass covered slopes	shrub covered slopes	tree covered slopes	vegetation covered channel	channel	fine sediments (L2)	snow + ice (L2)	coarse sediments (L2)	bare rock <50°	bare rock >50°	cirque wall W >50°	cirque wall W <50°	cirque wall E >50°	cirque wall E <50°	lake	alluvial fan	rockfall deposits	sum L2
shrub covered talus	1426	0	24	0	0	0	0	0	0	0	0	0	0	0	0	0	0	0	0	0	0	1450
tree covered talus	238	2081	0	0	0	0	0	0	0	0	0	0	0	0	0	0	0	0	0	0	0	2319
debris/grass cov. talus	397	61	316	0	0	0	0	0	0	0	0	0	0	0	0	0	0	0	0	0	0	774
floodplain	0	0	0	732	0	0	0	0	0	0	0	0	0	0	0	0	0	0	0	94	0	826
grass covered slopes	0	0	0	0	873	0	0	0	0	0	0	0	0	0	0	0	0	0	0	0	0	873
shrub covered slopes	0	0	0	0	0	1553	68	169	0	0	0	0	0	0	0	0	0	0	0	0	0	1790
tree covered slopes	0	0	0	0	0	0	1178	0	0	0	0	0	0	0	0	0	0	0	0	0	0	1178
veg. covered channel	0	0	0	0	156	0	0	514	0	0	0	0	0	0	0	0	0	0	0	0	0	670
channel	0	0	0	0	0	0	0	0	772	0	0	0	0	0	0	0	0	0	0	54	0	826
fine sediments (L2)	0	0	0	0	0	0	0	0	0	756	0	38	0	0	0	0	0	0	0	0	0	794
snow + ice (L2)	0	0	0	0	0	0	0	0	0	0	1932	0	0	0	0	0	0	0	0	0	0	1932
coarse sediments (L2)	0	0	0	0	0	0	0	0	0	0	0	991	27	0	0	0	0	0	0	12	0	1030
bare rock <50°	0	0	0	0	0	0	0	0	0	0	0	0	507	0	0	0	0	0	0	0	0	507
bare rock >50°	0	0	0	0	0	0	0	0	0	0	0	0	0	740	0	0	0	0	0	0	0	740
cirque wall W >50°	0	0	0	0	0	0	0	0	0	0	0	0	0	13	642	0	0	0	0	0	0	655
cirque wall W <50°	0	0	0	0	0	0	0	0	0	0	0	0	34	0	0	794	0	0	0	0	0	828
cirque wall E >50°	0	0	0	0	0	0	0	0	0	0	0	0	0	37	0	0	396	0	0	0	0	433
cirque wall E <50°	0	0	0	0	0	0	0	0	0	0	0	0	14	0	0	0	0	869	0	0	0	883
lake	0	0	0	0	0	0	0	0	0	0	0	0	0	0	0	0	0	0	70	0	0	70
alluvial fan	0	0	0	0	0	0	0	0	0	0	0	0	0	0	0	0	0	0	6	592	138	744
rockfall deposits	0	0	0	0	0	0	0	0	0	0	0	0	0	0	0	0	0	0	0	0	646	646
sum test pixels	2061	2142	340	732	1029	1553	1246	683	780	756	1932	1029	582	790	642	794	396	896	76	752	784	19968
producer´s accuracy	0.692	0.972	0.929	1	0.848	1	0.945	0.753	0.99	1	1	0.963	0.871	0.937	1	1	1	1	0.921	0.787	0.824	
user´s accuracy	0.983	0.897	0.408	0.886	1	0.868	1	0.767	0.935	0.952	1	0.962	1	1	0.98	0.959	0.915	0.984	1	0.796	1	
kappa per class	0.668	0.968	0.927	1	0.841	1	0.942	0.744	0.989	1	1	0.961	0.868	0.934	1	1	1	1	0.921	0.779	0.818	
overall accuracy	0.92																					
kappa	0.915																					

for centuries or millennia and therefore leave no characteristic marks on the land surface. Then again, some target classes (Tab. 5.1) are further differentiated than previously expected. For instance, the vegetation cover of slopes and taluses was subdivided into high, medium and low natural cover, leading to 20 thematic landform classes (Tab. 5.2) in Figure 5.3.

The final landform classification scores high in the assessments of both overall accuracy (92 %), kappa coefficient (0.915), user's and producer's accuracy (Tab. 5.2). Only a few misclassifications occur, but they concern high amounts of pixels, as level L2 consists of image objects of ten to hundreds of pixels. Fuzzy classification stability, i.e. the degree of distinctness between most and second most probable class affiliation, is lower (Fig. 5.4), but best membership assignments score generally high, too. Alluvial fans tend to intermingle with floodplains, while talus sheets and cones could not be differentiated from one another. This owes to the fact that in situ, these landforms tend to mostly coalesce, so that their exact assignment relies on interpretation by the observer. Overall, the vegetation covers of talus show the highest confusion.

5.5 Discussion

Image segmentation represents an additional, time consuming step in the classification routine. Finding an optimal segmentation for L2 constituted a veritable challenge, because the often very faint signals from avalanche and debris flow tracks should still be captured without ending at too small a resolution. VNIR bands have to be given considerable weight, as they trace landforms best. Yet the object-oriented approach makes the difficult high mountain terrain manageable (Schneevoigt et al., 2008) and leads to sound results.

The good results partially owe to the fact that two distinct data sources were combined for analysis: some target classes appear spectrally distinct (e.g. sediments, rocks vs. vegetation covered features), whereas other landforms could be separated by topographic information. For instance, Giles & Franklin

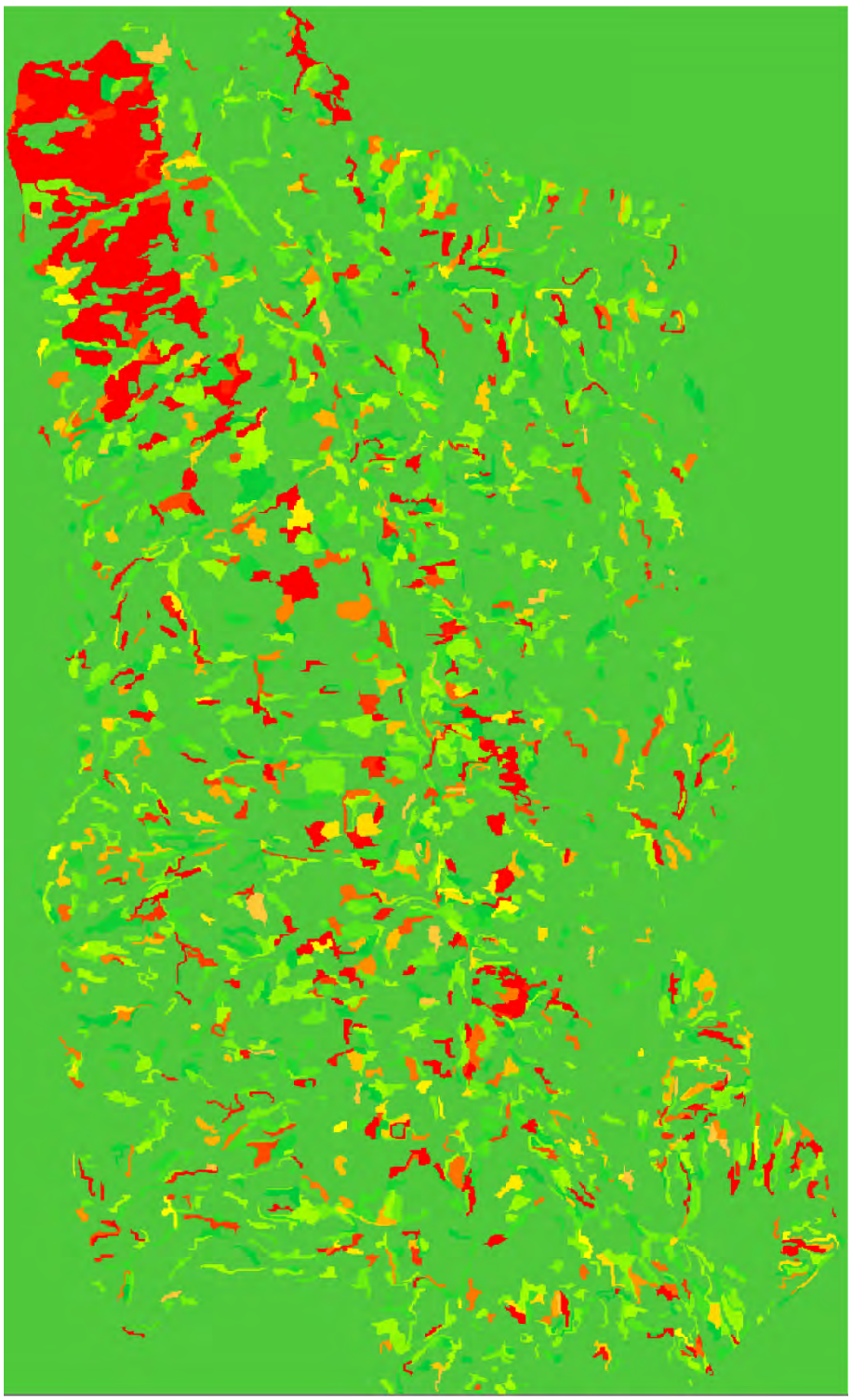

Figure 5.4: Fuzzy Classification Stability of Level L2
Red = close proximity of best and second best membership assignment; green = distal, stable assignments. The north-easternmost part of the valley shows the most unstable memberships.

(1998) investigating geomorphological slope units reach an overall accuracy of 88.5 % in their supervised classification based on prior image segmentation and subsequent classification from training areas. However, the values in the confusion matrix (Tab. 5.2) have to be taken with care: on the one hand, object-oriented accuracy assessments tend to overestimate as they are based on the previously generated, averaged image objects and not on individual pixels. On the other, test areas were selected randomly, but without following a regular spatial pattern. Hence further accuracy assessment with different, pixel-based software is required. Besides, the classification quality of older rockfall and moraine deposits could not be assessed, as they form no classes in the hierarchy.

Varying illumination constitutes a problem in high mountain areas. It can partially be mended by band ratio formation, i.e. the division of adjacent satellite image bands: discrepancies between them are reinforced, while similar structures are simultaneously eliminated. Hence while useful features like outlines of vegetation or ice/snow appear more clearly, atmosphere and relief induced variations in illumination disappear, as they are highly correlated in neighbouring bands (Paul, 2000). NDVI and other ratios form important thresholds in the classification hierarchy (Fig. 5.2).

5.6 Conclusions and outlook

To further evaluate the results, the exact influences of image and DEM data respectively should be assessed by analysing them individually. Moreover, the transferability both of the segmentation parameterisation and the classification hierarchy still has to be investigated. One can assume that the application of such a two-step routine poses double problems. Conversely, Blaschke et al. (2002) argue that object-oriented classification rules should be easier transferable than pixel-based ones, as the former depend less on reflection values and atmospherical conditions. When transferring the methodology developed in

this study both to other datasets and regions, the appropriateness of NDVI application should also be compared to soil-adjusted vegetation indices (for details see Schneevoigt et al., 2008).

Many open questions remain to be answered in this interdisciplinary work linking geomorphology and remote sensing. Albertz (2001) stresses that the appropriate analysis of remotely sensed imagery can become highly difficult when operating between disciplines, as remote sensing methods are not delivered with problem-adapted assessment factors. Then again, a broadened knowledge on sediment storage features represents the prerequisite for further insights into processual behaviour and landform development in the fragile mountain environment (Schrott et al., 2003). Considering the good match of the final landform classification and ground truth, the object-oriented approach constitutes a valuable tool for the Alpine sediment cascade, especially in inaccessible regions. It remains to be investigated to which extend a purely pixel-based classification scheme may handle this data.

5.7 Acknowledgements

Many thanks go to the Remote Sensing Laboratories, University of Zürich (K. Itten), the Center for Remote Sensing of Land Surfaces (M. Braun) and the Remote Sensing Research Group (G. Menz, H.-P. Thamm), both University of Bonn, for providing workplace and software. The DEM was generated by SEDAG partners using photogrammetric data by the Bavarian Geodetic Survey. The ASTER scene was provided by EOS Data Gateway (NASA) and is courtesy of NASA/GSFC/METI/ERSDAC/JAROS and the US/Japan ASTER science team. This study was embedded in the SEDAG projects, which were funded by the German Research Foundation (DFG) from 2000 to 2008. N.J. Schneevoigt was supported by the German National Academic Foundation until 2004, then by SEDAG and in 2006 within the International

Scholarship Programme of the Gottlieb Daimler and Karl Benz Foundation. Sebastian van der Linden was funded by the scholarship programme of the German Federal Environmental Foundation (DBU) until 2007.

5.8 References

Albertz, J., 2001: Einführung in die Fernerkundung. Grundlagen der Interpretation von Luft- und Satellitenbildern. Wissenschaftliche Buchgesellschaft, Darmstadt.

Baatz, M., Schäpe, A., 2000: Multiresolution segmentation - an optimization approach for high quality multi-scale image segmentation. In: Strobl, T., Blaschke, T., Griesebner, G. (eds.), Angewandte Geographische Informationsverarbeitung XII, Beiträge zum AGIT-Symposium Salzburg 2000. Herbert Wichmann Verlag, Heidelberg, 12-23.

Benz, U.C., Hofmann, P., Willhauck, G., Lingenfelder, I., Heynen, M., 2004: Multiresolution, object-oriented fuzzy analysis of remote sensing data for GIS-ready information. ISPRS Journal of Photogrammetry & Remote Sensing, 58, 239-258.

Blaschke, T., Gläßler, C., Lang, S., 2000: Bidverarbeitung in einer integrierten GIS/Fernerkundungsumgebung - Trends und Konsequenzen. In: T. Blaschke (ed.): Fernerkundung und GIS. Neue Sensoren - innovative Methoden. Herbert Wichmann Verlag, Heidelberg, 1-9.

Caine, N.T., 1974: The geomorphic processes of the alpine environment. In: Ives, J., Barry, R. (eds.): Arctic and Alpine environments. Methuen, London, 721-748.

Costantini, M. 1998. A novel phase unwrapping method based on network programming. IEEE Transactions on Geoscience and Remote Sensing, 36(3): 813–821.

Giles, P.T., Franklin, S.E., 1998: An automated approach to the classification of the slope units using digital data. Geomorphology, 21(3-4), 251-264.

Kääb, A., 2002: Monitoring high-mountain terrain deformation from repeated air- and spaceborne optical data: examples using digital aerial imagery and ASTER data. ISPRS Journal of Photogrammetry & Remote Sensing, 57, 39-52.

Klug, H., 2002: Tutorial Version 1.1: Eine Einführung in die Verwendung von ASTER. Asterdaten und ihre Verwendung im landschaftsökologischen Kontext. LARG Technical Report, Universität Salzburg, http://www.geo.sbg.ac.at/larg/Astertutorial.pdf, 12.07.2010.

Paul, F., 2000: Evaluation of different methods for glacier mapping using Landsat-TM data. In: Wunderle, S. (ed.): EARSeL Workshop on Remote

Sensing of Land Ice and Snow, Juni 2000, Dresden, 239-245.

Schneevoigt, N.J., Schrott, L., 2006: Linking geomorphic systems theory and remote sensing. A conceptual approach to Alpine landform detection (Reintal, Bavarian Alps, Germany). Geographica Helvetica, 61(3), 181-190.

Schneevoigt, N.J., van der Linden, S., Thamm, H.-P. & L. Schrott, 2008) Detecting Alpine landforms from remotely sensed imagery. A pilot study in the Bavarian Alps. Geomorphology, 93, 104-119.

Schrott, L., Hufschmidt, G., Hankammer, M., Hoffmann, T., Dikau, R., 2003: Spatial distribution of sediment storage types and quantification of valley fill deposits in an alpine basin, Reintal, Bavarian Alps, Germany. Geomorphology, 55, 45-63.

6 Paper V
Modelling mass movement from radar elevation data

published as
Ortega, R.Z. & N.J. Schneevoigt (2012):
Modelling potential debris flows from SRTM data in the upper Chama river watershed, northwestern Venezuela.
Revista Geográfica Venezolana 53(1): 93-108.

Debris flows in the Venezuelan Andes are common geomorphologic processes which reflect the sediment supply capacity of this regional mountain system. In this study, a regional model for potential debris flows on soil- and vegetation-covered hillslopes in watershed domains is presented. The method consists of a combination of remote sensing techniques, morphometric and hydrological parameters using a Shuttle Radar Topography Mission (SRTM) digital elevation model and an Advanced Spaceborne Thermal Emission and Reflection Radiometer (ASTER) scene. The study area comprises the upper Chama river basin, located in the central Andean region of Venezuela. Source, runout and deposition areas for the potential debris flows are modelled as a function of topography and sediment dynamics, implementing the Distributed Melton´s Ruggedness Number (DMRN) and the Modified Single Flow Model (MSFM).

6.1 Introduction

Hydrologically induced debris flows are the most common mass movement types in the Venezuelan Andes (Laffaille, 2005). They often occur in forested areas of watershed domains, and are usually associated with the seasonal variation of precipitation patterns in this region (Ferrer, 1993; Laffaille, 2005). The debris flow events in the upper Chama river basin, central Andean region of Venezuela, are characterised by coarse, poorly sorted, non-cohesive weathered material, including large boulders (Ingeomin, 2007; Roa, 2007). Their source areas are mainly located in the proximity of ridges, e.g. Montalbán debris flow, or close to primary and secondary stream channels, e.g. Las Calaveras debris flow, with slopes ranging from 20° to 40° (Ingeomin, 2007; Roa, 2007).

Debris flows are caused by intensive downpours over a short period of time and occur mainly at the end of the second precipitation season (October - November). This indicates a relationship between the first precipitation season (April - May), soil moisture conditions, runoff infiltration in hillslopes and the triggering of debris flows in the basin (Ferrer and Laffaille, 2005). Runouts range from 4 km length, e.g. Las Calaveras debris flow, to 11,5 km, e.g. Montalbán debris flow. They differ from place to place as a function of distance between source areas and potential deposition areas, slope and rheological characteristics of the flow (Ingeomin, 2007). The last one is beyond the scope of this study. In spite of the threat that these geomorphological processes pose for inhabited areas along the upper Chama river basin, a regional debris flow hazard assessment has not been proposed yet. Furthermore, the contribution of these natural phenomena to the overall sediment dynamics of the regional river system, and their influence on the torrential behaviour of the Chama River and its tributaries, is poorly understood.

In this study, a regional model for potential debris flows on soil- and vegetation-covered catchment areas is proposed for the upper Chama river basin, north-western Venezuela. It models source, run-out and deposition ar-

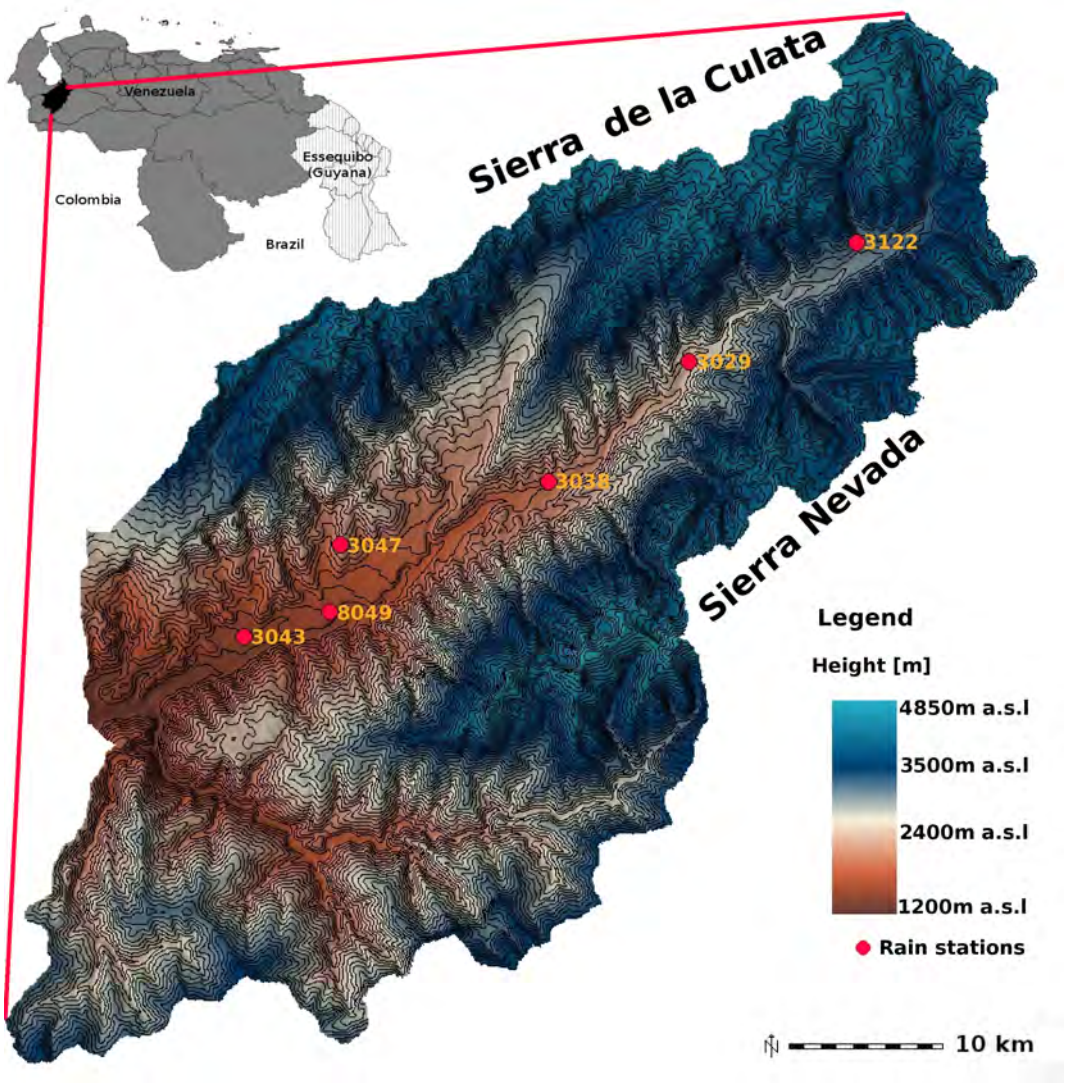

Figure 6.1: Relief Map of the upper Chama river basin

Relative location map (upper left) modified from Corporación Andina de Fomento (CAF, 2008). The yellow numbers indicate the rain stations displayed in Fig. 6.2.

eas for potential debris flows along the Chama River and its tributaries as a function of topography and sediment dynamics. A set of morphometric and geomorphological parameters are applied to determine potential source areas using the Distributed Melton's Ruggedness Number (DMRN) in combination with primary topographic derivatives.

6.2 Study area

The area of study is located in the central region of the Venezuelan Andes in the Mérida Mountain Range (Fig. 6.1). It comprises the upper Chama river basin between 8° 29' and 8° 53' N and 71° 19' and 70° 53' S, and covers a total area of 1900 km^2. In the north, it is flanked by Sierra de La Culata, with maximum heights of 4800 metres above sea level (m a.s.l), and in the south by the Sierra Nevada reaching 5000 m a.s.l (Schubert, 1980; Bellizzia et al., 1981; Ferrer, 1993). Both Sierras are formed by a Precambrian crystalline basement that consists mainly of igneous and metamorphic rocks, and present very distinctive periglacial, alluvial and fluvial landforms (Cabello, 1966; Bellizzia et al., 1981; Ferrer, 1993; Schubert and Vivas, 1993; Silva, 1999; Ferrer and Laffaille, 2005). Regarding precipitation patterns, the study area is characterised by a bimodal precipitation regime, with two maxima in April and October and two minima in February and August (Ponte, 1976; Rojas and Alfaro, 2000) (Fig. 6.2).

6.3 Methods

The methodology employed in this study consists of a combination of morphometric and geomorphological analyses. Their inputs are a Shuttle Radar Topography Mission (SRTM) digital elevation model (DEM) collected in C-band (90 m resolution) in February 2000 and an Advanced Spaceborne Thermal Emission and Reflection Radiometer (ASTER) satellite image (15 m resolution) of 1 February 2004. Their geomorphological assessment involves three

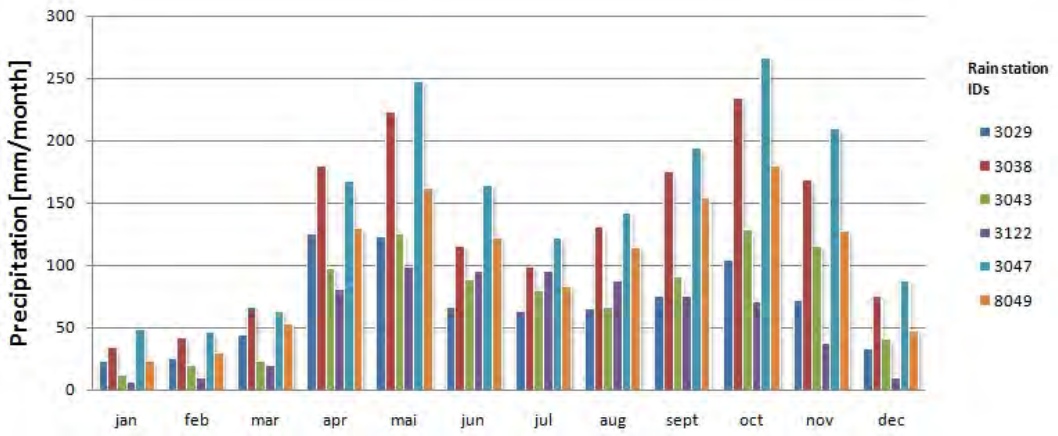

Figure 6.2: Monthly Precipitation along Chama River.
The locations of the respective rain stations (MARN, 2006) are shown in Fig. 6.1.

distinct steps: DEM optimisation and evaluation, identification of source areas and identification of probable run-out areas (Fig. 6.3).

6.3.1 DEM optimisation

The information gaps in the original SRTM DEM (SRTM FTP server, 2006) were filled by spline interpolation and the random errors removed using a low-pass filter (Li et al., 2005; Neteler and Mitasova, 2007). The accuracy of the SRTM DEM was assessed with the root mean square error (RMSE) equation:

$$RMSE = \sqrt{\frac{1}{n}\sum_{i=1}^{n} {d_i}^2} \tag{6.1}$$

where ${d_i}^2 = Z_{est} - Z_{obs}$. Z_{est} is the DEM value, Z_{obs} the field-measured elevation value and n the number of ground control points (GCPs) collected. For this purpose, 76 GCPs were collected with a hand-held GPS receiver during a field excursion.

6.3.2 Identification of source areas using the DMRN

In this step, the processed SRTM DEM is used to calculate the hydrological parameters, i.e. flow accumulation, flow direction and pour points, required to extract the basin area extent and catchment height. These DEM derivatives are further used as main input parameters for calculating Melton´s Ruggedness number (MRN) in a distributed form. MRN is a dimensionless index of basin ruggedness, that normalises the basin relief by areas (Marchi and Fontana, 2005; Rowbotham et al., 2005). Ruggedness is one of the most commonly used morphometric measures to identify debris torrent basins, since it reflects the relief potential of a landscape (Rowbotham et al., 2005). The MRN was also successfully used to differentiate debris flow prone basins from non debris flow prone basins (cf. Jackson et al., 1987; Rowbotham et al., 2005), and to identify channels with high versus low sediment transport capacity (Marchi and Fontana, 2005).

For the purpose of this study, the original MRN was calculated as a concentrated morphometric indicator from

$$MRN = \frac{H_{max} - H_{min}}{A^{0.5}} \tag{6.2}$$

where H_{max} and H_{min} are maximum and minimum elevation values within the basin and $A^{0.5}$ is the drainage basin area (Melton, 1958). Equation 6.2 is modified, resulting in the Distributed Melton´s Ruggedness Number (DMRN):

$$DMRN = \frac{H_{ave} - H_c}{A^{0.5}} \tag{6.3}$$

where H_{ave} represents the average height of all upslope cells over each other, H_c the height of the considered cell in the SRTM DEM, and $A^{0.5}$ the drainage basin area in square metres (Marchi and Fontana, 2005). Catchment height $H_{ave} - H_c$, also referred to as the *average expected relative altitude of the*

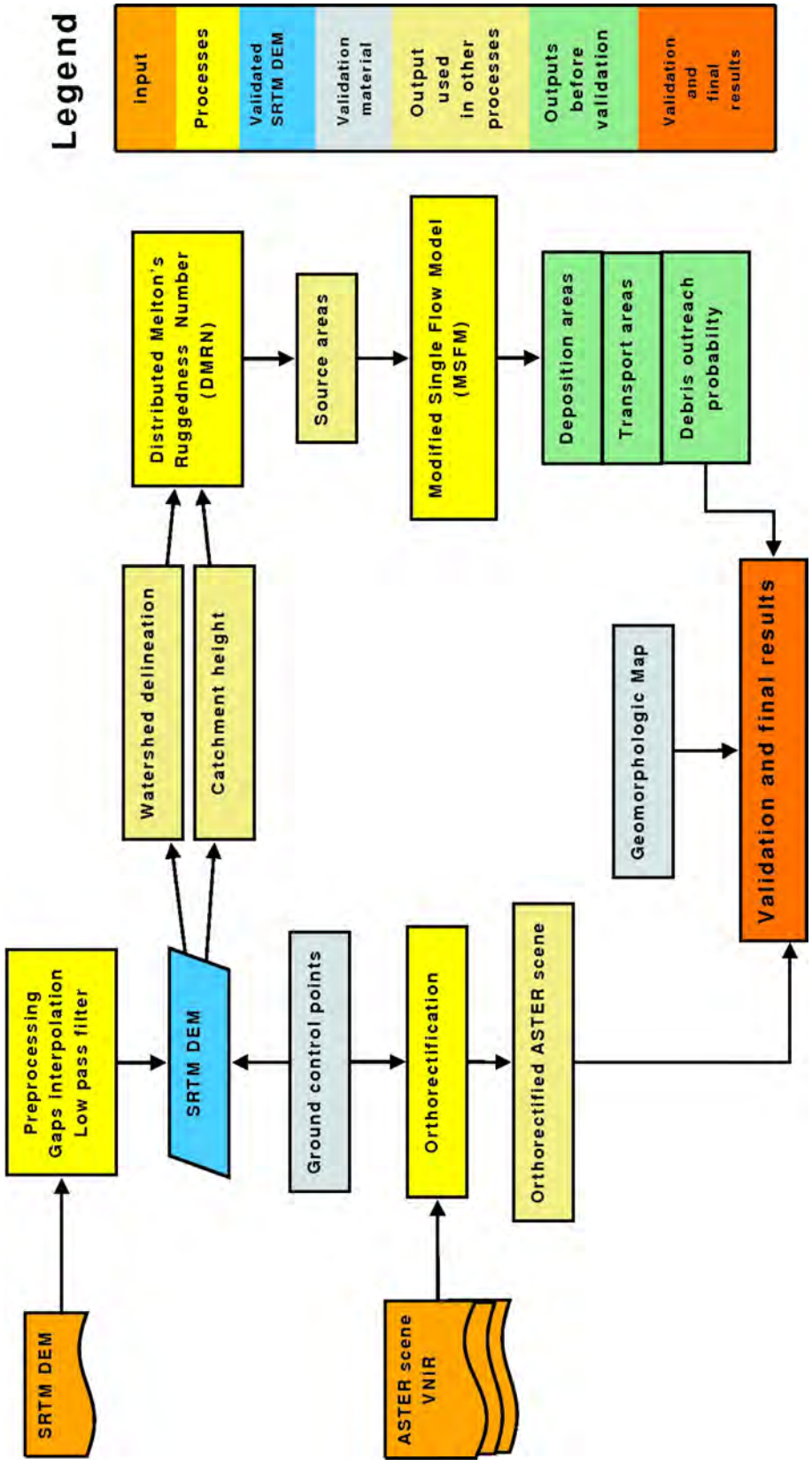

Figure 6.3: Structure and Workflow of the Investigation

upslope catchment area (cf. Gacetta, 1999), is obtained by assigning a value equal to the average upslope catchment elevation minus the pixel elevation in the SRTM DEM. This calculation uses an upward recursive method based on the Multiple-Flow Direction Algorithm (MFDA) (Quinn et al., 1991),

$$d_i = \frac{(\tan \beta_i)^f L_i}{\sum_{j=1}^{n} (\tan \beta_j)^f L_j} \tag{6.4}$$

where j is the total amount number of downhill directions, $\tan \beta$ the local slope, f a flow apportioning weight, L_i the contour length weighting factors for each flow direction i, and d_i represents the flow fraction allocated to each pixel in the direction of i (Quinn et al., 1991; Holmgren, 1994). The reason for selecting the MFDA lies in its high ability to capture spatial variability of geomorphological features, when compared to other algorithms, i.e. Single-Flow Algorithms (McNamara et al., 1999).

6.3.3 Identification of probable runout areas

Based on former empirical studies (cf. Eisbacher and Clague, 1984; Jackson et al., 1987; Patton, 1987; Wieczorek, 1987; Marchi and Fontana, 2005; Rowbotham et al., 2005), the results of the DMRN, local slope calculation and field observations, three criteria were established to delineate potential source areas:

1) Only cells with DMRN values equal or higher than 0,17 were considered (cf. Jackson et al., 1987; Marchi and Fontana, 2005; Rowbotham et al., 2005)

2) Slope values of the considered cells were equal or higher than 20° and lower or equal 40°(cf. Wieczorek, 1987; Patton, 1987)

3) Cells were located in the proximity of ridges and close to expected primary and secondary stream channels (cf. Eisbacher and Clague, 1984; Patton, 1987; Wieczorek, 1987).

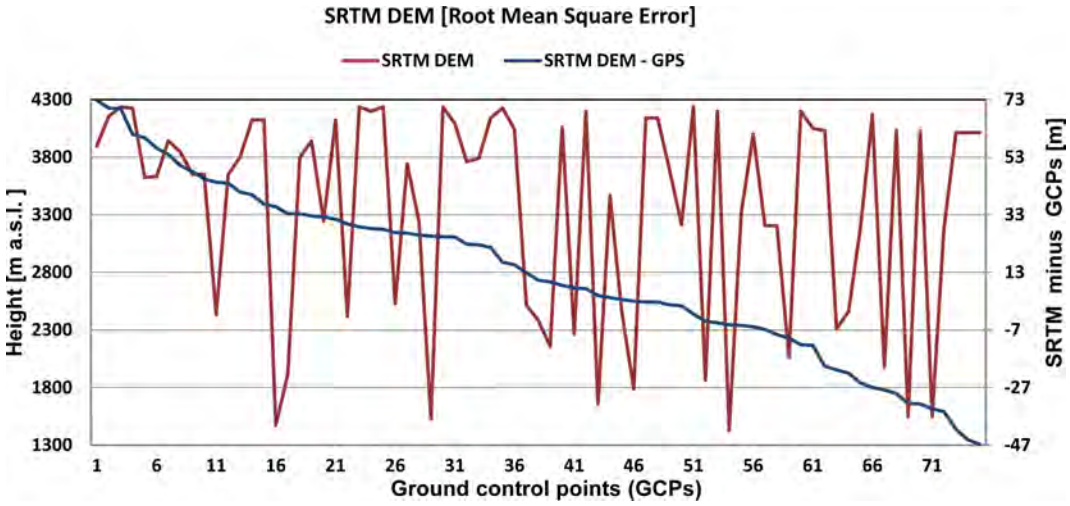

Figure 6.4: SRTM DEM RMSE versus GCPs

SRTM DEM root mean square error (RMSE) compared to manually collected GCPs.

Based on these three criteria, 53 potential source areas containing one or more cells, were selected, and used as input to the Modified Single Flow Model (MSFM). The MSFM is based on a single flow direction algorithm, where the central flow line follows the direction of the steepest descent, and was developed by Huggel et al., (2003, 2004). However, single flow algorithms are unable to adequately simulate the spreading behaviour of debris flows in less steep terrain and unconfined zones (Huggel et al., 2004). To solve this limitation, Huggel et al., (2004) modified the model by integrating a function that allows the flow to diverge up to 45° in unconfined and less steep areas. This modification enables the model to simulate different characteristics of debris flows in confined channel sections (stream channels) and in flat or convex terrain, e.g. alluvial fans (Huggel et al., 2004).

Modelled debris flows stop when an average slope of eleven degrees ($\leq 11°$) is reached. This last parameter is based on the H/L ratio (H is the difference in elevation and L the path length) and can be modified to fit site specific characteristics, where detailed information regarding the behaviour of debris flows exists. For the study area, this information was not available; so that an

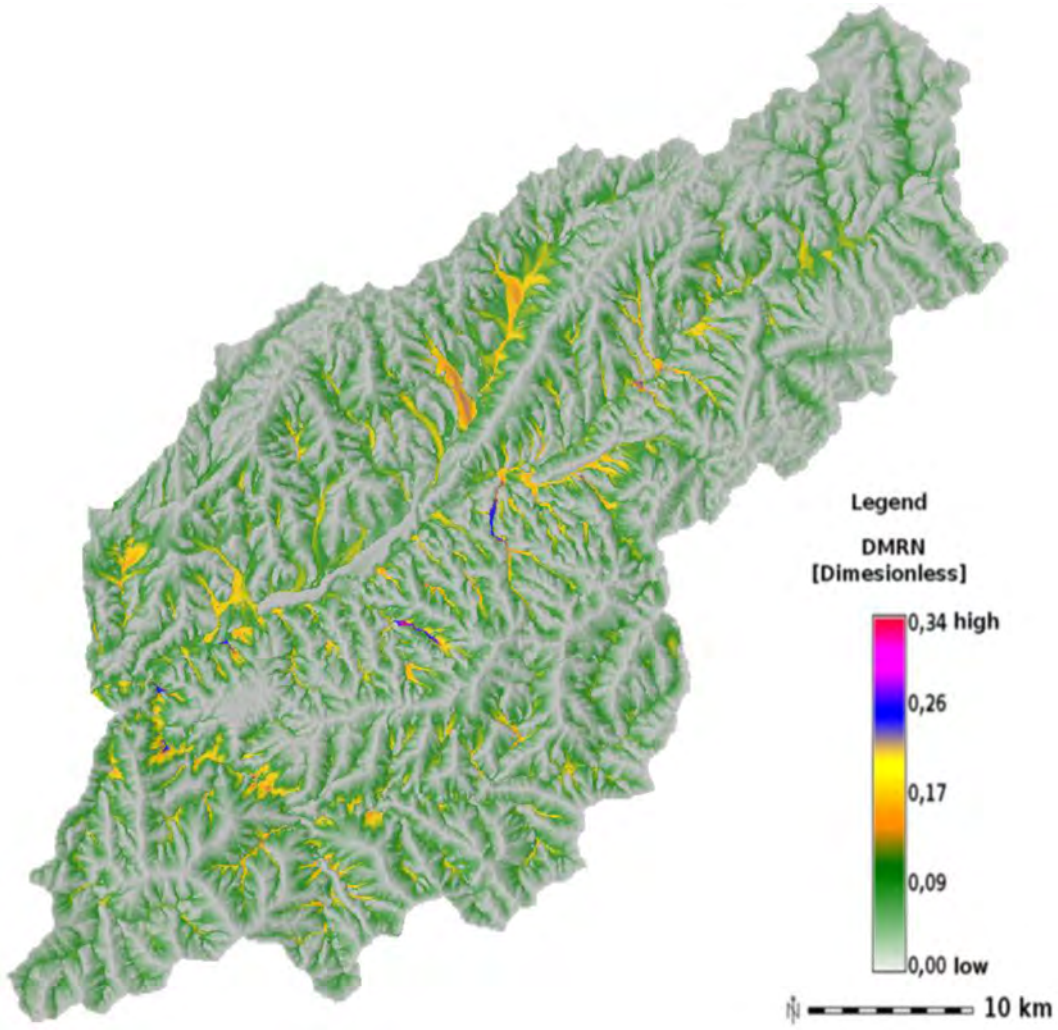

Figure 6.5: Distributed Melton's Ruggedness Numbers
DMRN values for the upper Chama river basin, where 0,34 indicates high and 0 low sediment dynamics.

average slope of 11°, originally calculated by Huggel et al., 2004 for the Swiss Alps region (equivalent to a minimum H/L ratio of 0,19), had to be used. The model also delineates the potential areas to be affected and assigns to each cell the relative probability it has to be affected by a mass movement. It is based on a linear function that defines that the more the flow diverges from the steepest descent direction, the greater becomes the resistance, and therefore the lower the probability for a point or cell to be reached (Huggel et al., 2004).

6.4 Results

6.4.1 DEM evaluation

The RMSE shows that the SRTM instrument over- and underestimates the terrain elevation of the study area. A subtraction of the SRTM DEM values and the observed values (GCPs) also reveals that the overestimation occurs above 2800 m a.s.l and the underestimation below this elevation. These values vary between +73 m and -49 m (Fig. 6.4). Furthermore, the elevation errors of the SRTM DEM also indicate a slope/aspect dependency, which has been already addressed by former studies (cf. Miliaresis, 2008).

In this particular case, the SRTM DEM underestimates the elevation in east-facing slopes, and overestimates it in southeast-facing slopes. However, to determine if the errors found in SRTM DEM are systematic it is necessary to collect more GCPs, which is beyond the scope of this investigation.

6.4.2 Potential source areas

The 53 potential source areas for debris flows used in this study were delineated with help of the DMRN and the local slope. For this purpose, hillslopes with high relief potential, as a function of ruggedness and slope, were determined. Using map algebra, the DMRN map was obtained by dividing the catchment

height map by the entire catchment area map. In Figure 6.5, the grey colour represents areas with very low sediment dynamics, which are mainly found on ridges and plateaus. The green colour represents areas with low sediment dynamics and constitutes the transition zones towards areas with medium to high sediment dynamics (yellow and red colours). In addition, the DMRN map also provides a general overview of the potential hazardousness of the Chama river basin, especially of those hazards that are related to sediment dynamics, e.g. sediment mobilisation as well as slope and fluvial erosion.

6.4.3 Modelled runout areas

48 potential debris flow runouts, out of the 53 source areas were delineated with the MSFM. This represents 91 % of the total potential source areas. The remaining 5 potential source areas (9 %), for which the MSFM did not model the runout, are attributed to the existence of grid cells with slope values below 11°, which is the average slope where the modelled debris stops. The results of the MSFM are presented in Figure 6.6 which depicts the areas potentially affected by debris flows (relative probability), the potential maximum inundation zones, as well as the flow reach of these events. The relative probability indicates that the more the flow diverges from the steepest descent direction, the greater becomes the resistance, and therefore the lower the probability for a point or cell to be affected.

The flow reach component, on the other hand, is determined by the H/L ratio used for calculating the MSFM. In this case, a H/L ratio 0,19 (equivalent to an average slope 11°) is used (Huggel et al., 2004). The value of the modelled debris ranges from 0,5 to 1,0 and is expressed as a probability function, where 1,0 represents the highest and 0,5 the lowest probability for a point to be reached by the modelled debris flow (Fig. 6.6).

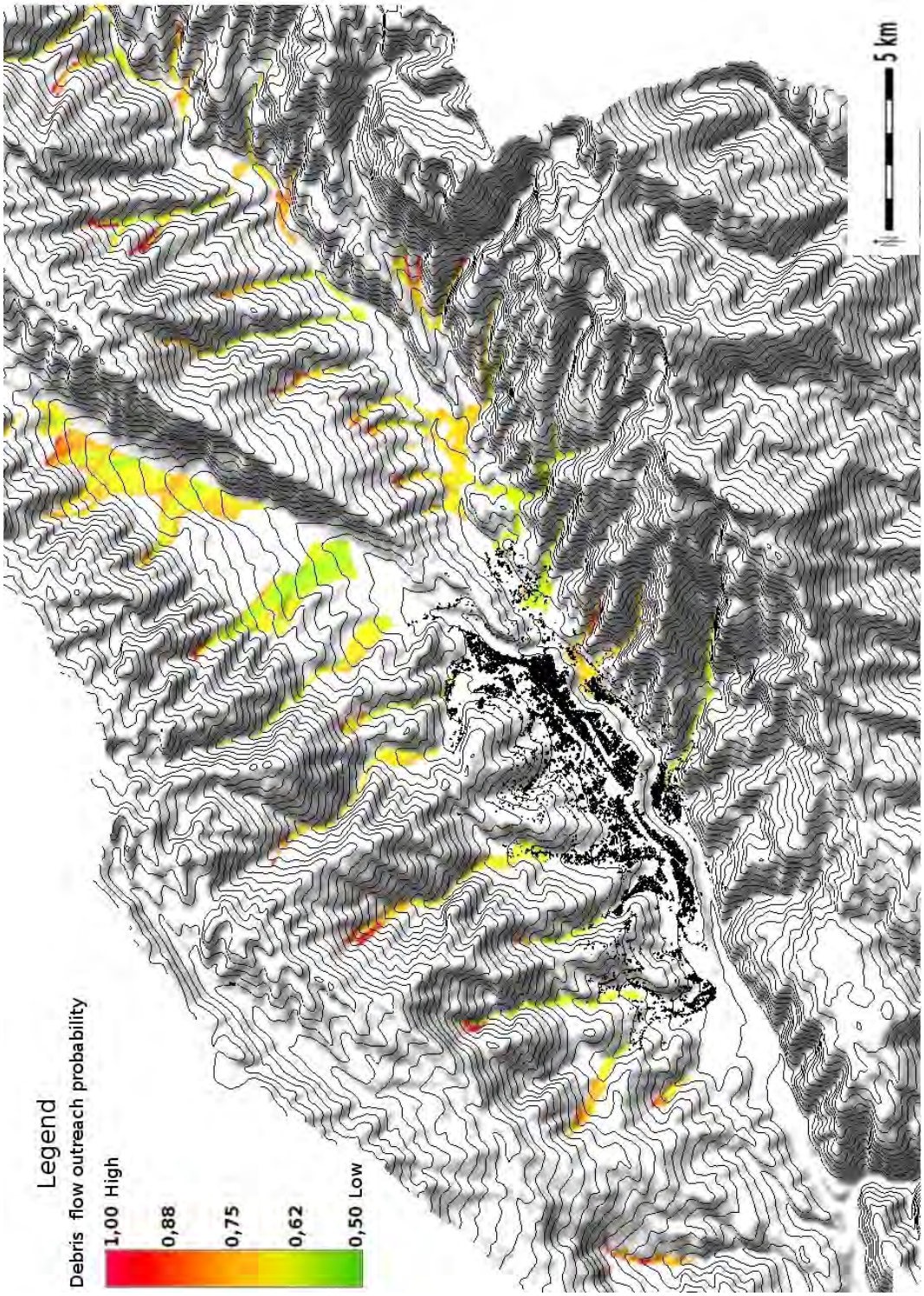

Figure 6.6: Modelled Debris Flows

DEM with 100 m contour lines shows modelled debris flows around the city of Mérida. 1,0 represents the highest probability and 0,5 the lowest probability for any point to be reached by a debris flow.

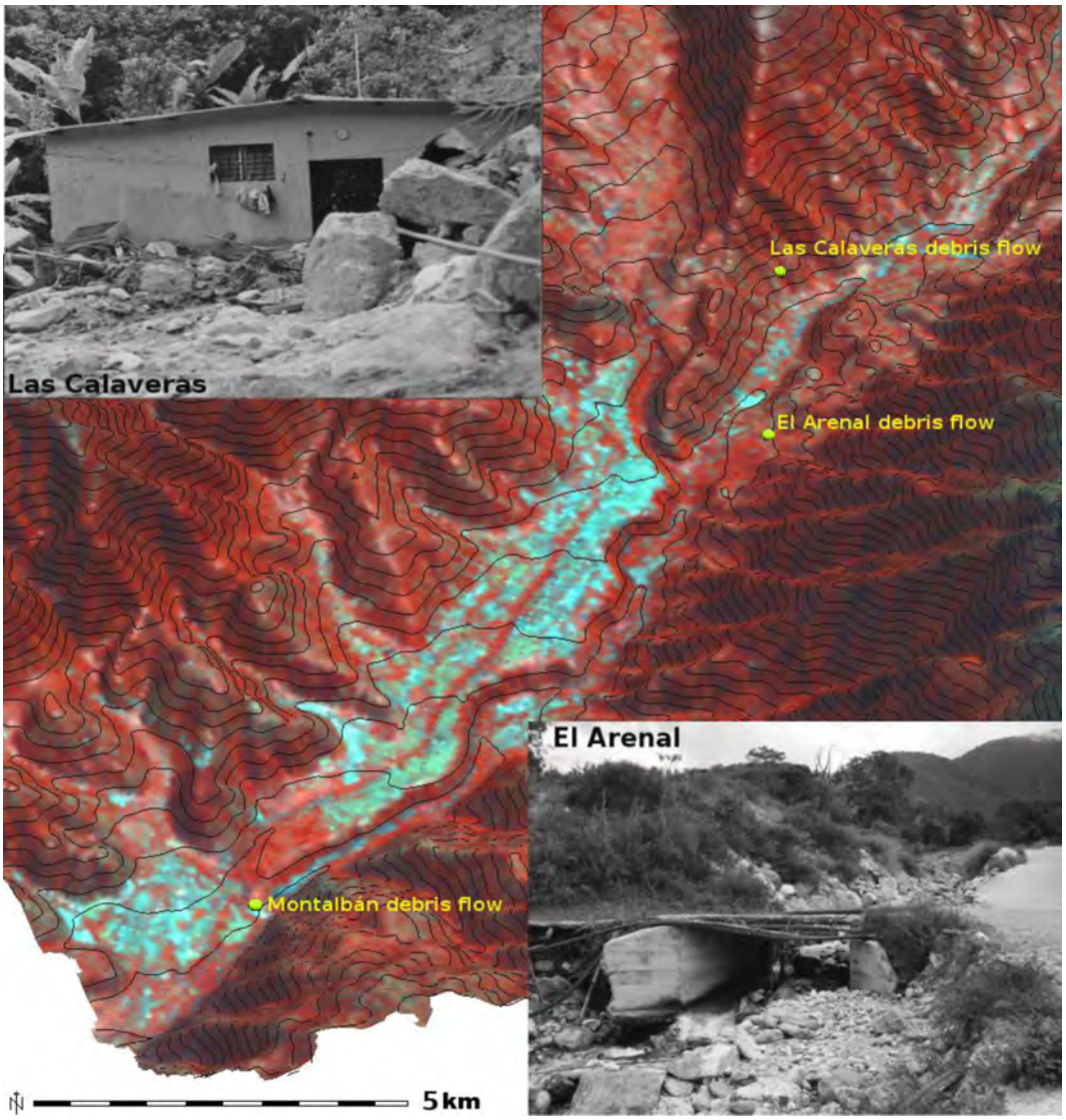

Figure 6.7: False Colour Composite ASTER image

False colour composite ASTER image (Bands 2, 3 and 4), light green represents sparse vegetation and agricultural land, bright purple urban areas/bare soil and dark purple shows densely vegetated areas. Debris flow El Arenal, Nov. 2007 (lower right; photo taken by George Volkhard); debris flow Las Calaveras, Nov. 2006 (upper left). Regarding debris flow Montalbán, Oct. 1947, Fig. 6.9. The contour line interval is 100 m.

6.5 Discussion

Whenever a new model is applied on a theoretical basis, it needs to be validated with respect to its practical applications. In this case, it is of interest to determine in which extent the DMRN and the MSFM correspond to the reality of the study area. In order to establish qualitative statements about the performance of the model, a comparative visual assessment was carried out using the following materials: a historical air photo (1947) with spatial resolution of 1:40000 (Ingeomin, 2006), a morphopedological map with a 1:50000 scale (Contreras, 2005) and an orthorectified ASTER image (1 February 2004) with a resolution of 15 m. This visual assessment was validated through three fieldwork excursions between November 2006 and March 2007. During these excursions, GPS points were collected and complemented with further imagery, i.e. digital photos (Figs. 6.7 and 6.8).

In general, the MSFM determined the relative probability for a cell to be affected, the potential maximum inundation extent of the modelled debris flows and flow reach of the events. The discrepancies between the model and reality resulted from the usage of a H/L ratio of 0,19 equivalent to overall slope 11°, originally calculated for the Swiss Alps region in Europe. Another source of discrepancies lies in DEM model dependency. The MSFM used the steepest descent path approach (single flow algorithm) and the H/L ratio to calculate the direction and the outreach of debris flows. Both calculations implied the use of slope as main parameter. In former studies, slope values were found to exhibit variations with the change of the DEM resolution (cf. Deng et al., 2007), resulting in a systematic decrease or increase of slope values by coarsening or fine-graining DEM resolution.

Regarding the DMRN, the model showed not only areas of the subbasins where sediment transport initiates, but also locations along stream channels suitable for trapping debris material from upstream areas. These areas represent transition zones from debris flows to bedload transport and are very

Figure 6.8: Montalbán Debris Flow Event

Aerial photo taken in 1947 in the aftermath of the Montalbán debris flow event (Ingeomin, 2006).

important to predict the flow process at the outlet of the basin. The DMRN also determined deposition areas, which are consistent with the deposition areas modelled by the MSFM and with the alluvial fans mapped by Contreras (2005) and Roa (2007) (Fig. 6.9). The results of the DMRN were satisfying with regard to their function as geomorphologic indicator, i.e. differentiating between areas with high and low sediment transport (cf. Jackson et al., 1987; Marchi and Fontana, 2005; Rowbotham et al., 2005). Besides, they provided a general overview of the distribution of the topographic ruggedness.

Regarding the relative probability of being affected, the highest probability (1,0) is found in the proximity of the defined source areas, at the base of steep slopes, while low and medium values of relative probability characterised diverting areas, i.e. alluvial fans. In general, MSFM results indicated that the relative probability for cells or areas to be affected varies from high to

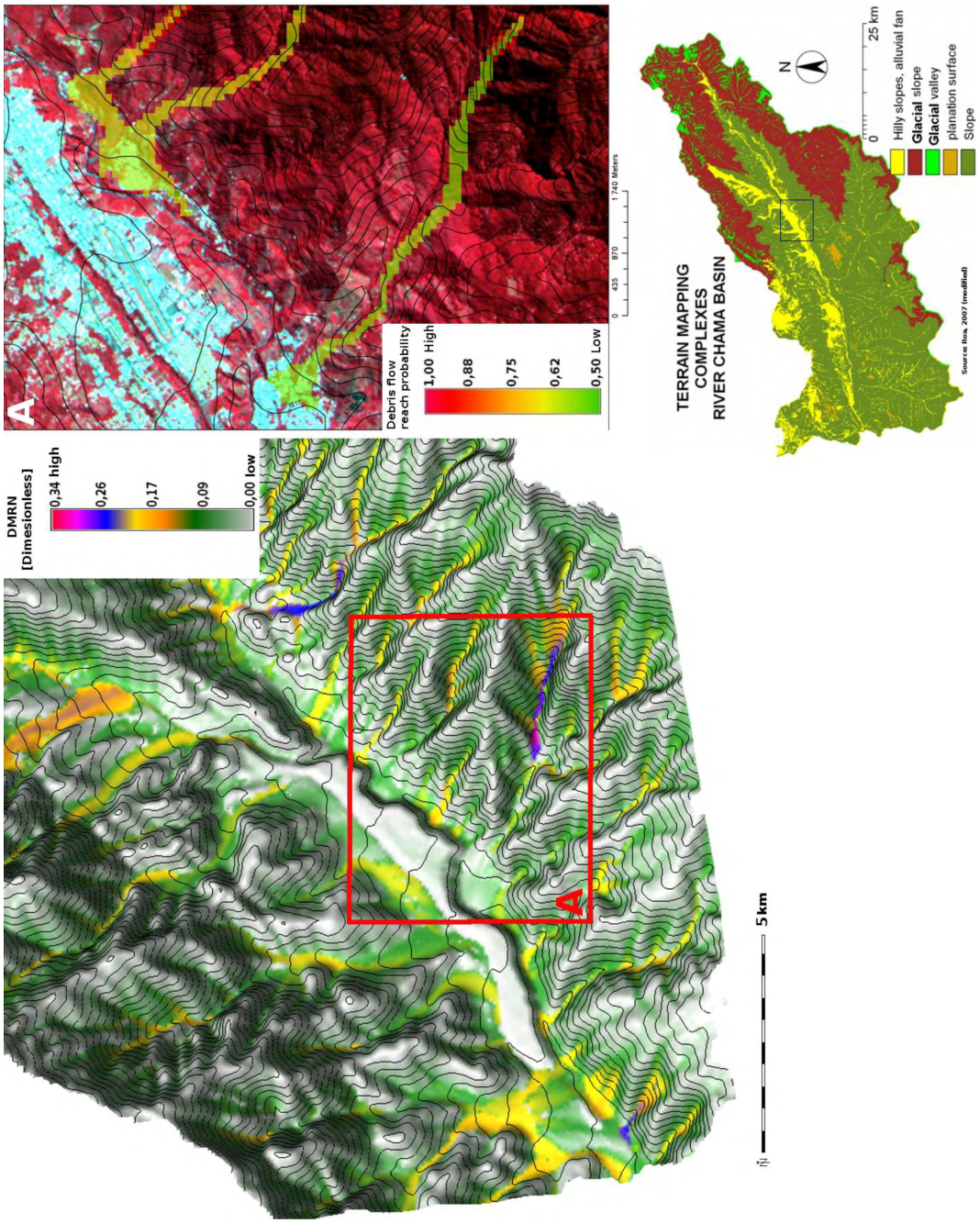

Figure 6.9: Modelled Debris Flow Deposition Zones

Example of deposition zones as modelled by the DMRN and MSFM, draped over the SRTM DEM (box A) and the false colour ASTER image (urban areas appear in light blue colour). The contour line interval in both images is 100 m. To the lower right, a terrain complexes map of the Chama river Basin depicting the predominant landforms.

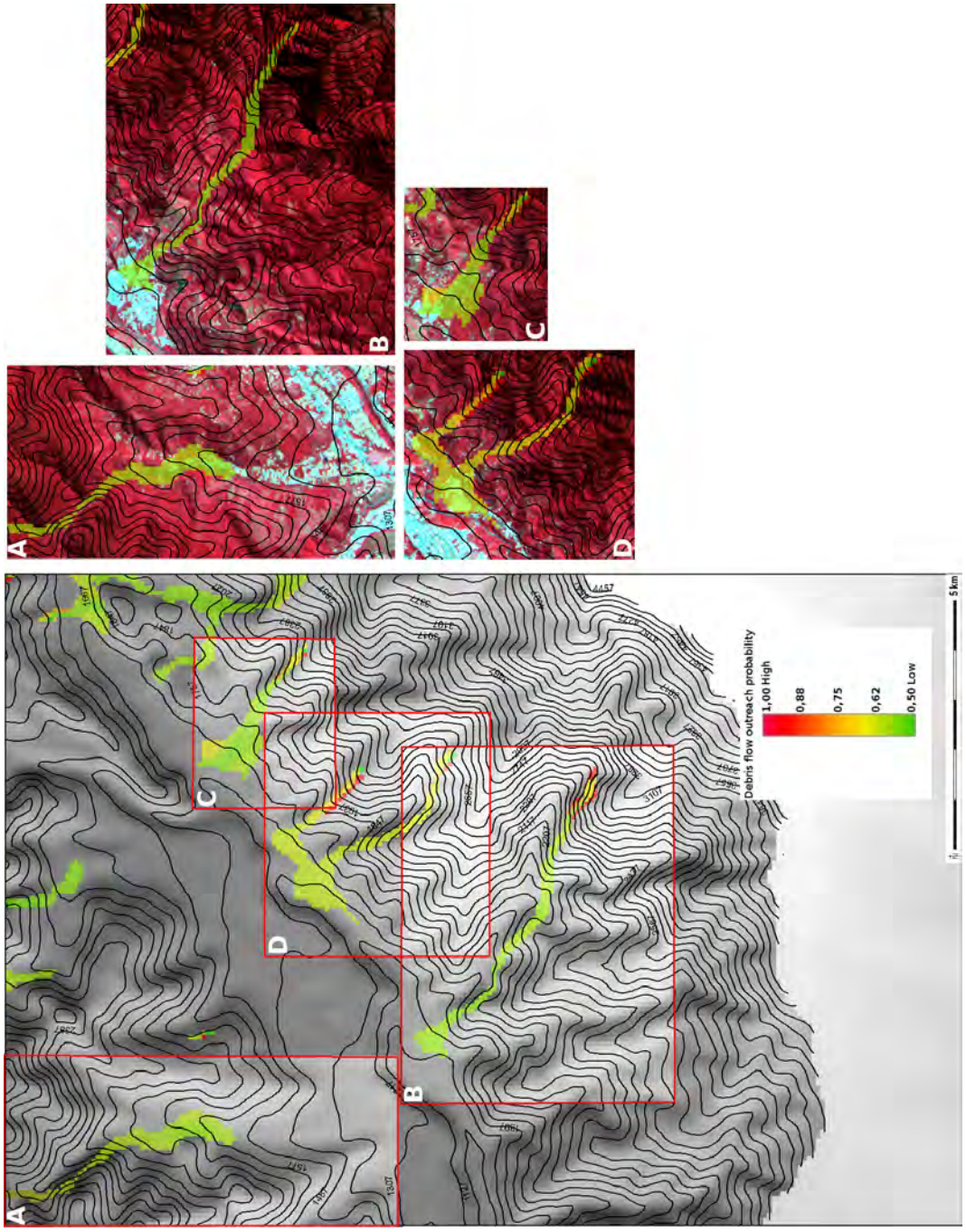

Figure 6.10: Debris flows reaching Alluvial Fans

Examples of modelled debris flows reaching alluvial fan areas, e.g. urban areas, draped over the SRTM DEM. Urban areas are shown in black on the DEM (A, B, C and D). The same areas are shown in the ASTER image (A, B, C and D). Ruby colour implies vegetated areas, light blue represents buildings. The contour line interval is 100 m.

low along the entire upper Chama river basin with the highest values located in tributary watershed systems (Fig. 6.6). Through a visual assessment of the orthorectified ASTER image, it is estimated that 48 potential debris flows out of 53 modelled source areas will reach an alluvial fan, i.e. farmland or residential areas (Fig. 6.10 A, B, C and D). The five remaining potential source areas exhibit a short runout, which can be attributed to overall slope value lower than the threshold of 11°.

6.6 Conclusions

This investigation demonstrates that the combination of remote sensing data (SRTM DEM) with morphometric and hydrologic parameters is suitable for modelling geomorphologic processes on the regional scale of the study area. Despite the complex characteristics of rugged terrain and the limitations stemming from the structure of the models used and their DEM dependency, the results of the DMRN and MSFM in the Venezuelan Andes are considered to be realistic. They reflect the sediment dynamics of the study area and coincided with vulnerability and susceptibility studies conducted in recent years (cf. Maldonado, 2007; Roa, 2007; Caritas, 2010).

The following main conclusions can be drawn:

1. The DMRN is useful to determine potential debris source areas in watershed domains. Furthermore, it provides a general overview of the level of dissection of the basin based on relief variation, thus allowing to differentiate areas with high sediment dynamics from those with low sediment turnover.

2. MSFM is able to model runout and deposition zones for potential debris flows along the upper Chama river basin using a SRTM DEM with a resolution of 90 m. The areas where the potential debris flow model shows a short runout are consistent with the presence of grid cells with overall slopes $\leq 11°$, which is the stopping threshold value (H/L ratio) for the modelled debris.

3. MSFM and DMRN render divergent results in some sections of the potential deposition zones on flat terrain, i.e. on alluvial fans. These differences originate from the different flow algorithms used for the calculation of both models.

Regarding the limitations of this model, it is important to mention that both DMRN and MSFM consider neither the volume of the potential source areas, nor the type of material available. This deficiency can however be counterbalanced by extensive surveying in the respective basin domains or by using advanced models in combination with the model proposed here, e.g. 3D dynamic models. For further studies, a downscaling of this approach and the use of detailed geological maps are suggested. The inclusions of topographic parameters like curvature and wetness index are recommended, as well as a landcover classification with emphasis on stream channel domains.

6.7 Acknowledgements

We thank Andreas Kääb at the University of Oslo (UiO) for providing guidance, feedback, the ASTER scene and the MSFM script, and the Department of Geosciences (UiO) for financial support. NASA and USGS provided the SRTM DEM, USGS and the Japan ASTER Program the ASTER scene. Carlos Pacheco at the Andes University (ULA), Greta Roa and Rigüey Valladares (Ingeomin), Jaime Laifalle (ULA), Carlos Ferrer (ULA) and Guido Ochoa (ULA) shared their experience and provided important geomorphologic, pedologic and geologic information about the study area. Special thanks to Regula Frauenfelder and Jachym Cepicky for their technical support, George Volkhard for his photos and Bernd Etzelmüller for commenting the paper.

6.8 References

Bellizzia, A., Pimentel, N. and Muñoz, M. 1981. Geology and Tectonics of Northern South America. Geodynamic investigations in Venezuela. Special publication 9, 79 pp.

Cabello, O. 1966. Estudio geomorfológico del área de Mérida y sus alrededores. Facultad de Ciencias Forestales y Ambientales. Universidad de los Andes. Mérida Venezuela. 138 pp. (Inédito).

Caritas 2010. Zonificación de las areas suceptibles a procesos hidrogeomorfológicos en el eje Vega de San Antonio, urbanización Don Perucho - El Arenal - La Pueblita, Municipio Libertador, Estado Mérida, 64pp. (Inédito). http://www.caritasvenezuela.org.ve/zonificacion.pdf, last access: November 30, 2010.

Contreras, A. 2005. El cadastre multiutilitario: Herramienta clave para el análisis territorial y el ordenamiento rural. Caso del Municipio Rangel en el Estado Mérida. Facultad de Ciencias Forestales y Ambientales, Universidad de los Andes. Mérida Venezuela. Trabajo de investigación para optar al grado de Magister Scientiae en Ordenación de territorio y ambiente, Facultad de Ciencias Forestales y Ambientales, 186 pp. (Inédito).

Corporación Andina de Fomento (CAF) 2008. Sistema de información geográfica Cóndor. Servicio regional de mapas. http://www.caf.com/view/index.asp?pageMs=45207&ms=17, last access: June 15, 2008.

Deng, Y., Wilson, J.P. and Bauer B.O. 2007. DEM resolution dependencies of terrain attributes across a landscape. International Journal of Geographical Information Science. 21(2): 187-213.

Eisbacher, H., G. and Clague, J.J. 1984. Destructive mass movements in high mountains: hazard and management. Geological Survey Canada. Paper 84-16: 12-29.

Ferrer, C. 1993. Procesos de erosión de los suelos y los problemas del uso de la tierra en las cuencas superiores de los rios Chama y Santo Domingo. In: Ferrer, C. (ed.): Guía de excursión. Reunión internacional. Procesos de erosión en tierras de alta pendientes. Evaluación y modelaje. Mérida, Venezuela. 1-10.

Ferrer, C. and Lafaille, J. 2005. Un estudio de las amenazas múltiples en la cuenca media del río Chama (Andes centrales venezolanos): Caso zanjón El Paraíso. Revista Geográfica Venezolana. Número especial 2. 93-117.

Gacetta, P. 1999. Some methods for deriving variables from digital elevation models for the purpose of analysis, portioning of terrain and providing decision support for what-if scenarios. CSIRO Mathematical and Information Science (CMIS). Australia. (unedited). http://www.cmis.csiro.au/rsm/research/dems/index.htm, last access: May 10, 2007.

Holmgren, P. 1994. Multiple flow direction algorithms for runoff modeling

in grid based elevation models: An empirical evaluation. Hydrological Processes. 8(4): 327-334.

Huggel, C., Kääb, A. and Salzmann, N. 2004. GIS-based modeling of glacial hazards and their interactions using Landsat-TM and IKONOS imagery. Norsk Geografisk Tidsskrift. 58: 61-73.

Huggel, C., Kääb, A., Haeberli, W. and Krummenacher, B. 2003. Regional scale GIS models for assessment of hazards from glacier lake outbursts: evaluation and application in the Swiss Alps. Natural Hazards and Earth Systems Sciences. 3: 647-662.

Ingeomin, 2006. Efecto social del evento de Santa Cruz de Mora. Emergencia en el Mocotíes. Encuentro Binacional Colombo-Venezolano en el marco del Proyecto Multinacional Andino: Geociencias para las Comunidades Andinas. Instituto Nacional de Geología y Minería de Venezuela. Mérida Venezuela, 64 pp.

Ingeomin, 2007. Estudio de suceptibilidad de la cuenca Montalbán - la ceibita, Municipio campo Elías - Edo. Mérida. Instituto Nacional de Geología y Minería de Venezuela. Mérida Venezuela, 212 pp.

Jackson, E., Kostaschuk, A. and MacDonald, M. 1987. Identification of debris flow hazard on alluvial fans in the Canadian Rocky Mountains. In: Costa, J.E. and Wieczorek, G.F. (eds.). Debris flows/avalanches: process, recognition and mitigation. Boulder Colorado. Geological Society of America: 115-124.

Lafaille, J. 2005. Antecedentes de los eventos meteorológicos ocurridos en el valle del río Mocotíes y su impacto geomorfológico. Revista Geográfica Venezolana. Número Especial 1: 297-311.

Li, Z., Zhu, Q. and Gold, C. 2005. Digital terrain modeling: Principles and methodology. CRC Press, Boca Raton, 323pp.

McNamara, J. P., Kane, D. and Hinzman, L. 1999. An analysis of an arctic channel network using a digital elevation model. Geomorphology. 29: 339-353.

Maldonado, J.J. 2007. Propuesta para la zonificación de vulnerabilidad socionatural de la microcuenca Quebrada La Resbalosa, Mérida. Instituto Universitario de Ejido. Tésis de grado, 75p. (Inédito). http://www.monografias.com/trabajos-pdf/zonificacion-la-resbalosa/zonificacion-la-resbalosa.pdf, last access: December 1, 2010.

Marchi, L. and Fontana, G. 2005. GIS morphometric indicators for the analysis of sediment dynamics in mountain basins. Journal of Environmental Geology. 48 (2): 218-228.

MARN 2006. Sistema de información hidrológica y metereológica. Datos pluviométricos sobre la Cuenca del río Chama (1947-2001). Mérida Venezuela. (Inédito).

Melton, M.A. 1958. Geometric properties of mature drainage systems and

their representation in E4 space. Journal of Geology. 66: 35-56.

Miliaresis, G.C. 2008. The landcover impact on the aspect/slope accuracy dependence of the SRTM-Elevation Data for the Humboldt Range. Sensors. 8: 3134-3149.

Neteler, M. and Mitasova, H. 2007. Open Source GIS. A GRASS GIS Approach. 3rd Edition. Springer, Heidelberg, 393pp.

Patton, P.C. 1987. Drainage basin morphometry and floods. In: Baker, V.R., Kochel, R.C. and Patton, P.C., (eds.). Flood geomorphology. New York: Wiley. 51-110.

Ponte, R. 1976. Investigación de la variabilidad y distribución de la precipitación en Cuenca de los ríos Chama y Mocotíes, Estado Mérida, Venezuela. Universidad de Los Andes. Mérida Venezuela. Trabajo presentado ante la Facultad de Ciencias Forestales para los efectos de ascenso a la categoría de profesor asistente, 49 pp. (Inédito).

Quinn P., Beven K. Chevallier, P. and Planchon, O. 1991. The prediction of hillslope flow paths for distributed hydrologic modeling using digital terrain models. Hydrologic Processes. 5: 59-79.

Roa, J.G. 2007. Identifying landslides hazards in a tropical mountain environment, using geomorphologic and probabilistic approaches. University of Maryland. Maryland, USA, 182 pp. (Inédito). http://drum.lib.umd.edu/handle/1903/7825, last access: December 1, 2010.

Rojas, M. and Alfaro, E. 2000. Influencia del oceano atlántico tropical sobre el comportamiento de la primera parte de la estación lluviosa en Venezuela. Topicos Meteorologicos y Oceanograficos. 7 (2): 88-92.

Rowbotham, D., Scally, D.F. and John, L. 2005. The identification of debris torrent basins using morphometric measures derived within a GIS. Geografiska Annaler. 87A (4): 527-537.

Scally, D.F., Slaymaker, O. and Owens, I. 2001. Morphometric controls and basin response in the Cascade Mountains. Geografiska Annaler. 83A (3): 55-65.

Schubert, C. 1980. Morfología neotectónica de una falla rumbo-deslizante e información preliminar sobre la falla de Boconó. Andes Merideños. Acta Científica. 31: 98-11.

Schubert, C. and Vivas, C. 1993. El Cuaternario de la Cordillera de Mérida. Andes Venezolanos: Mérida. Universidad de Los Andes/Fundación Polar. Mérida Venezuela, 345 pp.

Silva, G. 1999. Análisis hidrográfico e hipsométrico de la cuenca alta y media del río Chama, Edo Mérida, Venezuela. Revista Geográfica Venezolana. 40 (1): 9-42.

SRTM FTP Server 2006. ftp://e0srp01u.ecs.nasa.gov/srtm/version2/SRTM3/South_America/, last access: May 20, 2006.

Wieczorek, G.F. 1987. Effect of rainfall intensity and duration on debris flows

in central Santa Cruz Mountains, California. In: Costa, J.E. and Wieczorek, G.F. (eds.). Debris flows/avalanches: process, recognition and mitigation. Geological Society of America. Boulder, Colorado. 93-104.

7 Paper VI
Glacier movement from radar image and optical elevation data

published as
Schneevoigt, N.J., Sund, M., Bogren, W., Kääb, A. & D.J. Weydahl (2012):
Glacier displacement on Comfortlessbreen, Svalbard, using 2-pass differential SAR interferometry (DInSAR) with a digital elevation model.
Polar Record 48(244): 17-25.

Differential synthetic aperture radar interferometry (DInSAR) exploits the coherence between the phases of two or more satellite synthetic aperture radar (SAR) scenes taken from the same orbit to separate the phase contributions from topography and movement by subtracting either phase. Hence pure terrain displacement can be derived without residual height information in it, but only the component of movement in line-of-sight direction is represented in a differential interferogram. Comfortlessbreen, a recently surging glacier, flows predominantly in this direction with respect to the European Remote Sensing satellites ERS-1 and ERS-2. Four C-band SAR scenes from spring 1996 were selected because of the high coherence between the respective pairs of

the one-day repeat-pass tandem mission of the ERS sensors. 2-pass DInSAR is performed in combination with a SPOT 5 (Satéllite pour l´Observation de la Terre 5) SPIRIT (SPOT 5 stereoscopic survey of Polar Ice: Reference Images and Topography) digital elevation model (DEM) from 2007. The different processing steps and intermediate image products, including unwrapping and generation of displacement maps, are detailed in order to convey the DInSAR processing chain to the beginner in the field of interferometry. Maximum horizontal displacements of 18 to 20 cm d^{-1} in ground range direction can be detected at the glacier terminus, while a few centimetres per day characterised most of the middle and upper portions of Comfortlessbreen in spring 1996.

7.1 Introduction

Spaceborne interferometric synthetic aperture radar (InSAR) was introduced by Goldstein and others (1988) and first applied to glaciers by Goldstein and others (1993). It takes advantage of the coherence between the phases of two SAR scenes from the same satellite orbit, even in areas with poor visual contrast like ice caps and glaciers. As it depends on active microwave sensing, SAR data can also be acquired through clouds and at night. Information on movement and elevation are both contained in a single interferometric phase (Gens and van Genderen 1996; Joughin and others 1996).

Differential interferometry represents a means to separate displacement from topographic information. While Gabriel and others (1989) described DInSAR using three SAR scenes (3-pass DInSAR without DEM) over land, Kwok and Fahnestock (1996) obtained glacier velocities by differentiating the fringe structures in two independent interferograms (4-pass DInSAR without DEM). Cumming and others (1997) applied 2-pass DInSAR with DEM to measure alpine glacier flow. These different approaches have become established glacier monitoring tools, which are constantly being refined (Rosen and others, 2000; Rott, 2009). Because of the short 24 h time span and hence the

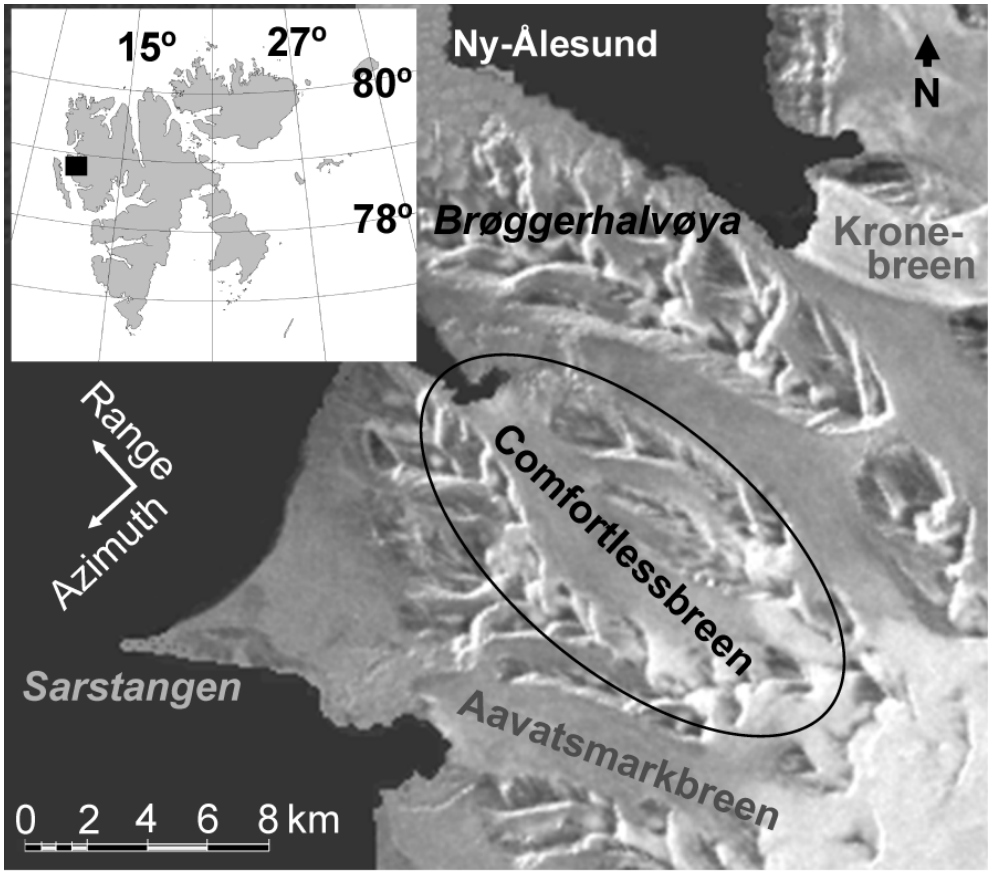

Figure 7.1: Comfortlessbreen on Svalbard Archipelago
Background: section of a modified C-band SAR amplitude image (5 April 1996) by ERS 1.

high potential for coherence between SAR scene acquisitions, the ERS-1/-2 tandem mission of 1995/96 still represents a unique data source for interferometric and glaciological analyses (Eldhuset and others 2003; Wangensteen and others 2005; Rott 2009). Examples of interferometric surge research are given in Joughin and others (1996), Murray and others (2003) and Pritchard and others (2005).

This study focuses on glacier dynamics, aiming at a reconstruction of glacier flow with ERS-1/-2 data from April and May 1996 and a SPOT 5 DEM from 2007 (Tab. 7.1). This allows a look into the past quiescent phase of Comfortlessbreen (Fig. 7.1) about a decade before its surge (Sund and others 2009;

Sund and Eiken 2010), to infer 1996 velocities. The goal of this paper is to render a thorough and well illustrated, low threshold description of the DInSAR workflow necessary to arrive at movement information. The entry into differential interferometry shall thus be facilitated.

7.2 Geographical setting and glacier surges

Svalbard lies in the North Atlantic (74° to 84° N, 10° to 34° E), south of the Arctic Ocean (Fig. 7.1). Glaciers cover about 60 % of the archipelago. Many of them are surgetype (Hagen and others 1993; Sund and others 2009) with typically low quiescent-phase velocities around 10 m a^{-1} (Melvold and Hagen 1998; Nuttall and others 1997).

Glacier surges are sudden increases in velocity of 10 to 1000 times the quiescent flow, rapidly transferring large ice masses from higher to lower areas (Meier and Post 1969; Murray and others 2003). In Svalbard, surges tend to last in total at least $\sim$ 10 a (Dowdeswell and others 1991; Sund and others 2009) and quiescence 30 to 500 a (Dowdeswell and others 1991; Hagen and others 1993). Between surges, velocities remain too low to maintain balance, which causes build-up of glacier mass (Melvold and Hagen 1998). More knowledge on surge dynamics is important because surges can have great impact on glacier geometry, and may affect assessments relating to climate change.

Some 20 km south of Ny Ålesund on Spitsbergen, the glacier Comfortlessbreen (Fig. 7.1), with an area of $\sim$ 65 km^2 and a length of $\sim$ 15 km, is flowing in a northwesterly direction from 1000 m above sea level (a.s.l.) to its partly tidewater terminus (Hagen and others 1993). Its recent surge is described by Sund and others (2009) and Sund and Eiken (2010).

7.3 Data basis

Four C-band SAR scenes from April and May 1996 from the one-day repeat-pass tandem mission of ERS-1/-2 are used for differential SAR interferometry over Comfortlessbreen together with a SPOT 5 HRS (High Resolution Stereoscopic) SPIRIT DEM from 2007 (Korona and others 2009) with 40 m resolution and 5 m height accuracy (Table 7.1). Each SAR image covers an area of $\sim$ 100 x 100 km and was provided in single look complex (SLC) format to be read into the Gamma Remote Sensing software (Wegmüller and Werner 1997) in which all data processing was done.

Table 7.1: Data Basis of the Study.

Sensor	Date	Data type
ERS 1	05.04.1996	SAR SLC
ERS 1	10.05.1996	SAR SLC
ERS 2	06.04.1996	SAR SLC
ERS 2	11.05.1996	SAR SLC
SPOT5-HRS	01.09.2007	SPOT DEM

7.4 Differential SAR interferometry

7.4.1 Interferometric SAR (InSAR) principles

An SLC SAR image s consists of amplitude, magnitude or intensity information $|s|$ representing backscatter from the ground as perceived in Fig. 7.1, and phase angles φ recorded as fractions (0 - 2π) of a radar wavelength λ with an ambiguous number of full wavelengths. The number of fully completed wavelengths of a radar signal is not measured (Hanssen 2001):

$$s = |s| e^{i\varphi} = |s| (\cos \varphi + i \sin \varphi) \tag{7.1}$$

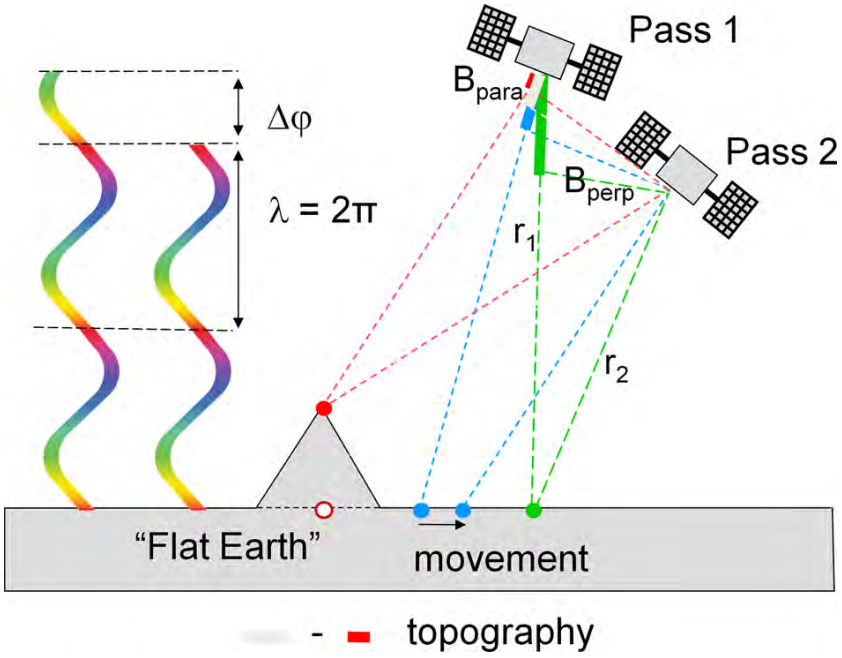

Figure 7.2: Schematic Principles of SAR Interferometry
Two colour fringes with their interferometric phase $\Delta\varphi$ (left). Across-track InSAR geometry with fat parallel baseline B_{para}, perpendicular baseline B_{perp} and antenna distances r_1 and r_2 (right). Satellite flight direction perpendicular to figure plane.

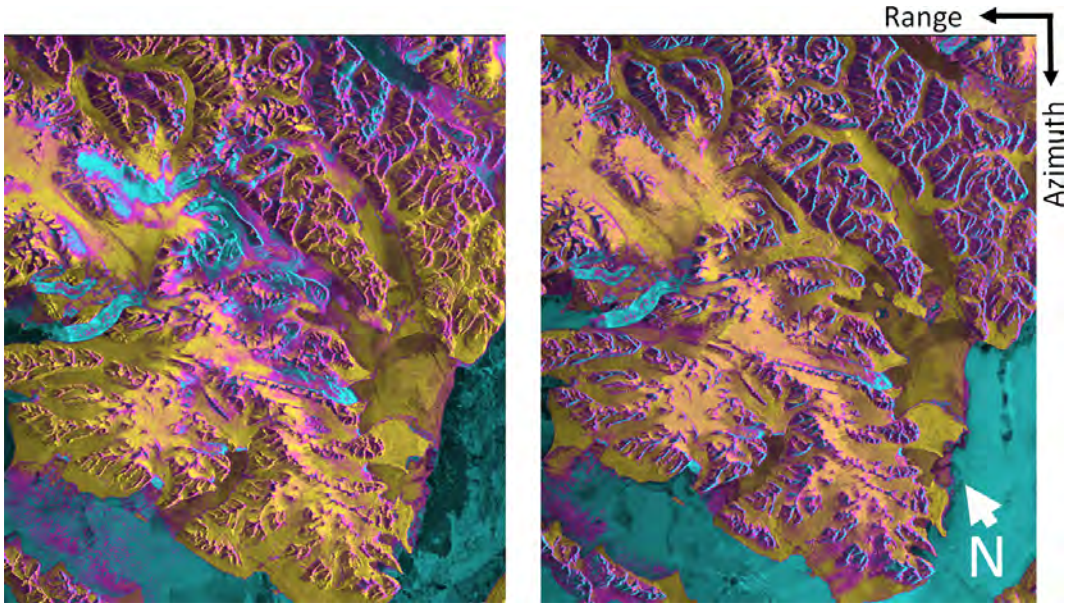

Figure 7.3: Phase Coherence between Image Pairs
Left: 5–6 April 1996, right: 10–11 May 1996. Bright, yellow areas represent high coherence values. Intermediate, pink tones indicate moderate correlation, while darker, turquoise zones imply low coherence.

The phases of one SAR image alone contain few interpretable features, yet when using the phase differences or interferometric phases $\Delta\varphi$ between two images of the same orbit and area (Fig. 7.2), the phase differences $\Delta\varphi$ can be represented in an interferogram to infer ground information (Gens and van Genderen 1996; Moholdt 2010):

$$\begin{aligned} \Delta\varphi \;=\; \varphi_2 \;-\; \varphi_1 \;&=\; \frac{4\pi}{\lambda}\,(r_2 \;-\; r_1) \\ &=\; \frac{4\pi}{\lambda}\,(B_{para}\;\sin\theta \;-\; B_{perp}\;\cos\theta) \end{aligned} \tag{7.2}$$

with the distances r_1 and r_2 from a point on the ground to the satellite antenna on the first and the second pass respectively (Fig. 7.2) and the radar look angle θ between nadir and the target on the ground (topographic information). Those two orbit passes are separated from one another temporally by a temporal baseline $B_t = 24$ h in the case of the ERS-1/-2 tandem mission, and in space by the spatial baseline B_s, corresponding to the distance between the two satellite orbits. B_s can be expressed by parallel baseline B_{para} and perpendicular baseline B_{perp} (Fig. 7.2); those are calculated and refined during interferogram generation.

In case of terrain displacement or deformation within the time interval corresponding to B_t, this will lead to a distinct signal in phase difference next to the inherent topographic contribution (Fig. 7.2). Hence Eq. 7.2 needs to be expanded with a deformation term (Kwok and Fahnestock 1996; Wangensteen and others 2005):

$$\begin{aligned} \Delta\varphi \;&=\; \frac{4\pi}{\lambda}\,(B_{para}\;\sin\theta \;-\; B_{perp}\;\cos\theta) \;+\; \frac{4\pi}{\lambda}\,\Delta\rho \\ &=\; \Delta\varphi_{topo} \;+\; \Delta\varphi_{disp} \end{aligned} \tag{7.3}$$

where $\Delta\rho$ represents the displacement component in line-of-sight direction. This shows that the topography summand $\Delta\varphi_{topo}$ is dependent on a spatial baseline B_s, while the movement summand only depends on B_t, but not on any B_s (Wangensteen and others 2005; Moholdt 2010).

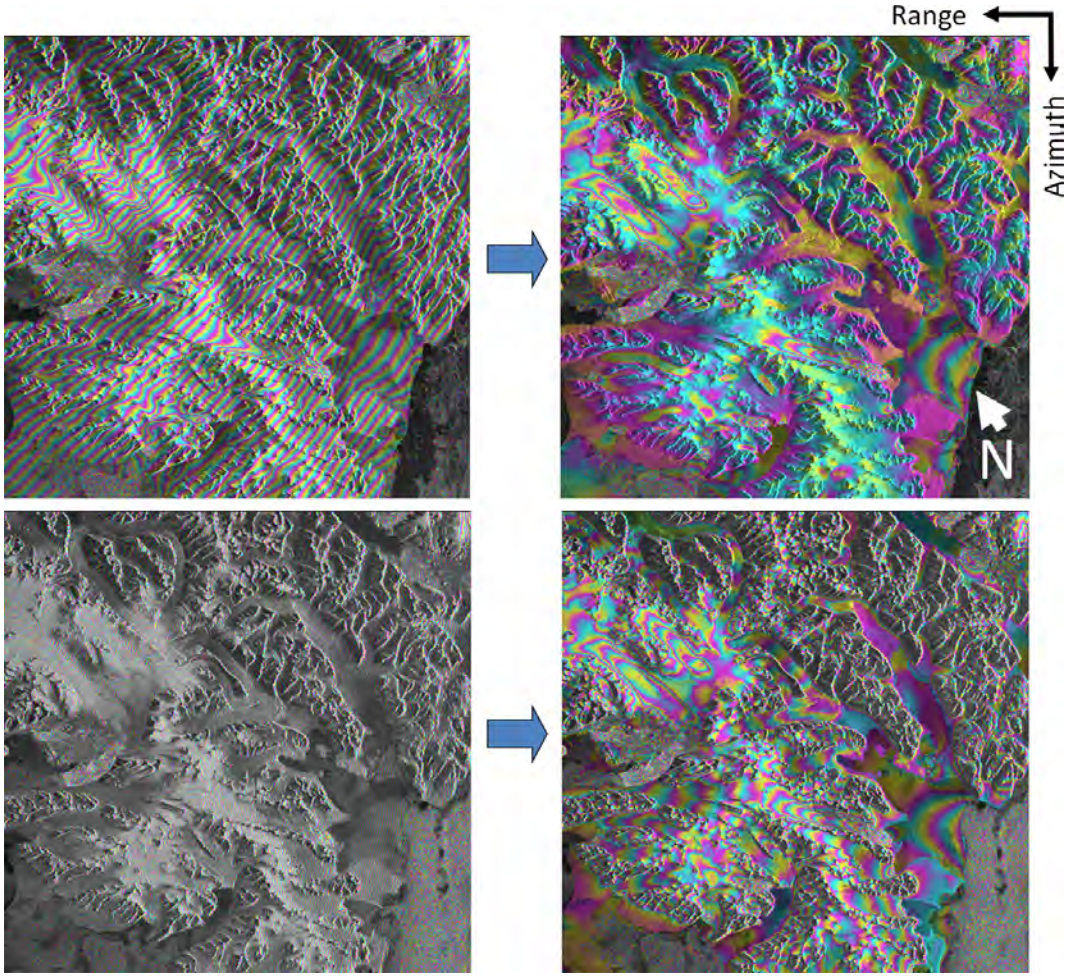

Figure 7.4: Flat Earth Correction in Wrapped Interferograms
Interferograms of 5–6 April 1996 (top) and 10–11 May 1996 (bottom) wrapped around modulus 2π with amplitude images as background. Phases from flat Earth, topography, movement, atmosphere and noise (left). Flat Earth phase corrected (right).

7.4.2 Phase coherence and interferogram generation

Very accurate image co-registration as well as high coherence (Fig. 7.3), that is only slight differences within a SLC image pair, are mandatory for interferogram generation (Rosen and others 2000; Weydahl 2001). Offset estimation via iterative image matching was used to co-register the two respective image pairs (Table 1), which were selected because of their high coherence (Weydahl 2001), with sub-pixel precision. Then one complex ERS-1 SAR image was multiplied with the complex conjugate of the other ERS-2 image taken 24 h later (Rosen and others 2000; Rott 2009). In the resulting raw interferogram, the phase differences $\Delta\varphi$ between the two satellite images are displayed modulo 2π as colour fringes (Figs. 7.2, 7.4). Those phase differences contain a mixed signal made up not only of topography ($\Delta\varphi_{topo}$) and displacement ($\Delta\varphi_{disp}$) as represented in Eq. 7.3, but also of contributions from flat Earth trend ($\Delta\varphi_{flat}$), and possibly atmospheric influences ($\Delta\varphi_{atmo}$) and noise ($\Delta\varphi_{noise}$) (Weydahl and others 2001; Fig. 7.4, left):

$$\Delta\varphi = \Delta\varphi_{flat} + \Delta\varphi_{topo} + \Delta\varphi_{disp} + \Delta\varphi_{atmo} + \Delta\varphi_{noise} \qquad (7.4)$$

$\Delta\varphi_{flat}$ and $\Delta\varphi_{topo}$ result from the sideward SAR viewing geometry and can be precisely computed with accurate orbit data and DEMs; $\Delta\varphi_{disp}$ only captures displacements in range line of sight of the sensor (Cumming and others 1989; Kwok and Fahnestock 1996; Rott 2009). Fast movements appear blurred in radar applications due to decorrelation or coherence loss (Weydahl, 2001; Eldhuset and others, 2003). Therefore, radar imagery better reflects glacial accumulation areas and slowflowing glacier parts (Goldstein et al, 1993; Joughin and others, 1996; Eldhuset and others, 2003; Pritchard and others, 2005).

Flat Earth phase removal constitutes the first step in interferometric processing (Fig. 7.4), followed by filtering (Rott 2009; Wegmüller and Werner 1997). Remaining phase differences are then due to topography, movement, atmosphere and noise (Fig. 7.4, right). When working with only one single SLC pair as in basic InSAR processing (Goldstein and others 1993), the $\Delta\varphi$

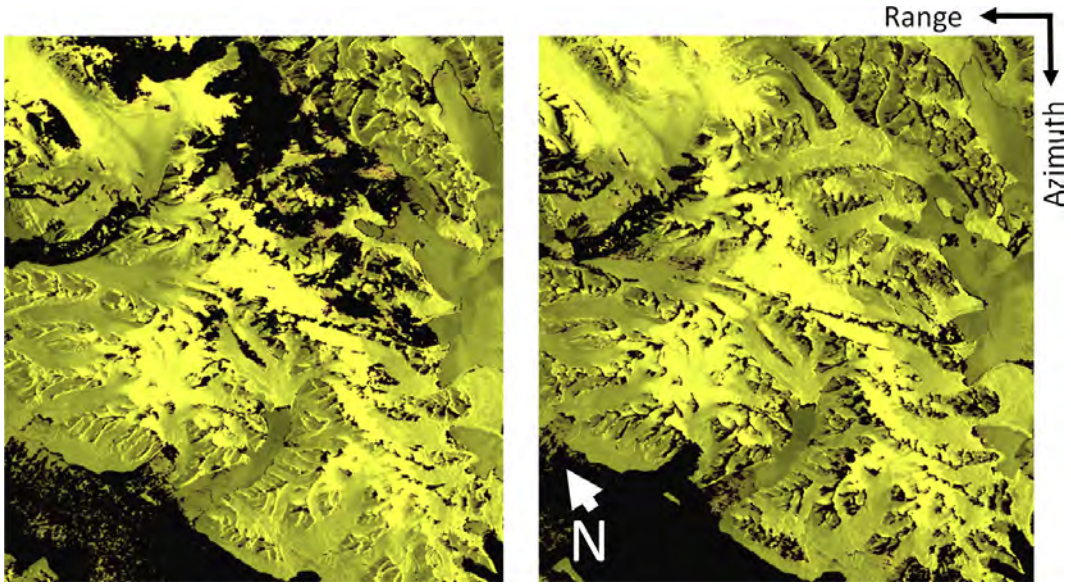

Figure 7.5: Removal of badly correlated Image Sections
Coherence masks with threshold 0.8 for the interferograms of April (left) and May 1996 (right). Coherence ≤ 0.8 is masked out for unwrapping (black colour).

constituents (Eq. 7.4) cannot be further resolved without additional supporting data; ground control points, other ground truth or DInSAR applications (see 4.4.) are necessary to this end.

7.4.3 Phase unwrapping

Fig. 7.4 represents intermediate InSAR results; phase unwrapping must be effectuated in order to obtain a final interferogram. This can then be interpreted correctly, as its fringes represent continuous values instead of being wrapped around modulus 2π. Phase unwrapping means adding integer multiples of 2π to $\Delta\varphi$ whenever it jumps back to 0 from 2π; a crucial and difficult step (Gens and van Genderen 1996; Wegmüller and Werner 1997; Moholdt 2010). Low coherence cannot be unwrapped and has to be masked out (Fig. 7.5). Several algorithms have been developed for unwrapping; implemented in Gamma (Wegmüller and Werner 1997) are the branchcut region growing algorithm (Goldstein and others 1988) and the minimum cost flow (MCF)

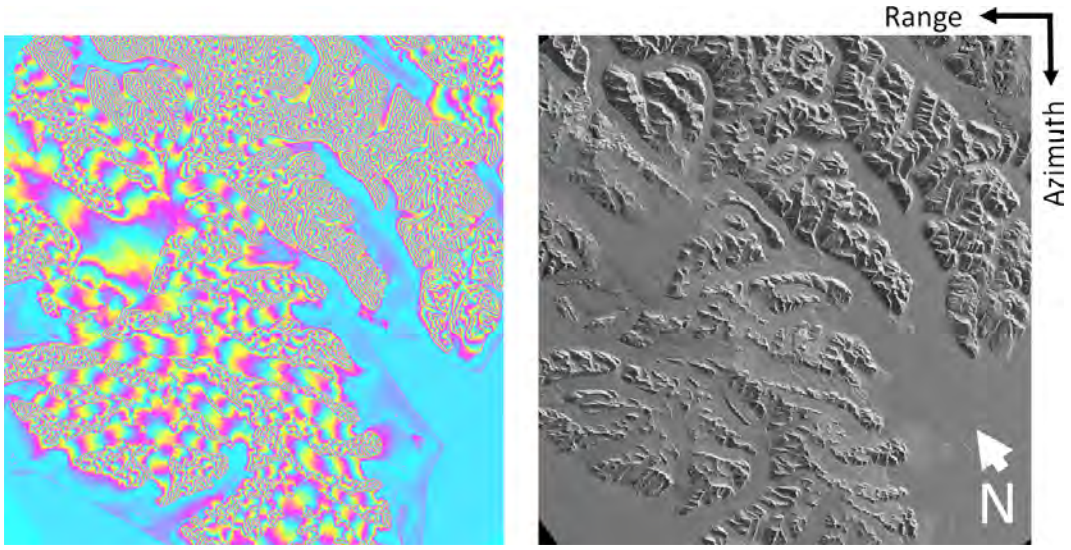

Figure 7.6: Interferogram Simulation from Elevation Data
Simulated interferogram from SPOT 5 DEM of 2007 transformed from map projection into radar geometry (left) based on simulated amplitude image from DEM in RDC (right).

technique with a triangular irregular network (TIN) (Costantini 1998). Both approaches were tested in this study.

7.4.4 2-pass differential InSAR (DInSAR) with DEM

DInSAR consists in subtracting the interferometric phases of one interferogram ($\Delta\varphi_1$) from another one ($\Delta\varphi_2$) to separate the phase contributions from topography and movement (Eqs. 3, 4) by subtracting and thus removing either of those phases. Hence pure terrain displacement can be derived without residual height information, or alternatively pure DEM information without motion signals. The InSAR baselines B_{s_1} and B_{s_2} must differ for this effect, while motion is assumed to be constant (Rott 2009):

$$\begin{aligned}\Delta\varphi_{1-2} &= \Delta\varphi_1 - k\,\Delta\varphi_2 \\ &= (\Delta\varphi_{topo_1} - k\,\Delta\varphi_{topo_2}) + (\Delta\varphi_{disp_1} - k\,\Delta\varphi_{disp_2}) \\ &\quad + (\Delta\varphi_{atmo_1} - k\,\Delta\varphi_{atmo_2}) + (\Delta\varphi_{noise_1} - k\,\Delta\varphi_{noise_2})\end{aligned} \tag{7.5}$$

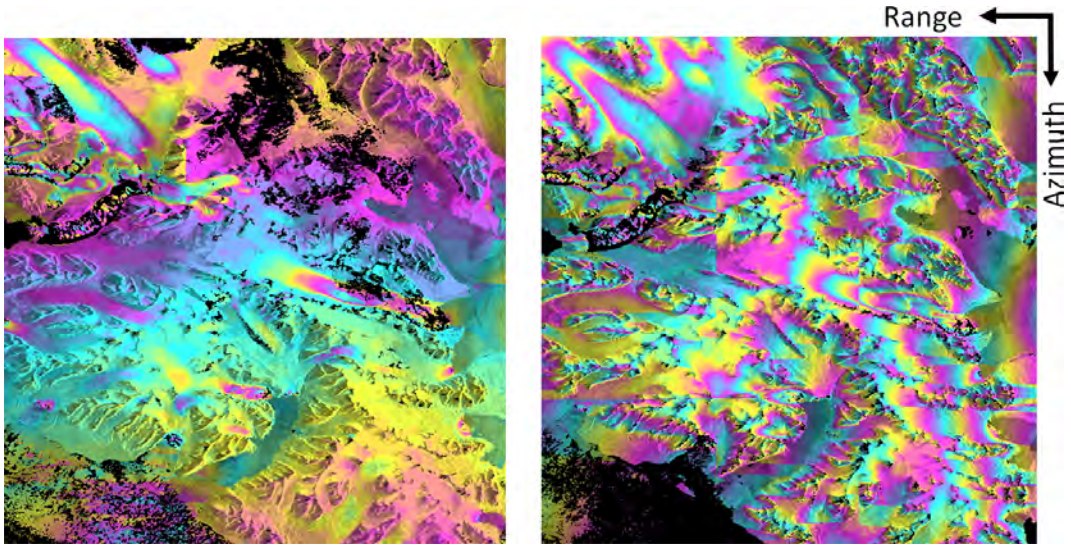

Figure 7.7: InSAR Phase Unwrapping using MCF
Linear jumps due to tile borders, phase inconsistencies and some baseline effects. Left: 5-6 April 1996 ($B_{perp} \sim 12$ m), right: 10-11 May 1996 ($B_{perp} \sim$ -66 m).

A scaling factor k is introduced at this point. When aiming at the topographic phase component $\Delta\varphi_{1-2} = \Delta\varphi_{topo_{12}}$, k must equal 1 (Moholdt 2010). As topography depends on B_s, while movement does not (Eq. 7.3), constant movement becomes fully subtracted for $k = 1$. Then topography or DEM information can be generated from Eq. 7.5. However, when aiming at displacement $\Delta\varphi_{1-2} = \Delta\varphi_{disp_{12}}$, a scaling factor $k \neq 1$ has to be used to allow for a complete removal of the perpendicular baseline and hence the topographic phase. Phase noise may increase due to interferogram scaling (Eq. 7.5).

Differential interferometry can be done by 2-pass DInSAR with two tandem SAR scenes and a DEM (Cumming and others 1989) as in this study, or by combining three (3-pass DInSAR) or more satellite scenes from the same orbit. Two interferograms are generated and then subtracted from one another (Joughin and others 1996; Kwok and Fahnestock 1996; Eldhuset and others 2003). In 2-pass DInSAR, a reference interferogram with $\Delta\varphi$ corresponding to surface topography is simulated based on a DEM in radar geometry (Fig. 7.6). Thus the DEM must be read into radar doppler coordinates (RDC). An

initial geocoding look-up table links Universal Transverse Mercator (UTM) coordinates to range-doppler geometry (Fig. 6, left). Then a SAR intensity image is simulated based on DEM and SAR imaging geometry (Fig. 6, right). Offsets are iteratively improved via pixel matching and subsequently the look-up table, so that a fine registration of the DEM becomes possible. Forward geocoding finally allows the transformation of the DEM UTM projection into RDC with improved coordinate relationships (Wegmüller and Werner 1997).

Afterwards, a first wrapped differential interferogram (Fig. 7.8, top) is generated by subtracting the unwrapped simulated phase $k\Delta\varphi_2$ (Eq. 7.5) from the complex, that is wrapped interferogram $\Delta\varphi_1$ (Fig. 7.4, left); both still contain $\Delta\varphi_{flat}$. Residual linear phase trends are determined by Fast Fourier Transform and removed by baseline model refinement. The corresponding unwrapped unflattened topographic interferometric phase is then resimulated with a baseline refined with help of the RDC DEM, and a second differential interferogram produced (Fig. 7.8, bottom).

7.5 Results

When unwrapping the interferograms, the MCF technique with a TIN (Costantini 1998) led to smoother and more continuous results than the branch-cut algorithm (Goldstein and others 1988), therefore it was given preference in this study. Figure 7.7 shows the maximum spatial unwrapping extent when using 5 x 5 tiles, which divide the image into 25 rectangles. Those tiles are unwrapped individually with a certain overlap and then reassembled by the algorithm. A few horizontal and vertical linear jumps in the colour fringes remain from tiling in Fig. 7.7. Besides, some baseline effects from the lower right to the higher left corner can be observed (Fig. 7.7, left). The final interferograms were generated using 3 x 2 tiles and a reduced image subset.

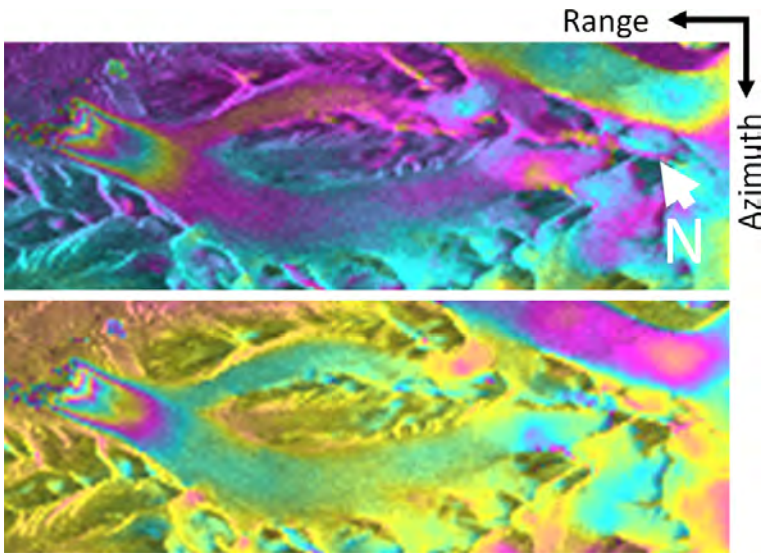

Figure 7.8: Differential Interferograms of Comfortlessbreen
Top: first complex-valued differential interferogram based on ERS-1/-2 data of 5-6 April 1996 and the SPOT-5 DEM. Linear colour shift from top left to bottom right due to small errors in the baseline model. Bottom: refined complex-valued differential interferogram after removal of linear phase trends via baseline residual correction.

The elevation difference corresponding to one 2π fringe in an unwrapped interferogram is (Weydahl and others 2001):

$$\Delta h_{2\pi} = \frac{\lambda \, r_a \, \sin \theta}{2 \, B_{perp}} \tag{7.6}$$

with r_a being antenna distance r_1 or r_2. For 5-6 April 1996 with $B_{perp} \sim 12$ m, one fringe represents $\Delta h_{2\pi} = 793$ m of altitude, and for 10-11 May 1996 ($B_{perp} \sim$ -66 m) 144 m.

Glacier velocities in line-of-sight between scene acquisitions can be derived from the differential phase (Murray and others 2003; Wangensteen and others 2005) after filtering and unwrapping by MCF, leading to orthonormal displacement maps for horizontal, vertical and look vector movement component respectively (Fig. 7.9). The DInSAR analysis of Comfortlessbreen reveals horizontal displacements of ~ 20 cm d^{-1} (5-6 April 1996) and ~ 18 cm d^{-1} (10-11 May 1996) at the glacier terminus and < 3 cm d^{-1} in the middle and upper

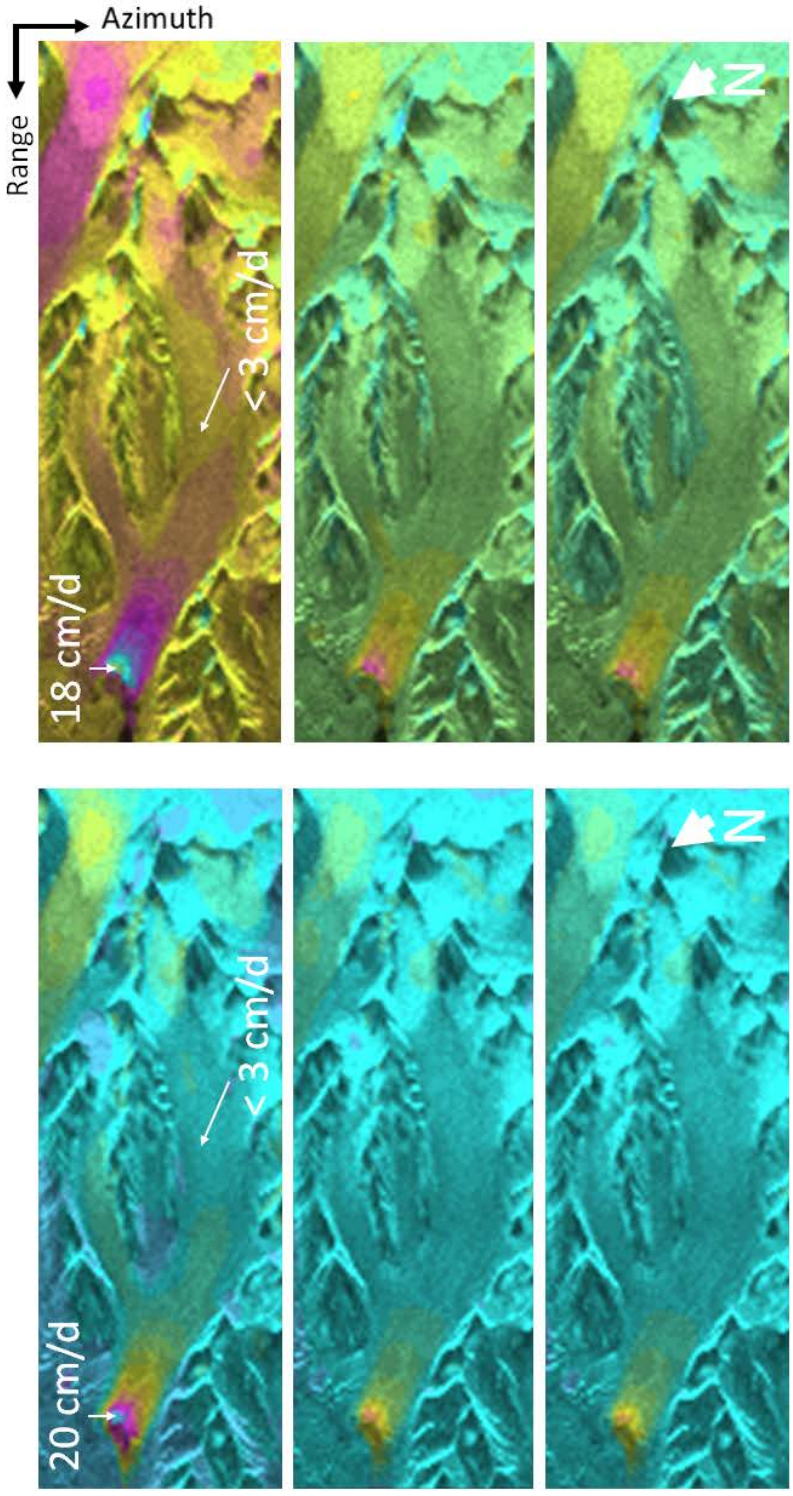

Figure 7.9: Comfortlessbreen Glacier Flow
Filtered and unwrapped differential interferograms transformed into displacement maps (left: 5–6 April 1996 and SPOT5 DEM, right: 10–11 May 1996 and SPOT5 DEM): horizontal (top), vertical (middle) and movement along the look vector (bottom) with 20 cm d^{-1} displacement per full colour cycle (from cyan to magenta).

glacier portions (Fig. 7.9). These measured velocities correspond to < 11 m a^{-1} along most of the glacier, while they increase towards 73 m a^{-1} in the lowermost 2.5 km, respectively. In the topmost area of the glacier, velocities of around 6 cm d^{-1} can be noted, which is commensurate to 22 m a^{-1}.

7.6 Discussion

The DInSAR displacement rates stated above are consistent for both April and May scenes and indicate a pre-surge velocity level on Comfortlessbreen in 1996. For Svalbard glaciers known to have surged, low velocities around 10 m a^{-1} are typically measured during quiescence (Nuttall and others 1997; Melvold and Hagen 1998) due to their polythermal regime. Tidewater glaciers commonly increase velocities towards the terminus (Vieli and others 2004), as is the case here (Fig. 7.9). The ratio from lowest (< 3 cm d^{-1}) to highest (20 cm d^{-1}) velocities is 7 (11 m a^{-1} to 73 m a^{-1}). Increasing velocities in the cirque region in spring 1996 (Fig. 7.9, top) may represent the first indicator of surge initiation, surge stage 1 as suggested by Sund and others (2009). During surge in 2008 however, this pattern changed. Despite generally increased velocities of ~ 2 m d^{-1} (730 m a^{-1}), the velocity gradient, was reduced, ranging from 1.17 m d^{-1} (427 m a^{-1}) at mid-glacier to 2.06 m d^{-1} (752 m a^{-1}) at the terminus (Sund and Eiken 2010; M. Sund, personal communication, 2011), hence reducing the velocity ratio along glacier to < 2. DInSAR thus provides a basis for the comparison of changes from quiescence displacement levels to surge.

The potential accuracy of repeat-pass InSAR surface change detection lies in the millimeter range (Gabriel and others 1989; Goldstein and others 1993; Weydahl 2001). Yet $\Delta\varphi$ decorrelates for ERS SAR images at ~ 7.2 cm for horizontal movements in line of sight (Weydahl 2001). To the central west in Fig. 7.3, fast flowing Kronebreen with its 2 m d^{-1} (Weydahl 2001; Eldhuset and others 2003) appears very blue and decorrelated especially towards its

margins. Such speeds as also reached in the Comfortlessbreen surge in 2008 (Sund and Eiken 2010) cannot be captured by DInSAR; SAR offset tracking and optical image matching represent possible alternatives.

Atmospheric influences, imprecise orbit information, signal noise and assumption of displacement along the elevation gradient represent the principal error sources in InSAR (Strozzi and others 2010). An assumed error in line-of-sight displacement of < 0.7 cm for ERS-1/-2 results from a total phase error of a quarter wavelength (Crosetto and others 2008; Strozzi and others 2010). As shown in Eqs. 4 and 5, contributions from atmospheric influences ($\Delta\varphi_{atmo}$) and noise ($\Delta\varphi_{noise}$) are still contained in the generated (differential) interferograms (Weydahl and others 2001; Rott 2009). Ideally, $\Delta\varphi_{atmo}$ and $\Delta\varphi_{noise}$ would be fully subtracted in the DInSAR process. However, $\Delta\varphi_{atmo}$ may differ between repeat pass acquisitions due to varying atmospheric water vapour content. This cannot easily be corrected for, as the necessary additional data would have to cover the entirety of the atmospheric strata and is seldom available (Gens and van Genderen 1996; Hanssen 2001; Rott 2009). As shown in Fig. 7.3, the phase coherence of the May image set is higher than in the April one, in which some temporal decorrelation over the northern central part of the scene occurs, possibly due to snowfall, snow drift, melting or atmospheric influences (Rott 2009). Besides, SAR data penetrates the ground surface to a certain extent. Hence inferences on and even below the glacier surface are possible, concerning roughness, wetness and melting conditions amongst others.

Because of the introduction of k, $\Delta\varphi_{noise}$ may increase. In order to reduce noise or speckle, a salt-and-pepper effect due to interferences between the many scatterers within one image pixel, the image grid can be spatially transformed to a lower resolution by averaging several looks at the same pixel, resulting in a multilook image (MLI) with better amplitude correlation and phase coherence between images at the expense of a lower spatial resolution (Kwok and Fahnestock 1996). MLI generation represents a means to find out how much

noise is left in the interferograms; therefore different MLI parameter settings should be compared to the results given here. With regard to the velocities given earlier, the errors cannot be precisely calculated within Gamma for all pixel values of a DInSAR scene. Testing all possible combinations of ERS-1/-2 SAR scenes together with more DEMs represents a means to account for the various possible error sources.

A short B_{perp} is advantageous for deriving displacement such as glacier flow, as it leads to extremely high topographic height spans represented within one fringe, like $\Delta h_{2\pi} = 793$ m as given for the April pair. This reduces DEM influence to a minimum, as most fringes in the corresponding interferogram then result from movement. The tallest peaks on Svalbard reach $\sim$ 1700 m a.s.l., thus a maximum of only two entire colour cycles stem from topography in the case of $B_{perp} \sim 12$ m (Fig. 7.4, top). As Comfortlessbreen reaches up to 1000 m a.s.l., some 1.3 colour cycles represent the maximum possible topographic contribution which might still be found in the unwrapped interferogram in Fig. 7.7 (left) which has not been differentiated from a simulated radar DEM phase. Since interferometric sensitivity to displacement is independent of the baseline B_{perp}, while it increases with the baseline for topography, short (or zero) spatial baselines are advantageous for InSAR displacement assessments and provide better coherence (Rott 2009).

7.7 Conclusion and outlook

This study provides a step-by-step introduction to differential interferometry exemplified by Comfortlessbreen. 2-pass DInSAR with DEM yields useful and consistent displacement maps for 1996, a period where little ground truth is available for the glacier. The results allow for comparison between surge and quiescence levels, showing a reduction in velocity gradient along glacier within $\sim$20 years to a fourth, even though velocities increased 10 to 60 times. More flow analyses are necessary to assess surge behaviour.

It would be interesting to look further into atmospheric influences by comparing our results to local meteorological data, which are limited to ground observations in 1996. No accurate corrections are hence possible. By assessing different DInSAR combinations of the ERS-1/-2 scenes with and without DEMs, conclusions could be drawn on whether the decorrelation in the April set is due to changes in the atmosphere or on the ground.

Our results are also valuable with regard to new tandem missions which allow for interferometric analyses again. For example, the COSMO/SkyMed constellation with its current four satellites (X-band SAR) can be flown in InSAR modus with either one-day, four-day, eight-day or 16-day tandem recording. TerraSAR-X and TanDEM-X or the C-band Radarsat Constellation Mission represent other sources of interferometry-compliant SAR data.

7.8 Acknowledgements

The European Space Agency (ESA) provided the SAR data (AOPOL 4127), the French Space Agency (CNES) the SPOT5-HRS DEM obtained through the IPY-SPIRIT programme (Korona and others 2009) ©CNES 2008 and SPOT Image 2008 all rights reserved. We thank R.G. Way and G. Moholdt for Gamma scripting support. G. Moholdt and the Remote Sensing Colloquium at the Department of Geosciences, University of Oslo, kindly reviewed an earlier manuscript. We are also grateful for the reviews by Polar Record and an Early Career Scientist Travel Grant for the International Circumpolar Remote Sensing Symposium (ICRSS) by the UK Polar Network. The Center for Remote Sensing of Land Surfaces, University of Bonn, Germany, currently hosts N.J. Schneevoigt. M. Sund was partly at the University Centre in Svalbard.

7.9 References

Costantini, M. 1998. A novel phase unwrapping method based on network programming. IEEE Transactions on Geoscience and Remote Sensing 36(3): 813–821.

Crosetto, M., O. Monserrat, C. Bremmer, R. Hanssen, R. Capes, and S. Marsh. 2008. Ground motion monitoring using SAR interferometry: quality assessment. European Geologist 26: 12–15.

Cumming, I., J.L. Valero, P.W. Vachon, K. Mattar, D. Geudtner, and L. Gray. 1997. Glacier flow measurements with ERS tandem mission data. ESA Fringe 1996 Proceedings, Zurich (ESA SP–406): 353–362.

Dowdeswell, J.A., G.S. Hamilton, and J.O. Hagen. 1991. The duration of the active phase on surge–type glaciers: contrasts between Svalbard and other regions. Journal of Glaciology 37(127): 388–400.

Eldhuset, K., P.H. Andersen, S. Hauge, E. Isaksson, and D.J. Weydahl. 2003. ERS tandem InSAR processing for DEM generation, glacier motion estimation and coherence analysis on Svalbard. International Journal of Remote Sensing 24(7): 1415–1437.

Gabriel, A.K., R.M. Goldstein, and H.A. Zebker. 1989. Mapping small elevation changes over large areas: differential radar interferometry. Journal of Geophysical Research 94(B7): 9183–9191.

Gens, R., and J.L. van Genderen. 1996. SAR interferometry – issues, techniques, applications. International Journal of Remote Sensing 17(10): 1803–1835.

Goldstein, R.M., H.A. Zebker, and C.L. Werner. 1988. Satellite radar interferometry: two–dimensional phase unwrapping. Radio Science 23(4): 713–720.

Goldstein, R.M., R. Engelhard, B. Kamb, and R. Frolich. 1993. Satellite radar interferometry for monitoring ice sheet motion: application to an Antarctic ice stream. Science 262: 1525– 1530.

Hagen, J.O., O. Liestøl, E. Roland, and T. Jørgensen. 1993. Glacier atlas of Svalbard and Jan Mayen. Oslo: Norwegian Polar Institute (Meddelelser 129).

Hanssen, R.F. 2001. Radar interferometry: data interpretation and error analysis. Remote sensing and digital image processing. Dordrecht: Kluwer.

Joughin, I., S. Tulaczyk, M.A. Fahnestock, and R. Kwok. 1996. A mini–surge on the Ryder Glacier, Greenland, observed by satellite radar interferometry. Science 274: 228– 230.

Korona, J., E. Berthier, M. Bernard, F. Remy, and E. Thouvenot. 2009. SPIRIT. SPOT 5 stereoscopic survey of polar ice: reference images and topographies during the fourth International Polar Year (2007–2009). ISPRS Journal of Photogrammetry and Remote Sensing 64: 204–212.

Kwok, R., and M.A. Fahnestock. 1996. Ice sheet motion and topography from radar interferometry. IEEE Transactions on Geoscience and Remote Sensing 34(1): 189–200.

Meier, M.F., and A. Post. 1969. What are glacier surges? Canadian Journal of Earth Sciences 6(4): 807–817.

Melvold, K., and J.O. Hagen. 1998. Evolution of a surge– type glacier in its quiescent phase: Kongsvegen, Spitsbergen, 1964–95. Journal of Glaciology 44(147): 394– 404.

Moholdt, G. 2010. Elevation change and mass balance of Svalbard glaciers from geodetic data. PhD dissertation. Oslo: University of Oslo, Department of Geosciences.

Murray, T., A. Luckman, T. Strozzi, and A.M. Nuttall. 2003. The initiation of glacier surging at Fridjovbreen. Annals of Glaciology 36: 110–116.

Nuttall, A.M., J.O. Hagen, and J. Dowdeswell. 1997. Quiescent–phase changes in velocity and geometry of Finsterwalderbreen, a surge–type glacier in Svalbard. Annals of Glaciology 24: 249–254.

Pritchard, H., T. Murray, T. Strozzi, S. Barr, and A. Luckman. 2005. Surge–related topographic change of the glacier Sortebræ, east Greenland, derived from synthetic aperture radar Interferometry. Journal of Glaciology 49(166): 381–390.

Rosen, P. A., S. Hensley, I.R. Joughin, F.K. Li, S.N. Madsen, E. Rodriguez, and R.M. Goldstein. 2000. Synthetic aperture radar interferometry. Proceedings of the IEEE 88(3): 333– 382.

Rott, H. 2009. Advances in interferometric synthetic aperture radar (InSAR) in earth system science. Progress in Physical Geography 33(6): 769–791.

Strozzi, T., R. Delaloye, A. Kääb, C. Ambrosi, E. Perruchoud, and U. Wegmüller. 2010. Combined observations of rock mass movements using satellite SAR interferometry, differential GPS, airborne digital photogrammetry, and airborne photography interpretation. Journal of Geophysical Research 115: F01014 (doi:10.1029/2009JF001311).

Sund, M., and T. Eiken. 2010. Recent surges of Blomstrandbreen, Comfortlessbreen and Nathorstbreen, Svalbard. Journal of Glaciology 56(195): 182–184.

Sund, M., T. Eiken, J.O. Hagen, and A. Kääb. 2009. Svalbard surge dynamics derived from geometric changes. Annals of Glaciology 50(52): 50–60.

Vieli, A., J. Jania, H. Blatter, and M. Funk. 2004. Short–term velocity variations on Hansbreen, a tidewater glacier in Spitsbergen. Journal of Glaciology 50(170): 389–398.

Wangensteen, B., D.J. Weydahl, and J.O. Hagen. 2005. Mapping glacier velocities on Svalbard using ERS tandem DInSAR data. Norwegian Journal of Geography 59: 276-285.

Wegmüller, U., and C. Werner. 1997. Gamma SAR processor and interfe-

rometry software. Florence: ERS (Third ERS symposium on space at the service of our environment, Florence, Italy): 1687–1692.

Weydahl, D.J. 2001. Analysis of ERS tandem SAR coherence from glaciers, valleys, and fjord ice on Svalbard. IEEE Transactions on Geoscience and Remote Sensing 39(9): 2029– 2039.

Weydahl, D.J., K. Eldhuset, and S. Hauge. 2001. Atmospheric effects on advanced modes. Kjeller: Norwegian Defence Research Establishment (Report 2001/04826).

List of Figures

List of Tables

Conference presentations

Schneevoigt, N.J., van der Linden, S., Sund, M., Bogren, W., Moholdt, G., Kääb, A., L. Schrott & D.J. Weydahl (2011):
Fernerkundung im geographischen Kontext - Ergebnisse eines Forschungsprojekts zwischen Bonn, Zürich und Oslo.
Annual Alumni Meeting of the Daimler and Benz Foundation, Ladenburg, Germany (talk).

Schneevoigt, N.J., Bogren, W., Sund, M., Weydahl, D.J. & A. Kääb (2011):
Gletscherbewegungen auf Spitzbergen aus differentieller SAR-Interferometrie.
Annual Workshop of the Center for Remote Sensing of Land Surfaces (ZFL), Bonn, Germany (talk).

Schneevoigt, N.J., Kääb, A., Bogren, W., Sund, M. & D.J. Weydahl (2010):
Comparison of 2-pass differential SAR interferometry (DInSAR) using two elevation models to 4-pass DInSAR. A test study near Ny Ålesund, Svalbard.
Fall Meeting of the American Geophysical Union (AGU), San Francisco, California, USA: C51A-0497 (poster).

Schneevoigt, N.J., Bogren, W., Sund, M., Weydahl, D.J. & A. Kääb (2010):
Glacier displacement of Comfortlessbreen, Svalbard, estimated by differential SAR interferometry (DInSAR) with digital elevation model (DEM).
11th International Circumpolar Remote Sensing Symposium, Cambridge, UK. Abstract volume: 39 (poster).

Schneevoigt, N.J., Bogren, W., Sund, M., Weydahl, D.J. & A. Kääb (2010):
Deriving glacier flow of Comfortlessbreen, Svalbard, with 2-pass differential SAR interferometry.
International Polar Year (IPY) Oslo Science Conference, Lillestrøm, Norway. Abstract volume: PS3-B.92 (poster).

Nuth, C., Moholdt, G., Schneevoigt, N.J., Sund, M., Svanem, M., Chapuis, A., Bogren, W. & A. Kääb (2010):
SPIRIT DEM applications over Svalbard.
SPOT SPIRIT IPY DEM Workshop, Centre National d'Études Spatiales (CNES), Toulouse, France (talk).

Schneevoigt, N.J., Moholdt, G., Sund, M. & A. Kääb (2009):
InSAR glacier observation near Ny Ålesund - first results.
Nordic Branch Meeting of the International Glaciological Society, Höfn, Iceland. Abstract volume: 75 (talk).

Schneevoigt, N.J., & A. Kääb (2009):
Remote sensing of geomorphological and glaciological features.
UNIS graduate course AG 325 Glaciology, Longyearbyen, Svalbard, (talk).

Schneevoigt, N.J., Moholdt, G., Nuth, C. & A. Kääb (2008):
Optical and SAR glacier observation near Ny Ålesund - first results.
Nordic Branch Meeting of the International Glaciological Society, Helsinki, Finland (talk).

Schneevoigt, N.J., Moholdt, G., & A. Kääb (2008):
Mapping glacial and periglacial environments with optical and radar data.
4th ESA EO Summer School on Earth System Monitoring and Modelling, ESA ESRIN Frascati, Rome, Italy (poster).

Schneevoigt, N.J., Moholdt, G. & A. Kääb (2007):
Remote sensing for mapping glacial and periglacial environments.
Nordic Branch Meeting of the International Glaciological Society, Uppsala, Sweden (poster).

Schneevoigt, N.J., Moholdt, G., & A. Kääb (2007):
Remote sensing for mapping glacial and periglacial mountain environments. Examples from geomorphic landforms in the Bavarian Alps and from Norwegian glaciers.
European Geosciences Union (EGU) General Assembly, Vienna, Austria. Geophysical Research Abstracts 9: 09464 (poster).

Schneevoigt, N.J., Kellenberger, T., Schrott, L. & A. Kääb (2006):
Object-oriented classification of alpine landforms from ASTER scenes (Reintal, Bavarian Alps).
9th International Symposium on High Mountain Remote Sensing Cartography (HMRSC-IX), Graz, Austria. Abstract volume: 89 (talk).

Schneevoigt, N.J. & L. Schrott, (2006):
Remote sensing of Alpine landforms. A geomorphic systems approach as exemplified in the Bavarian Alps (Germany).
BRGR Annual Conference on Geomorphology and Earth System Science, Loughborough, England. Abstract volume: 116 (poster).

Schneevoigt, N.J. (2005):
Fernerkundung alpiner Reliefformen - Ein Forschungsprojekt zwischen Bonn, Zürich und Oslo.
Ph.D. assessment fair of the Daimler and Benz Foundation, Ladenburg, Germany (talk).

Schneevoigt, N.J., Schrott, L., Schiefer, S. & H.-P. Thamm (2005):
Spaceborne detection of geomorphological landforms as visualisations of past and ongoing processes.
Arbeitskreis Oberflächenprozesse, Göttingen, Germany. Tübinger Geowissenschaftliche Arbeiten A (73): 64 (poster).

Schneevoigt, N.J., Schrott, L., Schiefer, S. & H.-P. Thamm (2005):
Können alpine Reliefformen fernerkundlich detektiert werden? Fallstudie im Reintal, Bayerische Alpen.
Annual session of "Arbeitskreis Hochgebirge", Geographentag, Trier, Germany. Abstract volume: 11 (talk).

Otto, J.-C. & N.J. Schneevoigt (2005):
Form- und Prozesserkennung aus digitalen Geländemodellen in der Geomorphologie.
Workshop Laserscanning, alpS-Zentrum für Naturgefahrenmanagement, Innsbruck, Austria (talk).

Schneevoigt, N.J., Schrott, L., & H.-P. Thamm (2005):
To what extent can Alpine landforms be predicted by remotely sensed imagery (Reintal, Bavarian Alps)?
EGU General Assembly, Vienna, Austria. Geophysical Research Abstracts 7: 08605 (poster).